

# **Pathological Alterations Induced by Intraneuronal A $\beta$ in Alzheimer's Disease**

## **Doctoral Thesis**

In partial fulfillment of the requirements  
for the degree "Philosophical Doctorate (Ph.D.)"

in the Molecular Medicine Program  
at the Georg-August University Göttingen

Faculty of Medicine

**submitted by**

DITTE ZERLANG CHRISTENSEN

**born in**

Hillerød, Denmark

**2009**

Members of the Thesis Committee:

Supervisor

Name, Institute: Prof. Thomas A. Bayer, Abteilung Molekulare Psychiatrie

Second member of the thesis committee

Name, Institute: Prof. Hannelore Ehrenreich, MPI Experimentelle Medizin

Third member of the thesis committee

Name, Institute: Prof. Uwe-Karsten Hanisch, Institut für Neuropathologie

Date of Disputation:

## **Affidavit**

Here I declare that my doctoral thesis entitled “Pathological Alterations Induced by Intraneuronal A $\beta$  in Alzheimer’s Disease” has been written independently with no other sources and aids than quoted.

Ditte Zerlang Christensen,

Göttingen, August 2009

## List of Publications

### Publications

**Christensen DZ**, Bayer TA, and Wirths O. Intracellular A $\beta$  triggers neuron loss in the cholinergic system of the APP/PS1KI mouse model of Alzheimer's disease. *Neurobiology of Aging*, in press. (EPUB Sep 3<sup>rd</sup> 2008, DOI: 10.1016/j.neurobiolaging.2008.07.022)

**Christensen DZ**, Kraus SL, Flohr A, Cotel MC, Wirths O, Bayer TA. Transient intraneuronal A $\beta$  rather than extracellular plaque pathology correlates with neuron loss in the frontal cortex of APP/PS1KI mice. *Acta Neuropathol* 116(6):647-55 (2008)

Thomsen MS, **Christensen DZ**, Hansen HH, Redrobe JP, Mikkelsen JD. Alpha 7 Nicotinic acetylcholine receptor activation prevents behavioral and molecular changes induced by repeated phencyclidine treatment. *Neuropharmacology* 56(6-7):1001-9 (2009)

### Abstracts from presentations

**Christensen DZ**, Bayer T, Wirths O. A $\beta$ -induced Pathology and Neuron Loss in the Cholinergic System of the APP/PSKI Mouse Model of Alzheimer's Disease. *Biochemical Pharmacology* 74(8): SMA-27 (2007)

**Christensen DZ**, Bayer TA, Wirths O. Intracellular A $\beta$  triggers neuron loss in the cholinergic system of the APP/PS1KI mouse model of Alzheimer's disease. *Alzheimer's & Dementia* 4(4) Suppl.2: T213 (2008)

Wirths O, **Christensen DZ**, Breyhan H, Duan K, Rettig J, Bayer TA. Intraneuronal A $\beta$  triggers loss of hippocampal and cholinergic neurons in the APP/PS1KI mouse model of Alzheimer's disease. *6th FENS Forum, Geneva (Switzerland), July 12-16 (2008)*

**Christensen DZ**, Bayer TA, Wirths O. Intracellular A $\beta$  correlates with neuron loss in Alzheimer's disease. *Neurodegenerative Diseases* 6, Suppl. 1:504 (2009)

**Christensen DZ**, Kraus SL, Flohr JCA, Cotel MC, Wirths O, Bayer TA. Intracellular A $\beta$  correlates with neuron loss in Alzheimer's disease. *Neuroforum* 1, Suppl.: T11-6A (2009)

Wirths O, **Christensen DZ**, Bayer TA. Increasing A $\beta$  peptide levels aggravate axonal degeneration in an Alzheimer mouse model. *Journal of Neurochemistry* 110, Suppl.1: 1-106 (2009)

# Table of Contents

<b>ACKNOWLEDGEMENTS</b> .....	<b>1</b>
<b>ABSTRACT</b> .....	<b>2</b>
<b>LIST OF FIGURES</b> .....	<b>3</b>
<b>LIST OF TABLES</b> .....	<b>4</b>
<b>ABBREVIATIONS</b> .....	<b>5</b>
<b>1 INTRODUCTION</b> .....	<b>6</b>
<b>1.1 Alzheimer's disease</b> .....	<b>6</b>
1.1.1 Clinical features .....	6
1.1.2 Neuropathology .....	8
1.1.3 Risk factors .....	11
<b>1.2 APP processing</b> .....	<b>13</b>
1.2.1 APP physiological functions .....	15
1.2.2 A $\beta$ toxicity .....	16
<b>1.3 Mouse models of Alzheimer's disease</b> .....	<b>19</b>
1.3.1 Generation of mouse models .....	19
1.3.2 FAD mutations in mouse models of AD .....	22
1.3.3 The APP/PS1KI mouse model .....	23
<b>1.4 The amyloid hypothesis</b> .....	<b>25</b>
1.4.1 The intraneuronal amyloid hypothesis .....	26
<b>1.5 Transmitter deficits in Alzheimer's disease</b> .....	<b>28</b>
<b>1.6 Introduction to experiments</b> .....	<b>32</b>
1.6.1 Neuron loss in the cholinergic system of APP/PS1KI mice .....	33
1.6.2 Effect of intraneuronal A $\beta$ versus plaques on neurodegeneration .....	33
1.6.3 Intraneuronal A $\beta$ staining in AD patients and transgenic AD mouse models .....	34
1.6.4 Effect of A $\beta$ on axonopathy in transgenic AD mouse models .....	35
1.6.5 Interaction between $\alpha$ 7 nAChR and A $\beta$ .....	37
1.6.6 Functional integrity of immediate early gene responses following novelty stimulation .....	38
<b>2 METHODS AND MATERIALS</b> .....	<b>40</b>
<b>2.1 Transgenic mice</b> .....	<b>40</b>
2.1.1 Genotyping .....	41
<b>2.2 Novelty exposure</b> .....	<b>43</b>
<b>2.3 Tissue collection and preservation</b> .....	<b>44</b>
<b>2.4 Histological staining</b> .....	<b>45</b>
2.4.1 Free-floating immunohistochemistry .....	47
2.4.2 Immunohistochemistry of paraffin embedded sections .....	48
2.4.3 Thioflavin-S staining .....	49

2.4.4	Cresyl violet histochemistry .....	49
2.5	Microscopy and photography .....	50
2.6	Quantification of plaque independent dystrophic neurites .....	50
2.7	Quantification of A $\beta$ staining .....	51
2.8	Stereology.....	51
2.9	qRT-PCR.....	53
2.10	Western blot.....	55
2.11	Radioactive ligand binding.....	56
2.12	In situ hybridization.....	57
2.13	AD brain tissue .....	58
2.14	Statistical analysis .....	59
3	RESULTS .....	60
3.1	Neuron loss in the cholinergic system of APP/PS1KI mice .....	60
3.2	Effect of intraneuronal A $\beta$ versus plaques on neurodegeneration.....	66
3.3	Intraneuronal A $\beta$ staining in AD patients and transgenic AD mouse models .....	71
3.4	Effect of A $\beta$ on axonopathy in transgenic AD mouse models.....	82
3.5	Interaction between $\alpha$ 7 nAChR and A $\beta$ .....	88
3.6	Functional integrity of immediate early gene responses following novelty stimulation.....	90
4	DISCUSSION .....	94
4.1	Neuron loss in the cholinergic system of APP/PS1KI mice .....	94
4.2	Effect of intraneuronal A $\beta$ versus plaques on neurodegeneration.....	96
4.3	Intraneuronal A $\beta$ staining in AD patients and transgenic AD mouse models .....	99
4.4	Effect of A $\beta$ on axonopathy in transgenic AD mouse models.....	105
4.5	Interaction between $\alpha$ 7 nAChR and A $\beta$ .....	107
4.6	Functional integrity of immediate early gene responses following novelty stimulation.....	109
5	SUMMARY AND CONCLUSIONS.....	113
6	REFERENCES.....	115
7	CURRICULUM VITAE.....	137

## Acknowledgements

I thank my primary supervisor Dr. Oliver Wirths for his excellent guidance with everything concerning the thesis from practical experimental work to scientific discussions. Especially, many thanks are given for his great patience and always present helpfulness, which have been an invaluable support throughout the work of my thesis.

Prof. Thomas A. Bayer I thank for his enthusiasm and strong will to educate us and allowing us to travel far and actively participate in an international scientific environment. In addition, many thanks are given for the many interacting scientific discussions and teaching us the necessity of criticism towards the scientific literature.

Five months of my PhD was spent at Neurosearch A/S in Ballerup, Denmark for which I owe many thanks to Jens D. Mikkelsen for great cooperation, inspiration, excellent advices, and giving me the opportunity to work in the industrial scientific environment at Neurosearch A/S. Special thanks are also given to all the people of the Department of Molecular Anatomy at Neurosearch for welcoming me in the laboratory and making my stay at Neurosearch a pleasant experience.

For instructing me at the confocal microscope, I thank Miso Mitkovski from the department of Experimental Medicine at the Max Planck Institute for his valuable time.

From the Department of Molecular Psychiatry in Göttingen, I thank Uta Engelhardt and Petra Tucholla for helping hands when time was short and their always pleasant company in the laboratory. Also, a great many thanks are given to all the students of the department through the years for pleasant company and an entertaining working atmosphere. Special thanks are given to Marie-Caroline Cotel for endless conversations on science as well as life, the many cups of tea, and all the sweets that I would probably have been better without.

To the European commission I owe many thanks for donating the money for the NEURAD PhD School, which has funded my entire PhD and made it possible to travel around the world participating in international scientific life. Also, I thank all the researchers of the NEURAD consortium for their enthusiastic spirits creating a welcoming scientific atmosphere at our NEURAD meetings.

Finally, I thank my family for their never failing support in my decision to travel abroad and participate in the European scientific community of the NEURAD PhD School. Special thanks are given to Nikolaj for his understanding and willingness to travel.

## Abstract

Alzheimer's disease (AD) is pathologically characterized by the deposition of amyloid beta ( $A\beta$ ) and neurofibrillary tangles (NFT) consisting of hyperphosphorylated tau protein. Since familial mutations in proteins involved in the  $A\beta$  generating cascade inevitably lead to AD, the deposition of  $A\beta$  is widely believed to be the underlying pathological mechanism of AD. In contrast, mutations in tau lead to frontotemporal dementia. The amyloid hypothesis states that the accumulation of  $A\beta_{42}$  is the underlying cause of AD driving neuron and synapse impairment and loss, eventually leading to behavioral deficits. For many years, the focus of the  $A\beta$  hypothesis has been the extracellular deposition of  $A\beta$  plaques; however numerous mouse models have been generated based on the familial AD mutations successfully modeling the deposition of  $A\beta$  plaques, but with little or no behavioral deficits and only seldom showing a loss of neurons. Furthermore,  $A\beta$  plaque deposition does not correlate well with cognitive decline in AD patients and can be found in non-demented controls as well as in AD patients. Recently, a modification of the amyloid hypothesis has been introduced suggesting that intraneuronal accumulation of  $A\beta$  rather than extracellular  $A\beta$  plaque deposition may be an early pathological hallmark of AD initiating pathological events. However, the presence of intraneuronal  $A\beta$  in the human AD brain is currently under debate. The present thesis investigates the presence of intraneuronal  $A\beta$  in human AD brain tissue and studies the role of intraneuronal  $A\beta$  versus plaques in transgenic mouse models of AD focusing on neuron loss, fiber pathology, and functional deficits concerning immediate early gene (IEG) regulation. Concerning pathological alterations, the present thesis corroborates the intraneuronal  $A\beta$  hypothesis, supporting the view of intraneuronal  $A\beta$  as an early pathological initiator and showing strong implications for intraneuronal  $A\beta$  in the generation of large plaque-independent axonal fiber pathology and neuronal loss. In contrast, plaques are found likely to cause functional disturbances such as deficits in the induction of IEGs upon neuronal activity, but seem not to be involved in the loss of neurons. Optimization of the immunohistochemical staining method for the detection of intraneuronal  $A\beta$  peptides provided a strong and robust staining of intraneuronal N-terminal  $A\beta$  peptides as well as fibrillar oligomeric  $A\beta$  and  $A\beta$  fibrils in neurons of the hippocampal formation of AD brain tissue. Finally, a highly significant correlation was identified between the accumulation of intraneuronal N-terminal  $A\beta$  peptides and the well-recognized AD risk factor of having one ApoE4 allele, emphasizing an important role of intraneuronal  $A\beta$  in AD pathology.



## List of Figures

<b>Fig. 1</b> Progression of amnesic mild cognitive impairment to AD .....	7
<b>Fig. 2</b> A $\beta$ pathologies visualised by A $\beta$ immunohistochemistry .....	8
<b>Fig. 3</b> Confocal image of neurofibrillary tangle (NFT) .....	9
<b>Fig. 4</b> Brain atrophy in AD .....	10
<b>Fig. 5</b> APP-positive dystrophic neurites surrounding neuritic plaque .....	11
<b>Fig. 6</b> Aging is a major risk factor of AD .....	11
<b>Fig. 7</b> Proteolytic processing of APP .....	13
<b>Fig. 8</b> Sorting of APP and BACE1 .....	14
<b>Fig. 9</b> The structure of $\gamma$ -secretase .....	15
<b>Fig. 10</b> A $\beta$ fibrillogenesis .....	17
<b>Fig. 11</b> Generation of transgenic mice by pronuclear microinjection .....	20
<b>Fig. 12</b> Specific modification of target gene by homologous recombination in ES cells .....	21
<b>Fig. 13</b> Pathogenic mutations in APP .....	22
<b>Fig. 14</b> Data from APP/PS1KI mice .....	24
<b>Fig. 15</b> The intraneuronal A $\beta$ hypothesis of AD .....	26
<b>Fig. 16</b> Overview of Ch1-6 nomenclature and projections .....	28
<b>Fig. 17</b> The avidin-biotin complex (ABC) method .....	45
<b>Fig. 18</b> The optical dissector method .....	51
<b>Fig. 19</b> Identification of homozygous YFP animals by RT q-PCR .....	55
<b>Fig. 20</b> Cholinergic fiber pathology in APP/PS1KI mice .....	60
<b>Fig. 21</b> Expression of APP transgene and A $\beta$ 1-x deposition in the cholinergic system of APP/PS1KI mice .....	61
<b>Fig. 22</b> Definition of counting areas .....	62
<b>Fig. 23</b> Stereological quantification of ChAT-positive neurons in APP/PS1KI mice .....	63
<b>Fig. 24</b> Intracellular A $\beta$ accumulation in the cholinergic motor neurons of Mo5 and 7N in APP/PS1KI mice .....	64
<b>Fig. 25</b> Fibrillar oligomeric A $\beta$ and Thioflavin S positive material in motor neurons of the Mo5 and 7N .....	65
<b>Fig. 26</b> A $\beta$ peptides in frontal cortex and thalamus of APP/PS1KI mice .....	66
<b>Fig. 27</b> Confirmation of intracellular A $\beta$ accumulation in APP/PS1KI mice by A $\beta$ [N] antibody .....	67
<b>Fig. 28</b> APP transgene expression and further confirmation of intracellular A $\beta$ in APP/PS1KI mice .....	68
<b>Fig. 29</b> Quantification of A $\beta$ accumulation in frontal cortex and thalamus .....	69
<b>Fig. 30</b> Schematic presentation of counting areas and stereological quantification of neuron numbers .....	70
<b>Fig. 31</b> Quantitative optimization of intracellular A $\beta$ <sub>1-x</sub> staining in APP/PS1KI mice .....	71
<b>Fig. 32</b> Optimization of intraneuronal A $\beta$ [N] staining in APP, APP/PS1KI, APP/PS1, and 5xFAD mice .....	72
<b>Fig. 33</b> Optimization of intraneuronal 4G8 staining in APP, APP/PS1KI, APP/PS1, and 5xFAD mice .....	74
<b>Fig. 34</b> Fluorescent double labeling of 4G8 and APP in APP/PS1KI mice .....	75
<b>Fig. 35</b> Optimization for intraneuronal A $\beta$ [N] staining in the CA4 region of AD brain tissue .....	76
<b>Fig. 36</b> Double labeling of A $\beta$ <sub>1-x</sub> and astrocytes .....	77
<b>Fig. 37</b> Intraneuronal staining detected by OC and 4G8 antibodies in sporadic AD brain tissue .....	78
<b>Fig. 38</b> Analysis of 4G8 and A $\beta$ [N] cross reactivity with lipofuscin in CA4 of an AD case .....	78
<b>Fig. 39</b> Rating of intraneuronal A $\beta$ [N] staining intensity .....	79
<b>Fig. 40</b> Analysis of APP transgene expression in APP, APP/PS1KI <sup>he</sup> , and APP/PS1KI <sup>ho</sup> mice .....	82
<b>Fig. 41</b> Immunostaining of A $\beta$ in APP, APP/PS1KI <sup>he</sup> , and APP/PS1KI <sup>ho</sup> mice .....	83
<b>Fig. 42</b> Intraneuronal A $\beta$ accumulation in APP, APP/PS1KI <sup>he</sup> , and APP/PS1KI <sup>ho</sup> mice .....	83
<b>Fig. 43</b> Dystrophic fibers together with A $\beta$ pathology in APP, APP/PS1KI <sup>he</sup> , and APP/PS1KI <sup>ho</sup> mice .....	84

<b>Fig. 44</b> Quantification of plaque-independent dystrophic fibers in APP, APP/PS1K1 <sup>hc</sup> , and APP/PS1K1 <sup>ho</sup> mice.....	85
<b>Fig. 45</b> Ubiquitin in APP, APP/PS1K1 <sup>hc</sup> , and APP/PS1K1 <sup>ho</sup> mice.....	85
<b>Fig. 46</b> A $\beta$ deposits in the vicinity of large dystrophic neurites .....	86
<b>Fig. 47</b> Confocal images of fibrillar A $\beta$ oligomers and A $\beta$ fibrils inside dystrophic fibers .....	86
<b>Fig. 48</b> Confocal images of intraneuronal A $\beta$ accumulation in cortical neurons.....	87
<b>Fig. 49</b> A $\beta$ staining in saline, SSR180711, and nicotine treated APP/PS1 $\Delta$ E9 mice .....	88
<b>Fig. 50</b> $\alpha$ -BTX radioactive ligand binding in wild-type and APP/PS1 $\Delta$ E9 mice .....	89
<b>Fig. 51</b> Quantified areas of the in situ hybridization analysis.....	90
<b>Fig. 52</b> <i>Arc</i> in situ hybridization in wild-type and APP/PS1 $\Delta$ E9 novelty stimulated and control mice .....	90
<b>Fig. 53</b> Quantification of <i>Arc</i> , <i>c-fos</i> and <i>synaptophysin</i> expression.....	92
<b>Fig. 54</b> Plasma corticosterone in wild-type and APP/PS1 $\Delta$ E9 novelty stimulated and control mice.....	93
<b>Fig. 55</b> Summary of A $\beta$ -mediated cell death in the cholinergic system .....	96

## List of Tables

<b>Table 1</b> Mutations in mouse models specified according to APP isoform, promoter, and amino acid exchange.....	41
<b>Table 2</b> Summary of tissue preservation, storage, and applied analyses.....	45
<b>Table 3</b> Details of primary antibodies applied for immunohistochemistry .....	46
<b>Table 4</b> Details of polyclonal secondary antibodies applied for immunohistochemistry.....	46
<b>Table 5</b> Definition of stereological parameters. ....	52
<b>Table 6</b> Sampling scheme for stereological analysis of the cholinergic system.....	52
<b>Table 7</b> Sampling scheme for stereological analysis of neurons in the frontal cortex and thalamus. ....	53
<b>Table 8</b> Patient data.....	80
<b>Table 9</b> Statistical analysis of intraneuronal A $\beta$ .....	81

## Abbreviations

Below is listed the most important abbreviations used in the present thesis.

$\alpha 7$ nAChR	alpha 7 nicotinic acetylcholine receptor
$\alpha$ -BTX	$\alpha$ -bungarotoxin
A $\beta$	amyloid beta
A $\beta$ 40/42	amyloid beta ending at amino acid 40/42
A $\beta$ N <sub>3pE</sub>	amyloid beta starting with a pyroglutamate modification at position 3
ADAM	a disintegrin- and metalloproteinase enzyme
APP	beta amyloid precursor protein
ACh	acetylcholine
AChE	acetylcholine esterase
AD	Alzheimer's disease
ADDLs	beta-amyloid derived diffusible ligands
ANOVA	analysis of variance
ApoE	apolipoprotein E
BACE	beta-site amyloid precursor protein cleaving enzyme
CAA	cerebral amyloid angiopathy
ChAT	choline acetyltransferase
DAB	3,3-diaminobenzidine
DAPI	4'6-diamidino-2'-phenylindole dihydrochloride
DG	dentate gyrus
ES cells	embryonic stem cells
FA	formic acid
FAD	familial alzheimer's disease
FCS	fetal calf serum
GSK3 $\beta$	glycogen synthase 3 $\beta$
HPA	hypothalamic-pituitary-adrenal
HRP	horseradish peroxidase
KI	knock in
KO	knock out
MAPT	microtubules-associated protein tau
MCI	mild cognitive impairment
NFTs	neurofibrillary tangles
NGF	nerve growth factor
NMDA	N-Methyl-D-Aspartat
PBS	phosphate buffered saline
PCR	polymerase chain reaction
PHFs	paired helical filaments
PS1/2	presenilin 1/2
PSD-95	postsynaptic density 95 protein
rpm	rounds per minute
TGN	trans-Golgi network
qRT-PCR	quantitative real time polymerase chain reaction
SDAT	senile dementia of the Alzheimer type
SDS	sodium dodecyl sulphate
YFP	yellow fluorescent protein

# 1 Introduction

## 1.1 *Alzheimer's disease*

Alzheimer's disease (AD) is a severely disabling neurodegenerative disorder characterized by progressive cognitive decline and accounts for 50-70% of all cases of dementia, thereby representing the main cause of dementia among the elderly population. Alzheimer's association reports that AD was the fifth-leading cause of death for those aged 65 and older in 2006 in US, only surpassed by heart disease, breast cancer, prostate cancer, and stroke (Alzheimer's Association Report 2009). However, AD was the only one of these indications actually showing an increasing rate of deaths from 2000 to 2006 of as much as 47%, which emphasizes a continuing lack of effective treatments of AD. Patients often live about 10 years after appearance of the first symptoms and end up completely dependent on care givers. Thus WHO predicted the direct costs of AD in US alone to be about US\$ 500 billion in year 2000 making AD a major socioeconomic problem that will expand in near future (Vas et al. 2002).

### 1.1.1 Clinical features

The final diagnosis of AD is based on neuropathological hallmarks and can therefore only be given for certain after autopsy. In the clinic, the diagnosis is described as senile dementia of the Alzheimer type (SDAT) until confirmed by neuropathology. Unlike dementia, AD does not only affect memory function, but also other cognitive functions such as language, planning ability, attention, and orientation in time and space. Many patients start to forget recent events and appointments and progress to forgetting year and location. As the disease progresses, patients may have difficulties finding words and suffer from impairments in abstract thinking and judgment such as related to the concept of money. Problems start to arise with familiar tasks as buttoning a shirt or placing things at their right location. Mood changes can also appear with the patient showing anger for no apparent reason and with changes in personality showing paranoia, jealousy, and confusion. Eventually, patients often end up without initiative and completely passive without any language having reached the so called "bed-state" (Alzheimer's Association Brochure 2005). To give the clinical diagnosis of SDAT, an individual is assessed by for example the Mini-Mental State Examination (MMSE),

which is a practical method for grading the cognitive state of patients (Folstein et al. 1975). Still, the symptoms vary with each patient often complicating the assignment of a diagnosis, but appearance of any of the early symptoms may be a sign of AD. Clinicians assign the term “mild cognitive impairment” (MCI) to patients where problems with memory, language, or other cognitive functions are severe enough to be noticed by others and show up on cognitive tests, but are not severe enough to interfere with daily life (Alzheimer's Association Report 2009). It is estimated that as many as 10-20% of people age 65 and older have MCI (Alzheimer's Association Report 2009; Levey et al. 2006), but not all of these develop AD. The definition of MCI is broad and encompasses several subtypes. Amnesic MCI is characterized by memory deficits. Multiple-domain MCI is characterized by impairments in several cognitive functions such as language, executive functions, and visuospatial skills, but may also include memory deficits. A third subtype of MCI involves patients with impairment in a single cognitive domain that does not involve memory. Multiple-domain MCI without memory impairment can progress to dementia with Lewy bodies as can MCI affecting a single non-memory domain, which in addition can progress to frontotemporal dementia. Only MCI patients with memory impairment are likely to progress into AD. Although they may also suffer from depression, patients with amnesic MCI are very likely to develop AD with an incidence of 10-15% per year compared to 1-2% in healthy controls (Levey et al. 2006). All three types of MCI can also show complete remission; however, in a longitudinal study from the Mayo clinic, 80% of 76 patients with amnesic MCI had converted to AD after 6 years, translating into the annual incidence of 15% (Fig. 1) (Levey et al. 2006; Petersen et al. 2001; Petersen et al. 1999).

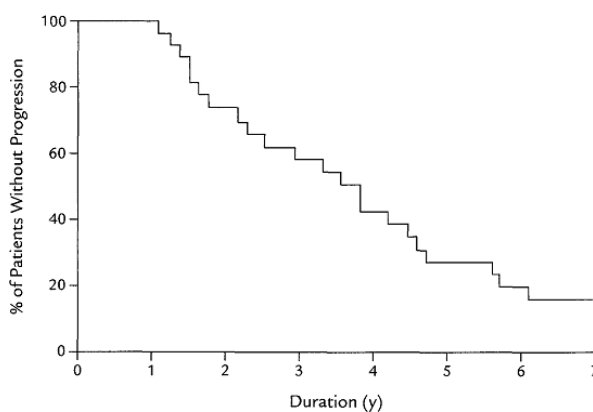


**Fig. 1 Progression of amnesic mild cognitive impairment to AD.** After 6 years, one study showed a rate of 80% conversion to Alzheimer's disease for individuals with amnesic mild cognitive impairment (Petersen et al. 2001; Petersen et al. 1999).

### 1.1.2 Neuropathology

Already in 1906, two major neuropathological lesions of AD were identified by the German psychiatrist Alois Alzheimer in his investigations of the most famous AD patient, Auguste D, a woman in her early 50s that suffered from progressive senile dementia (Hardy 2006). At that time, life expectancy was low compared to today, and what Alois Alzheimer thought to have identified as a rare dementia occurring in the “presenile” period of life, was only much later recognized to be the most common cause of dementia with an incidence rising exponentially with age. Using the limited microscopic technology of the time, Alois Alzheimer identified extracellular senile plaques and intracellular neurofibrillary tangles (NFTs) as the two major neuropathological lesions of AD, which are still thought to underlie AD pathogenesis and to date defines the final diagnosis of AD that can only be given after neuropathological examination following autopsy (Selkoe 2001).

Much later, the extracellular plaques were found to consist of amyloid beta ( $A\beta$ ) peptides, and two types of plaques were identified (Dickson 1997; Masters et al. 1985; Selkoe 1989). Neuritic plaques, or cored plaques (Fig. 2A), are microscopic foci of extracellular filamentous  $A\beta$  deposits surrounded by dystrophic neurites, which are swollen axons and

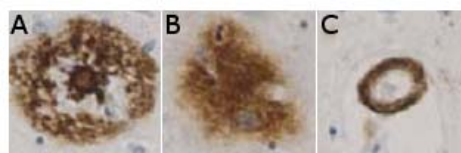


**Fig. 2  $A\beta$  pathologies visualised by  $A\beta$  immunohistochemistry.** A) Cored or neuritic plaque. B) Diffuse amorphous plaque. C) cerebral amyloid angiopathy (CAA) (Alafuzoff et al. 2008).

dendrites that accumulate amongst others enlarged lysosomes and numerous mitochondria. The neuritic plaques are surrounded by microglia and Optimization for intraneuronal  $A\beta_{1-x}$  staining in reactive astrocytes and are found in large numbers throughout limbic and association cortices. In contrast, diffuse amorphous plaques are not surrounded by dystrophic fibers or glial changes (Fig. 2B). They are thought to consist of less aggregated  $A\beta$  and might represent a stage of precursor lesions for neuritic plaques. Another form of  $A\beta$  deposition often observed in AD brains is cerebral amyloid angiopathy (CAA), where  $A\beta$  is found to accumulate inside the walls of blood vessels (Fig. 2C) (Alafuzoff et al. 2008; Selkoe 1989).

The NFTs are large non-membrane bound bundles of fibers occupying much of the perinuclear cytoplasm and consist of paired helical filaments (PHFs) wound into larger helices (Fig. 3). During the 1980's, the PHFs were found to be composed of microtubule-associated protein tau (MAPT) commonly referred to as “tau”, which is a protein normally

associated with microtubules supporting their assembly (Selkoe 1989). The tau protein in PHFs is hyperphosphorylated, which is thought to be an initiating factor promoting the tau protein to dissociate from the microtubules and aggregate into PHFs forming the NFTs. Many kinases have been found capable of phosphorylating tau at various sites, amongst others the glycogen synthase kinase 3 (GSK3), mitogen-activated protein kinase (MAPK), cyclic AMP-dependent protein kinase (PKA), and, more recently, cyclin-dependent kinase 5 (cdk5). Nevertheless, the identities of the true physiological and pathological kinases *in vivo* remain unknown (Hanger et al. 2009). Many *in vitro* studies show neurotoxicity of hyperphosphorylated tau protein, however, the *in vivo* consequences of the hyperphosphorylation are still a matter of debate. One study of European ground squirrels in torpor during hibernation described the formation of highly phosphorylated tau in large amounts especially in the entorhinal cortex, hippocampus, and isocortical areas. The PHF-like phosphorylation of tau did not lead to fibril formation and was fully reversible after arousal, indicating that hyperphosphorylation itself is not the irreversible step in a fatal cascade (Arendt et al. 2003). Still, tau pathology has been found to correlate better with cognitive decline than A $\beta$  plaques and the extent of tau pathology in AD brains is therefore used to stage the severity of the disease into six stages, Braak I-VI (Braak et al. 2006; Braak and Braak 1991).

Another pathological determinant of AD is brain atrophy and loss of neurons, which occurs predominantly in the cortex, hippocampal formation, and nucleus Basalis of Meynert. The loss of cholinergic neurons of the nucleus basalis of Meynert provided the first evidence of neuron loss, where as much as 90% neuron loss can be observed (Davies and Maloney 1976; Whitehouse et al. 1982). In comparison, neuron losses of approximately 50% have been established in the superior temporal cortex as well as in the enthorinal cortex proximate to the hippocampal formation (Gomez-Isla et al. 1997; Gomez-Isla et al. 1996). Concerning the hippocampal formation, there are some disagreements concerning the specific loss of neurons in subregions, but one study reported neuron losses of 23% in the subiculum and granule cell layer of the dentate gyrus (DG) (Simic et al. 1997), and another reported as much as 68% in the CA1, 47% in the subiculum and 25% in the hilus also named the CA4 region of the hippocampal formation (West et al. 1994). Accordingly, only the CA2-3 region of the

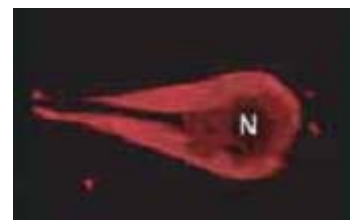


**Fig. 3 Confocal image of neurofibrillary tangle (NFT).** Aggregated hyperphosphorylated tau protein stained by immunohistochemistry (red) accumulates in the cytoplasm and surrounds the nucleus (N) (Luna-Munoz et al. 2005).

hippocampal formation seems to be somewhat resistant to neuronal loss in AD. The brain atrophy is evident by macroscopic examination and is characterized by enlargement of the ventricles and loss of volume especially in the hippocampal region concerned with memory processing and in cortical regions concerned with amongst others language skills, correlating well with the deficits in cognitive functions observed in AD patients (Fig. 4). Thus a total volume loss of about 30% has been found in the hippocampal formation using *in vitro*

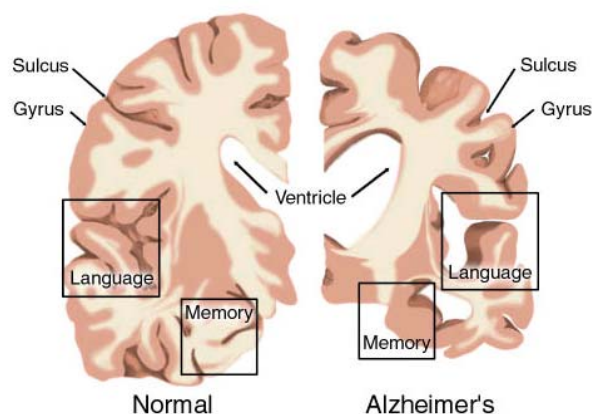


**Fig. 4 Brain atrophy in AD.** Coronal brain sections of normal control subject (left) and a patient with Alzheimer's disease (right) showing enlargement of ventricles and evident tissue loss especially in the hippocampal region concerned with memory and in the cortex amongst others dealing with language function ([www.ahaf.org/alzdis/about/BrainAlzheimer.htm](http://www.ahaf.org/alzdis/about/BrainAlzheimer.htm)).

microscopy (Huesgen et al. 1993; Simic et al. 1997), which is in line with *in-vivo* magnetic resonance imaging (MRI) studies showing hippocampal and entorhinal cortical atrophy of 40-50% (Erkinjuntti et al. 1993; Kesslak et al. 1991). Recently, significant atrophy of the olfactory bulb has been reported that probably accounts for the decrease in olfactory function also observed in AD patients (Thomann et al. 2009).

Also synapses are lost in AD and is believed to be an early pathological alteration in the brain, especially in the frontal cortex where a loss of 30-40% of the synapses in layer III and V of AD biopsy tissue has been reported (Scheff et al. 1990; Tiraboschi et al. 2000). As synaptic plasticity is a key player in cognitive function, the loss of synapses could very well result in cognitive impairments. Accordingly, the loss of synapses seems to strongly correlate with the cognitive decline in AD patients (DeKosky and Scheff 1990; Dickson et al. 1995; Terry et al. 1991).

In addition, abnormalities and impairments in axonal transport have been reported in a variety of neurodegenerative diseases (Yagishita 1978) and are suggested to be an important pathological alteration underlying AD (Roy et al. 2005; Stokin and Goldstein 2006; Zhu et al. 2005). The axonal pathology in AD is evident by swollen dystrophic fibers in which various proteins accumulate including APP (Cras et al. 1991), synaptic proteins like alpha-synuclein (Wirhth et al. 2000), glycogen (Mann et al. 1987), or abnormal filaments (Praprotnik et al. 1996) (Fig. 5). With the implementation of new imaging techniques it has recently been



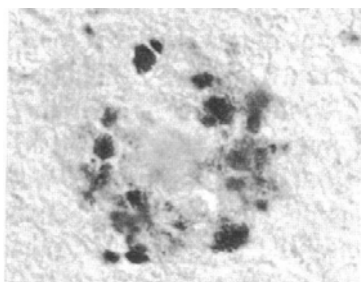


**Fig. 5 APP-positive dystrophic neurites surrounding neuritic plaque (Cras et al. 1991).**

shown in *in-vivo* studies that impairment of axonal transport mechanisms and decreased axonal transport rates early in the disease process might have a significant impact on the pathogenesis of AD (Cross et al. 2008; Minoshima and Cross 2008; Smith et al. 2007; Teipel et al. 2007).

### 1.1.3 Risk factors

The major risk factor of AD is aging, which is evident by the exponential increase in AD incidence with age. Thus, a study performed by the American National Institute on Aging estimated a fairly low incidence rate of 0.08% per year in the 60-65 year age group that was found to double each 4.4 years resulting in 6.48% new AD cases each year in the 85+ age group (Fig. 6A) (Kawas et al. 2000). In prevalence, this means that 1.4% of the population aged 60-65 suffers from AD, whereas this applies to 23.6% of people aged 85 or more (Fig. 6B). The world health organization (WHO) estimates that there are currently 18 million people worldwide suffering from AD and expects this number to have doubled by 2025 (Vas et al. 2002). Since aging is the major risk factor of AD, much of this dramatic

increase in the number of AD patients is expected to be caused by an ongoing demographic change with an increasing proportion of elderly people owing to higher living standards, medical improvements, and better care that altogether prolongs life expectancy.

Alzheimer's association reports a higher prevalence of AD in women compared to men in the US, but also concludes that this is caused by the longer life span of women, and not by

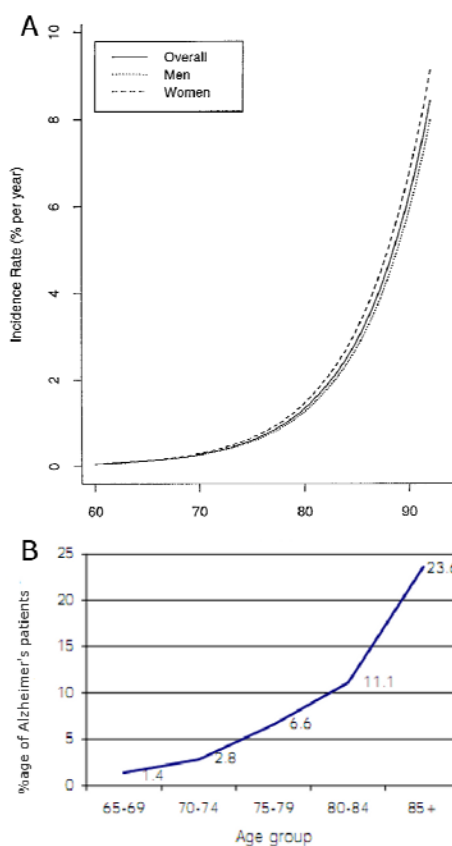


**Fig. 6 Aging is a major risk factor of AD.** AD incidence rate increases exponentially with age (A) (Kawas et al. 2000) causing a dramatic increase in AD prevalence in older age (B) (Vas et al. 2002).

women having a higher risk of developing AD. This is in line with reports of no differences in AD risk factor between men and woman as well as the observed incidence rate in men and woman rising equally exponentially with age (Fig. 6A) (Kawas et al. 2000; Sandberg et al. 2001).

Whereas the majority of all cases of AD occur sporadically, 2-5% are caused by familial inherited mutations most often resulting in an early onset of the disease before the age of 65 years that can be as early as around 30 years of age (Bentahir et al. 2006; Kumar-Singh et al. 2006). So far, all mutations resulting in familial AD (FAD) have been identified in only three genes encoding the beta amyloid precursor protein (APP), presenilin 1 (PS1) or presenilin 2 (PS2), which are all proteins involved in the cascade leading to A $\beta$  deposition (Janssen et al. 2003). Most of these mutations have been shown to elevate the levels of the A $\beta$  isoform ending at amino acid 42 (A $\beta$ 42), which is considered to be highly neurotoxic and tends to aggregate into amyloid fibrils more rapidly than the isoform ending at amino acid 40 (A $\beta$ 40) (Iwatsubo 1998). Mutations in the *MAPT* gene encoding the tau protein have also been identified; however, these cause frontotemporal dementia and not AD (Kumar-Singh and Van Broeckhoven 2007).

Whereas FAD can be caused by a single mutation, sporadic AD is generally believed to be a multifactorial disease and is therefore not expected to be caused by a single genetic mutation or variation. So far, the strongest genetic variation linked to AD is that of apolipoprotein E (ApoE) of which three different alleles can be found in the general population: 2, 3, and 4. The ApoE3 is the most common allelic form and is found in 77-78% of the general population. The ApoE2 is rather rare and is found in only 7-8% of the population. The ApoE4 constitutes the remaining 14-16%, however, in people with AD, the ApoE4 genotype is found in about 40% of the patients being much more common than in the general population. Thus the ApoE4 genotype is believed to be a major risk factor of AD, and individuals with one ApoE4 allele are considered 3-4 times as likely to develop AD as those without ApoE4 (Bu 2009; Corder et al. 1993; Schmechel et al. 1993; Strittmatter et al. 1993). Why ApoE4 predisposes to AD is yet unclear, however, ApoE4 has been shown to directly influence APP processing to A $\beta$ . More indirectly, apolipoproteins are the major carriers of cholesterol in the blood and delivers cholesterol to cells that incorporate it into cell membranes, where cholesterol is considered important for the function of lipid rafts that are considered to regulate the cleavage of APP to A $\beta$  (Riddell et al. 2001; Vetrivel et al. 2004).

## 1.2 APP processing

The major breakthrough in AD biochemistry happened in the mid 1980's when A $\beta$  was isolated and characterized as the core peptide of amyloid plaques (Glennner and Wong 1984; Masters et al. 1985), which was shortly followed by the identification of the gene encoding the peptide's parent protein, the APP (Kang et al. 1987; Tanzi et al. 1987). The APP gene was mapped to the Down's syndrome region of chromosome 21, which was especially intriguing since Down's syndrome is a chromosomal disorder where the patients have three copies of chromosome 21 and invariably develops AD at an early age (Kang et al. 1987; Wisniewski et al. 1978). The APP protein turned out to be a type 1 transmembrane glycoprotein (Tanzi et al. 1987) that is widely expressed in many cell types of the brain including neurons, glial cells, astrocytes, and endothelial cells as well as in many peripheral tissues (Beer et al. 1995; Schmechel et al. 1988). Anchored in the membrane, full-length APP undergoes post-translational proteolytic processing through at least two distinct pathways, differing in the proteases involved and the resulting production of protein fragments (Fig. 7A). In the non-amyloidogenic pathway, cleavage of APP by  $\alpha$ -secretase results in release of the large soluble ectodomain fragment  $\alpha$  (sAPP $\alpha$ ) from the membrane. The resulting membrane-associated 83-amino-acid long C-terminal fragment (C83) remains associated with the membrane and is in turn processed by the  $\gamma$ -secretase generating the so-called P3 peptide and the APP intracellular domain (AICD, also referred to as CTF $\gamma$ ). In this pathway, cleavage within the A $\beta$  sequence

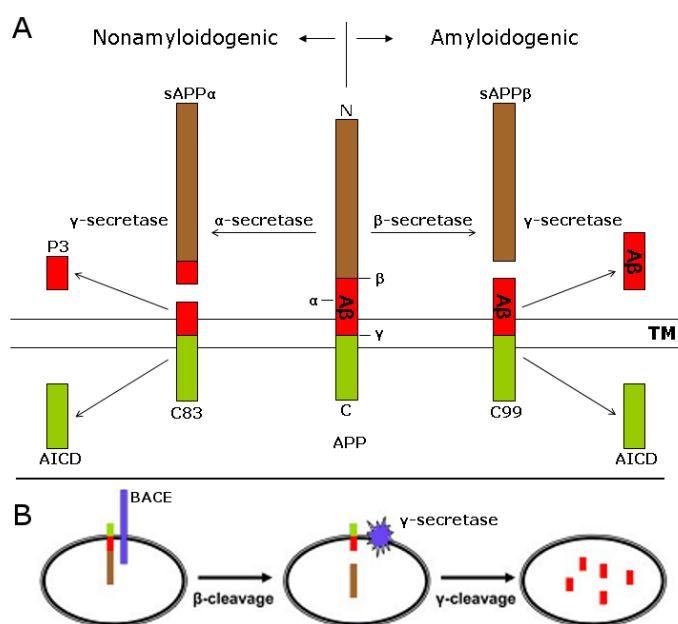


**Fig. 7 Proteolytic processing of APP.** A) In the nonamyloidogenic pathway (left) cleavage of APP by the  $\alpha$ -secretase results in the release of the large soluble ectodomain fragment  $\alpha$  (sAPP $\alpha$ ). The membrane-associated 83-amino-acid long C-terminal fragment (C83) is further processed by the  $\gamma$ -secretase within the transmembrane domain (TM) liberating the P3 peptide and the APP intracellular domain (AICD/CTF $\gamma$ ). Alternatively, APP can undergo the amyloidogenic pathway (right) in which APP is initially cleaved by the  $\beta$ -secretase releasing the soluble ectodomain fragment  $\beta$  (sAPP $\beta$ ). Subsequent processing of the C-terminal derivative (C99) by the  $\gamma$ -secretase generates the A $\beta$  peptide and the C-terminal AICD fragment (inspired by (Senechal et al. 2006)) B) The generation of A $\beta$  is believed to take place in the membranes of intracellular compartments, most likely the endosomes, accumulating A $\beta$  inside the vesicle structures (adapted from (Small and Gandy 2006)).

by the  $\alpha$ -secretase prevents the formation of A $\beta$  peptides. Alternatively, APP can be cleaved in the amyloidogenic pathway in which APP is initially cleaved by the  $\beta$ -secretase resulting in the formation of an N-terminal ectodomain fragment  $\beta$  (sAPP $\beta$ ) that is released from the membrane and a membrane-bound 99-amino-acid long C-terminal derivative (C99). Subsequent processing of C99 by the  $\gamma$ -secretase within the transmembrane domain releases the A $\beta$  peptide and the C-terminal AICD fragment from the membrane (Senechal et al. 2006).

The nature of the secretases as well as the intracellular localization of the cleavage process has been of great interest and many questions are not yet finally answered. Three enzymes have been identified having  $\alpha$ -secretase activity, ADAM9, ADAM10, and ADAM17, all belonging to the ADAM family (a disintegrin- and metalloproteinase-family enzyme) of integral membrane proteins (Allinson et al. 2003). They are thought to cleave the APP at the cell surface membrane releasing sAPP $\alpha$  into the extracellular space (Laferla et al. 2007). Several groups have identified the  $\beta$ -secretase to be the  $\beta$ -site APP-cleaving enzyme 1 (BACE 1), which is, like APP, a type 1 integral membrane protein (Hussain et al. 1999; Sinha et al. 1999; Vassar et al. 1999). Like most transmembrane proteins, APP and BACE1 are sorted via the secretory and endocytic pathways where the trans-Golgi network (TGN) and the endosomes function as coordinators of the complex movement of transmembrane proteins within the cell (Fig. 8A) (Small and Gandy 2006). The sorting through the different compartments is highly regulated and clathrin has been identified to mediate the movement from the TGN to endosomes and between the endosomes and the

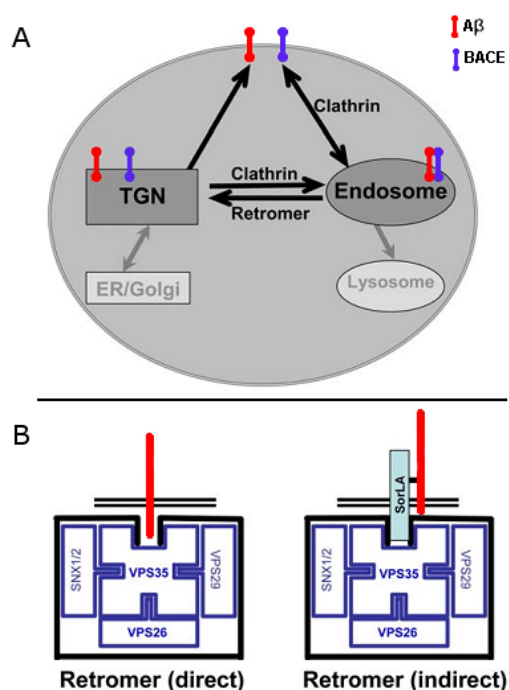


**Fig. 8 Sorting of APP and BACE1.** A) Both are sorted via the secretory and endocytic pathways where the trans-Golgi network (TGN) and the endosomes function as coordinating compartments. B) The retromer complex transports type-I transmembrane proteins from the endosome to the TGN. VPS35 is the core of the retromer and binds directly to the protein cargo (red bar). VPS26, VPS29, and sortin nexins (SNX) 1 or 2 assemble onto VPS35 to generate the complete functional retromer complex. The retromer sorts APP and BACE1, either by direct binding to the retromer or by indirect binding through the adaptor protein sorLA (light blue) (Small and Gandy 2006).

cell surface (Wahle et al. 2005). A novel coat complex, the retromer, has been found to be involved primarily in retrograde transport from the endosome to the TGN where an adaptor protein, sorLA, is thought to bind the retromer complex to cargo proteins such as APP and BACE1 and could provide interaction between the two proteins (Seaman 2004). Both APP and BACE1 can be found, at least transiently, in almost all membranous compartments of these pathways as well as on the cell surface, but biochemical studies suggest maximal BACE1 activity in an acidic environment, making the lysosomes a likely compartment for the initial cleavage. However, mature BACE1 is found predominantly in the endosomes with lower levels on the cell surface and in the TGN and not in lysosomes or in the endoplasmic reticulum (Small and Gandy 2006). A fluorescence resonance energy transfer (FRET) study analyzed the interaction between APP and BACE1 and confirmed that wild-type APP binds BACE1 with greatest efficiency in the endosomes, lesser on the cell surface, and to a negligible degree in the TGN and secretory pathway (Kinoshita et al. 2003). The  $\gamma$ -secretase has been identified as a multimeric complex of at least 4 enzymes being the PS1 or PS2, nicastrin, anterior pharynx defective enzyme 1 (APH-1), and presenilin enhancer 2 (PEN-2) (Fig. 9) (Gandy 2005). The multimeric nature of the  $\gamma$ -secretase has made the localization of its cleavage even more complicated than that of  $\beta$ -secretase. The best clue is that  $\gamma$ -secretase cleavage takes place in presynaptic terminals of neurons where the only existing organelles involved in the  $\gamma$ -cleavage are the endosomes (Kamenetz et al. 2003). Thus both  $\beta$ - and  $\gamma$ -cleavage is thought to take place in endosomes (Fig. 7B), but it remains unsolved whether  $\gamma$ -secretase cleavage also takes place in other compartments of the secretory and endocytic pathways.

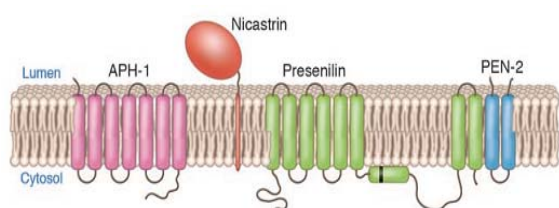


**Fig. 9 The structure of  $\gamma$ -secretase.**  $\gamma$ -secretase is a complex of 4 enzymes: presenilin (PS1 or PS2), nicastrin, anterior pharynx defective enzyme (APH-1), and presenilin enhancer 2 (PEN-2). The complex is a zymogen being inactive until the presenilin is cleaved at the black bar causing the complex to self associate and form the active enzyme (Gandy 2005).

### 1.2.1 APP physiological functions

The *APP* gene sequence shows extensive conservation throughout evolution suggesting an important physiological function of the APP protein (Coulson et al. 2000), which is alternatively spliced resulting in three major isoforms differing in length, functional domains,

and expression pattern in the brain (Sola et al. 1993; Tanaka et al. 1989). The APP695 consists of 695 amino acids and is the most abundant form in the brain expressed predominantly in neurons, whereas the APP751 and APP770 isoforms have one additional domain and are present mostly in glial cells and other non-neuronal tissues. Within neurons, the highest expression levels of APP are found in the hippocampal formation and cerebellum, where APP undergoes fast anterograde axonal transport, is expressed at neuronal synapses, and is found throughout vesicular structures of the cell bodies, axons, and dendrites (Koo et al. 1990; Sola et al. 1993). The physiological role of APP is not as extensively investigated as its pathological role and is thus not very well understood, however, some information are supplied from KO or knock-down studies of APP expression as well as mutations of the different domains. APP KO or deficient mice are in fact viable but show weight loss, reduced forelimb grip strength and decreased locomotor activity, suggesting impairment in muscular or motoneuronal function (Muller et al. 1994; Zheng et al. 1995). On the biochemical level, the APP protein has been found to contain many domains capable of interacting with a variety of proteins as well as metal ions. For example, the extracellular part of APP was shown to interact with ApoE and Notch receptors involved in development, during which APP expression actually increases in correlation with intense neurite outgrowth and synaptogenesis (Moya et al. 1994; Senechal et al. 2006). Thus APP is thought to play an important role in synaptic development, cell migration, early postnatal survival, and neurogenesis, and possibly has a role in maintenance and repair (Senechal et al. 2006). In the periphery, APP is highly expressed in Sertoli cells, follicle cells, secretory cells, podocytes, and macrophages found in the spleen, liver, kidney, testis, ovary, pancreas, and salivary glands (Beer et al. 1995). Common to these cells is their high membrane turnover and their functional characteristics mediating endocytosis and exocytosis supporting a peripheral role of APP in tissue maintenance and repair.

### **1.2.2 A $\beta$ toxicity**

A $\beta$  is a 4 kDa peptide that shows a high tendency to polymerize and aggregate. Thus A $\beta$  can self-associate to form oligomers ranging from dimers and trimers to larger oligomers of more than 100 kDa, although it mostly forms low-n oligomers (dimers to octamers). The oligomers are described as soluble as they are soluble in aqueous buffer and remain in solution following high speed centrifugation. Monomers are thought to be in equilibrium with the oligomers, but

when a certain threshold amount of monomers is reached, they initiate a nucleation-dependent polymerization process in which monomeric A $\beta$  forms nuclei that are polymerized into A $\beta$ -derived diffusible ligands (ADDLs), which assemble into larger protofibrils. The ADDLs and protofibrils are plastic structures that can again dissociate to monomers, but the protofibrils can also aggregate further into full-length fibers (Fig. 10). A $\beta$  fibers are insoluble and represent the major constituents of plaques, whereas the solubility of ADDLs and protofibrils following high speed centrifugation has not yet been addressed (Roychaudhuri et al. 2008; Walsh et al. 1997; Walsh and Selkoe 2007).

A $\beta$  peptides have been shown to have toxic properties in cell cultures (Kihara et al. 1997; Loo et al. 1993; Yankner et al. 1990), but so far, the mechanism whereby A $\beta$  induces cell death has not been clarified and there is an ongoing debate concerning which type of A $\beta$  peptides represents the most toxic species. Most people agree that A $\beta$ 42 peptides are more neurotoxic than A $\beta$ 40, probably owing to their increased tendency to aggregate (Small and McLean 1999). However, variations also exist at the N-terminal region where a considerable part of the A $\beta$  found in AD brains is N-terminally truncated beginning for example with phenylalanine at position 4, or with a pyroglutamate modification at position 3 (A $\beta$ N<sub>3pE</sub>) (Masters et al. 1985; Saido et al. 1995). The N-terminal truncated A $\beta$  peptides generally show

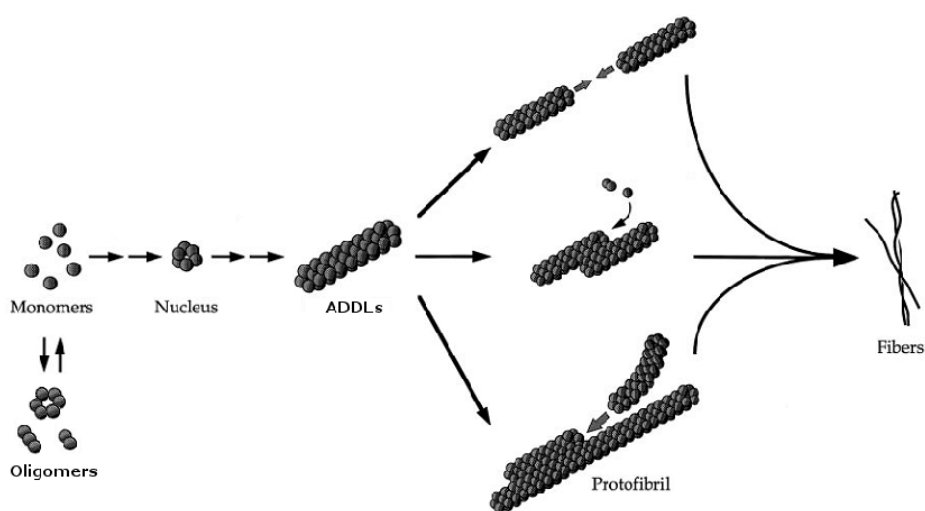


**Fig. 10 A $\beta$  fibrillogenesis.** Monomers are in equilibrium with oligomers that can be of low-n (2-12) or further associate to larger oligomers. Monomers initiate a nucleation-dependent polymerization process in which nuclei are the basis for generation of A $\beta$ -derived diffusible ligands (ADDLs) that further assemble into protofibrils. Protofibrils give rise to full-length fibers by simple end-to-end annealing, lateral association of protofibrils followed by addition of monomers or oligomers to ends, and lateral association followed by end-to-end annealing (adapted from (Walsh et al. 1997)).

enhanced tendency to aggregate in vitro (Pike et al. 1995), and especially A $\beta$ N<sub>3pE</sub> shows increased cellular toxicity compared to full-length A $\beta$  (Russo et al. 2002) and has been shown to mediate neuron death in a mouse model expressing specifically A $\beta$ N<sub>3pE</sub> (Wirhth et al. 2009). A $\beta$ N<sub>3pE</sub> also shows high stability (Kuo et al. 1998) and aggregation propensity (He and Barrow 1999), and is thought to have seeding properties inducing the aggregation of other A $\beta$  peptides (Schilling et al. 2006). Thus prevention of the aggregation of A $\beta$  peptides by inhibition of A $\beta$ N<sub>3pE</sub> generation is considered a potential target in AD (Schilling et al. 2008). Not only the A $\beta$  species, but also the confirmation of A $\beta$  peptides is currently under discussion. Early studies demonstrated that aggregation of A $\beta$  is essential for its toxicity (Yankner 1996), however, it has recently been suggested that soluble oligomeric A $\beta$  is more toxic than the aggregated fibers (Walsh et al. 2000), and one study even isolated a specific oligomeric A $\beta$  species, the A $\beta$ 56\*, claiming that this is solely responsible for the memory impairment caused by A $\beta$  in a mouse model of AD (Lesne et al. 2006). Thus there seems to be a lack of agreement within the field as to which primary species of A $\beta$  is actually mediating its toxic effects. Supporting the hypothesis of the toxic oligomers to be the most toxic is the lack of correlation between the accumulation of aggregated A $\beta$  in plaques and the deterioration in memory and cognitive functions of AD patients (Aizenstein et al. 2008; Dickson et al. 1995; Terry et al. 1991), whereas soluble A $\beta$  species have recently been reported to correlate much better with the cognitive decline in AD (McLean et al. 1999; Naslund et al. 2000).

Only very little is known about the physiological role of A $\beta$ , but the peptide has been reported to play a role in the regulation of neuronal excitation (Kamenetz et al. 2003), and a very recent finding identifies A $\beta$  as an antimicrobial peptide of the innate immune system (Moir et al. 2009). Others have found a link between APP processing and the metabolism of cholesterol and sphingomyelin, both part of cellular membranes. According to these studies, A $\beta$ 42 should reduce the level of sphingomyelin by activating the sphingomyelin degrading enzyme, whereas A $\beta$ 40 reduces cholesterol de novo synthesis by inhibiting its synthesizing enzyme. This regulation strictly depends on  $\gamma$ -secretase, and cholesterol and sphingomyelin should directly affect the  $\gamma$ -secretase activity providing a feedback mechanism where cholesterol induces the activity of the  $\gamma$ -secretase (Grimm et al. 2005). Corroborating these results, hypercholesterolemia has been suggested as an early risk factor in the development of



AD, and cholesterol-lowering drugs are being evaluated as a potential treatment for AD (Cutler et al. 2004; Simons et al. 2002; Sparks et al. 2005).

### **1.3 Mouse models of Alzheimer's disease**

The knowledge of identified FAD mutations can be used to generate model systems for studying the pathology and course of AD. The most widely used model organism is the mouse. The choice is a compromise between having a mammalian organism being in many ways similar to humans and practical considerations such as handling, generation time, and the extensive knowledge of the mouse genome obtained in 2002 by complete sequencing. Owing to the complicated techniques of introducing mutations, the mouse is in fact the only mammal in which targeted mutation is yet possible (Pluck and Klasen 2009). However, *drosophila* is also quite often applied because of its very easy handling, extremely fast generation time, low costs, and the ability to conduct fast screenings of drug candidates (Sang and Jackson 2005).

#### **1.3.1 Generation of mouse models**

Presently, two technically different approaches can be applied to generate a mouse model. Pronuclear injection of a vector containing a relevant DNA sequence into fertilized oocytes generates transgenic mice by introducing a foreign target gene, however, with random integration into the genome. Targeted mutagenesis using homologous recombination in embryonic stem (ES) cells can be used to specifically modify a target gene and is thus used to produce genetically modified mice where a gene is knocked in (KI) to obtain a gain of function or knocked out (KO) to obtain inactivation of gene expression.

Pronuclear injection is the most widely used technique to generate transgenic animals as it is a straightforward method to consistently integrate a transgene at a single site in the chromosome (Ittner and Gotz 2007). Female mice are superovulated, mated to fertile males and sacrificed the following day to recover fertilized oocytes from the oviducts. The DNA of interest is injected into the male pronucleus of the oocytes using a micro injection pipette, and surviving oocytes are reimplanted into the oviducts of a pseudopregnant foster female (Fig. 11). During this procedure, the microinjected DNA randomly integrates into the chromosomal DNA at nicks, usually at a single site, however, often containing multiple head-to-tail copies

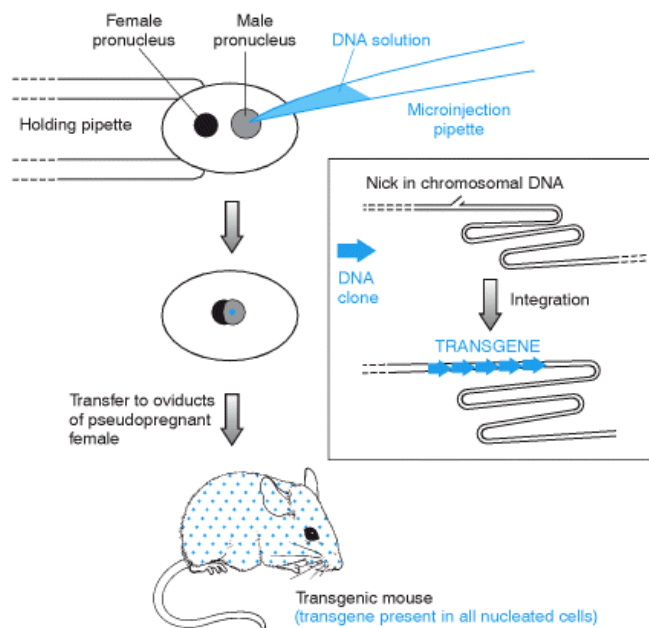


**Fig. 11 Generation of transgenic mice by pronuclear microinjection.** A micro injection pipette is used to inject the DNA into the male pronucleus of the oocyte. The introduced DNA clones integrate into the chromosomal DNA at nicks, forming transgenes, usually containing multiple head-to-tail copies. The oocytes are reimplanted into the oviducts of pseudopregnant foster females. Newborn mice resulting from development of the implanted embryos are checked by PCR for the presence of the desired DNA sequence (Strachan and Read 1999).

of the transgene. To target specific tissues and cell types, e.g. neurons of the brain, expression vectors are applied containing promoters specific for the target tissue. To express APP in neurons of the brain and spinal cord, the prion or Thy1 promoter are often used of which the latter has shown to give a high APP mRNA level throughout the brain, being most notably in the hippocampal formation and cerebral cortex (Ittner and Gotz 2007). If the foreign DNA has integrated at the one-cell stage of development, it should be transmitted to 50% of the offspring, which is checked by polymerase chain reaction (PCR) for the presence of the desired DNA sequence. The advantage of the pronuclear injection is that the molecular

biology work is quite simple and development time to first offspring is rather low (~22 weeks), however, as the transgenic integration is random it can disrupt an existing gene possibly causing phenotypic changes or lethality. Also, the transgene usually integrates with a non-predictable copy number, and expression patterns and levels are usually highly variable in different transgenic founders. Therefore, several mouse lines have to be screened for the optimal transgenic phenotype until one is chosen for further breeding and characterization. Extensive housing capacity must therefore be available for the breeding procedure and it takes approximately a year from making the DNA construct for pronuclear injection to the establishment of a new transgenic mouse strain with some phenotypic characterization (Ittner and Gotz 2007; Strachan and Read 1999).

Specific genetic modifications in a mouse genome can be obtained by isolating and culturing ES cells from the inner cell mass of blastocysts. While in culture, the ES cells can be genetically modified by homologous recombination. The modified ES cells are injected back

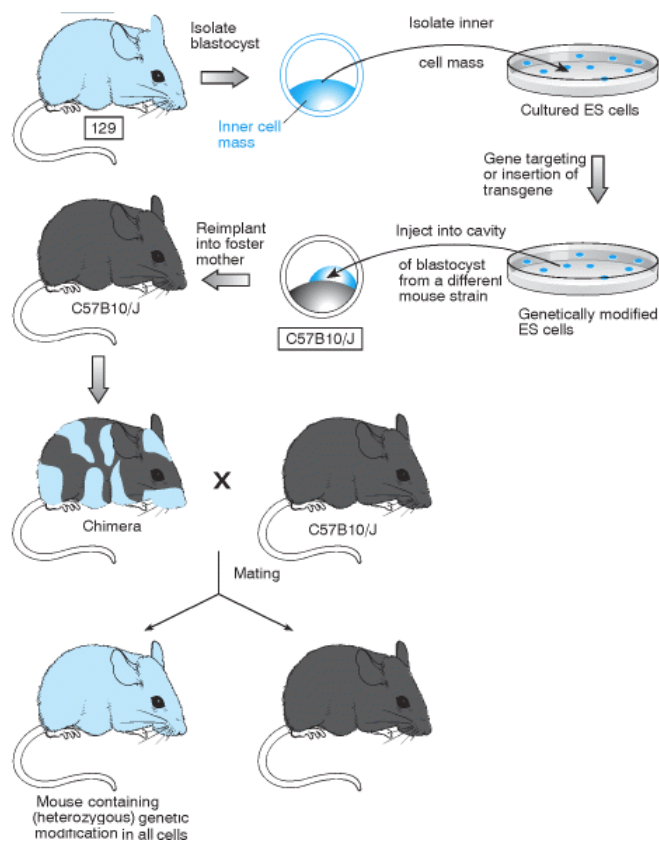


**Fig. 12 Specific modification of target gene by homologous recombination in ES cells.** Embryonic stem (ES) cells from the inner cell mass of blastocytes are cultured, genetically modified, injected into isolated blastocyte of another mouse strain with different fur color, and then implanted into pseudopregnant foster mother. Development of introduced blastocyst results in a chimera containing two populations of cells evident by the presence of differently colored coat patches. Backcrossing produces mice that are heterozygous for the genetic modification (Strachan and Read 1999).

into isolated host blastocysts and reimplanted into a pseudopregnant foster mother. The developing embryo is a chimera which contains two populations of cells derived either from ES cells of the host blastocyst or from the implanted ES cells (Fig. 12). If the two strains of cells are derived from mice with different coat colors, chimeric offspring can be easily identified on their mixed fur coat color. Backcrossing of the chimeras can then generate mice that are heterozygous for the genetic modification, and subsequent cross-breeding of heterozygous mutants can generate homozygous animals (Pluck and Klasen 2009; Strachan and Read 1999). The specific DNA changes performed on the cultured ES cells are introduced using vectors designed to target the locus of interest through sequence homology between the

introduced DNA and the target gene. Two types of vectors are used. Insertion vectors target the locus of interest by a single homologous sequence causing insertion of the entire introduced DNA including the vector sequence. By inserting foreign DNA into the target gene, this is the most reliable way of causing a KO mutation. Replacement vectors target the locus of interest by containing the DNA of interest flanked by two homologous sequences that then recombine with the chromosomal DNA resulting in replacement of some of the sequence in the chromosomal gene. The result can inactivate the gene of interest if the introduced sequence contains a premature termination codon or lacks a critical coding sequence, but can also be used to change the coding sequence producing a change of function for the encoded protein thus producing a KI mutation (Strachan and Read 1999). The main

disadvantage of the ES cell method is that gene cloning and construction of the targeting vector is quite time consuming and technically advanced. However, a huge advantage is that specific genetic modifications can be obtained and that these can be verified in the tissue culture, before insertion of the genetically modified cells are implanted into the foster mother. This renders the genetic manipulation highly effective and minimizes the time spend on breeding and phenotypic screening as the insertion can be performed in a single mouse line.

### 1.3.2 FAD mutations in mouse models of AD

Even though FAD only makes up 2-5% of AD cases, the many identified FAD mutations have the major advantage of being able to modulate the pathology of the disease in model organisms. Many mouse models of AD have been generated utilizing FAD mutations of APP and PS1 or PS2 causing the mice to develop an age-dependent A $\beta$  deposition. FAD mutations in APP are generally named after the population in which they were first identified thus leading to amongst others the Swedish, Flemish, Dutch, Italian, Arctic, Iowa, French, German, Florida, London, Indiana, and Australian mutations of which the Swedish and London mutations are probably the most extensively studied (Fig. 13) (Janssen et al. 2003). The mutations segregate around the secretase cleavage sites affecting the activity of the restriction enzymes. Only one mutation has been identified at the  $\beta$ -cleavage site, the Swedish double mutation, which generally increases the production of A $\beta$  (Scheuner et al. 1996).

Mutations near the  $\gamma$ -secretase cleavage site generally increase the production of the more amyloidogenic A $\beta$ 42 (Scheuner et al. 1996), although the French mutation results in a reduction of A $\beta$ 40 without affecting A $\beta$ 42 production, suggesting that it is the increase in the ratio of A $\beta$ 42 to A $\beta$ 40 that is important rather than the absolute amount of A $\beta$ 42 (Ancolio et al. 1999).

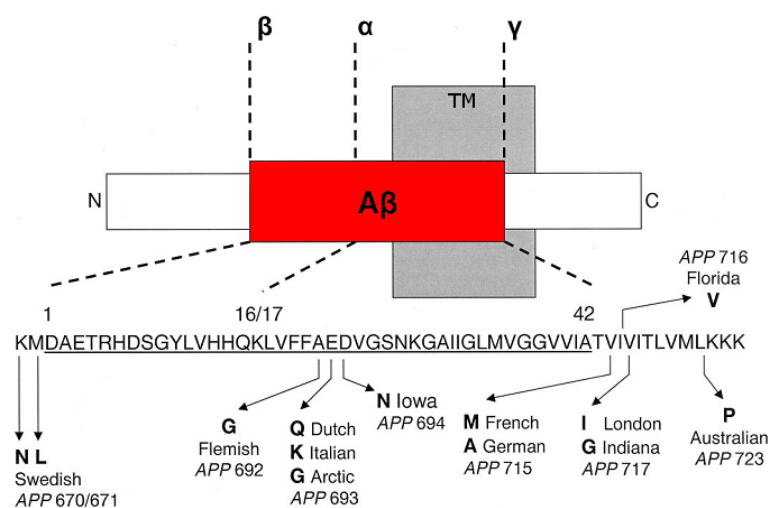


**Fig. 13 Pathogenic mutations in APP.** The mutations are given according to the APP amino acid sequence producing the A $\beta$  peptide, related to  $\beta$ -,  $\alpha$ -, and  $\gamma$ -cleavage sites as well transmembrane domain (TM). For each mutation is given name, amino acid mutation, and number in APP sequence (Janssen et al. 2003).

Intra-A $\beta$  mutations near the  $\alpha$ -secretase cleavage site as the Dutch and Flemish mutations are generally associated with CAA amyloid deposition in blood vessels in addition to amyloid plaque formation, however, the effect of these mutations on the levels of A $\beta$ 40 and A $\beta$ 42 are less clarified with evidence of reduced A $\beta$ 42 or generally reduced A $\beta$  levels in cell culture studies (Janssen et al. 2003). More than 150 mutations have been identified in PS1 and PS2, which are part of the  $\gamma$ -secretase complex. PS1 mutations are the major cause of FAD accounting for 18-55% of all families. The PS1/PS2 mutations are scattered throughout the presenilin protein and generally result in an increased ratio of A $\beta$ 42/A $\beta$ 40 causing early and aggressive forms of AD (Bentahir et al. 2006; Kumar-Singh et al. 2006).

The mouse models generated by introduction of, often several, FAD mutations are numerous. Much important information has come from the analysis of these mouse models; however, the differences in background, transgenic expression pattern, and combination of mutations render the comparison between the models almost impossible and irrelevant. Still, many show pathological features also observed in AD patients. For example, extracellular deposition of A $\beta$  in plaques and vasculature as well as the accumulation of different forms of A $\beta$  having N-terminal modifications and being of different aggregation states correlates with findings in AD patients (Duyckaerts et al. 2008). Disturbances of neuronal structure in the form of dystrophic neurites surrounding plaques, decreased fiber and synapse density, and synaptic dysfunctions also correlate to observations in AD patients (Aucoin et al. 2005; Bellucci et al. 2006; Bronfman et al. 2000; Hu et al. 2003; Luth et al. 2003; Wong et al. 1999), as does the observation of inflammatory changes (Baron et al. 2007; Eikelenboom et al. 2006). Neuron loss, however, assessed by stereological quantification is a feature only observed in very few mouse models, which complicates the study of the mechanism behind the massive neuron loss observed in AD patients and weakens the hypothesis of the A $\beta$  deposition driving the AD pathogenesis (Casas et al. 2004; Schmitz et al. 2004). Also, none of the mouse models containing FAD mutations develop tau pathology in the form of NFT, making the link between A $\beta$  and tau pathology a still unsolved mystery.

### 1.3.3 The APP/PS1KI mouse model

The bigenic APP/PS1KI mouse model is a result of the breeding of two different lines, a PS1KI mouse line and a transgenic APP Swedish London (APP<sup>SL</sup>) mouse line. The PS1KI mouse line was derived using a two-step mutagenesis strategy, based on the construction of a

targeting vector that bears base changes in the coding region at codons M233T and L235P and surrounding introns of the murine *Ps1* gene. Homozygous mice were established and referred to as PS1KI. PS1KI mice on a mixed 129SV-C57BL/6 genetic background were bred with APP<sup>SL</sup> transgenic mice generated by pronuclear injection overexpressing human APP751 carrying the London (V717I) and Swedish (K670N, M671L) mutations under the control of the Thy1 promoter on a mixed C57BL/6-CBA genetic background. When present, the APP transgene was heterozygote, and the resulting APP/PS1KI animals statistically have the same genetic background: 50% C57BL/6, 25% CBA, and 25% 129SV (Casas et al. 2004).

The bigenic APP/PS1KI mice accumulates almost exclusively A $\beta$ 42, but with different N-terminal modifications. The model is one of the currently most interesting as the mice develop an extensive neuron loss of about 30% in the CA1 region of the hippocampal formation already at 6 months, which is even more obvious in 10-month-old mice (Fig. 14A) (Breyhan et al. 2009; Casas et al. 2004). The bigenic mice are smaller and have a thoracolumbar kyphosis observed as a characteristic bend in the spinal cord compared to PS1KI control mice and they show a severe motor pathology evident by a hind limb clasping phenotype when dispensed by the tail. Significant impairments in the balance beam, string suspension, and vertical grip hanging tasks become obvious at the age of 6 months (Wirhth and Bayer 2008). The APP/PS1KI mice also show inflammatory changes (Wirhth et al. 2008a) and many dystrophic neurites marking axonal degeneration throughout the brain and spinal cord (Fig. 14B) (Wirhth et al. 2007; Wirhth et al. 2006). The observed extensive pathology apparently results in behavioral deficits, which can be detected in working memory assessed by Y- and T-maze at the age of 6 months (Fig. 14C) (Wirhth et al. 2008b).

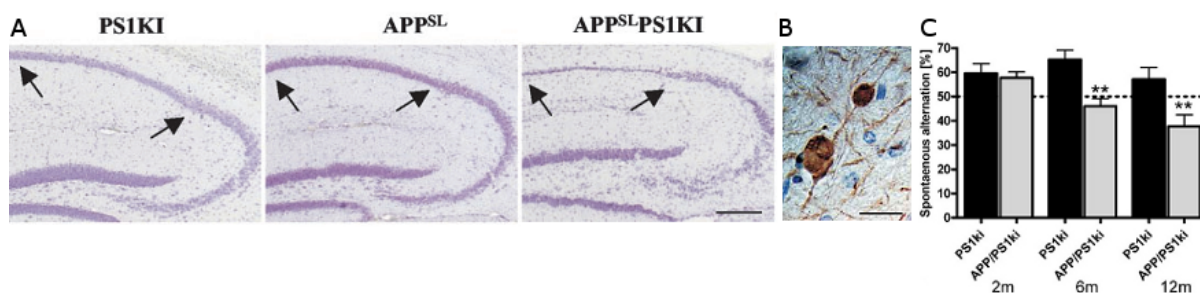


**Fig. 14 Data from APP/PS1KI mice.** A) Micrographs of hippocampal cresyl violet stained sections from 10-month-old PS1KI, APP<sup>SL</sup>, and APP<sup>SL</sup>PS1KI mice. Massive cell loss is observed in the CA1 of bigenic APP<sup>SL</sup>PS1KI mice only (arrows) (Casas et al. 2004). B) Large axonal spheroids stained with antibody against NF200 labeling neurofilaments in neurons of 10-month-old APP/PS1KI mice (Wirhth et al. 2007). C) Analysis of alternation behavior in T-maze revealed significant impairment in working memory at the age of 6 and 12 months in the APP/PS1KI mice compared to PS1KI controls (Wirhth et al. 2008b).

## **1.4 The amyloid hypothesis**

For many years, scientists have been split concerning the etiology of AD depending on their belief in A $\beta$  or tau as the driving pathological mechanism of AD. The amyloid hypothesis states that the accumulation of A $\beta$ , preferable A $\beta$ 42, is the underlying cause of AD driving neuron and synapse impairment and loss, eventually leading to behavioral deficits (Hardy 2006; Hardy and Allsop 1991). The major argument for the amyloid hypothesis is the genetics of FAD in which mutations have been identified only in genes linked to the A $\beta$  generating cascade, whereas mutations in tau lead to frontotemporal dementia (Kumar-Singh and Van Broeckhoven 2007). Thus at present, the amyloid hypothesis is widely believed to be the primary pathological mechanism of AD, whereas the tau pathology is believed to be downstream of A $\beta$  pathology since FAD also show NFTs, but frontotemporal dementia caused by tau mutations shows no A $\beta$  pathology. Another argument for the A $\beta$  hypothesis is the discovery of the familial British and Danish dementias. These dementias are caused by two different mutations in the *BRI2* gene generating two similar proteins of 34 amino acids varying in their C-terminal part (Vidal et al. 1999; Vidal et al. 2000). These two proteins aggregate and form amyloid plaques similar to A $\beta$  plaques in AD and the proteins are thus named amyloid Bri (ABri) and amyloid Dan (ADan) according to their presence in British and Danish dementia. Interestingly, the processing of the *BRI2* gene reminds a lot of that of APP as it can also be cleaved by ADAM10 and has been shown to undergo regulated intramembrane proteolysis (Martin et al. 2008), and the British and Danish dementias also develop tau pathology, which further suggest that tau pathology is downstream of the amyloid pathology (Holton et al. 2001).

Plaques have been shown to cause toxic effects such as disturbances in the fiber network with development of dystrophic swellings in surrounding fibers and loss of dendritic spines, as well as decreased synaptic bouton density, preferably of cholinergic cortical fibers (Blanchard et al. 2003; Delatour et al. 2004; Hu et al. 2003; Tsai et al. 2004; Wirths et al. 2007). Still, much remains to be resolved about their actual toxicity as the accumulation of extracellular A $\beta$  plaques does not seem to correlate with the cognitive decline observed in AD patients and can be found in non-demented control subjects (Aizenstein et al. 2008). Furthermore, loss of neurons is rarely observed in the various mouse models generated accumulating abundant A $\beta$  plaque pathology (Duyckaerts et al. 2008; Games et al. 2006).

### 1.4.1 The intraneuronal amyloid hypothesis

A possible modification of the amyloid hypothesis is that the driving pathological factor is not A $\beta$  accumulation in extracellular plaques, but rather A $\beta$  accumulation inside neurons. Intraneuronal accumulation of A $\beta$  has received considerable attention in the past recent years and is believed to precede extracellular plaque deposition (Gouras et al. 2005; Gyure et al. 2001; Laferla et al. 2007; Wirths et al. 2004). Thus the intraneuronal A $\beta$  hypothesis of AD is a modification of the original amyloid hypothesis and suggests that risk factors such as aging, ApoE4 polymorphism, trisomy 21 (Down Syndrome), or FAD mutations

initially cause A $\beta$  accumulation inside neurons, leading to functional deficits and loss of neurons and synapses ending up in cognitive decline (Fig. 15) (Gouras et al. 2005; Laferla et al. 2007; Wirths et al. 2004). In this model, plaques are considered a result of A $\beta$  leakage or release from the intraneuronal pool, or to originate from the lysis of neurons accumulating intraneuronal A $\beta$ . The plaques are believed to cause disturbances of the neuronal network, but they are not considered the primary cause of AD pathogenesis (D'Andrea et al. 2001; Gouras et al. 2005; Wang et al. 2002).

The accumulation of intraneuronal A $\beta$  peptides in AD brains has been sporadically reported since the late 1980's (Grundke-Iqbal et al. 1989), however, initial problems with the inability of the antibodies to distinguish full length APP from A $\beta$  founded a skepticism towards the presence of intraneuronal A $\beta$  that has been exceedingly difficult to eliminate (Gouras et al. 2005; Laferla et al. 2007). Despite the initial technical complications, several studies using A $\beta$ 40/42 end-specific antibodies have since reported the presence of intraneuronal A $\beta$  in AD

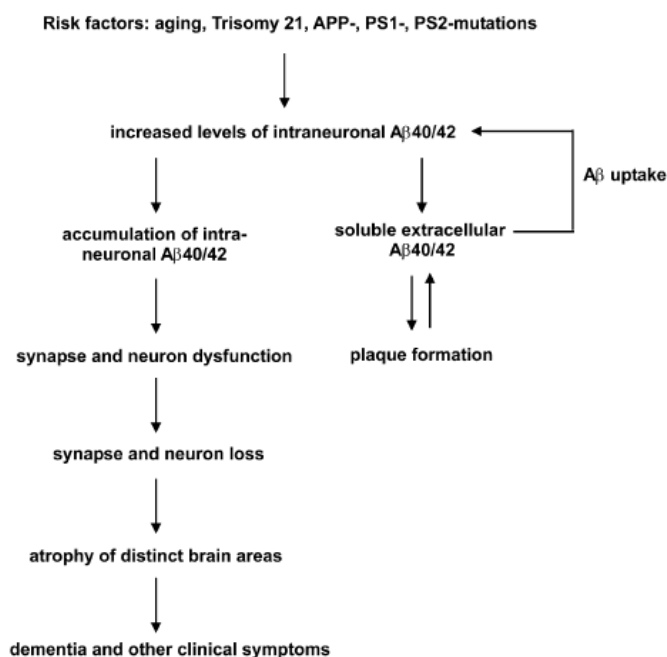


**Fig. 15 The intraneuronal A $\beta$  hypothesis of AD.** Due to risk factors as ageing, Trisomy 21 and FAD mutations, intraneuronal A $\beta$ 42 levels increase and leads to synaptic and neuronal dysfunction followed by neurodegeneration. In parallel, increased release and deposition of A $\beta$ 42 leads to extracellular plaque formation, from which A $\beta$  can possibly again be internalized and contribute to the intraneuronal pool of A $\beta$  peptides. (Wirths et al. 2004).



brains (D'Andrea et al. 2002a; D'Andrea et al. 2002b; D'Andrea et al. 2001; Fernandez-Vizarra et al. 2004; Gouras et al. 2000; Mochizuki et al. 2000; Nagele et al. 2002; Wegiel et al. 2007), as well as in Down Syndrome patients who are known to develop AD in early age (Gyure et al. 2001; Mori et al. 2002). One study even isolated human hippocampal granular neurons from the CA1 of AD patients by laser capture microdissection and identified an increased intraneuronal ratio of A $\beta$ 42/A $\beta$ 40 in AD patients compared to controls (Aoki et al. 2008). However, people still remain skeptical towards the presence of intraneuronal A $\beta$  in human AD brains, probably because most of the studies show pictures of variable quality and often reports of findings in only one or a very low number of AD cases. Also, some antibodies, especially monoclonal, directed toward an internal part of A $\beta$  seem to cross-react with lipofuscin, which is a protein that accumulates abundantly in neurons with age showing a very distinct cap-like granular staining nearby the nucleus (Bancher et al. 1989). The reports of intraneuronal A $\beta$  have thus been inconsistent with pictures showing very different patterns of intraneuronal A $\beta$  accumulation of which some have actually been lipofuscin, and the accumulation of intraneuronal A $\beta$  remains under discussion (Duyckaerts et al. 2008).

In AD mouse models, intraneuronal A $\beta$  was first reported in familial PS1 transgenic mice that also showed neurodegeneration without the formation of plaque pathology (Chui et al. 1999), and has since been convincingly reported in several mouse models including APP<sup>SDL</sup>PS1<sub>M146L</sub> (Wirhns et al. 2001), Tg2576 (Takahashi et al. 2002), 3xTg-AD (Oddo et al. 2003), 5xFAD (Oakley et al. 2006), APP<sup>Arc</sup> (Knobloch et al. 2007; Lord et al. 2006), APP<sub>T714I</sub> (Van Broeck et al. 2008), as well as in APP/PS1KI mice (Casas et al. 2004). In the mouse models, intraneuronal A $\beta$  has amongst others been reported to disrupt fast axonal transport in isolated axoplasms (Pigino et al. 2009) and impair multivesicular body sorting by inhibiting the ubiquitin-proteasome system (Almeida et al. 2006). In addition, it induces synaptic dysfunction leading to reduced postsynaptic density 95 protein (PSD-95) levels and consequently reduces the levels of the glutamate receptor subunit, GluR1, in synapses (Almeida et al. 2005). Strikingly, of the very few mouse models based on FAD mutations which have been documented to show robust neuron loss, two are accumulating intraneuronal A $\beta$ : the APP<sup>SL</sup>PS1<sub>M146L</sub> and the APP/PS1KI models (Casas et al. 2004; Schmitz et al. 2004). The 5xFAD mice, which also accumulate intraneuronal A $\beta$  peptides, have been described to have a lower density of neurons in the cortex and subiculum based on a qualitative evaluation of a cresyl violet staining, however, this needs to be confirmed by unbiased stereological

quantifications (Oakley et al. 2006). This renders the mouse models accumulating intraneuronal A $\beta$  especially interesting for studying the neuron loss in AD, which most likely symbolizes the irreversible step in the pathological cascade of AD where clinical deficits become apparent (Price et al. 2001).

### 1.5 Transmitter deficits in Alzheimer's disease

The first transmitter specific deficits to be identified in AD were of the cholinergic system utilizing acetylcholine (ACh) as a neurotransmitter that were reported already in the 1970s leading to the cholinergic hypothesis of AD (Davies and Maloney 1976). Parallel to Parkinson's disease, which is primarily a neurodegenerative disease of the dopaminergic neurons of the substantia nigra, AD was hypothesized to be a neurodegenerative disease of the cholinergic system, owing mainly to degeneration of cholinergic neurons of the nucleus basalis of Meynert, which is the largest cholinergic nucleus of the human basal forebrain projecting to the cortex (Coyle et al. 1983). The cholinergic system of the brain comprises two projecting neuron complexes: the basal forebrain and the pons complex, as well as motor nuclei projecting to the periphery and interneurons located mainly in the striatum. In the present thesis, the cholinergic projecting nuclei will be designated according to the Ch1-6 nomenclature, which is based on common connectivity patterns that are virtually identical in human and rodents (Lucas-Meunier et al. 2003; Mesulam et al. 1983). From the basal forebrain complex, cholinergic neurons from the medial septum (Ch1) and the vertical limb of the diagonal band (Ch2) project to the hippocampal formation, whereas those of the basal nucleus of Meynert (Ch4) mainly project to the cortex (Fig. 16). The Ch3 is a minor nucleus of the horizontal part of the diagonal band and its cholinergic neurons project to the olfactory bulb. The cholinergic neurons of Ch5-6 belong to another projecting complex located in the pons projecting mainly to the thalamus. Initially, a reduction in the activity of

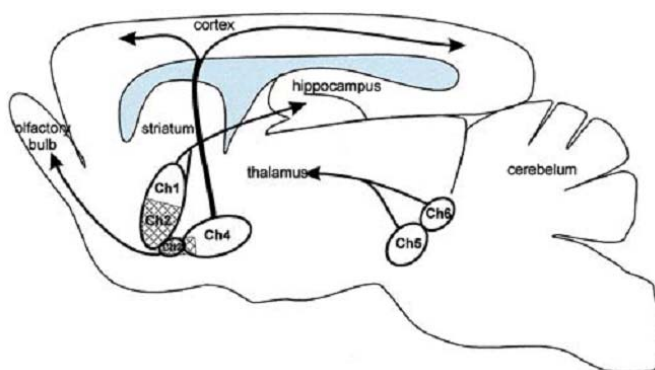


**Fig. 16 Overview of Ch1-6 nomenclature and projections.** The figure is based on a sagittal section of the rat brain. Hatched area: the diagonal band (Lucas-Meunier et al. 2003).

both the ACh synthesizing enzyme, choline acetyltransferase (ChAT), and the ACh degrading enzyme, acetylcholine esterase (AChE), was reported being most severe in the cortex (Davies 1979; Davies and Maloney 1976). Subsequently, a loss of cholinergic forebrain neurons of the nucleus basalis of Meynert was discovered as the first evidence of neuron loss in AD (Arendt et al. 1988; Mufson et al. 1989; Whitehouse et al. 1981). These cholinergic forebrain neurons projecting to the cortex participate in the mediation of attention, and their degeneration is thus thought to cause part of the cognitive decline observed in AD (Sarter et al. 2005).

Based on the cholinergic hypothesis, AD patients have long been treated with AChE inhibitors to decrease the breakdown of ACh and thereby prolong its action in the synaptic cleft. However, the clinical impact of the AChE inhibitors has turned out to be quite disappointing with only minor beneficial effects and it was soon recognized that AD is a complex disease affecting multiple transmitter systems, although perhaps with the cholinergic basal forebrain neurons being especially vulnerable. According to the nerve growth factor (NGF) hypothesis, this vulnerability is thought to be caused by decreased NGF stimulation of the cholinergic basal forebrain neurons as their survival is highly dependent on NGF being retrogradely transported from the hippocampal formation or cortex (Counts and Mufson 2005). Thus in vivo, cholinergic Ch4 neurons of the nucleus basalis degenerated following experimental neocortical infarction in monkeys (Burgos et al. 1995) or excitotoxic neocortical lesions in rats (Charles et al. 1996), but were rescued by exogenous NGF treatment. In parallel, infusion of NGF can prevent death of cholinergic Ch1/2 neurons following septohippocampal axotomy (Hefti 1986; Tuszynski and Gage 1995; Williams et al. 1986) or hippocampal lesions (Burke et al. 1994). Finally, transgenic mice that express anti-NGF antibodies in adulthood display an age-dependent specific loss of cholinergic basal forebrain neurons (Capsoni et al. 2000; Ruberti et al. 2000). In AD patients, the NGF system has been found to be dysregulated early in the disease progress and in end-stage AD patients, cholinergic basal forebrain neurons have reduced protein levels of NGF and its high and low affinity receptors, TrkA and p75, whereas both stable, increased, as well as decreased levels of NGF have been reported in the cortical and hippocampal projection regions of end-stage AD (Mufson et al. 1995; Scott et al. 1995). Thus impairment in retrograde transport of NGF is thought to be responsible for the lack of trophic support of Ch4 neurons, rendering the cholinergic neurons more vulnerable, or directly mediate their degeneration (Lad et al. 2003). NGF treatment is therefore another potential treatment for AD directly targeting the

degeneration of the cholinergic basal forebrain neurons, however, there is a need for highly specific delivery to avoid aberrant sprouting of neuronal fibers. So far, one successful phase I clinical trial has been conducted in which mild AD subjects received grafts of autologous fibroblasts genetically modified to secrete human NGF (Tuszynski et al. 2005). The cells were implanted directly in the nucleus basalis of Meynert bypassing putative defects in the retrograde transport of NGF and avoiding systemic exposure. The patients showed minor improvements in cognitive decline and cortical glucose uptake; still, more studies are needed to confirm a positive effect of NGF treatment in AD patients. Apart from administration, a major challenge of NGF treatment will be early intervention, as NGF must be given prior to degeneration of the cholinergic neurons to have any effect on their survival (Montero and Hefti 1988).

To date, only 5 drugs have been approved by the food and drug administration (FDA) in the US for treatment of AD. These are tacrine (Cognex), rivastigmine (Exelon), galantamine (Razadyne), donepezil (Aricept), and memantine (Namenda), of which the first four are all AChE inhibitors. It has been evaluated that at least rivastigmine, galantamine, and donepezil have similar efficacy showing only minor benefits of treatment on cognitive function, activities of daily living, and behavior and there is currently a debate concerning whether the AChE inhibitors have any effect at all (Birks 2006).

Also receptors of the cholinergic system are being discussed as potential targets for future treatments of AD. Two types of cholinergic receptors exist, the nicotinic ACh receptors (nAChRs) which are ligand-gated ion channels, and the muscarinic receptors that are 7-transmembrane receptors coupled to G proteins. The muscarinic receptors, especially the M1 receptor, have received much attention in the past showing stimulation of  $\alpha$ -secretase cleavage by Protein Kinase C (PKC) activation (Nitsch et al. 1992), but presently, the nAChRs are at the center of most attention (D'Andrea and Nagele 2006). The nAChRs are composed of 5 transmembrane subunits of which there are 2 major types,  $\alpha$  and  $\beta$ . At least 9  $\alpha$ -type subunits ( $\alpha 2$  through  $\alpha 10$ ) and 3  $\beta$ -type subunits ( $\beta 2$  through  $\beta 4$ ) are expressed throughout the CNS, where two of the most abundant neuronal nAChRs are the heteromeric high affinity  $\alpha 4\beta 2$  and the homomeric low affinity  $\alpha 7$  receptors (Alkondon and Albuquerque 2004). All the nAChRs are stimulated by ACh and nicotine with varying affinities and are cation selective, being permeable to small monovalent and divalent cations, where the  $\alpha 7$  nAChR has a high relative permeability of  $\text{Ca}^{2+}$  to  $\text{Na}^{+}$  of  $\geq 10$  as compared to  $\sim 2.0$  for the

heteromeric neuronal receptors (Dani and Bertrand 2007). The nAChRs mediate fast synaptic signal transmission and are involved in learning, memory, and attention (Hasselmo 2006; Sarter et al. 2005). In AD post-mortem studies, reductions in both  $\alpha 4$  and  $\alpha 7$  subunits have been reported in the cortex and hippocampal formation (Guan et al. 2000; Teaktong et al. 2004). Although, increased immunohistochemical staining of  $\alpha 7$  reactive neuropil was observed in some areas of the hippocampus (Teaktong et al. 2004) and cholinergic neurons of the nucleus basalis of Meynert express an increased level of  $\alpha 7$  nAChRs, probably as a compensatory mechanism in reaction to their dysfunction and degeneration (Counts et al. 2007). In contrast, little depletion or dysregulation of muscarinic cholinergic receptors has been found in patients with AD (Nordberg et al. 1992).

The nAChR showing most implication in AD is the  $\alpha 7$  nAChR, of which a direct interaction with A $\beta$ 42 has been repeatedly reported, and genetic variation in the  $\alpha 7$  nAChR gene has recently been shown to influence AD susceptibility (Carson et al. 2008). In human AD brain tissue,  $\alpha 7$  nAChRs show co-localisation with A $\beta$ 42, and also co-immunoprecipitate with A $\beta$ 42 in AD hippocampal neurons, as does  $\alpha 7$ nAChRs purified from culture and incubated with synthetic A $\beta$ 42 (Wang et al. 2000). In membranes, the same study found that A $\beta$ 42 displaces  $\alpha$ -bungarotoxin ( $\alpha$ -BTX) binding specific for  $\alpha 7$ nAChRs (Wang et al. 2000). In contrast, another study in cultured cells found that A $\beta$  does not bind to  $\alpha 7$ nAChRs, but binds to lipids within the plasma membrane that could, potentially, influence the function of a variety of receptors and channels on the cell surface (Small et al. 2007). However, A $\beta$ 42 specifically blocks the response evoked by ACh or nicotine of  $\alpha 7$  nAChRs in cell culture and hippocampal neurons (Liu et al. 2001; Pettit et al. 2001; Spencer et al. 2006), and  $\alpha 7$  nAChR activation protected against A $\beta$ -induced neurotoxicity (Kihara et al. 1997). Interestingly, the  $\alpha 7$  nAChR has been suggested to mediate endocytosis of A $\beta$ 42, facilitating intraneuronal accumulation of A $\beta$  (Nagele et al. 2002).

In addition to direct cholinergic behavioral deficits, the  $\alpha 7$  nAChRs can cause behavioral symptoms by interaction with other transmitter systems. For instance,  $\alpha 7$  nAChRs are located presynaptically at excitatory synapses and enhance both glutamatergic and cholinergic synaptic transmission by increasing presynaptic intracellular Ca<sup>2+</sup> levels (McGehee et al. 1995). This suggests that fluctuations in  $\alpha 7$  receptor levels may lead to functional deficits in the glutamatergic excitatory system thus influencing processes of learning, memory, and synaptic plasticity, or even influence excitotoxicity. In fact, the AChE inhibitor, galantamine,

is thought to also block glutamate toxicity through  $\alpha 7$  mediated phosphatidylinositol 3-kinase (PI3K) activation (Kihara et al. 2004).

The involvement of the cholinergic system in the pathogenesis of AD is supported by the observation that nicotine reduces A $\beta$  levels in APP<sup>SWE</sup> mice (Hellstrom-Lindahl et al. 2004a), which correlated with the finding that smoking had a lowering effect on A $\beta$  and an increasing effect on radioactive-ligand binding of nicotinic receptors in the brains of AD patients and control subjects (Hellstrom-Lindahl et al. 2004b). These studies indicate that selective nicotinic agonists may be beneficial in AD by lowering A $\beta$  levels and even increasing nAChR levels. Accordingly, some pharmaceutical companies are presently developing  $\alpha 7$  agonists for AD patients; however, many believe that the best strategy to treat neurotransmitter deficits in AD will be to use a combination of drugs toward multiple targets within neurotransmission (Geerts and Grossberg 2006; Grossberg et al. 2006; Gsell et al. 2004).

## **1.6 Introduction to experiments**

The loss of neurons in AD represents a fatal irreversible step in the cascade of AD development; however, thus far, the mechanism of the neuron loss remains unclear. As specified, very few mouse models generated by use of FAD mutations have so far shown any loss of neurons, and especially, the specific loss of the cholinergic neurons of the nucleus basalis of Meynert lacks to be modeled. The intraneuronal A $\beta$  hypothesis is a fairly new modulation of the amyloid hypothesis, stating that intraneuronal A $\beta$  rather than plaque pathology is the primary toxic mechanism of AD pathogenesis. The present thesis focuses on the impact of intraneuronal A $\beta$  on neuron function and degeneration, mainly utilizing the APP/PS1KI model, which is one of the presently most interesting mouse models of AD showing cognitive deficits, extensive neuron degeneration in the CA1, and abundant accumulation of intraneuronal A $\beta$  in many regions prior to development of plaque pathology in early age (Casas et al. 2004; Wirths et al. 2008b; Wirths et al. 2007). The following studies were undertaken to investigate the impact of A $\beta$ , especially intraneuronal, on neuron function and degeneration, and their backgrounds are further explained below:

1. The neuron number in selected parts of the cholinergic system of the APP/PS1KI mouse model was quantified and correlated to the accumulation of intraneuronal A $\beta$ .

2. The impact of intraneuronal A $\beta$  versus plaques on neuronal survival was studied in the APP/PS1KI mouse model by neuron quantification in an area with plaques only compared to an area with plaques as well as intraneuronal A $\beta$ .
3. Intraneuronal A $\beta$  staining was optimized in four AD mouse models as well as human AD tissue, and subsequently used to semi-quantify the intensity of intraneuronal A $\beta$  staining in human sporadic AD brains that was correlated to patient data.
4. The toxic effect of A $\beta$  on axonal pathology was studied in APP/PS1KI mice.
5. Collaboration was established with Neurosearch A/S in Denmark to evaluate the impact of the potential interaction between A $\beta$  and the  $\alpha 7$  nAChR in AD.
6. Through collaboration with Neurosearch as well as the group of Mark West in Århus, Denmark, the potential dysfunction of the *Arc* system was investigated in the APP/PS1 $\Delta$ E9 mouse model of AD following novelty stimulation.

#### **1.6.1 Neuron loss in the cholinergic system of APP/PS1KI mice**

Because the APP/PS1KI mice develop an extensive neuron loss in the CA1 region of the hippocampal formation, the present study investigated A $\beta$  accumulation and its influence on neuronal survival in the cholinergic system of this bigenic mouse model. The objective of the study was to establish whether the APP/PS1KI mouse model represents a valid model for the cholinergic neuron loss observed in AD. The expression of the APP transgene and accumulation of intraneuronal A $\beta$  was initially investigated by qualitative fluorescent immunohistochemistry using antibodies towards ChAT to indentify neurons of the cholinergic system. The pattern of APP transgene expression and corresponding intraneuronal A $\beta$  accumulation was applied as a model system to study the effect of intra- and extracellular A $\beta$  accumulation on neuron loss in the cholinergic system analyzed by design-based stereology quantifying ChAT-positive neurons stained by free-floating immunohistochemistry.

#### **1.6.2 Effect of intraneuronal A $\beta$ versus plaques on neurodegeneration**

The study of the impact of intraneuronal A $\beta$  on neuronal survival in the cholinergic system was extended to a study comparing the impact of intraneuronal A $\beta$  versus plaques on neuron loss. For this purpose, the APP/PS1KI mice presented an optimal model system as they have regions of the brain not accumulating intraneuronal A $\beta$ , but with abundant deposition of

plaques as well as regions accumulating intraneuronal A $\beta$  together with the deposition of plaques. The thalamus was chosen as a region accumulating plaques only, whereas the frontal cortex was used to study the impact of the combined accumulation of plaques and intraneuronal A $\beta$ . Initially, the A $\beta$  deposition was thoroughly investigated in the two chosen regions and neuron quantifications were subsequently performed using design-based stereology comparing the APP/PS1KI mice to PS1KI control mice showing no A $\beta$  pathology.

### **1.6.3 Intraneuronal A $\beta$ staining in AD patients and transgenic AD mouse models**

Many scientists remain skeptical toward the presence of intraneuronal A $\beta$  in human AD brains. Thus the present study had the objective of optimizing and confirming the staining of intraneuronal A $\beta$  in human AD tissue using a highly specific N-terminal A $\beta$  antibody, whereas other studies have mainly targeted the C-terminus of A $\beta$ . Compared to mouse tissue, human tissue offers challenges such as post-mortem delay and less consistent tissue fixation, which might cause problems with the immunohistochemical staining techniques. Also, the staining protocols so far applied to study intracellular A $\beta$  accumulation in human tissue have been inconsistent with varying use of heat and formic acid (FA) for antigen retrieval. Microwave heat treatment has been reported to enhance the staining of intraneuronal A $\beta$  as compared to no or enzymatic pretreatment (D'Andrea et al. 2002b). FA is widely used to increase the staining of plaque pathology in AD, yet, the effect of FA on intraneuronal A $\beta$  staining has been reported to be low and similar to the effect of heat (D'Andrea et al. 2003) or even to counteract the enhancing effect of heat pretreatment on intraneuronal A $\beta$  immunohistochemical detection (Ohyagi et al. 2007).

The study was divided in two parts. First, the staining protocol for intraneuronal A $\beta$  was optimized in relation to heat and FA in four different mouse models being positive controls known to accumulate intraneuronal A $\beta$ . Secondly, the optimization was extended to human brain tissue from AD patients.

#### **Optimization for staining of intraneuronal A $\beta$ in mouse models of AD**

The effect of FA versus microwave heating on the staining of plaques and intracellular A $\beta$  was quantified in the APP/PS1KI mouse model utilizing the regional discrepancy of A $\beta$  deposition in relation to plaques and intraneuronal A $\beta$  accumulating in the thalamus and CA1,



respectively. The quantification of A $\beta$  staining was performed using ImageJ, where a fixed intensity threshold was applied to micrographs defining the 3,3-diaminobenzidine (DAB) staining, and the percentile area covered by A $\beta$  staining was calculated. The results of the quantification were confirmed in a qualitative optimization in three other mouse models using two different A $\beta$  antibodies, where four conditions were compared; no pretreatment, FA pretreatment, heat pretreatment, and combined FA and heat pretreatment, applying time intervals optimized in the quantitative study in the APP/PS1KI mice.

#### **Staining of intraneuronal A $\beta$ in brain tissue of AD patients**

The four optimized conditions from the studies in the mouse models were applied to human brain tissue of sporadic, familial Swedish and familial Arctic AD cases as well as non-demented controls. The best protocol was used to screen 10 controls and 20 sporadic AD cases for the intensity of intraneuronal A $\beta$  staining, which was correlated to patient data including gender, Braak stage, plaque load, and ApoE genotype.

#### **1.6.4 Effect of A $\beta$ on axonopathy in transgenic AD mouse models**

Abnormalities and impairments in axonal transport are suggested to strongly contribute to the pathological alterations underlying AD (Roy et al. 2005; Stokin and Goldstein 2006; Zhu et al. 2005). Indications for axonopathy resulting in disturbances in axonal transport have also been described in various APP-based transgenic AD mouse models (Salehi et al. 2006; Stokin et al. 2005; Wirths et al. 2007; Wirths et al. 2006). Surprisingly, it has recently been shown that an increase in the A $\beta$ 42/A $\beta$ 40 ratio, as well as an increased deposition of A $\beta$  peptides, resulted in a suppression of APP-induced axonal deficits in both transgenic mouse and drosophila models, leading to the suggestion that APP-induced axonal defects are not caused by A $\beta$  peptides (Stokin et al. 2008). To evaluate the effect of A $\beta$  accumulation on axonopathy in our APP/PS1KI model, the present study quantified large plaque-independent axonal spheroids in the brain of APP single transgenic mice overexpressing APP751 with the Swedish and London mutations under control of the Thy-1 promotor, as well as in APP transgenic mice co-expressing the mutant PS1KI gene on endogenous levels in either a hemi- (APP/PS1KI<sup>he</sup>) or homozygous (APP/PS1KI<sup>ho</sup>) manner. Using this strategy, APP expression levels did not differ between the different mouse lines, however, increased PS1KI gene

dosage caused a dramatic increase in A $\beta$  peptide levels, allowing the study of the impact of A $\beta$  independently of APP expression.

APP can be applied as a marker of axonopathy since it is transported into fibers and accumulates in dystrophic swellings and APP is thus often used in the detection of axonal pathology for example in the analysis of traumatic brain injury (Pierce et al. 1996) and has previously been used to detect axonal degeneration in APP/PS1KI<sup>ho</sup> mice (Wirhth et al. 2007). However, a problem of using APP as a marker of axonal degeneration in APP-transgenic mouse models is its very broad staining pattern. This includes cell bodies, axonal swellings and dystrophic neurites in the vicinity of amyloid plaques, thereby complicating the analysis of distinct pathological alterations like axonal pathology especially in plaque-rich brain areas. One solution is to use an antibody which detects APP phosphorylated at T668 (anti-pT668) that has proved not to stain cell bodies, but only stains dystrophic neurites that can be plaque-associated or plaque-independent. NF-200 is a 200 kDa neurofilament and is another possible marker of axonopathy. Neurofilaments are the most abundant fibrillar components of the axon and serve as major elements of the cytoskeleton supporting the axonal structure and NF-200 has the advantage of mostly staining the large axonal swellings independent of plaques. Thus antibodies toward phosphorylated APP and NF-200 were applied as markers in the quantification of axonopathy in the APP, APP/PS1KI<sup>he</sup>, and APP/PS1KI<sup>ho</sup> mice.

Equal APP expression levels in the three mouse lines were confirmed qualitatively and quantitatively by APP immunohistochemical staining and western-blot. The accumulation of A $\beta$  was likewise evaluated by western-blot and A $\beta$  immunohistochemical staining, which was quantified by micrographs and Image-J software analysis.

To study possible mechanism of the axonopathy observed in the APP/PS1KI mice, the level of ubiquitin and ubiquitinated proteins was qualitatively investigated in the different mouse lines using immunohistochemistry and western-blotting. Furthermore, yellow fluorescent protein (YFP) transgenic mice expression YFP in 2-3% of neurons were crossed with APP/PS1KI<sup>he</sup> mice to obtain visualization of fibers in fluorescent analyses and the presence of intracellular A $\beta$  in dystrophic fibers was directly analyzed using confocal microscopy.

### 1.6.5 Interaction between $\alpha 7$ nAChR and A $\beta$

The cholinergic system modulates cognitive functions such as attention and memory, and smoking was found to have a lowering effect on A $\beta$  and an increasing effect on radioactive-ligand binding of nicotinic receptors in the brains of AD patients and control subjects, indicating that selective nicotinic agonists may be beneficial in AD (Hellstrom-Lindahl et al. 2004b). This was supported by a study in APP<sup>swc</sup> mice, where 10 days of treatment with nicotine reduced insoluble A $\beta$ 40 and A $\beta$ 42 levels with 80% in brain tissue (Hellstrom-Lindahl et al. 2004a). Which of the nAChRs that mediates the beneficial effects of nicotine is unknown, but many studies have reported a direct interaction between the  $\alpha 7$  nAChR and A $\beta$ 42, implicating the  $\alpha 7$  nAChR in AD. If A $\beta$  in fact interacts with the  $\alpha 7$  nAChR it could mediate part of its toxic effect by inducing desensitization of the  $\alpha 7$  nAChR. The present study thus set out to investigate if specific activation of the  $\alpha 7$  nAChR could mediate a lowering effect on the generation of A $\beta$ , and whether endogenous accumulation of A $\beta$  had an effect on the binding capacity of the  $\alpha 7$  nAChR in vivo.

The study was performed as cooperation with the group of Mark West at the department of Neurobiology, Anatomical Institute, Aarhus University, Denmark. Three groups of 9-month-old APP/PS1 $\Delta$ E9 mice were treated twice daily for 10 days with subcutaneous injections of saline, 10 mg/kg of the  $\alpha 7$  nAChR agonist SSR180711 (1,4-Diazabicyclo[3.2.2]nonane-4-carboxylic acid, 4-bromophenyl ester, synthesized at Neurosearch A/S, DK), or 10 mg/kg nicotine ((-)-1-Methyl-2-(3-pyridyl)pyrrolidine (+)-bitartrate salt, Sigma-Aldrich, St Louis, USA) as a positive control replicating the data from the APP<sup>swc</sup> mice. The mice were decapitated and half of the brains were directly frozen on dry ice and stored at -80°C, whereas the other halves were immersion fixated in 4% formaldehyde for 5 days until they were embedded in paraffin. A $\beta$  levels were quantified in micrographs of A $\beta$  immunohistochemistry on 2  $\mu$ m paraffin sections using Image-J software. A radioactively labeled  $\alpha$ -BTX binding assay was set up at Neurosearch A/S in Denmark and applied to brain sections from 9-month-old APP/PS1 $\Delta$ E9 and C57Bl6 control mice to evaluate the effect of in vivo A $\beta$  accumulation on  $\alpha 7$  nAChR binding levels in the brain.

### 1.6.6 Functional integrity of immediate early gene responses following novelty stimulation

Immediate-early genes (IEGs) are the first genes to be expressed following synaptic activity, they do not require *de novo* synthesis for expression, and are considered to play a key role in activity-dependent synaptic modification and memory consolidation (Guzowski 2002; Steward and Worley 2002). The activity-regulated cytoskeletal-associated protein (Arc) and the regulatory transcription factor, *c-fos*, are IEG products produced by the corresponding IEGs, *Arc*, and *c-fos*. An especially interesting feature of the Arc protein is that newly synthesized *Arc* mRNA is rapidly delivered into the active synaptic sites based on a targeting signal in the mRNA sequence and is translated locally in the synapse (Wallace et al. 1998). Taking part in the targeting of *Arc* mRNA, N-Methyl-D-Aspartate (NMDA) receptor activation has been shown to be sufficient and necessary to trigger the translocation of *Arc* mRNA into dendrites, and upon translation, the Arc protein forms an integral part of the synaptic junctional complex that also involves the NMDA receptor, which strongly support a role of Arc in synaptic plasticity underlying the consolidation of long-term memory (Steward and Worley 2001). Accordingly, infusion of *Arc* antisense oligonucleotides directly into the hippocampus *in vivo* not only blocked the expression of the corresponding protein, but also disrupted the maintenance of LTP and impaired memory in a spatial maze task (Guzowski et al. 2000). *In vivo*, IEGs take part in encoding observations from the surrounding environment. Thus a five-minute exposure to a novel environment has been shown to dramatically increase the expression of IEGs such as *Arc* and *c-fos* in neurons of the CA1, CA3, and upper DG of the hippocampal formation as well as in the parietal cortex, and medial prefrontal cortex (Chawla et al. 2005; Guzowski et al. 1999; Klebaur et al. 2002; Vazdarjanova and Guzowski 2004; Vazdarjanova et al. 2002). The population of neurons thereby upregulating *Arc* expression in the CA1 has even been shown to be specific for a certain environment, and the induction of IEG expression is therefore thought to be linked to neural encoding processes of the surrounding environment (Guzowski et al. 1999). An inability to upregulate expression of IEGs could thus lead to deficits in cognitive functions and disable the encoding of memories, which could underline part of the functional deficits observed in AD patients showing disturbances in cognitive functions such as memory deficits and orientation in time and space (Reisberg 2006). The present study therefore investigated the ability of APP/PS1 $\Delta$ E9 mice to upregulate the expression of the two IEGs, *Arc* and *c-fos*, upon experiencing a novel

---

environment. The study was performed as cooperation with the group of Mark West at the department of Neurobiology, Anatomical Institute, Aarhus University, Denmark, where 4 groups of 9-month-old APP/PS1 $\Delta$ E9 or C57BL6 wild-type control mice were either decapitated directly from their home-cage or stimulated for 5 min in a novelty paradigm after which they were returned to their home cage for 30 min before decapitation. The levels of *Arc* and *c-fos* mRNA were analyzed at Neurosearch A/S in Denmark by semi-quantitative in situ hybridization and compared to the expression levels of the house keeping gene *synaptophysin*. Because exposure to a novel environment is a light stressor and has been shown to induce the hypothalamic-pituitary-adrenal (HPA) axis, trunk blood was collected for plasma corticosterone quantification and used to verify the effect of the novelty paradigm (Briski 1996; Chandramohan et al. 2007).

## 2 Methods and Materials

### 2.1 *Transgenic mice*

Several mouse models of AD have been applied in the current thesis and their genetic modifications are described in Table 1. The most extensively used mouse model is the APP/PS1KI model which has been described in the introduction (Chapter 1.3.3) and was bred at the University of Göttingen, Germany. All mice designated PS1KI were homozygous for PS1KI mutations, in comparison to the APP/PS1KI mice that were hemizygous for the APP751 isoform carrying the Swedish and London mutations (APP751SL transgene). PS1KI mice showed no pathology or phenotype and were generally used as littermate controls. In the study of axonopathy were applied variations of the APP/PS1KI mouse model. APP mice were hemizygous for the APP751SL transgene, whereas APP/PS1KI<sup>he</sup> and APP/PS1KI<sup>ho</sup> mice additionally carried one or two alleles with the PS1KI mutations, respectively. YFP/APP/PS1KI mice were generated by crossing of APP/PS1KI<sup>he</sup> mice and yellow fluorescent protein (YFP) transgenic mice overexpressing YFP in a proportion of neurons in the brain under the control of the Thy 1 promoter (Feng et al. 2000) (The Jackson Laboratory, US). APP/PS1KI mice were a generous gift of Dr. Laurent Pradier, Sanofi-Aventis, France. Only female mice were applied for stereological quantifications, whereas males were also applied for qualitative immunohistochemical analyses.

APP/PS1 $\Delta$ E9 transgenic mice were hemizygous for the APP and PS1 mutations (Borchelt et al. 1996). Only female mice were applied and non-transgenic wild-type female littermates were used as controls. The mice were bred at the Anatomical Institute, Aarhus University, Denmark, where in vivo experiments were also carried out.

APP/PS1 transgenic mice (Blanchard et al. 2003; Wirths et al. 2002) were hemizygous for both transgenes and three 8-month-old mice were used in the qualitative optimization for intraneuronal A $\beta$ . APP/PS1 mice were a generous gift of Dr. Laurent Pradier, Sanofi-Aventis, France. The 5xFAD mice (Oakley et al. 2006) (The Jackson Laboratory, US) were likewise hemizygous for the APP and PS1 transgenes and three 6-month-old mice were used in the qualitative optimization study.

All animals were handled according to German guidelines for animal care and the European Communities Council Directive European Communities Council Directive of 24 November 1986 (86/609/EEC).

<b>Mouse model</b>	<b>Gene</b>	<b>Protein</b>	<b>Mutations</b>	<b>Promotor</b>
APP/PS1KI	<i>APP</i>	APP751	Swedish (K670N, M671L) and London (V717I)	murine Thy-1
	<i>PSEN1</i>	PS1	M233T and L235P	endogenous PS1
APP	<i>APP</i>	APP751	London (V717I) and Swedish (K670N, M671L)	murine Thy-1
APP/PS1	<i>APP</i>	APP751	Swedish (K670N, M671L) and London (V717I)	murine Thy1
	<i>PSEN1</i>	PS1	M146L	HMG-CoA reductase
5xFAD	<i>APP</i>	APP695	Swedish (K670N, M671L), Florida (I716V), and London (V717I)	murine Thy-1
	<i>PSEN1</i>	PS1	M146L, L286V	murine Thy-1
APP/PS1 $\Delta$ E9	<i>APP</i>	APP695	Swedish (K670N, M671L)	murine prion protein
	<i>PSEN1</i>	PS1	$\Delta$ E9	murine prion protein

**Table 1** Mutations in mouse models specified according to APP isoform, promoter, and amino acid exchange.

### 2.1.1 Genotyping

Genotyping of APP/PS1 $\Delta$ E9 mice was performed at the Anatomical Institute, Aarhus University, Denmark, and analysis of YFP hemizyosity or homozygosity was carried out by quantitative real time polymerase chain reaction (qRT-PCR) explained below. Genotyping of APP/PS1KI, APP/PS1, and 5xFAD mice was performed by a technician in our laboratory and will be briefly explained.

Using specially designed DNA-primers and PCR, a specific gene of interest can be amplified and its presence verified by agarose gel-electrophoresis. The PCR reaction is composed of cycles of brief temperature stages in which different reactions take place. First step is denaturation of the DNA strands at high temperature (95°C) followed by a lower temperature

(50-70°C) at which the oligonucleotide primers are allowed to anneal to the denatured DNA strands. The temperature is then raised to 70-75°C for optimal function of the DNA polymerase which synthesizes new DNA strands. The cycle is then repeated 35-40 times.

For DNA isolation, 500 µL of lysis buffer (100 mM Tris/HCl pH 8.5, 5 mM EDTA, 0.2 % sodium dodecyl sulphate (SDS), 200 mM NaCl, 10µL/mL Proteinase K) were added to mouse tail clippings obtained from the animal facility and shaken overnight at 55 °C and 400 rounds per minute (rpm) in a heating block. Next day, the solutions were centrifuged for 10 min at 13000 rpm and the supernatants were transferred to a new 1.5 mL tube containing 500 µL of isopropanol. Samples were again vortexed and centrifuged for 10 min at 13000 rpm. Pellets were then washed by vortexing in 500 µL of 70% ethanol and centrifuged for 10 min at 13000 rpm. The supernatants were discarded and the pellets dried on a heating block at 37 °C and subsequently dissolved in 70 µl H<sub>2</sub>O (Aqua ad iniectabilia) (37°C, 30 – 45 min or overnight at 4°C).

PCR was then used to exponentially amplify a DNA fragment of the transgene of interest. The reaction was performed in a total volume of 10 µL (0,5 µL 10 pM primer forward, 0,5 µL 10 pM primer reverse, 1 µL 10 x PCR-Puffer, 1 µL 200 µM dNTPs, 5.9 µl H<sub>2</sub>O, 0.1 µL Taq-Polymerase, 1 µL diluted DNA containing 25 ng of genomic DNA) and run with the following cycling parameters: heating at 94°C for 5 min followed by 35 cycles of 94°C for 60 sec, 55°C for 60 sec, and 72°C for 1.5 min mediating denaturing, annealing, and extension of the DNA. The PCR reaction was finished at 72°C for 5 min and stored at 4°C until further processing. Primers targeted the APP transgenes, forward: 5'-GTAGCAGAGGAGGAAGAAGTG-3', revers: 5'-CATGACCTGGGACATTCTG -3' generating a product of either a 505 bp (APP/PS1KI and APP/PS1 mice) or 324 bp (5xFAD mice).

The presence of the desired PCR products was verified by agarose gel-electrophoresis that separates DNA fragments according to size. A 2.5% agarose gel was prepared in a tris-acetate-EDTA (TAE) buffer with 1 µg/mL ethidiumbromide that intercalates into the double-stranded DNA structure and allows visualization of DNA bands by UV-light-transillumination at a wavelength of 366 nm. The 10 µL PCR products were loaded along with a suitable DNA ladder to enable analysis of the size of the separated DNA fragments, each were added an equal volume of loading dye and the gel was run at 170 V. PCR product



bands were visualized in an UV-chamber (Gel-Doc 2000, Bio-Rad) connected to a computer and using QuantityOne software program (Bio-Rad) producing a photo of the gel.

## **2.2 Novelty exposure**

APP/PS1 $\Delta$ E9 and wild-type littermate control mice were divided in 4 groups of 6 animals per cage and housed for 1 week before the experiment. The groups were as follows:

- Group 1: Wild-type non-handled, home-cage controls (n=6)
- Group 2: Wild-type novelty-exposed (n=6)
- Group 3: APP/PS1 $\Delta$ E9 non-handled, home-cage controls (n=6)
- Group 4: APP/PS1 $\Delta$ E9 novelty-exposed (n=6)

The mice to be exposed to novelty were transferred to a box one at a time. The box was 41 x 21 cm and 18 cm high and was made of see through plastic. Red and blue cardboard paper was placed at bottom and sides: blue paper on the longer sides and red at the ends, blue paper was placed underneath the box to be able to clean the box between each mouse. The room was enlightened by standard bright light and the box was placed in the middle of the room so that the mice could look up and find itself in a novel environment. The mice were placed in the box for a total of 5 min, and they were sitting still for more than 5 sec, they were moved to another area of the box by gently pulling them by the tail. The mice were replaced to the home-cage and killed 30 min after novelty-exposure. After each animal, the box was cleaned in 70% ethanol and allowed to evaporate for another 5 min. Non-handled home-cage control animals were taken directly from their cage and care was taken that non-handled animals were not exposed to novelty. All animals were killed by decapitation, trunk blood was collected in EDTA-vials (kept on ice), and brains were immediately removed and directly frozen in crushed dry-ice. Blood samples were centrifuged at 300 rpm for 10 min and plasma was collected and frozen at -20°C. Plasma corticosterone levels were measured directly without prior extraction using a commercial [<sup>125</sup>I]-radioimmunoassay kit (TKRC1, Siemens Medical Solutions Diagnostics).

### **2.3 Tissue collection and preservation**

Tissue is collected and preserved in different ways according to the following analyses. Directly frozen tissue is needed for mRNA and protein extractions as well as for ligand binding and in situ hybridization. For these purposes, mice were either directly killed by decapitation using a sharp scissor or briefly anaesthetized by 1 min exposure to CO<sub>2</sub> in a box with dry-ice and then killed by spinal dislocation and decapitated. Brain and spinal cord tissue was quickly removed and directly frozen on dry ice, and the tissue was kept at -80°C until further processing.

For immunohistochemical staining, the tissue must be preserved by fixation in 4% paraformaldehyde (PFA). The best is to do a perfusion fixation in which the mouse is anesthetized by 10 mL/kg intraperitoneal injection of 1% Ketamin (Pharmanovo GmbH, Hannover, Germany) and 0.1% Xylazin (Riemser, Gristow, Germany) in aqua ad injectabilia. When the mouse is deeply anesthetized transcardial perfusion is carried out through the left ventricle with 30 mL ice-cold phosphate buffered saline (PBS) followed by 30 mL 4% PFA dissolved in PBS. Brains and spinal cords are carefully removed and brains were divided at the midline. Alternatively, the tissue can be directly removed as for direct freezing and then immersion fixed by storage in 4% PFA over night, however, this method does not remove the blood cells as well as the perfusion fixation, which can increase background staining when applying immunohistochemistry. The PFA fixed tissue will be frozen or embedded in paraffin. For fixed frozen tissue preparation, the tissue is post fixed in 4% PFA for at least 2 hrs and then cryo protected in 30% sucrose in PBS overnight. Next day, the tissue is quickly frozen on dry ice and stored at -80°C until further processing. The fixed frozen tissue can be sectioned on a cryostat and was used for free-floating immunohistochemistry as well as for cresyl violet histochemistry. For paraffin embedding, the tissue is post fixed in 4% buffered formalin at 4°C for a minimum of 1 day before the tissue was embedded in paraffin by dehydration in a series of ethanol of 50%, 60%, 70%, 80%, 90%, and 2x 100% followed by Xylol treatment and a final emersion in liquid paraffin for 2 hours before being embedded in solid paraffin blocks. The paraffin embedded tissue was used for immunohistochemistry in thin slices of 2-4µm that gives the best pictures of pathological structures when using a normal transmitted light or fluorescent microscope. The tissue processing is summarized in Table 2.

<b>Tissue preservation</b>		<b>Storage</b>	<b>Analyses</b>
Directly frozen		-80°C	mRNA/protein extraction, radioactive
Fixed tissue	Frozen	-80°C	Free-floating immunohistochemistry and cresyl violet histochemistry
	Paraffin embedded	Room temperature	Immunohistochemistry on glass slide

**Table 2** Summary of tissue preservation, storage, and applied analyses.

### 2.4 Histological staining

Histological structures in tissue can be revealed by using various dyes specific for e.g. cell nucleic proteins or aggregated proteins, however, they can also be revealed by using highly specific antibodies recognizing a target protein of interest. The primary antibody is applied to the tissue of interest and its FC region can then be identified by a secondary antibody generated in another species. The secondary antibody

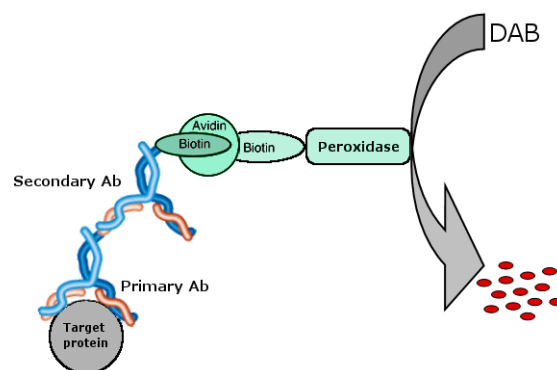


**Fig. 17 The avidin-biotin complex (ABC) method.** A primary antibody (Ab) is used to recognize a target protein, and the substrate diaminobenzidine (DAB) is applied to visualize the protein by a reddish brown color.

can be conjugated directly to different enzymes mediating colorimetric reactions or to fluorescent molecules, or be conjugated to proteins with specific affinities such as the avidin-biotin complex (ABC). In the ABC method, the secondary antibodies are biotinylated. Upon addition of avidin and a peroxidase enzyme bound to biotin, the peroxidase enzyme will be indirectly bound to the secondary antibody. When a colorimetric substrate is added such as DAB, the enzyme mediates accumulation of a reddish brown product (Fig. 17).

Free-floating immunohistochemistry was applied for antibody staining of rather thick sections for stereology or confocal microscope imaging. Immunohistochemistry of paraffin embedded tissue was performed directly on glass slides and was used for qualitative antibody staining as well as Aβ and dystrophic fiber quantifications. Immersion in cresyl violet solution provided a blue staining of nuclei that were used for general quantification of neurons by design-based

stereology, whereas immersion in Thioflavin S was used to visualize aggregated proteins. Primary antibodies applied for immunohistochemistry are specified in Table 3 and secondary antibodies in Table 4.

<b>Target</b>	<b>Name</b>	<b>Host</b>	<b>Dilution</b>	<b>Manufacturer</b>
A $\beta$ 1-x	A $\beta$ [N]	Rabbit	1:200 - 1:1000	IBL, Germany
A $\beta$ 1-x	A $\beta$ N1(D)	Rabbit	1:500	Takaimo Saido, RIKEN Institute, Japan
A $\beta$ 17-24	4G8	Mouse	1:1000 - 1:10.000	Covance, USA
Fibrillar A $\beta$ oligomers	OC	Rabbit	1:200 - 1:2000	Gift of C. Glabe and R. Kaye
A $\beta$ <sub>31-40</sub>	G2-10	Mouse	1:500	Genetics company, Switzerland
A $\beta$ N <sub>3pE</sub>	N3pE	Rabbit	1:500	American Research Products, USA
APP	22C11	Mouse	1:1000	Millipore, Germany
APP	23850	Rabbit	1:500	Gift of Gerd Multhaup
Phosphorylated APP	anti-pT668	Rabbit	1:500	Cell Signalling Technologies, Germany
Neurofilaments	NF-200	Rabbit	1:1000	Millipore, Germany
GFAP	GFAP	Mouse	1:1000	Synaptic Systems, Germany
ChAT	AB144P	Goat	1:300 - 1:1000	Millipore, Schwalbach, Germany
Ubiquitin	Z0458	Rabbit	1:500	DAKO, Denmark

**Table 3** Details of primary antibodies applied for immunohistochemistry. All mouse antibodies were monoclonal, whereas all rabbit and goat antibodies were polyclonal.

<b>Antibody</b>	<b>Product number</b>	<b>Manufacturer</b>
Rabbit anti-mouse immunoglobulins, biotinylated	E0465	DAKO, Denmark
Swine anti-rabbit immunoglobulins, biotinylated	E0353	DAKO, Denmark
Rabbit anti-goat immunoglobulins, biotinylated	E0466	DAKO, Denmark
AlexaFluor568-conjugated immunoglobulins, goat anti-rabbit	A11036	Invitrogen, Germany
AlexaFluor594-conjugated immunoglobulins, donkey anti-goat	A11058	Invitrogen, Germany
AlexaFluor488-conjugated immunoglobulins, chicken anti-rabbit, rabbit anti-mouse	A21441, A11059	Invitrogen, Germany

**Table 4** Details of polyclonal secondary antibodies applied for immunohistochemistry.

### 2.4.1 Free-floating immunohistochemistry

For ChAT stereology, fixed frozen brain tissue was cut on a cryostat in 10 series of 40  $\mu\text{m}$  coronal sections with collection of every 10<sup>th</sup> section throughout the brain. For qualitative evaluation of fiber pathology in YFP mice, the brains were cut in 8 series of 50  $\mu\text{m}$  coronal sections collecting every 8<sup>th</sup> section throughout the forebrain. All sections were stored frozen at  $-80^{\circ}\text{C}$  until further processing. One series from each animal comprising either every 8<sup>th</sup> or 10<sup>th</sup> section was carefully transferred to a net well and stained by free-floating technique with a 12-well net system (Costar, Corning, New York, USA) on a horizontal stirring table providing constant floating of the sections. Sections were hydrated for 15 min in PBS (0.01M, throughout staining techniques) and endogenous peroxidases were blocked in PBS containing 0.3%  $\text{H}_2\text{O}_2$  for 30 min (only for DAB staining). Antigen retrieval was achieved by 10 min incubation in 88% FA (only for  $\text{A}\beta$  staining) followed by thorough washing for 3 x 5 min in PBS. Sections were washed 3 x 10 min in PBS containing 0.1% Triton X-100 for membrane permeabilization, and unspecific binding was blocked by treatment with 4% skim milk powder and 10% fetal calf serum (FCS) in PBS for 1 hour prior to overnight incubation in primary antibodies with 10% FCS in PBS (Table 3). Next day, sections were washed 3 x 10 min in PBS containing 0.1% Triton X-100 followed by 2 hrs incubation with secondary antibodies in 10% FCS in PBS. Following secondary fluorescent antibody incubation, sections were washed 3 x 10 min in PBS, mounted onto super frost glass slides, and left to dry overnight. Following secondary biotinylated antibody incubation, sections were washed 3 x 10 min in PBS and then incubated 1.5 h in ABC Vectastain kit (1:300 in PBS, Vector Laboratories, Burlingame, USA). The staining was finally visualized in a DAB solution (Sigma, Taufkirchen, Germany) of 0.5 mg/mL in Tris/HCl pH 7.5 for 5-10 min providing a reddish brown color. Sections were washed 3 x 10 min in PBS, mounted onto super frost glass slides, and left to dry over night. Next day, sections were rehydrated for 10 min in PBS, after which fluorescent staining were counterstained for 1 min in 1  $\mu\text{g}/\text{ml}$  4'6-diamidine-2'-phenylindole dihydrochloride (DAPI, Sigma, Taufkirchen, Germany) and washed 3 x 5 min in PBS containing 0.1% Triton X-100. Embedding was performed in an aqueous fluorescent protecting mounting medium (Vectashield Hard Set, Linaris, Wertheim, Germany) and upon drying, the edges were sealed with transparent lacquer to prevent evaporation of the mounting medium. DAB stainings were counterstained with hematoxylin for 40s followed by 5 min under running tap water providing a blue staining of nuclei. The sections were then

dehydrated in a series of ethanol (1 min 70%, 5 min 95%, 10 min 100%) and xylol (2 x 5 min) and embedded in Roti-Histokitt mounting medium (Carl Roth GmbH, Germany).

#### **2.4.2 Immunohistochemistry of paraffin embedded sections**

Paraffin embedded fixed tissue blocks were cut on a microtome in 2-4  $\mu\text{m}$  sagittal sections and carefully transferred to a container with double distilled water of room temperature. The sections were collected on super frost glass slides, briefly dipped in a heated water bath containing double distilled water of 52-56°C, and left to dry on a hot plate of same temperature for about 15 min or until the sections had dried. Sections were left overnight at 37°C to dry completely before staining. Glass slides with paraffin embedded sections were deparaffinized 2 x 5 min in xylol and rehydrated in a series of ethanol (10 min 100%, 5 min 95%, 1 min 70%, 1 min H<sub>2</sub>O). Endogenous peroxidases were blocked for 30 min in 0.3% H<sub>2</sub>O<sub>2</sub> in PBS (only for DAB staining), and antigen retrieval was achieved by boiling sections 10 min in 0.01 M citrate buffer pH 6.0 in a microwave after which the sections were left 15 min at room temperature to cool down. Membrane permeabilization was carried out by 3 x 5 min washes in PBS containing 0.1% Triton X-100, followed by antigen retrieval in 88% FA for 3 min (only for A $\beta$  staining). Non-specific binding sites were blocked by 1 hour treatment with 4% skim milk and 10% FCS in PBS, prior to over night incubation in a humid chamber at room temperature with primary antibodies (Table 3) in PBS containing 10% FCS. Next day, sections were washed 3 x 5 min in PBS containing 0.1% Triton X-100 and incubated with secondary antibodies (DAKO, Glostrup, DK) at 37°C for 1 hour (DAB staining) or 1.5 hrs (fluorescent staining). Following secondary fluorescent antibody incubation, sections were washed 3 x 5 min in PBS, directly counterstained for 1 min in DAPI, washed 2 x 3 min in PBS, and embedding in Vectashield aqueous fluorescent protecting mounting medium. Following secondary biotinylated antibody incubation, sections were washed 3 x 5 min in PBS and incubated 1.5 h in ABC Vectastain kit (1:100) at 37°C. The staining was finally visualized in a 0.5 mg/mL DAB solution in Tris/HCl pH 7.5 for 1-5 min providing a reddish brown color, followed by 3 x 5 min PBS washes. DAB staining were counterstained with hematoxylin for 40s followed by 5 min under running tap water, and sections were dehydrated in a series of ethanol (1 min 70%, 5 min 95%, 10 min 100%) and xylol (2 x 5 min) and embedded in Roti-Histokitt mounting medium. For double ABC staining, DAB visualization was followed by repetition of the protocol from the blocking step in 4% skim milk applying a

second primary antibody produced in a species different from the first. The second primary antibody was visualized using the ABC method with Vectastain kit, however, with the HistoGreen kit (Linaris, Germany) as chromogen providing a blue color.

To prevent autofluorescence from lipofuscin, 20 min incubation was performed in a saturated Sudan Black B solution of 1g dissolved in 200 ml methanol following antigen retrieval in FA prior to non-specific blocking in 4% skim milk.

### **2.4.3 Thioflavin-S staining**

Thioflavin-S is a fluorescent dye that binds to aggregated  $\beta$ -sheet conformations thus labeling aggregated forms of A $\beta$ , but not monomers or dimers (LeVine 1993). The staining was performed in paraffin embedded sections with 1% Thioflavin S (Sigma, Taufkirchen, Germany) dissolved in distilled water. The sections were deparaffinized and rehydrated as for the immunostaining, washed 2 x 1 min in distilled water and immersed for 8 min in the Thioflavin S solution. Sections were then washed 2 x 1 min in distilled water and once more immersed for 4 min in the Thioflavin S solution. The last incubation was followed by 2 x 1 min washes in 80% ethanol and 3 x 1 min washes in distilled water before being counterstained with DAPI and embedding in Vectashield aqueous fluorescent protecting mounting medium.

### **2.4.4 Cresyl violet histochemistry**

For neuronal stereology, fixed frozen brains were cut in 10 series of 30  $\mu$ m coronal sections with collection of every 10<sup>th</sup> section throughout the brain and stored frozen at -80°C until further processing. One series comprising every 10<sup>th</sup> section from each animal was carefully mounted in PBS onto super frost glass slides. When dried, sections were washed 2 x 10 min in 0.04 M Sodiumacetate/0.1% acetic acid solution (B1), delipidated 20 min in 0.025% Triton X-100/75% ethanol, washed 2 x 10 min in B1 and stained for 2 x 8 min in 0.01% cresyl violet dissolved in B1. The sections were then washed 3 x 1 min in B1, 3 min in 100% ethanol, 10 min in isopropanol, and 2 x 5 min in xylol before being embedded in Roti-Histokitt mounting medium.

## **2.5 Microscopy and photography**

Photomicrographs were taken using an Olympus BX51 microscope equipped with an Olympus DP-50 digital camera. Final figures were constructed using Image-J (NIH, USA) and GIMP 2.6 software and only minor adjustments of contrast and brightness were made, which in no case altered the appearance of the original images.

Confocal microscopy was performed in cooperation with the Max Planck Institute for Experimental Medicine, Göttingen. Images were acquired with a Leica SP2 laser scanning confocal microscope equipped with an acousto-optical beam splitter (Leica, Germany) using a 63x/1.4 oil-immersion objective. The 405-nm line of a blue laser diode (DAPI), 488-nm line of an argon laser (YFP), and 561-nm line of a DPSS laser (AlexaFluor568) were used at 40%, 5-10%, and 5-10% power, respectively. Reasonable detector gains were used between 550 and 650 AU in the Leica LSC software. Pictures were processed in Image-J using a Median filter to smoothen the images.

## **2.6 Quantification of plaque independent dystrophic neurites**

For each animal, two series of three paraffin embedded sections at least 25  $\mu\text{m}$  apart were stained simultaneously using either the NF-200 or anti-pT668 antibodies with DAB as chromogen, followed by an ABC staining with the 4G8 antibody using Histogreen as chromogen marking A $\beta$  plaques in blue. Quantification of plaque-independent dystrophic neurites was performed using the meander scan option of StereoInvestigator 7 (MicroBrightField) and a BX51 microscope (Olympus) to count dystrophic fibers larger than 10  $\mu\text{m}$  that were not plaque-associated. The average of the counting from the three sections per animal was used for statistical analyzes. Quantifications were performed in two regions; pons and spinal cord as these regions had obvious dystrophic fiber pathology together with moderate plaque pathology, making it possible to distinguish plaque-associated from plaque-independent axonal swellings. Quantification was performed in 6 mice of each of the genotypes APP, APP/PS1KI<sup>he</sup>, and APP/PS1KI<sup>ho</sup>.



## 2.7 Quantification of Aβ staining

For each animal, 5 paraffin embedded sections at least 25 μm apart were stained simultaneously for Aβ immunoreactivity using DAB as chromogen. Micrographs of the Aβ staining were systematically captured in the region of interest with an Olympus BX-51 microscope equipped with an Olympus DP-50 camera. Using the ImageJ software (NIH, USA), pictures were binarized to 8-bit black and white pictures, a fixed intensity threshold was applied defining the DAB staining, and the percentile area covered by Aβ DAB staining was calculated together with the number and size of Aβ grains.

## 2.8 Stereology

Stereological counting procedures were developed in order to estimate a massive amount of cells in the brain in an unbiased systematic random fashion without considering size, shape and orientation of the cells being counted. Thus quantification of neurons can be obtained by the optical fractionator stereological method (Fig. 18), where the “fractionator” is the systematic

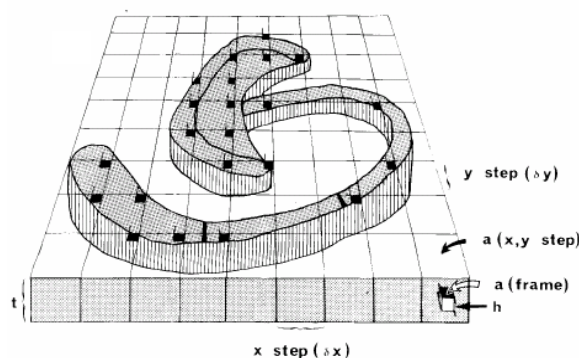


**Fig. 18 The optical dissector method.** An optical dissector with areal (a) and height (h) is defined by a superimposed counting frame (x,y) (West et al. 1991).

random sampling of sections, sampling e.g. every 10<sup>th</sup> with random selection of the first section in the area of interest, and the “optical dissector” is a three-dimensional probe associated with a set of rules for counting neurons (West 1993; West et al. 1991). In practise, an unbiased counting frame divided in grids is superimposed on the section being counted. The optical dissector is systematically applied to the grid taking up a defined area (a<sub>frame</sub>) of the grid area (a<sub>step</sub>). The optical dissector probe is three dimensional, and when counting through the thickness (t) of the section, guard zones of e.g. 2 μm can be left uncounted near the surfaces and counting is then performed within a certain dissector height (h) being less or equal to t. According to the principle of stereology (Schmitz and Hof 2005; West 2002; West et al. 1991), the total number of neurons (N) in an area of interest can be estimated by:

$$N = \sum Q^- \cdot \frac{1}{ssf} \cdot \frac{1}{asf} \cdot \frac{1}{tsf}$$

Where  $\sum Q^-$  is the sum of the neurons counted by the optical fractionator in the area of interest. The remaining stereological parameters are explained in Table 5.

Two overall quantifications were performed: One of ChAT-positive neurons throughout the brain cholinergic system, and another of

<b>Stereological parameters:</b>	
<i>ssf</i>	Fraction of sections sampled
<i>asf</i>	Fraction of area of sections sampled
<i>tsf</i>	Fraction of sections thickness sampled (h/t), $\mu\text{m}$
<i>a<sub>frame</sub></i>	Area of optical dissector counting frame, $\mu\text{m}^2$
<i>a<sub>step</sub></i>	Area associated with movement to next frame, $\mu\text{m}^2$
<i>h</i>	Height of optical dissector, $\mu\text{m}$
<i>t</i>	Section thickness, $\mu\text{m}$
<i>CE</i>	Coefficient of error

**Table 5** Definition of stereological parameters.

cresyl-violet stained neurons. The optical fractionator method was applied by probes constructed to count approximately 300-400 cells in each region for each animal resulting in coefficient of errors around 0.05, and the quantification was performed by an observer blinded to the genotype of the animals using StereoInvestigator 7 (MicroBrightfield) together with a BX51 microscope (Olympus). Only female mice were quantified, and the number of mice in each group is given directly in the graphs of the respective results chapters.

For quantification of ChAT-positive neurons, frozen fixed hemispheres were cut in 10 series of 40  $\mu\text{m}$  coronal sections that were systematically collected resulting in 10 series containing every 10th section throughout the forebrain to the ventral hippocampus (bregma 2.22 mm  $\rightarrow$  -3.64 mm) (Paxinos and Franklin 2001). The posterior brains were cut throughout in 40  $\mu\text{m}$  with collection of all sections (bregma -3.64 mm  $\rightarrow$  -6.84 mm) (Paxinos and Franklin 2001).

The following brain regions were selected for quantification: The caudate putamen (CPu); Ch1/2 comprising the medial septum and the vertical limb of the diagonal band; Ch4 comprising the horizontal limb of the diagonal band, the ventral pallidum, the basal nucleus, and substantia innominata; as well as the brainstem motor nuclei Mo5 and 7N. The identification of a neuron was

	<b>CPu</b>	<b>Ch1/2</b>	<b>Ch4</b>	<b>Mo5</b>	<b>7N</b>
<i>ssf</i>	10	5	10	1	1
<i>asf</i>	0.38	1	0.44	0.33	
<i>tsf</i>	1	1	1	1	1
<i>a<sub>frames</sub></i> $\mu\text{m}^2$	34500	28000	10000	10000	5625
<i>a<sub>grid</sub></i> $\mu\text{m}^2$	90000	28000	22500	30000	40000
<i>h</i> , $\mu\text{m}$	18.2	14.8	17.7	16.9	17.3
<i>t</i> , $\mu\text{m}$	18.2	14.8	17.7	16.9	17.3
<i>Sec.counted</i>	11	8	7	20	27
<i>CE</i>	0.040	0.09	0.052	0.052	0.046

**Table 6** Sampling scheme for stereological analysis of the cholinergic system. CE, t, and tsf are average values. Sec.counted is average number of sections counted per animal.

performed on the basis of the typical shape of a neuron with at least one visible process. The stereological parameters of the counting are given in Table 6.

Stereological quantification of neurons in the frontal cortex and thalamus was performed in 30  $\mu\text{m}$  cresyl-violet stained frozen hemisphere sections systematically collected in 10 series containing every 10th section throughout the brain. Neurons were identified based on their typical morphology with large nuclei. The frontal cortex was quantified from Bregma 3.08 to 0.26 (Paxinos and Franklin 2001), and the thalamus was quantified from Bregma -0.94 to -2.54 (Paxinos and Franklin 2001). Stereological parameters for the counting are given in Table 7.

	<i>Frontal cortex</i>	<i>Thalamus</i>
<i>ssf</i>	10	10
<i>asf</i>	0.00357	0.0246
<i>tsf</i>	0.61	0.65
$a_{frame}$ , $\mu\text{m}^2$	625	1600
$a_{grid}$ , $\mu\text{m}^2$	175000	65000
$h$ , $\mu\text{m}$	6	6
$t$ , $\mu\text{m}$	9.8	9.3
<i>Sec.counted</i>	11	6
<i>CE</i>	0.045	0.045

**Table 7** Sampling scheme for stereological analysis of neurons in the frontal cortex and thalamus. CE, t, and tsf are average values, and sec.counted gives the average number of sections counted per animal.

## 2.9 qRT-PCR

Assesment of gene dosage was carried out using qRT-PCR in YFP transgenic mice to identify homozygous mice for the breeding with APP/PS1KI<sup>he</sup> mice. In qRT-PCR, mRNA or DNA is purified from a sample of interest, and for analysis of mRNA, reverse transcription is performed to generate cDNA. A PCR reaction is initiated and continuously monitored by the incorporation of a dye that becomes fluorescent when incorporated into the PCR product as the reaction proceeds. The fluorescence of the sample correlates with the concentration of amplified product and is continuously plotted as a function of cycle number. As the amount of PCR product increases exponentially with time, the fluorescent will start to rise dramatically after a certain amount of cycles. The Threshold cycle ( $C_T$ ) is the cycle value at which a statistically significant increase in fluorescence is first detected. The  $C_T$  value is of a continuous scale and at this cycle, the concentration of the amplified gene will be the same in all samples, assuming the efficiency of the amplification is the same in all tubes. The lower the amount of starting DNA, the longer time it will take for the fluorescence to reach

threshold level and thus the higher the  $C_T$  value. Based on measured  $C_T$  values, the expression level of a gene or gene dosage can be quantified.

DNA isolation was performed from mouse tail biopsies in 500  $\mu\text{L}$  of lysis buffer (100 mM Tris/HCl pH 8.5, 5 mM EDTA, 0.2 % SDS, 200 mM NaCl, 10 $\mu\text{L}/\text{mL}$  Proteinase K) and shaken overnight at 55 °C and 400 rpm in a heating block. Next day, the solutions were centrifuged for 10 min at 13000 rpm and the supernatants were transferred to a new 1.5 mL tube containing 500  $\mu\text{L}$  of isopropanole. Samples were again vortexed and centrifuged for 10 min at 13000 rpm. Pellets were then washed by vortexing in 500  $\mu\text{L}$  of 70% ethanol and centrifuged for 10 min at 13000 rpm. The supernatants were discarded and the pellets dried on a heating block at 37 °C and subsequently dissolved in 70  $\mu\text{l}$   $\text{H}_2\text{O}$  (Aqua ad iniectabilia) (37°C, 30 – 45 min or overnight at 4°C).

qRT-PCR was performed using a Stratagene MX3000P Real-Time Cycler and 10 ng of DNA was used per reaction. For quantification of the PCR product was applied the SYBR-green based 2x SensiMix DNA Kit containing ROX as an internal reference dye (peqLab, Germany). Measurements of  $C_T$  values were performed in duplicates, and relative quantification was performed using APP as a housekeeping gene normalising the expression level of YFP to that of APP and calibrating it to a chosen YFP heterozygous animal using the  $\Delta\Delta C_T$  method (Livak and Schmittgen 2001):

$$\text{Amount}_{\text{Gene}} = 2^{-\Delta\Delta C_T}$$

For an animal (q) quantifying the level of YFP gene expression normalized to the expression of APP as a reference gene and calibrated to the animal (cb),  $-\Delta\Delta C_T$  is calculated as follows:

$$\Delta C_T = C_{T, YFP} - C_{T, APP}$$

$$-\Delta\Delta C_T = -(\Delta C_{T,q} - \Delta C_{T,cb})$$

An example of the identification of homozygous animals by qRT-PCR is given in Fig. 19. YFP and APP amplification efficiencies were analysed and found to be equal.

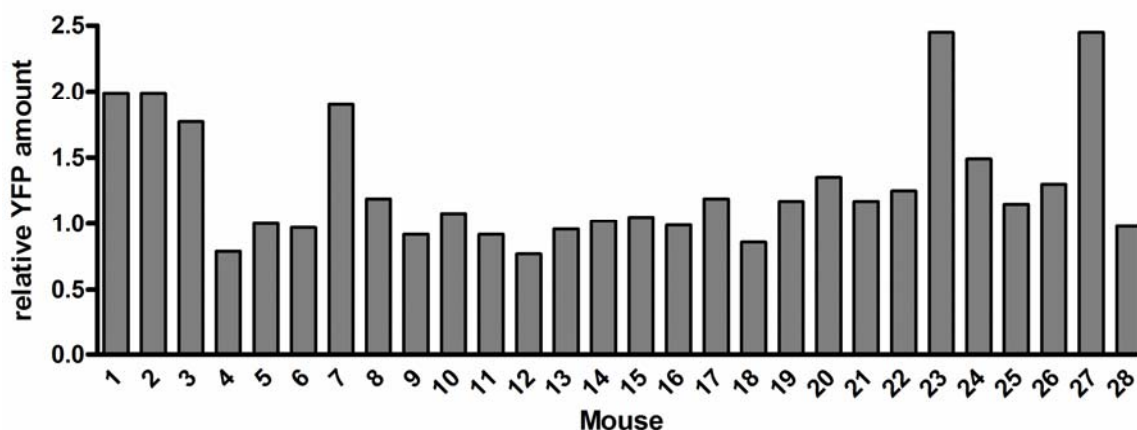


**Fig. 19 Identification of homozygous YFP animals by RT q-PCR.** The YFP expression is quantified relative to APP. All animals were calibrated according to mouse number 5. Mouse 1, 2, 3, 7, 23, and 27 were identified as homozygous for YFP, whereas the rest were considered to be heterozygous.

## 2.10 Western blot

Proteins can be separated based on their size by SDS polyacrylamide gel electrophoresis (SDS-PAGE) in which protein samples are loaded in equal amounts onto the gel. SDS is an anionic detergent that denatures secondary and non-disulfide-linked tertiary structures, and applies a negative charge to each protein in proportion to its mass as smaller proteins travel faster. Thus when an electric field is applied over the gel, the proteins will be separated based on their size. The proteins can then be blotted onto a nitrocellulose membrane where antibodies can be applied to recognize specific proteins of interest. Secondary antibodies proteins conjugated to horseradish peroxidase (HRP) can be used to visualize the proteins as HRP oxidizes amongst others luminol, after which protein bands can be detected by light sensitive films.

Qualitative western blots were made for two proteins: APP and ubiquitin. As ubiquitin is attached to many proteins of varying size, the protocol was varied to extract a higher proportion of high-molecular weight proteins. Directly frozen brain hemispheres stored at -80 °C were homogenized using 10 strokes of a glass Teflon homogenizer at 800 rpm in 150 mM NaCl, 50 mM Tris, 1% Triton X-100, 5 mM EDTA, pH 7.6 extraction buffer, supplemented with complete protease inhibitor cocktail (Roche, Germany). The amount of buffer was adjusted to the brain weight in a 10:1 ratio. Lysates were centrifuged at 4°C and 13.000 rpm

for 30 min, and the supernatant was collected and stored at  $-80^{\circ}\text{C}$  for quantification of soluble proteins. The pellets were dissolved in 0.01 M PBS buffer containing 2% SDS, pH 7.4 and homogenized on ice using a Branson Ultrasound Homogenizer followed by centrifugation at  $4^{\circ}\text{C}$  and 17,000 rpm for 30 min to obtain the SDS-soluble fraction. Protein concentrations were measured by the commercially available Roti-Quant universal solution (C. Roth, Germany). Of each sample, 20  $\mu\text{g}$  (APP) or 50  $\mu\text{g}$  (ubiquitin) proteins as well as 5  $\mu\text{L}$  color plus prestained protein marker (BioLabs, England) were mixed 1:1 with Vario loading buffer (Anamed Elektrophorese, Germany) and heated for 4 min at  $95^{\circ}\text{C}$ , after which they were loaded onto precast 4-12% vario gels (Anamed Elektrophorese, Germany) and run in Vario running buffer for approximately 45 min at 200 V. Proteins were transferred to nitrocellulose membranes (Hybond-ECL, Amersham Biosciences, USA) using either semidry blotting for 30 min at 25 V or wet blotting for 2 hr at 25 V in 48 mM Tris, 39 mM glycine, and 20% methanol, pH 9.2 transfer buffer. Membranes were blocked in 10% non-fat dry milk in Tris buffered saline buffer (0.01 M Tris, 0.15 M NaCl) containing 0.05% Tween-20 (TBS-T), pH=8.0 (TBS-T) for 1 hour. Monoclonal mouse anti-APP (1:5000, 22C11) or rabbit anti-ubiquitin (1:5000, DAKO, Denmark) primary antibodies were applied overnight in TBS-T buffer at  $4^{\circ}\text{C}$  followed by a 2 hrs incubation with goat anti-mouse or swine anti-rabbit HRP-conjugated secondary antibodies (1:3000, DAKO, Denmark) at room temperature. Blots were developed using light sensitive X-ray films and a 0.25 mg/mL luminol solution in 0.1 M Tris/HCl, pH 8.6 together with a 1.1 mg/mL para-hydroxycoumarine acid solution in DMSO mixed 9:1 just before use and with the addition of 0.03%  $\text{H}_2\text{O}_2$ . A mouse monoclonal  $\beta$ -Actin antibody (1:5000, Chemicon, USA) was used as a reference protein to assure equal loading of the samples.

### **2.11 Radioactive ligand binding**

The level of receptors expressed in a tissue can be semi-quantified using receptor autoradiography that can be conducted in tissue homogenates or in tissue slides in which the latter offers the advantage of anatomical resolution and was the method of choice in this thesis (Kuhar et al. 1990). The basic principle of receptor autoradiography is the addition of a radioactively labelled ligand (radioligand) that binds to the receptor of interest. The amount of bound radioactivity in the tissue will then be proportional to the amount of receptors. Non-

specific binding (NSB) to glass surfaces etc., is determined by displacing the radioligand with an excessive amount of non-labeled receptor ligand and is subtracted from the total binding resulting in the specific binding.

Directly frozen half brains were cut in 12  $\mu\text{m}$  serial coronal sections on a cryostat and directly mounted onto super frost glass slides. Sections were collected in parallel series with 4 sections per glass slide throughout the prefrontal cortex (8 series, bregma 1.98 mm) (Paxinos and Franklin 2001) and the dorsal hippocampal region (15 series, bregma -1.46 mm  $\rightarrow$  -2.18 mm) (Paxinos and Franklin 2001). Two slides from each animal were dried at room temperature for 30 min, followed by 30 min hydration in 50 mM Tris buffer, pH 7.3 (binding buffer). Slides were incubated 2 hrs in binding buffer with 0.5 nM [ $^{125}\text{I}$ ]Tyr54-mono-iodo- $\alpha$ -bungarotoxin (2,200Ci/mmol, #NEX126H, Perkin Elmer, DK) to assess total binding. For analysis of non-specific binding, incubation was performed together with 1 mM (-)-nicotine (#N5260, Sigma-Aldrich, DK). After the incubation, slides were dipped in buffer, followed by 2 x 30 min wash in ice-cold buffer. Finally, slides were rinsed briefly in ice-cold distilled water, dried for 24 hrs, and exposed to a radioactive sensitive Kodak Biomax MS film (GE Healthcare) for 24 hrs. Optical densities were measured using Quantity One software (BioRad) by bilateral delineation of PFC in at least two sections per animal and of the hippocampal formation in at least three sections per animal. Specific  $\alpha$ -BTX binding was calculated by subtracting non-specific binding from total binding.

## **2.12 *In situ hybridization***

The expression level of a particular gene expressed in a tissue can be semi-quantified using *in situ hybridisation* in which a radioactively labeled probe is applied to tissue sections. The amount of bound radioactivity in the tissue will then be proportional to the mRNA produced by the target gene.

Twelve- $\mu\text{m}$  parallel coronal brain sections were cut through the PFC, and the dorsal hippocampus as explained in the chapter of radioactive ligand binding (2.11). One glass slide with four brain sections from each animal was processed in the same experiment for one transcript to achieve the highest level of standardization. The slides were incubated for 5 min in 4% PFA in 0.2 M PBS, and then washed twice for 1 min in PBS. This was followed by acetylation (0.25% acetic anhydride, 0.1 M triethanolamine in 0.9% NaCl, pH 8.0) for 10 min

at room temperature. The slides were then delipidated and dehydrated in a series of ethanol (70%/5 min; 80%/1 min; 95%/2 min; and 99%/1 min) and finally incubated for 5 min in chloroform. Excessive chloroform was washed off the slides in 99% and 96% ethanol, and the slides were air-dried. Synthetic oligonucleotide DNA probes complimentary to the rat *Arc* mRNA (targeting bases 789-839; Genbank accession number: NM019361), *c-fos* (targeting bases 133-180; Genbank accession number: X06769), *synaptophysin* (codon 131-175, TGT TGG CAC ACT CCA CGC TCA GCC GAA GCT CCC CGG TGT AGC TGC), and *PSD-95* (codon 383-393, GTT TAT ACT GAG CGA TGA TCG TGA CCG TCT GAC CC) genes were applied (DNA Technology, Risskov, Denmark). The probes were labeled at the 3'-end with  $\alpha$ [<sup>35</sup>S]-dATP (>3000 Ci/mmol, Amersham Bioscience) using terminal transferase. Labeled probe was added at a specific activity of 10<sup>6</sup> cpm/100  $\mu$ L to the hybridisation buffer containing 45% formamid (v/v), 4X saline sodium citrate (SSC) (1XSSC is 0.15M NaCl, 0,015M NaCitrate\*2H<sub>2</sub>O, pH 7.2), 1X Denhardtts solution (0,02% ficoll, polyvinylpyrrolidone and BSA), salmon sperm ssDNA (0.5 mg/ml), 0.25 mg/mL yeast transfer RNA, 10% (w/v) dextran sulfate, and 10 mM dithiotreitol. After incubation overnight (37°C), the sections were initially transferred to 4 rapid consecutive washes in 1XSSC (room temperature) and then washed 4 times 15 min in 1XSSC (55°C) and 2 times 30 min in 1XSSC at room temperature. Finally, the sections were air dried and exposed together with [<sup>14</sup>C]-standards to a Kodak Biomax MR film (Amersham Bioescience) for 8-14 days. Optical densities were quantified in medial PFC, CA1, CA3, upper DG, and parietal cortex (S1) using Quantity One software (BioRad) performed by an observer blinded to the genotype and treatment of the animals. The optical densities were converted to nCi/g tissue using the [<sup>14</sup>C]-standards and the individual values for each animal were calculated as the average of three sections measured within the areas of interest. A background measurement outside the sections was subtracted from each measurement.

### **2.13 AD brain tissue**

Familial Swedish and Arctic brain tissue was kindly provided by Lars Lannfelt, Uppsalla University, Sweden. Sporadic AD brain tissue was supplied from the Netherlands Brain Bank, Amsterdam, The Netherlands.



## **2.14 Statistical analysis**

Data were analyzed using unpaired t-tests, two-way analysis of variance (ANOVA) or one-way ANOVA followed by post-hoc tests as specified in the figure legends of the results chapter (3). Data are presented as mean  $\pm$  s.e.m. Significance levels were given as follows: \*\*\* $P < 0.001$ ; \*\* $P < 0.01$ ; \* $P < 0.05$ . All statistical analyses were conducted using GraphPad Prism version 4.03 for Windows (GraphPad Software, San Diego, CA, USA).

The correlation analysis between intraneuronal A $\beta$  and the following parameters was performed by Thomas Schneider-Axmann. Diagnosis, gender, age, brain weight, post-mortem delay, number of ApoE4 alleles, and Braak stage data were supplied directly from the Brain bank. Atherosclerosis and plaque stage were extracted from a document describing the patients' disease history and post-mortem examination.

Kolmogorov-Smirnov test was applied to examine which variables showed significant deviations from normal distribution. Most of the parameters, especially intraneuronal A $\beta$ , showed significant deviation from normal distribution and thus the following tests are non-parametric. Non-linear Spearman correlations were used to analyze the correlation between intraneuronal A $\beta$  and atherosclerosis, followed by Spearman rank correlations between intraneuronal A $\beta$  and age, brain weight, and post-mortem delay. Non-parametric Mann Whitney U test was performed between intraneuronal A $\beta$  and the factors gender, diagnosis and number of ApoE 4 alleles. Non-parametric Kruskal Wallis tests were performed between intraneuronal A $\beta$  and Braak stage and plaque stage, where subgroup analysis between two groups was performed with Mann Whitney U tests. As the study is explorative, the p-values are given without Bonferroni adjustments.

### 3 Results

The background of the individual experiments is described in chapter 1.6. The details of the methods applied are given in the previous section. The results are discussed separately in section 4, and a final unified conclusion is given in section 5.

#### 3.1 Neuron loss in the cholinergic system of APP/PS1KI mice

##### Cholinergic pathology

To initially characterize cholinergic fiber pathology in the APP/PS1KI mice, staining for ChAT was qualitatively analyzed in relation to A $\beta$  deposition throughout the brain in a double ABC staining in paraffin embedded sections. ChAT-positive dystrophic neurites, which are swollen neuronal processes, were found to decorate amyloid plaques in the cortex and thalamus (Fig. 20A, B) as well as in the hippocampal formation occasionally disrupting the granular cell layer of the DG (Fig. 20C). This pathology starts already at 2 months of age, but is most abundant in 6- to 10-month-old mice. At later time points, ChAT-positive axonal varicosities independent of plaques were detected in some brain regions e.g. in the lateral septum (Fig. 20D, E), probably indicating axonal transport disturbance. Strong plaque associated

ChAT-positive dystrophic neurites were also detected in the striatum; whereas control animals were consistently negative (Fig. 20F, G).

To examine A $\beta$ -related effects on the number of cholinergic neurons in the present APP/PS1KI mouse model, we analyzed the expression pattern of the human mutant APP transgene and the associated A $\beta$  deposition in the brain

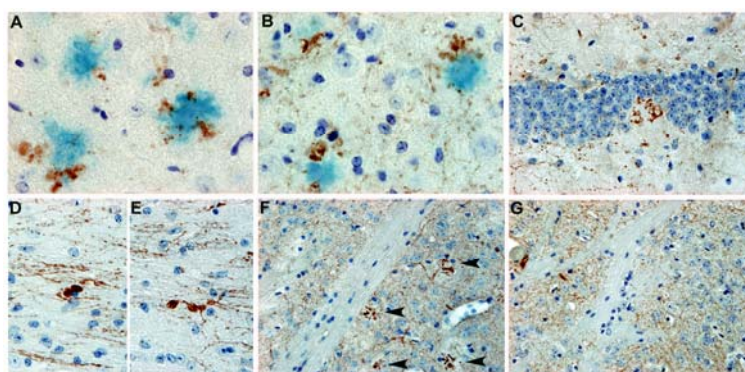


**Fig. 20 Cholinergic fiber pathology in APP/PS1KI mice.** Six to 10 months old APP/PS1KI mice showed ChAT-positive dystrophic neurites (reddish brown) decorating A $\beta$ [N]-positive amyloid plaques (blue) in the cortex (A) and thalamus (B), as well as occasionally in the granular cell layer of the dentate gyrus (C). ChAT-positive axonal varicosities independent of plaques were detected e.g. in the lateral septum (D, E). Strong plaque-associated ChAT-positive neurites were also detected in the striatum (F); whereas control animals were consistently negative (G). Scale bars: (A, B) 20  $\mu$ m, (C - E) 33  $\mu$ m, (F, G) 50  $\mu$ m.

cholinergic system by double-labeled fluorescent immunohistochemistry. In the brain cholinergic system, human APP was found to be expressed in motor nuclei of the brain stem that also accumulated intracellular A $\beta$  peptides (Fig. 21M - P). In contrast, no APP expression and almost no deposition of A $\beta$  plaques was observed in either of the two cholinergic projecting nuclei groups of the brain, the forebrain (Ch1-Ch4, Fig. 21K, L) and pons (Ch5-Ch6, Fig. 21I, J) complexes. However, fibers from these nuclei were severely affected as many plaques surrounded by cholinergic dystrophic neurites could be found in their projecting areas: cortex, hippocampus, and thalamus (Fig. 21A - F). The APP transgene was also found not to be expressed in the cholinergic interneurons of the caudate putamen, a region containing numerous smaller plaques and dystrophic neurites (Fig. 21G, H). Thus in the brain cholinergic system, only motor nuclei of the brain stem were found to express the APP transgene and consequently accumulate intracellular A $\beta$  peptides (Fig. 21N- P). Of the motor nuclei in the brain stem, Mo5 and 7N are fairly large and were chosen for stereological

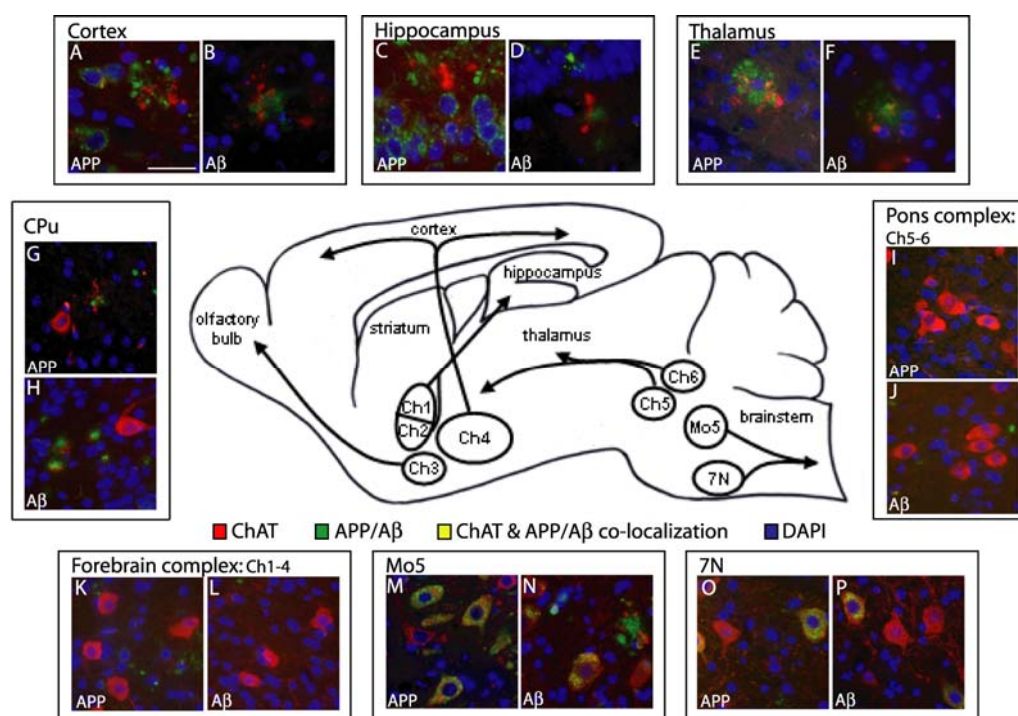


**Fig. 21 Expression of APP transgene and A $\beta_{1-x}$  deposition in the cholinergic system of APP/PS1KI mice.**

In 6-month old APP/PS1KI mice, ChAT is visualized in red, APP and A $\beta_{1-x}$  in green using the 23850 and A $\beta$ [N] antibodies, respectively, and cell nuclei in blue by DAPI staining. Cholinergic dystrophic neurites were found surrounding plaques in the cortex (A, B), hippocampus (CA1; C, D), and thalamus (E, F). No expression of the APP transgene or accumulation of intracellular A $\beta$  was observed in either the forebrain (K, L) or pons (I, J) complex. The same held true for the cholinergic interneurons of the caudate putamen (CPu: G, H). However, cholinergic neurons of the motor nuclei Mo5 and 7N were found to express the APP transgene (M, N) and accumulate intracellular A $\beta$  (N, P). Scale bars: (A-F) 33  $\mu$ m, (G-P) 50  $\mu$ m.

quantification representing areas with accumulation of intracellular A $\beta$ . In comparison, the forebrain cholinergic neurons projecting to the hippocampus (Ch1/2) and cortex (Ch4) were chosen representing areas with cholinergic fiber pathology, and the interneurons of the caudate putamen of the striatum were chosen representing an area with cholinergic fiber pathology as well as extracellular A $\beta$  plaque deposition surrounding the neuron bodies, however, without any intracellular A $\beta$  accumulation.

### Analysis of cholinergic neuron numbers

Cholinergic neuron numbers were quantified by stereology at 2, 6, and 12 months of age in APP/PS1KI and PS1KI control mice by counting ChAT-positive neurons in caudate putamen, the forebrain complex (Ch1/2 and Ch4), and in the two motor nuclei: Mo5 and 7N (Fig. 22A). Depending on age and genotype as cofactors, quantification revealed no changes in the number of cholinergic neurons in the caudate putamen or in any of the cholinergic projecting nuclei of the forebrain complex (Ch1/2, Ch4) (Fig. 23A - C). In contrast, Mo5 and 7N accumulating intracellular A $\beta$  peptides showed a significant loss of cholinergic neurons in the APP/PS1KI mice. Thus the number of cholinergic neurons was decreased by 27% in the Mo5 already at 6 months of age ( $P < 0.001$ ) and by 33% at the age of 12 months ( $P < 0.001$ ), whereas the cholinergic neuron number in the 7N was significantly decreased only at 12 months of age (-19%;  $P < 0.01$ ) (Fig. 23D, E).

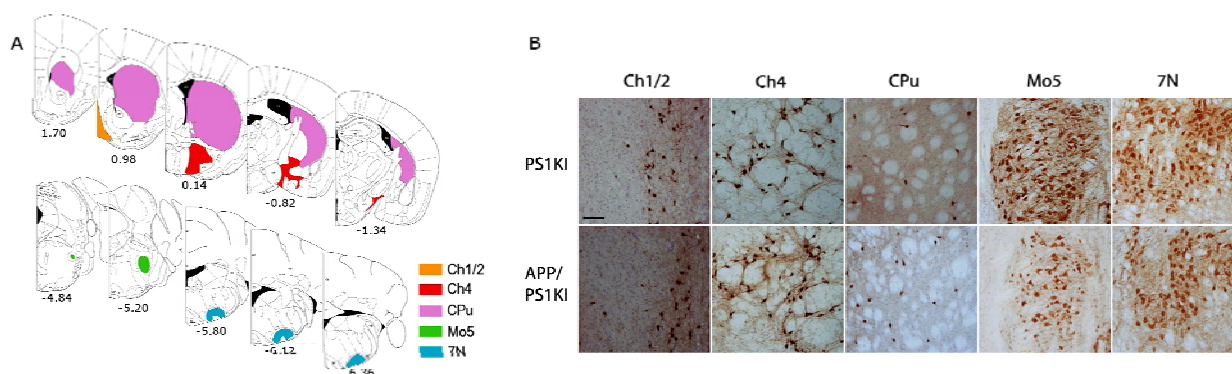


**Fig. 22 Definition of counting areas.** A) Schematic presentation of stereologically quantified cholinergic areas: Caudate putamen (CPu, Bregma 1.70 to -2.30 mm), Ch1/2 comprising the medial septal nucleus and vertical limb of the diagonal band of Broca (Bregma 1.34 to 0.26 mm), Ch4 comprising the horizontal limb of the diagonal band of Broca, ventral pallidum, nucleus basalis, and substantia innominata (Bregma 0.26 to -1.34 mm), as well as motor nuclei Mo5 (Bregma -4.84 to -5.34) and 7N (Bregma -5.68 to -6.48). Figures were created from the mouse atlas by Paxinos and Franklin (2001) with orientation according to Bregma beneath each section. B) 12-month-old APP/PS1KI and PS1KI control mice showing examples of the free-floating ChAT staining in the quantified regions. Scale bar = 100 $\mu$ m.

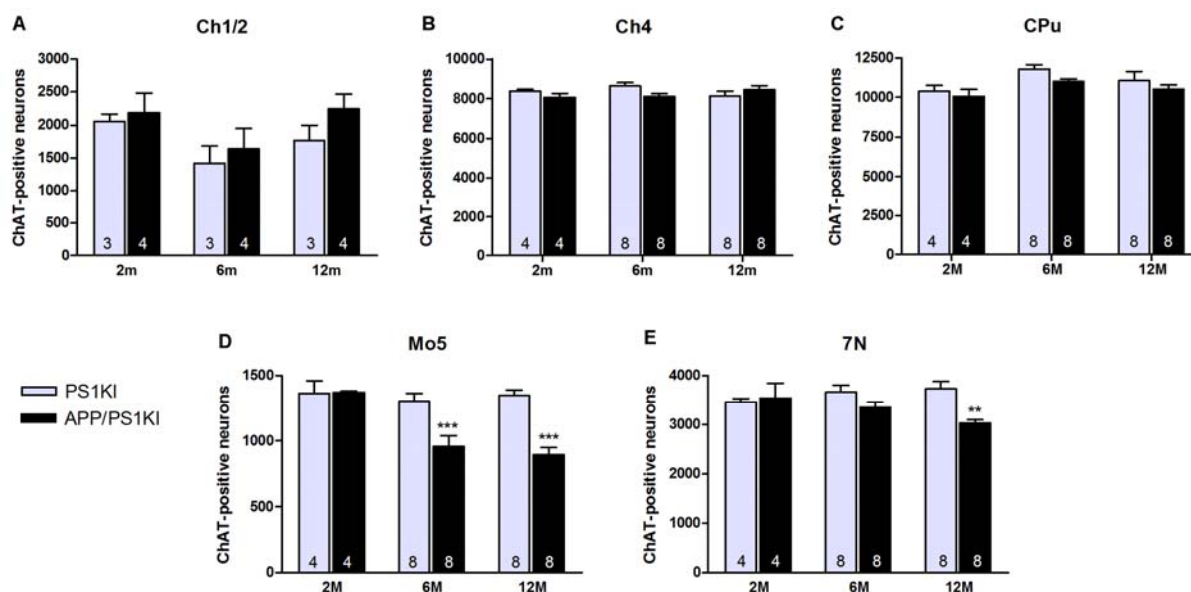


**Fig. 23 Stereological quantification of ChAT-positive neurons in APP/PS1KI mice.** No change in cholinergic neuron numbers was found depending on either age or genotype neither in the hippocampal projecting Ch1/2 nuclei (A), in the cortical projecting Ch4 nuclei of the forebrain complex (B), nor in the cholinergic interneurons of the caudate putamen (C). However, in the motor nuclei of the brain stem, a cholinergic neuron loss in the APP/PS1KI mice compared to the PS1KI control mice was found. In the Mo5 (D), the cell loss was 27% in 6-month-old mice and 33% in 12-month-old mice, whereas the cholinergic neuron number in the 7N was significantly decreased only in 12-month-old mice (E, -19%; P). Data were analyzed using two-way ANOVA followed by Newman-Keuls posthoc test. The number of animals per group is given directly in the bars. All error bars represent mean  $\pm$  s.e.m. \*\*\*P < 0.001; \*\*P < 0.01.

### Intracellular A $\beta$ accumulation and cell death

Loss of cholinergic neurons occurred earlier and to a larger extent in the motor nucleus Mo5 compared to the 7N (Fig. 23D, E). Therefore, a qualitative fluorescent immunohistochemical analysis was carried out in paraffin sections, comparing the accumulation pattern of different A $\beta$  species in the two motor nuclei. The accumulation of intracellular A $\beta_{1-x}$  began earlier and to a larger degree in the Mo5 than in the 7N. This difference in A $\beta_{1-x}$  accumulation was especially evident at 2 and 6 months of age where the Mo5 showed extensive accumulation of A $\beta$  peptides that were virtually absent in the 7N at these time points (Fig. 24A – F, J – O).



This distinction was less evident at 12 months, where substantial intracellular  $A\beta_{1-x}$  accumulation could be detected also in the 7N (Fig. 24P - R). The same held true for fibrillar oligomeric and fibrillar  $A\beta$ , visualized by use of OC antibodies (Kayed et al. 2007) (Fig. 25A - C, G - I), as well as for highly aggregated  $A\beta$  visualized by use of the amyloid binding dye

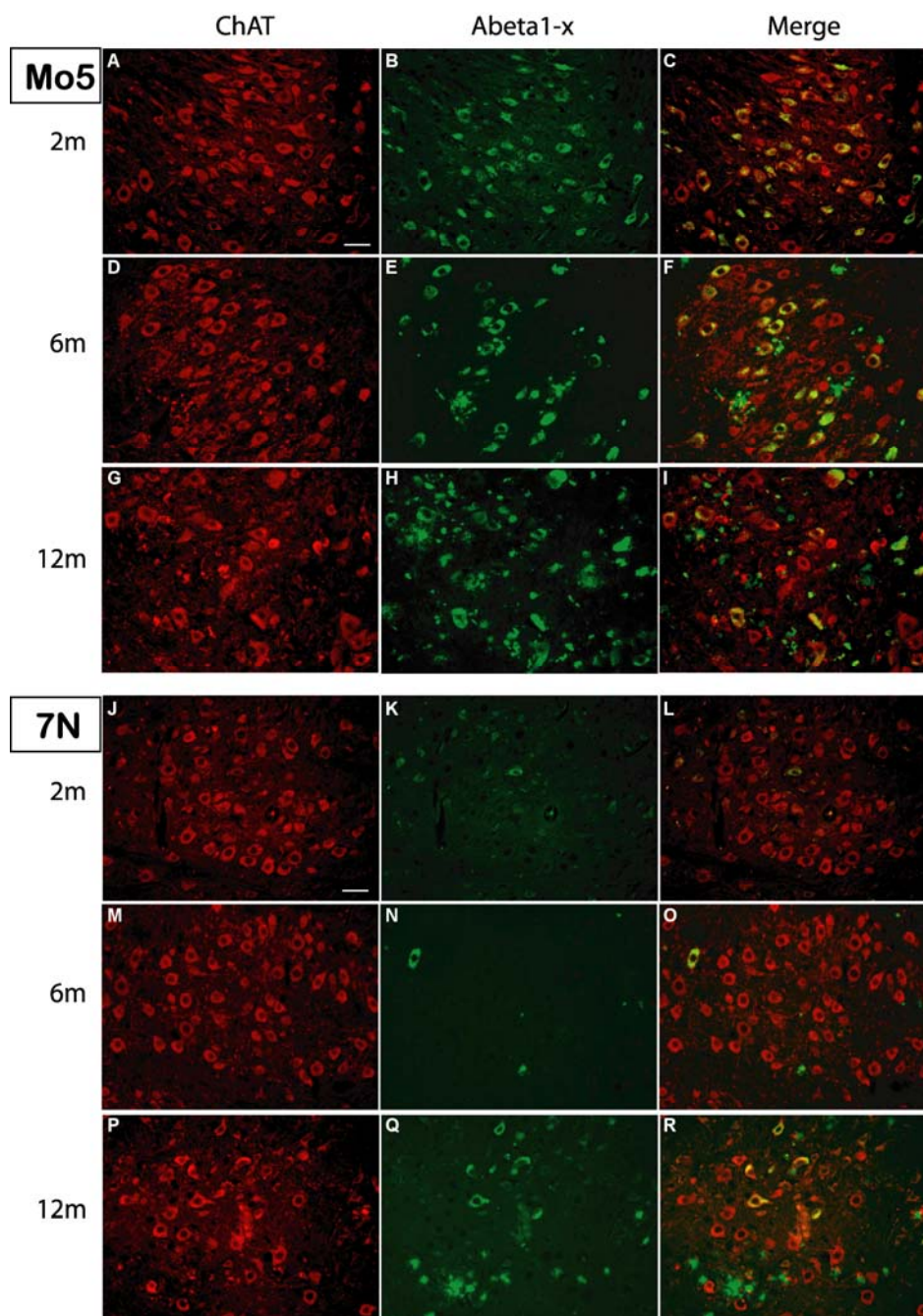


**Fig. 24 Intracellular  $A\beta$  accumulation in the cholinergic motor neurons of Mo5 and 7N in APP/PS1KI mice.** In 2-, 6-, and 12-month-old APP/PS1KI mice, the Mo5 was found to accumulate intracellular  $A\beta_{1-x}$  labeled by  $A\beta[N]$  antibodies at an earlier age than the 7N. ChAT staining is shown in red and  $A\beta_{1-x}$  in green. Merged images are shown in C, F, I, L, O, R. Scale bars: 50  $\mu$ m.

Thioflavine S, which detects aggregated beta sheet structures and disclosed a punctuate somatodendritic staining pattern already in 2-month-old mice in the Mo5 being much more prominent than in the 7N (Fig. 25D - F, J - L).

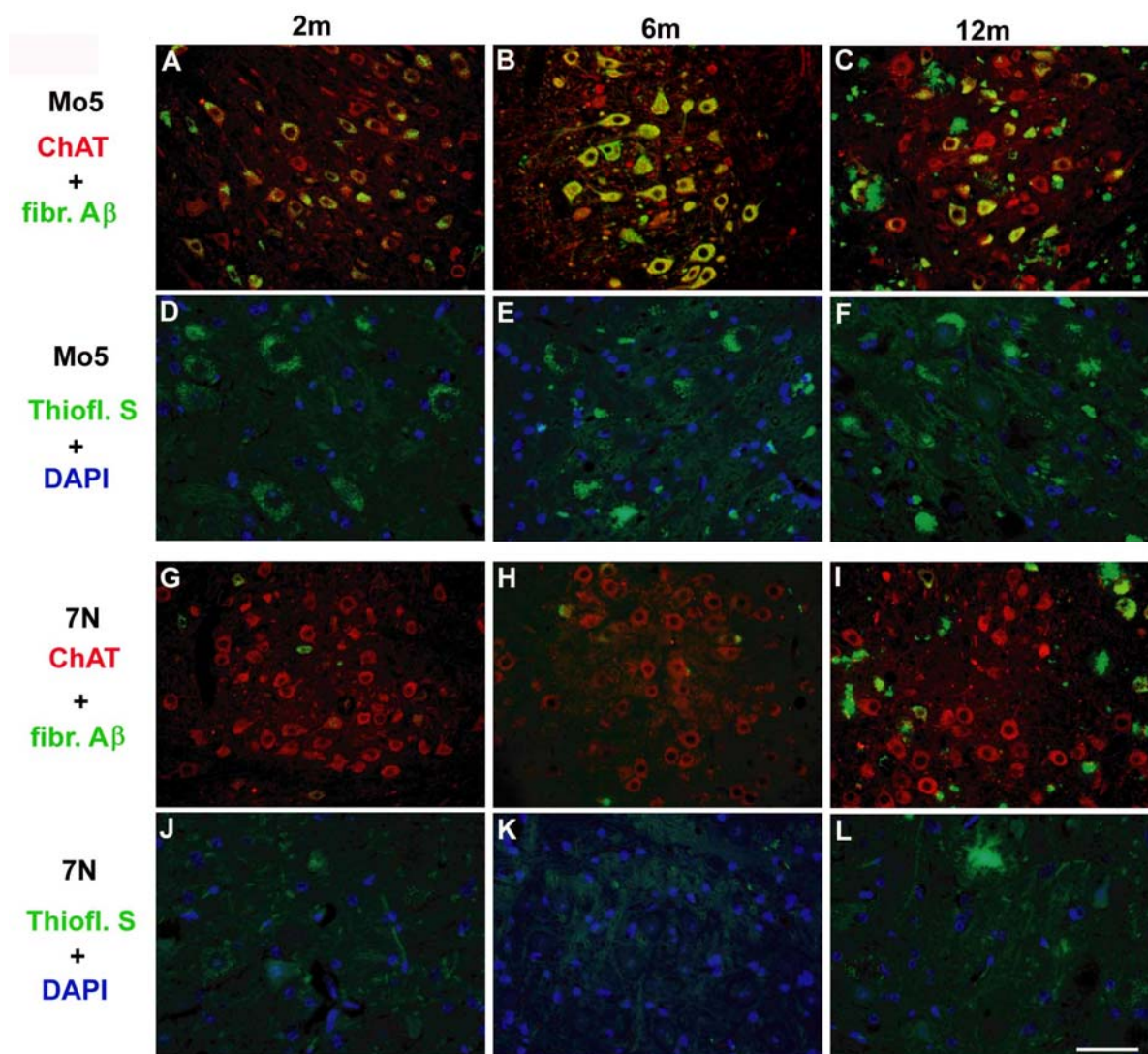


**Fig. 25 Fibrillar oligomeric A $\beta$  and Thioflavin S positive material in motor neurons of the Mo5 and 7N.** In 2-, 6-, and 12-month-old APP/PS1KI mice, fibrillar oligomeric and fibrillar A $\beta$  (OC antibody, green) as well as Thioflavin S positive material (green) were found to accumulate intracellular in a larger amount and at an earlier age in the Mo5 as compared to the 7N. DAPI staining in blue shows cell nuclei and only merged pictures are shown. Scale bars: A – C, G – I: 100  $\mu$ m; D – F, J – L: 50  $\mu$ m.



### 3.2 Effect of intraneuronal A $\beta$ versus plaques on neurodegeneration

#### A $\beta$ accumulation in the frontal cortex and thalamus

Massive intra- and extracellular A $\beta$  accumulations were observed in the frontal cortex by immunohistochemical staining using the 4G8 antibody recognizing the central epitope A $\beta$ <sub>17-24</sub> (Fig. 26A - H). The intraneuronal pathology of the frontal cortex is already very prominent at the age of 1.5 months, where virtually no or very few plaques are visible (Fig. 26A, E). Already at 2 months, plaque pathology starts to develop at a greater degree; however,

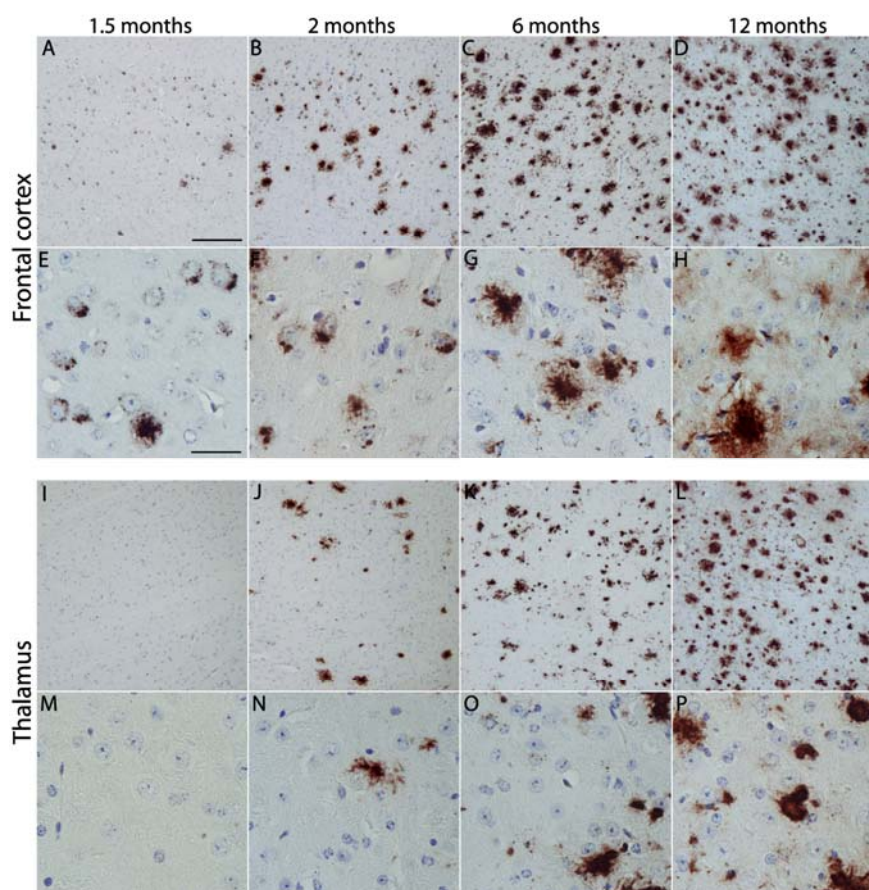


**Fig. 26 A $\beta$  peptides in frontal cortex and thalamus of APP/PS1KI mice.** Micrographs shows immunostaining of A $\beta$  peptides using 4G8 antibodies in frontal cortex (A - H) and thalamus (I - P) of 1.5-, 2-, 6-, and 12-month-old APP/PS1KI mice in paraffin embedded sections. Prominent accumulation of intraneuronal A $\beta$  is seen in the frontal cortex already at 1.5 months with only little plaque pathology (A, E). More plaques are evident in the frontal cortex of 2-month-old mice where intraneuronal A $\beta$  is still highly abundant (B, F). Plaque pathology dramatically increases in the frontal cortex from 2 to 6 months, with a concomitant decrease in intraneuronal A $\beta$  accumulation (C, G), whereas the pathology is mostly unchanged from 6 to 12 months (D, H). No A $\beta$  pathology is observed in the thalamus of 1.5-month-old mice (I, M) which start to develop plaques at the age of 2 months with no accumulation of intraneuronal A $\beta$  (J, N). Plaque pathology increased dramatically in the thalamus from 2- to 6-month-old mice (K, O) and even further to 12-month-old mice (L, P). Scale bars: A - D, I - L: 200  $\mu$ m; E - H, M - P: 33  $\mu$ m.



intraneuronal A $\beta$  is still abundantly present (Fig. 26B, F). At the age of 6 months, plaque pathology has been dramatically developed, however, the staining of intracellular A $\beta$  aggregates decreases and is no longer a dominating pathological feature (Fig. 26C, G). From 6 to 12 months, the pathology of the frontal cortex does not seem to change much except that the plaques may become more densely packed (Fig. 26D, H). The thalamus is found to develop only plaques and no intraneuronal aggregates (Fig. 26I - P). The pathology of this region starts later than in the cortex at about the age of 2 months with no pathology at 1.5 months (Fig. 26I, M). From 2 to 6 months, numerous plaques develop and the pathology even increases further till the age of 12 months (Fig. 26J - L, N - P). As the 4G8 antibody has been shown to weakly cross react with APP in western blots, the antibody was highly diluted (1:10,000) in order to recognize only A $\beta$ . Using a variety of different dilutions, this concentration was found to show no staining of APP. The presence of intracellular A $\beta$  aggregates was confirmed by immunostaining with the N-terminal specific A $\beta$  antibody, A $\beta$ [N]. Again, prominent accumulation of intraneuronal A $\beta$  staining was found in the frontal cortex already at the age of 1.5 and 2 months, but being absent at 6 and 12 months (Fig. 27A - D). Furthermore, confirming the 4G8-staining, no intraneuronal A $\beta$  immunoreactivity was

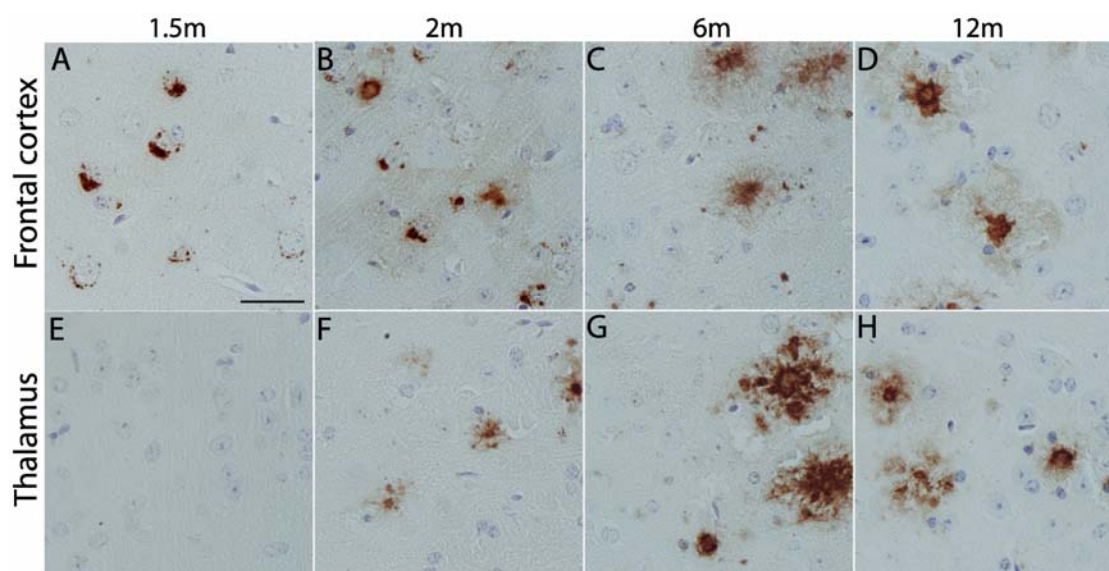


**Fig. 27 Confirmation of intracellular A $\beta$  accumulation in APP/PS1KI mice by A $\beta$ [N] antibody.** As observed with the 4G8 antibody, intracellular A $\beta_{1-x}$  staining was found to be prominent in AP/PS1KI mice already at 1.5 months of age (A) as well as at 2 months (B), but decreased at 6 and 12 months (C, D). No intraneuronal A $\beta_{1-x}$  staining was detected in the thalamus regardless of age (E - H). Scale bar: a - h: 33  $\mu$ m.

detected in the thalamus regardless of age (Fig. 27E - H). In addition, different end-specific A $\beta$  antibodies were used to demonstrate the specificity of intraneuronal A $\beta$  immunoreactivity in the frontal cortex (Fig. 28E - G). The regional difference in the accumulation of intraneuronal A $\beta$  seems to be a consequence of the APP transgene expression pattern, as the APP transgene is abundantly expressed in the pyramidal layers of the frontal cortex, whereas no expression is found in the thalamus (Fig. 28A - D). To further characterize the development of A $\beta$  pathology over time in the two regions chosen for stereology, the A $\beta$  accumulation was quantified using the 4G8 antibody and a software density measurement technique (Fig. 29). At 2 months of age, the area covered by A $\beta$  deposits was already 4.7 % in the frontal cortex owing to the massive accumulation of intraneuronal A $\beta$ , but only 1.5 % in the thalamus because of the absence of intracellular A $\beta$  and the later onset of extracellular plaque pathology. At 6 months of age, the percentage of the area covered by A $\beta$  deposits had increased to 12.1 % in the frontal cortex and 8.5 % in the thalamus. From the age of 6 to 12 months, the A $\beta$ -covered area remained stable in the frontal cortex, but increased further to 13.9 % in the thalamus (Fig. 29A, B). Looking at average A $\beta$  grain size and grain numbers in

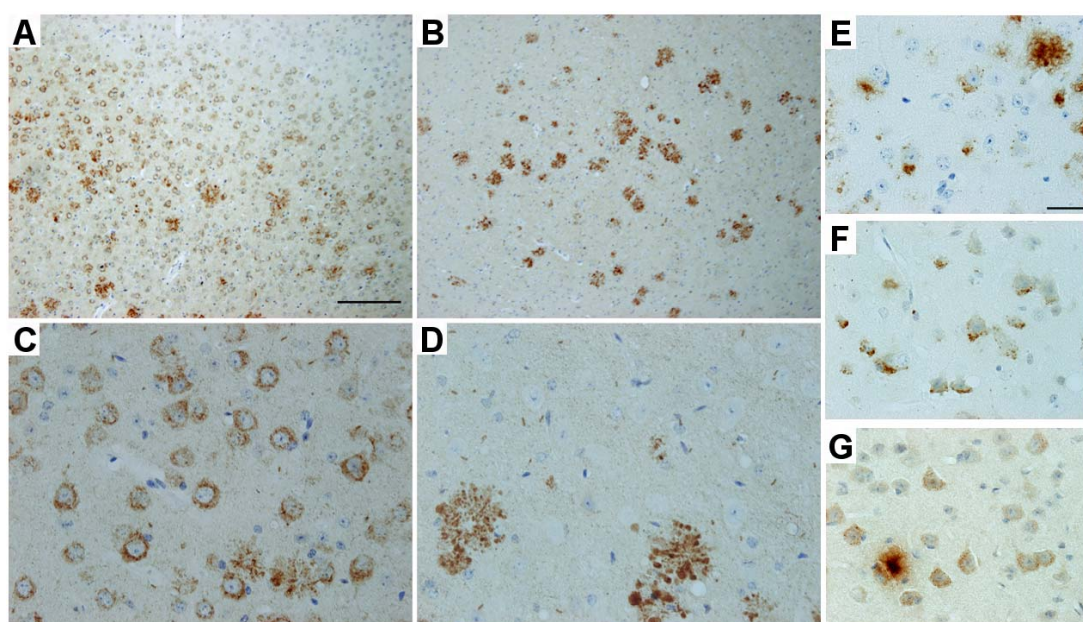
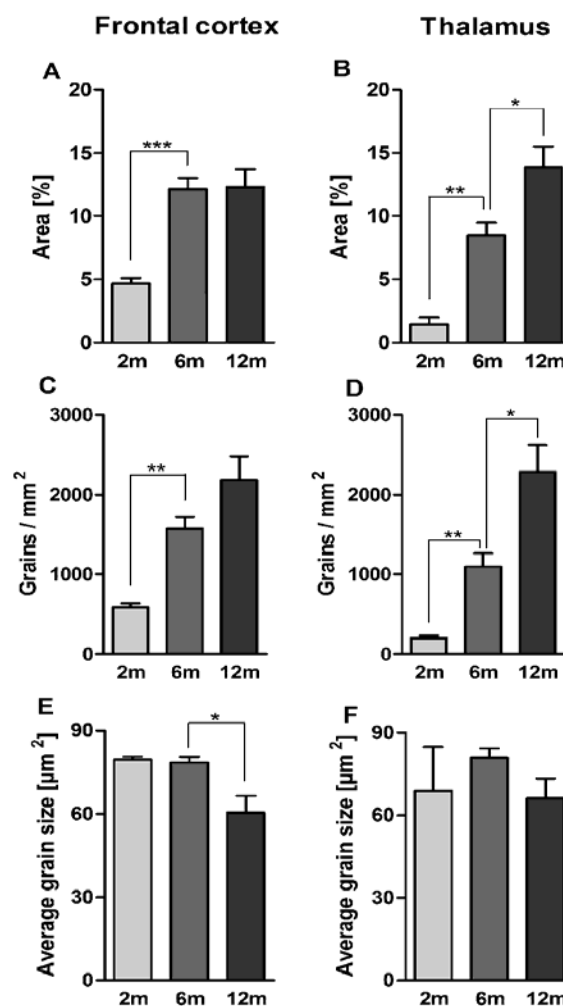


**Fig. 28 APP transgene expression and further confirmation of intracellular A $\beta$  in APP/PS1KI mice.** Immunostaining of human APP using the 23850 antibody in paraffin embedded sections of 2-month-old APP/PS1KI mice showed that the APP transgene is expressed in the neurons of the frontal cortex (A, C) but not of those in the thalamus, where only dystrophic fibers mostly surrounding plaques were stained (B, D). The following endspecific A $\beta$  antibodies were applied to further confirm the intraneuronal A $\beta$  staining in the frontal cortex: N1D (E, N-terminal A $\beta$  starting with aspartate at position 1), N3pE (F, N-terminal A $\beta$  starting with pyroglutamate at position 3), and G2-10 (G, C-terminal A $\beta$ 40 peptides). Scale bars: A, B: 200  $\mu$ m; C, D: 50  $\mu$ m; E - G: 33  $\mu$ m.

**Fig. 29 Quantification of A $\beta$  accumulation in frontal cortex and thalamus.** About 5% of the frontal cortical area is covered by A $\beta$  peptide in 2-month-old APP/PS1KI mice increasing to 12.1% in 6-month-old mice with no further increase in 12-month-old mice (A). Only 1.5% of the thalamic area was covered by A $\beta$  peptide in 2-month-old APP/PS1KI mice, which increased to 8.5% in 6-month-old mice, and further progressed to 13.9% at the age of 12 months (B). The increase in A $\beta$  load in the frontal cortex from the age of 2 to 6 months was due to an increased number of deposits (C) as no change in average deposit size was detected (E). In the thalamus, the steady increase in A $\beta$  load was solely due to increased number of deposits (D) as the average deposit size did not change with age (F). The number of animals analyzed was at 2 months: 3; 6 months: 5; and 12 months: 4. Data were analysed using one-way ANOVA followed by Tukeys post-hoc test. All error bars represent mean  $\pm$  s.e.m. \*\*\*P < 0.001; \*\*P < 0.01; \*P < 0.05.



each region, it is evident that the steady increase in the percentile A $\beta$ -covered area observed in the thalamus over time is solely due to a dramatic increase in plaque number, as the grain number increases a total of 11 times from 2 to 12 months, without major changes in their size (Fig. 29D, F). In the frontal cortex, the increase observed in the percentage of the A $\beta$ -covered area between 2 and 6 months of age is also exclusively dependent on a 2.7-fold increase in grain numbers as the average grain size is unchanged. However, in contrast to the thalamus, changes are seen in the composition of frontal cortical deposits as the average size decreases, confirming the observation that the plaques become more dense and the number of deposits tend to increase being close to significance.

In order to separate the effect of intracellular A $\beta$  and plaques on neuronal survival in the frontal cortex, we selected the thalamus as an appropriate region for comparison as the amount of extracellular accumulated plaques is in a comparable range to the A $\beta$  load

observed in the frontal cortex, however, without any accumulation of intraneuronal A $\beta$  peptides.

### Stereology in the frontal cortex and thalamus

The counting areas of the frontal cortex and thalamus were defined according to Fig. 30A. A loss of neurons of 28 % and 35 % was found in the frontal cortex of the APP/PS1KI mice compared to PS1KI control mice at the age of 6 and 12 months, respectively (Fig. 30B,  $P < 0.001$ ). However, the loss did not significant progress between these ages in APP/PS1KI mice correlating with the finding of no further changes in A $\beta$  accumulation in the frontal cortex after 6 months of age. Corresponding reductions in frontal cortical volumes were found at the age of both 6 (25%,  $P < 0.001$ ) and 12 months (23%,  $P < 0.01$ ) (Fig. 30D). Due to normal growth, frontal cortical volumes increased 86% and 50% between the age of 2 to 6 months in PS1KI control and APP/PS1KI mice, respectively. Strikingly, no change was observed in the neuron numbers of the thalamus between 2-, 6-, and 12-month-old mice despite the development of massive plaque pathology (Fig. 30C). Correspondingly, no differences in thalamic volume were found between APP/PS1KI and PS1KI control mice at any age investigated (Fig. 30E). As for the frontal cortex, normal growth from 2 to 6 months was

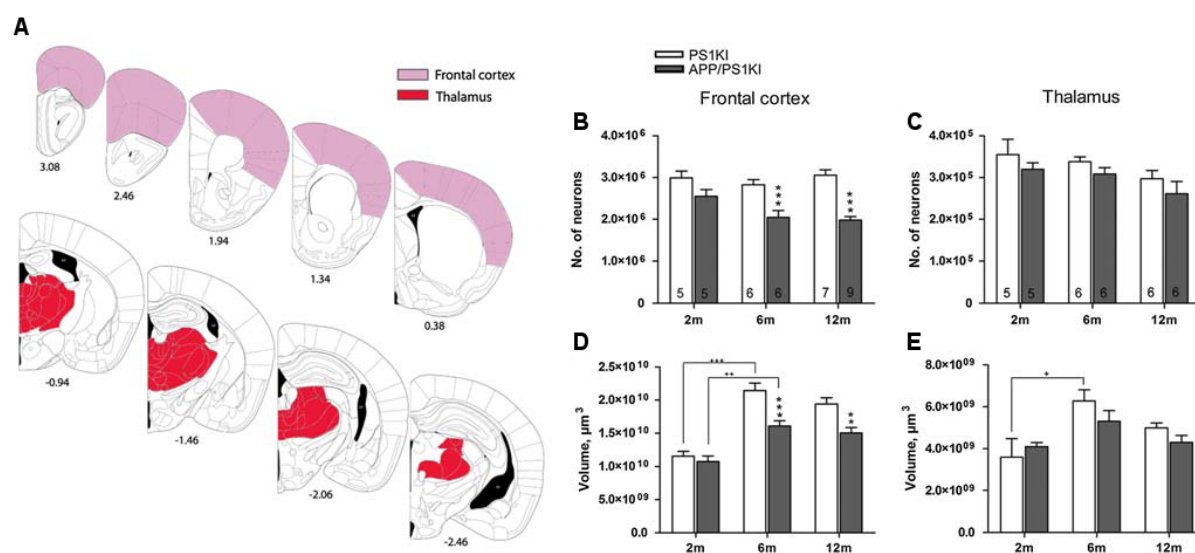


**Fig. 30 Schematic presentation of counting areas and stereological quantification of neuron numbers.** A) The frontal cortex was quantified from Bregma 3.08 to 0.26 and the thalamus from -0.94 to -2.54. Adapted from (Paxinos and Franklin 2001) with orientation according to Bregma below each section. Significant neuron losses of 28% and 35% were found in the frontal cortex of APP/PS1KI mice 6 and 12 months, respectively (B). Corresponding decreases of 25% and 23% were observed in frontal cortical volumes (D). No differences in neuron numbers or volumes were observed of the thalamus between APP/PS1KI and PS1KI control mice at 2-, 6-, and 12 months of age (C, E). The number of animals analyzed is given directly in the bars (B, C). Data were analyzed by two-way ANOVA followed by Tukeys post-hoc test. All error bars represent mean  $\pm$  s.e.m. \*\*\* $P < 0.001$ ; \*\* $P < 0.01$ ; \* $P < 0.05$ .



evident by an increase in the thalamic volume of 75 % ( $P < 0.05$ ) in the PS1KI mice and 30 % in the APP/PS1KI mice, however, only being close to significance ( $P = 0.072$ ).

### 3.3 Intraneuronal A $\beta$ staining in AD patients and transgenic AD mouse models

#### Optimization for staining of intraneuronal A $\beta$ in mouse models of AD

Quantitative optimization for staining of intracellular A $\beta$  as compared to plaques was performed in 6-month-old APP/PS1KI transgenic mice in the CA1 and thalamus

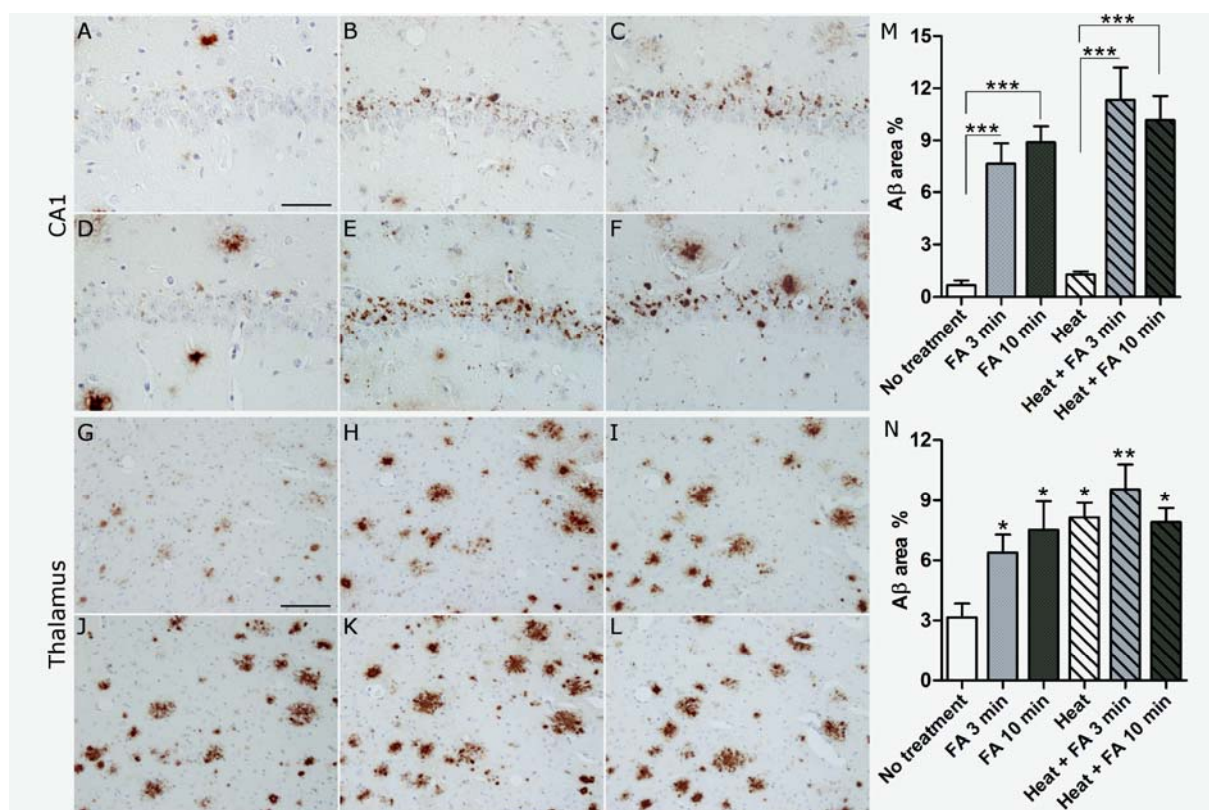


**Fig. 31 Quantitative optimization of intracellular A $\beta_{1-x}$  staining in APP/PS1KI mice.** Parallel sections from 6-month-old APP/PS1KI transgenic mice stained with A $\beta$ [N] antibodies in paraffin embedded sections showing micrographs of intracellular A $\beta_{1-x}$  in CA1 and plaque labeling in thalamus using protocols with either no antigen retrieval (A, G), 3 min formic acid (FA) pretreatment (B, H), 10 min FA pretreatment (C, I), 10 min microwave heating in a citric acid buffer pH 6 (D, J), combined heating and 3 min FA pretreatment (E, K), or combined heating and 10 min FA pretreatment (F, L). Area percentile quantifications of the corresponding A $\beta$  loads showed that FA pretreatment regardless of exposure time is essential for the intraneuronal staining of A $\beta$  in the CA1 (M), whereas heat and FA treatment have equal antigenic retrieval effect on extracellular A $\beta$  plaque pathology in the thalamus (N). Scale bars: (A-F) 50  $\mu$ m, (G-L) 100  $\mu$ m. Three sections from 5 mice were analyzed in each group. Data were analyzed by One-way ANOVA followed by Newman Keuls post-hoc test. \* $P < 0.05$ ; \*\* $P < 0.01$ ; \*\*\* $P < 0.001$ .

accumulating either intracellular A $\beta$  or plaques, respectively. Parallel sections containing the two areas of interest were stained with the A $\beta$ [N] antibody that recognizes A $\beta$ <sub>1-x</sub> comparing protocols with either no antigen retrieval, 10 min microwave heating in a citric acid buffer pH 6 (heat), 3 and 10 min FA pretreatments, or combined heat and FA pretreatments. Virtually no intracellular A $\beta$  staining and only very little labeling of A $\beta$  plaques were observed in the CA1 and thalamus without any pretreatment (Fig. 31A, G). FA pretreatments revealed an obvious

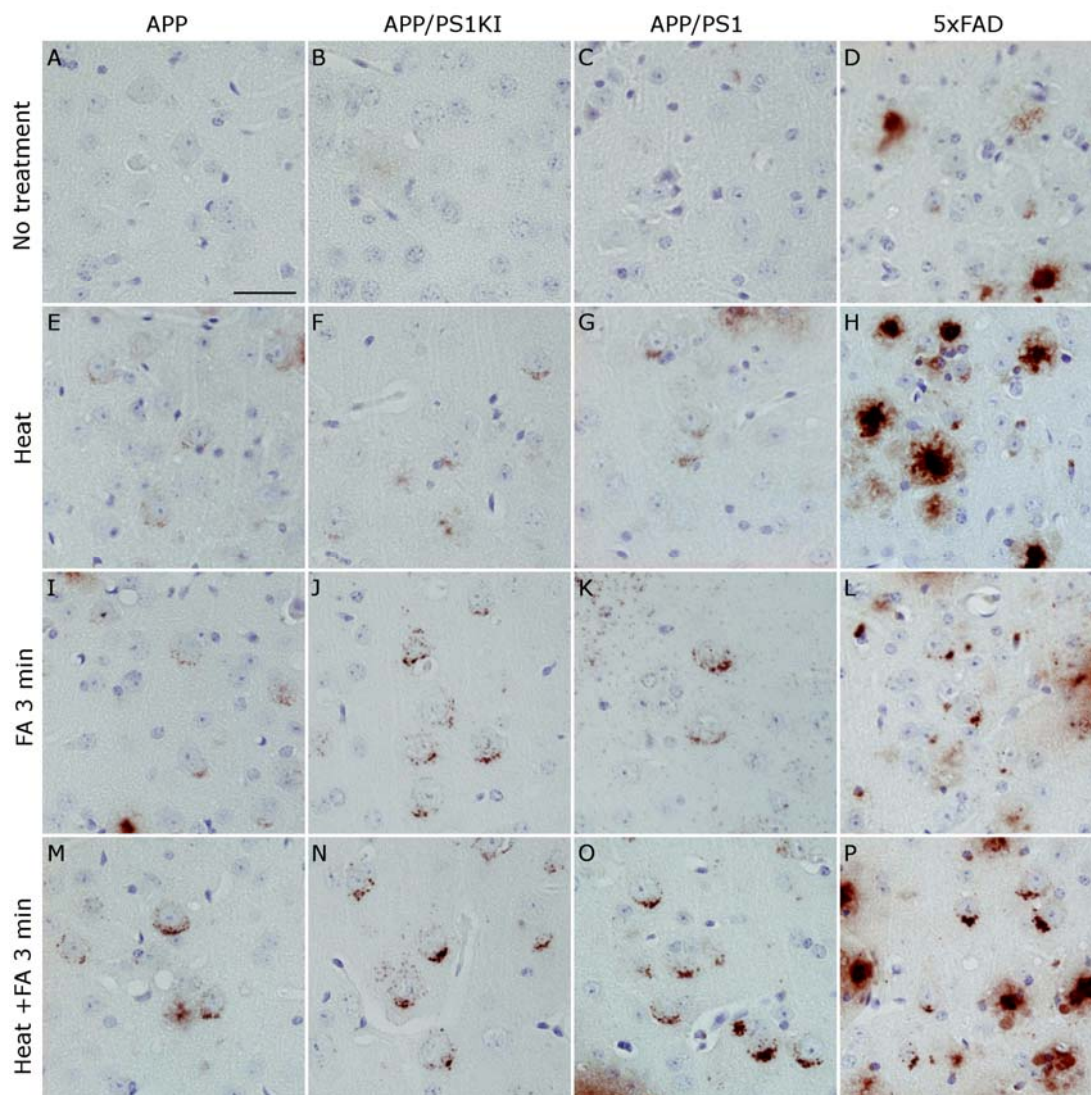


**Fig. 32 Optimization of intraneuronal A $\beta$ [N] staining in APP, APP/PS1KI, APP/PS1, and 5xFAD mice.** Qualitative optimization for intraneuronal A $\beta$  staining in the medial cortex of APP, APP/PS1KI, APP/PS1, and 5xFAD mice was performed with the N-terminal specific antibody A $\beta$ [N]. No clear intraneuronal A $\beta$ <sub>1-x</sub> staining was observed in APP, APP/PS1KI, and APP/PS1 mice without heat or FA treatment (A, B, C), whereas 5xFAD mice showed some intraneuronal A $\beta$  staining without any pretreatment (D). Ten min heat treatment in citric acid buffer pH 6 had a minor increasing effect on the intracellular staining in all 4 mouse models (E, F, G, H), however, 3 min FA pretreatment markedly increase the intracellular A $\beta$ <sub>1-x</sub> disclosing a distinct granular pattern being most obvious in the APP/PS1KI, APP/PS1, and 5xFAD mice (I, J, K, L). The combination of heat and FA pretreatment further increase the intracellular staining in APP mice and had a minor intensifying effect in the APP/PS1KI, APP/PS1, and 5xFAD mice (M, N, O, P). Scale bar: 33  $\mu$ m.

granular intracellular staining in CA1 as well as a much clearer labeling of plaques with both 3 and 10 min exposure times (Fig. 31B, C and H, I). Applying the heat pretreatment alone did not reveal much staining of intracellular A $\beta$  in the CA1, however, staining of plaques was dramatically increased in the thalamus (Fig. 31D, J). Combining the heat and FA treatments seemed to intensify the staining of intracellular A $\beta$  as compared to FA treatment alone, whereas plaques were equally well disclosed (Fig. 31E, F and K, L). These observations were confirmed by quantification of the area covered by A $\beta_{1-x}$  staining where it became evident that heat pretreatment alone did not increase the staining of intraneuronal A $\beta$  in the CA1. FA pretreatments for 3 and 10 min both significantly increased the intraneuronal staining independent of exposure time (Fig. 31M). The combined effect of heat and FA also significantly increased the area of intraneuronal A $\beta$  staining compared to no pretreatment, but not compared to FA pretreatment alone (Fig. 31M). Concerning plaque pathology in the thalamus, all pretreatments significantly increased the plaque staining in an equal manner as compared to no pretreatment (Fig. 31N).

The analysis of optimization for staining of intraneuronal A $\beta$  was extended to a qualitative comparison in four different AD mouse models: APP, APP/PS1KI, APP/PS1 and 5xFAD mice of ages where intraneuronal accumulation of A $\beta$  was evident in the medial cortex above the hippocampus. No pretreatment was compared to the antigen retrieving effect of heat, FA 3 min, and the combined effect of heat and FA 3 min. Applying the A $\beta$ [N] antibody, APP, APP/PS1KI, and APP/PS1 mice showed no detection of intraneuronal A $\beta_{1-x}$  without heat or FA pretreatment (Fig. 32A, B, C, respectively), in contrast to 5xFAD mice that showed some intraneuronal A $\beta$  staining without any pretreatment (Fig. 32D). Heat pretreatment had a minor increasing effect on the intracellular A $\beta_{1-x}$  staining in all mouse models (Fig. 32E, F, G, H), however, 3 min FA pretreatment revealed an intense granular intracellular staining being most evident in the APP/PS1KI, APP/PS1, and 5xFAD mice (Fig. 32I, J, K, L). The combination of heat and FA treatment further increased the intracellular staining of A $\beta_{1-x}$  in single transgenic APP mice and had an intensifying effect in the bigenic APP/PS1KI, APP/PS1, and 5xFAD mouse models (Fig. 32M, N, O, P).

The effect of heat and FA was additionally studied in the same four mouse models using the 4G8 antibody recognizing A $\beta_{17-24}$ . Applied in the concentration of 1:10.000 this antibody previously showed no cross-reaction with APP in immunostainings in APP/PS1KI transgenic



mice (Christensen et al. 2008). As observed with the A $\beta$ [N] antibody, weak intraneuronal A $\beta$  staining without any pretreatment was only observed in the 5xFAD model (data not shown) and 3 min FA pretreatment was found to reveal a granular intracellular staining pattern in all four mouse models being most intense in the APP/PS1KI mice (Fig. 33A, B, C, D). However, in contrast to the A $\beta$ [N] staining, heat pretreatment of 4G8 stained sections revealed a staining pattern of much smaller A $\beta$  granules dispersed throughout the cytoplasm of cortical neurons in all four mouse models (Fig. 33E, F, G, H). This heat-induced A $\beta$  staining was

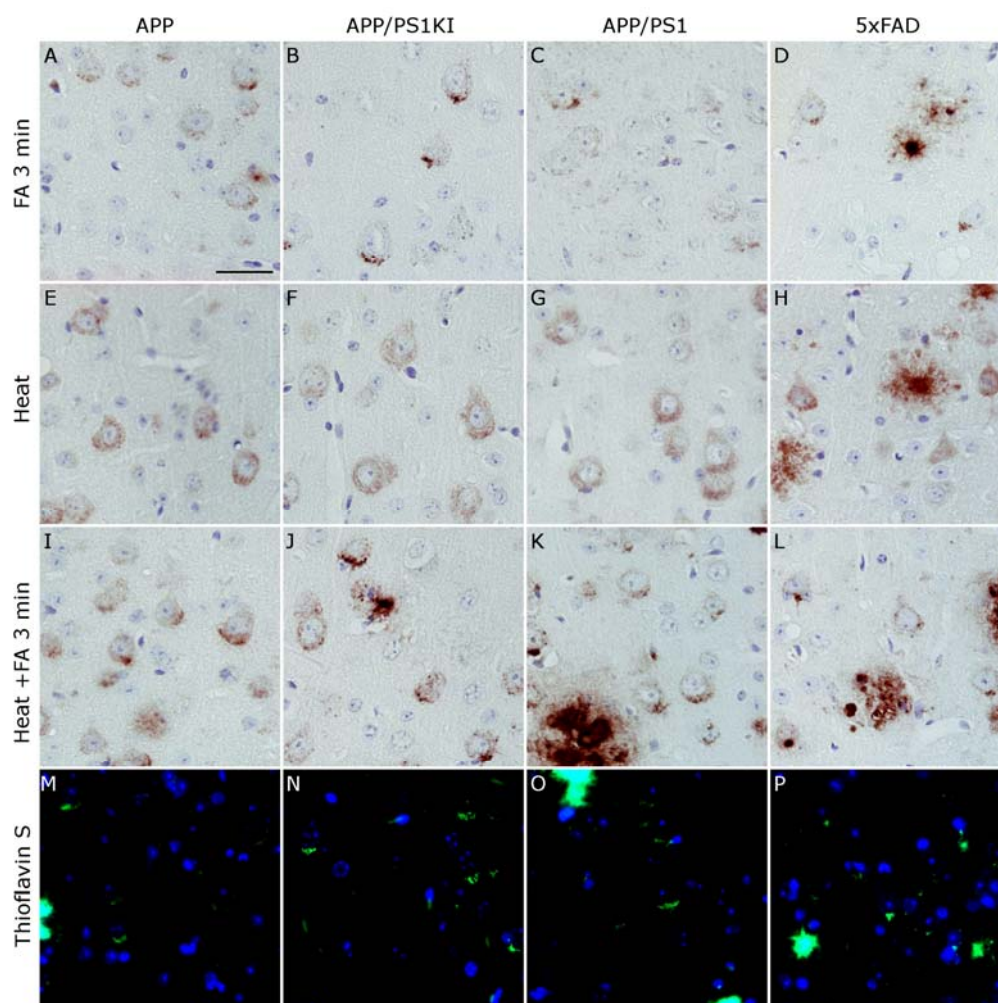


**Fig. 33 The effect of formic acid (FA), heat, and combined heat and FA antigen retrieval on intracellular 4G8 staining** was qualitatively compared in the medial cortex of APP, APP/PS1KI, APP/PS1, and 5xFAD mice. Three min FA pretreatment was found to reveal a distinct granular intracellular staining pattern as observed with the A $\beta$ [N] antibody (A, B, C, D). In contrast, 10 min heating in citric acid buffer pH 6 revealed a more homogenous intracellular staining pattern in all four mouse models (E, F, G, H), however, this seemed to decrease with combined pretreatment of heat and 3 min FA showing mainly the granular intracellular staining observed with FA pretreatment alone (I, J, K, L). Thioflavin S staining in green disclosed the same granular intracellular staining pattern as observed with the 3 min FA treatment alone in all four mouse models (M, N, O, P). Scale bar: 33  $\mu$ m.



decreased with combined pretreatment of heat and 3 min FA, disclosing mainly the granular intracellular staining similar to the effect of FA alone (Fig. 33I, J, K, L). To investigate the specificity of the heat-induced 4G8 staining, 4G8 (red) and APP (green) were fluorescently labeled in APP/PS1KI mice (Fig. 34). With application of the heat pretreatment alone, most of the 4G8 staining co-localized with the APP staining within the cytoplasm of cortical neurons (Fig. 34A, B, C). With the combination of heat and FA pretreatment, the 4G8 antibody mainly labeled the larger granules at the axon hillock, which did not co-localize with the APP staining (Fig. 34D,

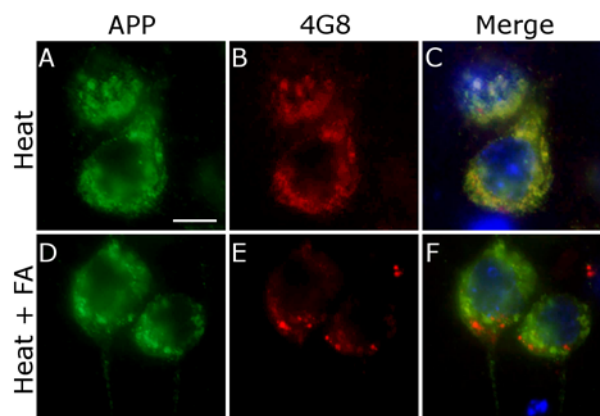


**Fig. 34 Fluorescent double labeling of 4G8 and APP in APP/PS1KI mice.** 4G8 (red) and APP (green) was fluorescently double labeled in heat and heat + FA pretreated sections from 1.5-month-old APP/PS1KI mice. With heat pretreatment alone, much of the 4G8 staining co-localized with the APP staining within the cytoplasm of cortical neurons (A, B, C). With the combination of heat and FA, the 4G8 antibody mainly labeled larger granules at the axon hillock of cortical neurons and did not co-localize with APP staining (D, E, F). Blue counterstaining of nuclei in the merged pictures was performed with DAPI. Scale bar: 10  $\mu$ m.

E, F). Fluorescent green Thioflavin S staining visualizing aggregated proteins was applied to analyze the aggregation state of the intraneuronal A $\beta$  peptides and disclosed the same granular intraneuronal staining pattern as observed with 3 min FA pretreatment alone or together with heat in all four mouse models (Fig. 33M, N, O, P), indicating that the intraneuronal A $\beta$  enhanced by FA is in an aggregated state.

### Staining of intraneuronal A $\beta$ in brain tissue from AD patients

Optimization for intraneuronal A $\beta$  staining was performed in hippocampal paraffin sections of sporadic, familial Swedish, and familial Arctic AD cases using the A $\beta$ [N] antibody. Even without any antigen retrieval, a faint fairly homogenous intraneuronal A $\beta_{1-x}$  staining could be detected in all three types of AD cases (Fig. 35A, E, I). Yet, 10 min heat treatment in 0.01 M citric acid buffer pH 6 dramatically increased the intraneuronal A $\beta_{1-x}$  staining that in higher magnification showed a granular appearance and concentration around the nucleus (Fig. 35B, F, J). Compared to no pretreatment, 3 min FA pretreatment did not improve the staining of intracellular A $\beta_{1-x}$  (Fig. 35C, G, K), and actually very clearly counteracted the enhancing effect of the heat pretreatment on intraneuronal A $\beta_{1-x}$  staining (Fig. 35D, H, L). In addition to

the fairly homogenous cytoplasm staining, some nuclei were observed to be surrounded by a highly granular A $\beta$  staining pattern, which were present in all three AD cases with all applied protocols (Fig. 35C, G, K; black arrows). Double labeling of A $\beta$ <sub>1-x</sub> and astrocytes using the A $\beta$ [N] antibody visualized by DAB and a GFAP antibody visualized by Histogreen proofed this highly granular staining pattern to be astrocytes accumulating A $\beta$ , which could be found abundantly in CA4 and CA3 of the hippocampal formation of many sporadic AD cases (Fig. 36A, B; black arrows). In a few cases, astrocytes with no granular A $\beta$  accumulation could be found in close proximity to neurons (Fig. 36C, D).

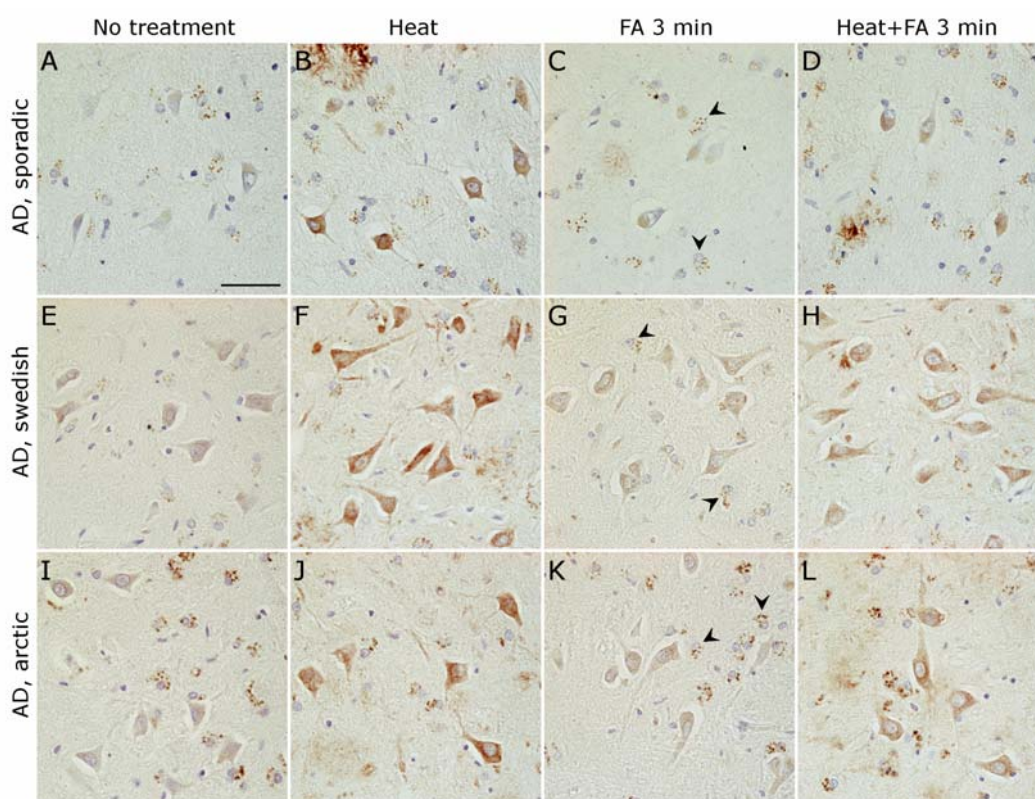


**Fig. 35 Optimization for intraneuronal A $\beta$ [N] staining in the CA4 region of AD brain tissue.** The optimization was performed in hippocampal sections from sporadic, familial Swedish, and familial Arctic AD cases using the A $\beta$ [N] antibody in paraffin embedded sections. A faint homogenous intraneuronal A $\beta$ <sub>1-x</sub> staining could be detected even without any antigen retrieval in all three types of AD cases (A, E, I). However, 10 min heat pretreatment in citric acid buffer pH 6 dramatically increased the intraneuronal A $\beta$ <sub>1-x</sub> staining that in higher magnification show granularity and concentration around the nucleus (B, F, J). Compared to no treatment, 3 min formic acid (FA) pretreatment did not improve the staining of intraneuronal A $\beta$ <sub>1-x</sub> (C, G, K) and in the combined treatment of heat and FA, FA actually counteracted the enhancing effect of the heat pretreatment (D, H, L). Besides the intraneuronal A $\beta$ <sub>1-x</sub> staining, smaller nuclei surrounded by a highly granular A $\beta$  staining pattern were observed in all three AD cases with all protocols (C, G, K, black arrowheads). Scale bar: 50  $\mu$ m.

The presence of intraneuronal A $\beta$  in the hippocampal region of sporadic AD cases was confirmed by staining with OC antibodies recognizing A $\beta$  fibrils and fibrillar oligomers (Kayed et al. 2007). The OC antibody produced an intraneuronal staining much like that of A $\beta$ [N] with heat pretreatment alone (Fig. 37A, B) as well as with combined heat and 3 min FA pretreatment, actually being slightly more intense than that enhanced by heat alone (Fig. 37C, D). The 4G8 antibody was applied to further confirm the presence of intraneuronal A $\beta$  using heat pretreatment, but was found to produce a highly abundant intense granular staining very different from that detected by OC or A $\beta$ [N] antibodies (Fig. 37E, F) with the granules being much larger and surrounding the nucleus in a cap-like manner. Fluorescent

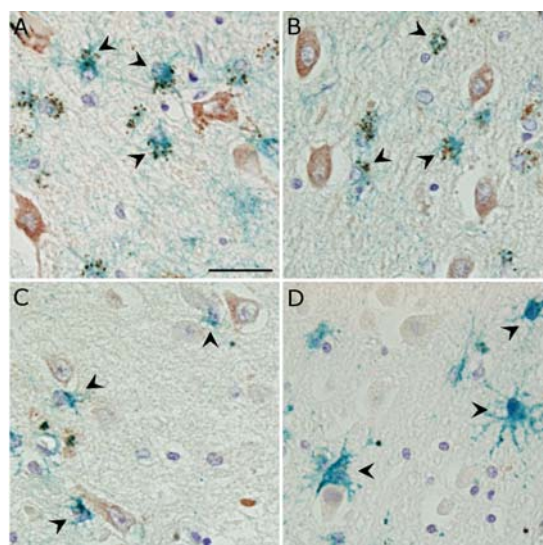


**Fig. 36 Double labeling of A $\beta$ <sub>1-x</sub> and astrocytes.** Using a double ABC labeling in paraffin embedded sections is shown A $\beta$ [N] staining in reddish brown (DAB) and GFAP in blue (Histogreen, black arrowheads). The highly granular staining pattern surrounding smaller nuclei was found to be astrocytes accumulating A $\beta$  and could be found in CA4 (A) as well as in CA3 (B) of many sporadic AD cases. However, in some AD cases, astrocytes without granular staining were found close to neurons in both CA4 (C) and CA3 (D). Scale bar: 33  $\mu$ m.

labeling of 4G8 and A $\beta$ [N] with and without Sudan Black B pretreatment proved this 4G8 staining to be a cross-reaction with lipofuscin (Schnell et al. 1999). Thus, staining with 4G8 antibodies using a green secondary antibody showed only the intense staining of large intracellular granules (Fig. 38B) which were also evident in the blue DAPI channel (Fig. 38A) and as red auto fluorescence (Fig. 38C). Merging of the pictures showed complete co-localization of this intense labeling of large cap-like granules (Fig. 38D). Pretreatment with Sudan Black B abolished the fluorescent staining observed in all channels (Fig. 38E, F, G), and merging of the pictures showed no remaining specific staining from the green 4G8 channel (Fig. 38H). In contrast, visualization of intraneuronal A $\beta$  using the A $\beta$ [N] antibody with a green fluorescent secondary antibody showed the same intense labeling of large intracellular granules, however, with an additional staining of smaller granules dispersed throughout the cytoplasm as well as at the axon hillock (Fig. 38J). DAPI and red auto fluorescence (Fig. 38I, K) showed only the very intense labeling of the larger granules, and merging of the pictures revealed co-localization of the very intense cap-like staining, but with



an additional green staining of the smaller granules (Fig. 38L). Pretreatment with Sudan Black B abolished the intense cap-like granular staining from all channels (Fig. 38M, N, O), and the merged picture showed only the green staining of the smaller granules specific for the A $\beta$ [N] antibody (Fig. 38P).

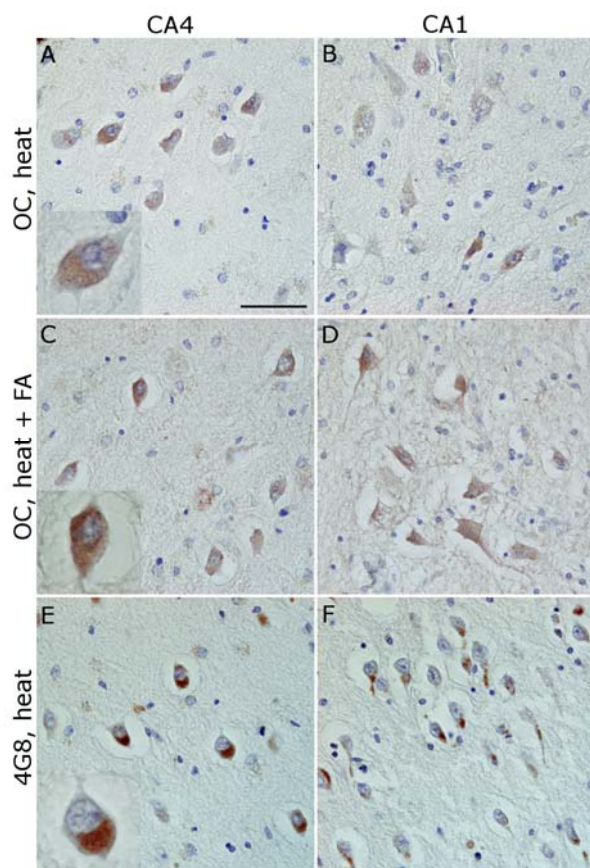


**Fig. 37 Intra-neuronal staining detected by OC and 4G8 antibodies in a sporadic AD brain tissue.** The OC antibody disclosed intra-neuronal A $\beta$  staining much like that of A $\beta$ [N] with both 10 min heat pretreatment alone (A: CA4, B: CA1) and combined heat and 3 min formic acid (FA) treatment (C: CA4, D: CA1). With 10 min heat pretreatment, the 4G8 antibody produced a much different highly abundant and granular intracellular staining (E: CA4, F: CA1). Bottom left corners of A, C, and E show intracellular staining in high magnification. Scale bar: 50  $\mu$ m.

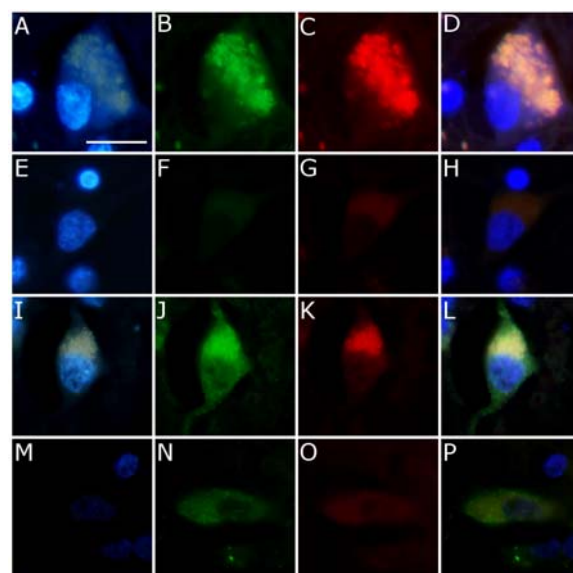


**Fig. 38 Analysis of 4G8 and A $\beta$ [N] cross reactivity with lipofuscin in CA4 of a sporadic AD case.** Fluorescent staining using 4G8 antibodies with a green secondary antibody showed an intense intracellular labeling of large granules (B). However, merging of the 4G8 staining in green (B) with autofluorescence from the DAPI (A) and red channel (C) showed complete co-localisation (D). Pretreatment with Sudan Black B abolished the fluorescence observed in all channels (E, F, G), and the merged picture showed no remaining specific staining in the green channel (H). In contrast, fluorescent staining using A $\beta$ [N] antibodies with a green fluorescent secondary antibody produced the same intense staining of large intracellular granules, but with an additional staining of smaller intracellular granules throughout the cytoplasm and in the axon hillock (J). The DAPI (I) and red channels (K) showed only the very intense large granules and merging of the pictures showed co-localisation only of the intensely labeled large granules (L). Pretreatment with Sudan Black B abolished the intense granular staining from DAPI (M), A $\beta$ [N] green labeling (N), and red autofluorescence (O), and the merged picture showed only the weaker green staining specific for the A $\beta$ [N] antibody (P). Scale bar: 20  $\mu$ m.

### Intraneuronal A $\beta$ staining intensity in sporadic AD patients

Hippocampal sections from 10 controls and 20 AD patients were stained with A $\beta$ [N] antibodies and their intraneuronal A $\beta_{1-x}$  intensity was analyzed based on evaluation of the staining intensity in CA4, CA3, and CA1. Thus “+++” was assigned to cases with very strong intraneuronal A $\beta$  staining in CA4, CA3, as well as in CA1 (Fig. 39A, B, C). “++” was assigned to cases with weaker but still obvious intracellular A $\beta$  staining in CA4 and CA3, but low or no staining in CA1 (Fig. 39D, E, F). “+” was assigned to cases with a very faint intracellular staining in CA4 and CA3 and no staining in CA1 (Fig. 39G, H, I), and “0” was assigned to cases showing no intracellular A $\beta_{1-x}$  staining either in CA4, CA3, or CA1 (Fig. 39J, K, L). Four AD patients and 2 controls were found to accumulate the highest degree of intraneuronal A $\beta_{1-x}$  peptides, whereas 9 AD patients and 2 controls accumulated a moderate amount of these A $\beta$  peptides. Six AD patients and 4 controls accumulated low amount of A $\beta$  peptides, whereas only 1 AD patient and 2 controls showed no accumulation of A $\beta_{1-x}$  peptides (Table 8). By non-parametric statistical analysis, the accumulation of intraneuronal A $\beta_{1-x}$  was found not to correlate with age, brain weight, post-mortem delay, gender, diagnosis, and Braak stage, whereas a weak but significant correlation was found with atherosclerosis and plaque pathology. Yet, ApoE genotype was found to very strongly correlate with the presence of intraneuronal A $\beta$  where having one ApoE4 allele highly significantly correlated with increased intraneuronal A $\beta_{1-x}$  staining (Table 9,  $P=0.002$ ), which was even significant after Bonferroni adjustment ( $P=0.023$ ).

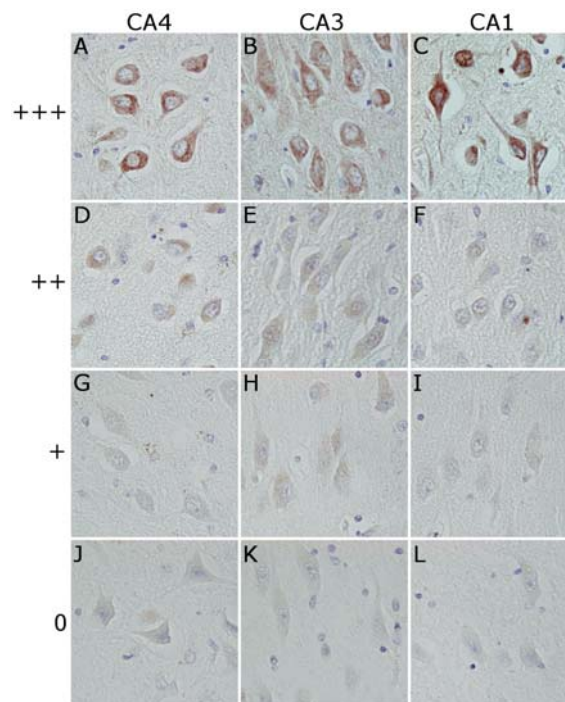


**Fig. 39 Rating of intraneuronal A $\beta$ [N] staining intensity.** +++ was assigned to cases with very strong intraneuronal A $\beta$  staining in CA4, CA3, as well as in CA1 (A, B, C). ++ was assigned to cases with weaker but still obvious intracellular A $\beta$  staining in CA4 and CA3 and low staining in CA1 (D, E, F). + was assigned to cases with a very faint intracellular A $\beta$  staining in CA4 and CA3 and apparently no staining in CA1 (G, H, I). 0 was assigned to cases showing no intracellular A $\beta$  staining either in CA4, CA3, or CA1 (J, K, L). Scale bar: 50  $\mu$ m.

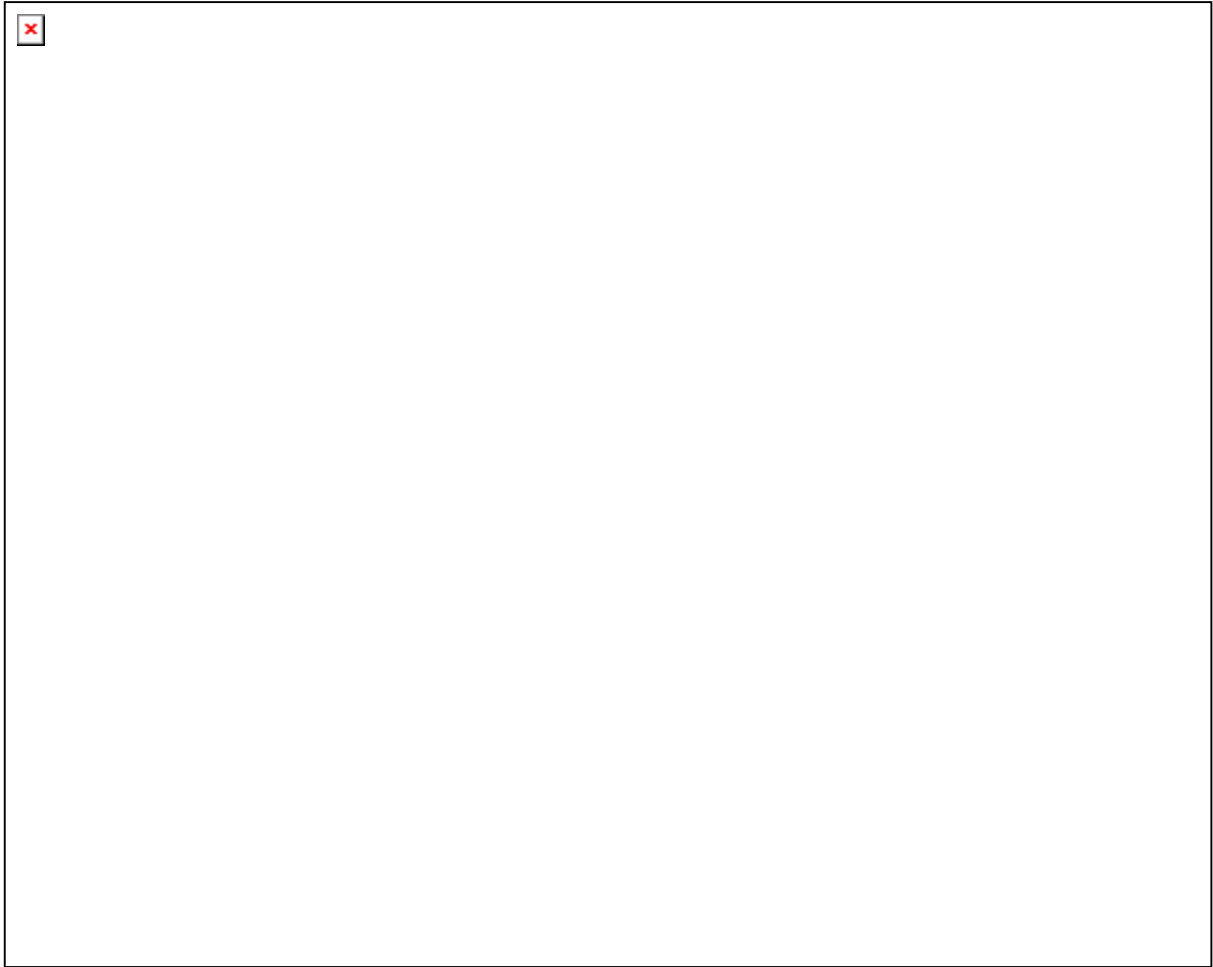


**Table 8** Patient data giving diagnosis, gender, age, post mortem delay (PMD, hrs:min), Brain weight (g), Braak stage, Plaque load, ApoE genotype (combination of alleles 2, 3, and 4), intraneuronal A $\beta_{1-x}$  staining intensity, and level of atherosclerosis.

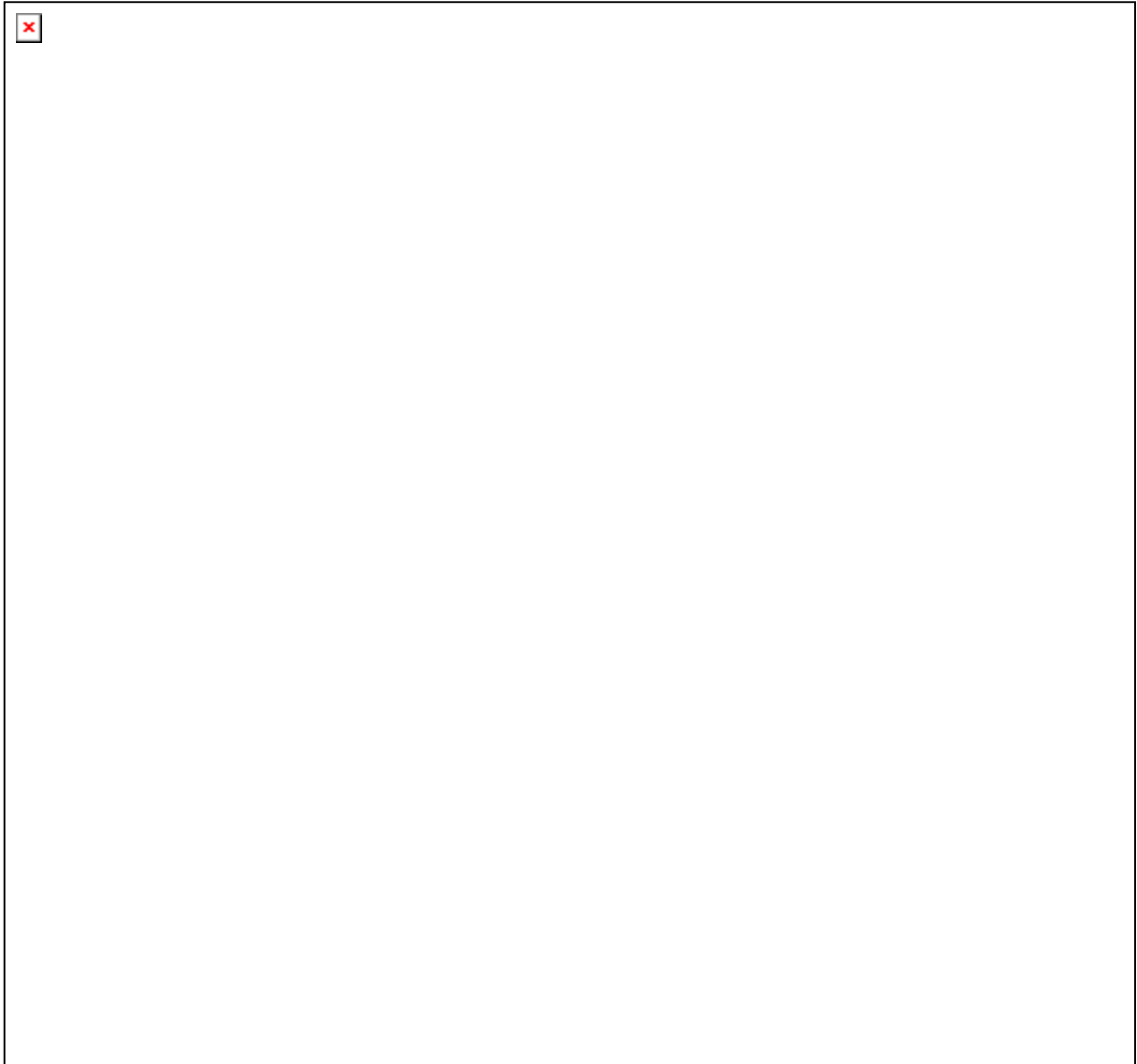


**Table 9** Statistical analysis of the correlation between intraneuronal A $\beta$  accumulation and the following data from AD patients and control cases: atherosclerosis, age, brain weight (g), post mortem delay, gender, diagnosis, number of ApoE4 alleles, Braak stage, and plaque stage. 20 AD patients and 10 controls were included in the statistical analysis, which is described in Chapter 2.14.

### 3.4 Effect of A $\beta$ on axonopathy in transgenic AD mouse models

#### APP expression and A $\beta$ load with increasing PS1KI gene dosage

Staining with antibodies against human APP revealed approximately equal numbers of APP-positive cells in APP, APP/PS1KI<sup>he</sup> and APP/PS1KI<sup>ho</sup> mice at 10 months of age, but with dystrophic fibers accumulating APP in APP/PS1KI<sup>he</sup> and APP/PS1KI<sup>ho</sup> mice (Fig. 40A – C). A qualitative western-blot analysis confirmed that the overall expression of human full-length APP in the three mouse lines was equal with no considerable variation between the different genotypes. In contrast, the levels of the  $\beta$ -secretase cleavage product C99 as well as A $\beta$  increased with increasing mutant PS1 gene dosage (Fig. 40D).

The accumulation of A $\beta$  was quantified in the frontal cortex, pons and spinal cords of

10-month-old APP, APP/PS1KI<sup>he</sup>, and APP/PS1KI<sup>ho</sup> mice using computer-based analysis of 4G8 DAB stained sections (Fig. 41). Very little or no A $\beta$  accumulation was observed in the pons and spinal cords of APP transgenic mice harboring no PS1KI mutations (Fig. 41E, H, I, L), whereas 3.9% of the frontal cortex was covered by A $\beta$  staining (Fig. 41A and D). Introducing one PS1KI allele generating APP/PS1KI<sup>he</sup> mice caused a significant increase in the A $\beta$  load in the frontal cortex by 80% leading to an overall A $\beta$  load of 7% (Fig. 41A). Also, considerable pathology was observed in the pons and spinal cord which had A $\beta$  loads of 3.6% and 3.3%, respectively (Fig. 41F, H, J, L). A further increase in the PS1KI gene dosage resulting in the APP/PS1KI<sup>ho</sup> mice caused an approximate doubling of the A $\beta$  load in all three

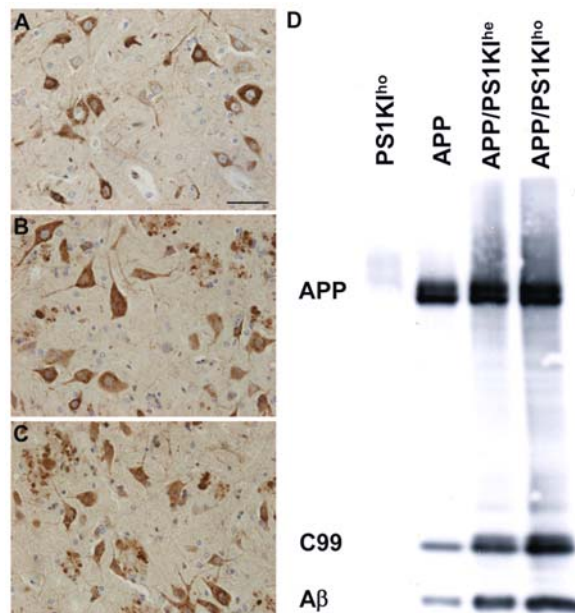


**Fig. 40 Analysis of APP transgene expression in APP, APP/PS1KI<sup>he</sup>, and APP/PS1KI<sup>ho</sup> mice.** Immunostaining of human APP in spinal cords of APP (A), APP/PS1KI<sup>he</sup> (B), and APP/PS1KI<sup>ho</sup> (C) mice showing comparable numbers of APP-expressing cells in all three genotypes. Western-blot analyses revealed no differences in the amount of human full-length APP among the three genotypes, however, the levels of C99 and A $\beta$  increased with increasing PS1KI gene dosage (D). Scale bar: 50  $\mu$ m.



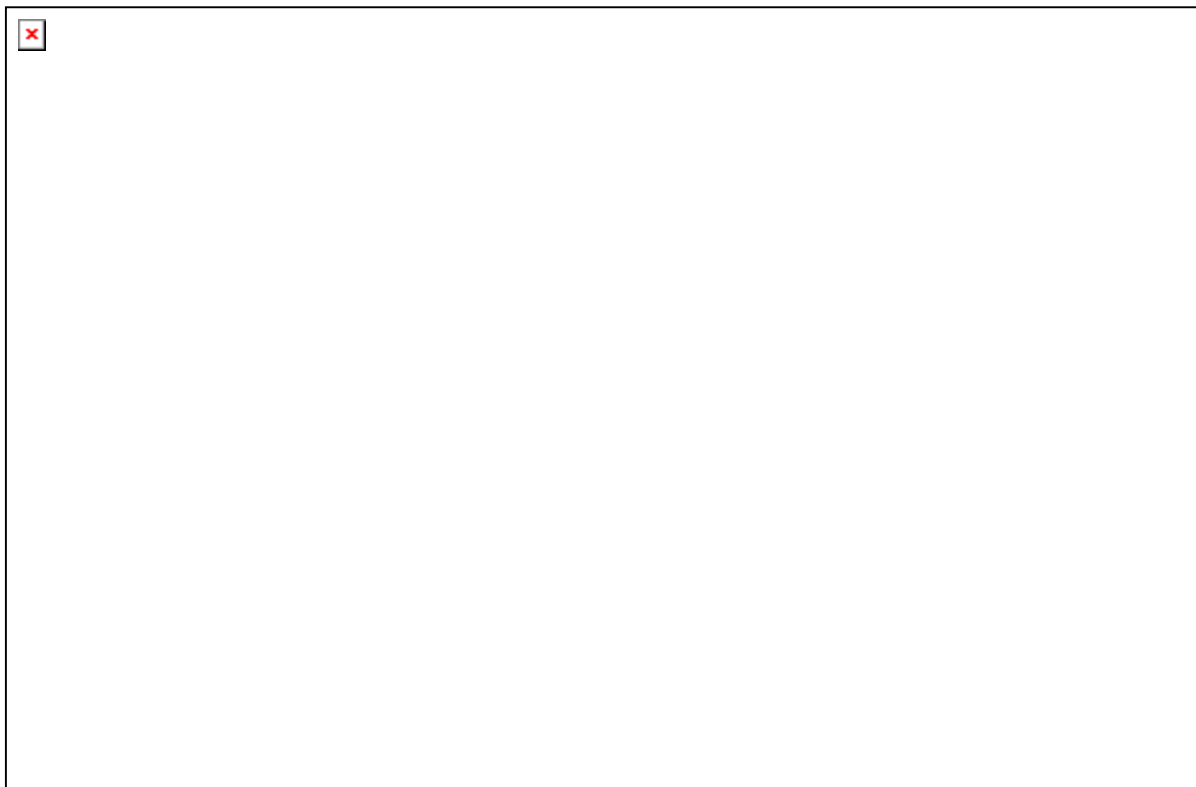


**Fig. 41 Immunostaining of A $\beta$  in APP, APP/PS1KI<sup>he</sup>, and APP/PS1KI<sup>ho</sup> mice.** A $\beta$  accumulation was analysed using 4G8 immunostaining, which is shown in 10-month-old APP, APP/PS1KI<sup>he</sup>, and APP/PS1KI<sup>ho</sup> mice in frontal cortex (A-C), pons (E-G), and spinal cord (I-K) together with their respective quantifications of the percentile area covered by DAB staining (D, H, L). Virtually no A $\beta$  peptide accumulation was detected in the pons and spinal cord of APP mice, whereas about 4% of the frontal cortical area was covered by A $\beta$  staining. Upon introduction of one PS1KI gene (APP/PS1KI<sup>he</sup> mice), the accumulation of A $\beta$  was found to rise significantly in all three regions investigated and further approximately doubled with the introduction of an additional PS1KI gene (APP/PS1KI<sup>ho</sup> mice), reaching percentile A $\beta$  covered areas of 14%, 8%, and 6.5% in the frontal cortex, pons, and spinal cord, respectively. Data was analyzed from 6 mice of each genotype and analyzed using one-way ANOVA followed by t-tests. All error bars represent mean  $\pm$  s.e.m. **\*\* $P < 0.01$ ; \* $P < 0.05$ .** Scale bar: 200 $\mu$ m.

regions measured (Fig. 41C-D, G-H, K-L), whereas PS1KI<sup>ho</sup> mice were consistently negative for 4G8 staining (data not shown). This directly proportional rise in A $\beta$  load observed with increasing PS1KI gene dosage in mice hemizygous for the APP transgene also applied to intraneuronal A $\beta$  as exemplified in motor neurons of the spinal cord (Fig. 42).

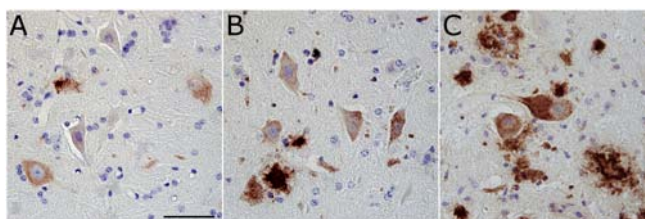


**Fig. 42 Intraneuronal A $\beta$  accumulation in APP, APP/PS1KI<sup>he</sup>, and APP/PS1KI<sup>ho</sup> mice.** In spinal cords, intraneuronal A $\beta$  accumulation was found to rise proportionally with increasing PS1KI gene dosage in 10-month-old APP (A), APP/PS1KI<sup>he</sup> (B), and APP/PS1KI<sup>ho</sup> mice (C) visualized by the 4G8 antibody. Scale bar: 50  $\mu$ m.

### Quantification of dystrophic fibers with increasing PS1KI gene dosage

The number of plaque-independent dystrophic neurites was quantified in the pons and spinal cord using antibodies toward phosphorylated APP (anti-pT668) and neurofilament (NF-200) as markers of axonopathy in double ABC-stainings with 4G8 visualizing A $\beta$  plaques. Examples of the quantification of plaque-independent dystrophic fibers in 10-month-old APP, APP/PS1KI<sup>he</sup>, and APP/PS1KI<sup>ho</sup> mice are visualized in Fig. 43, showing NF-200 staining in the pons (Fig. 43A-C) and anti-pT668 staining in the spinal cord (Fig. 43E-G). The quantification showed practically no dystrophic neurites in the pons and spinal cord of APP mice with either NF-200 (Fig. 44A, C) or anti-pT668 (Fig. 44B, D). In contrast, a considerable amount of dystrophic fibers was found in the APP/PS1KI<sup>he</sup> mice using both NF-200 and anti-pT668 in pons as well as spinal cord, and increased even further in APP/PS1KI<sup>ho</sup> mice (Fig. 44). No dystrophic fibers were found in PS1KI<sup>ho</sup> (Fig. 43D and H) or wildtype control mice (not shown). Thus using the two markers NF-200 and anti-pT668, the amount of dystrophic fibers was found to rise proportionally to the dosage of the PS1KI gene and was absent in mice harboring either only the APP transgene or the PS1KI<sup>ho</sup> gene alone.

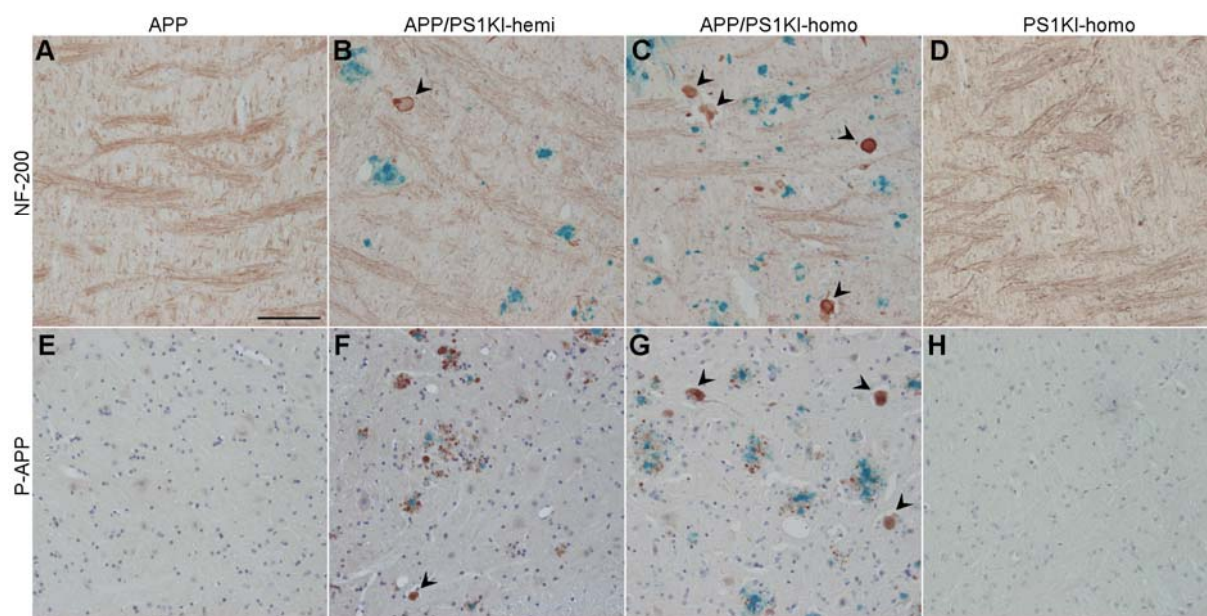


**Fig. 43 Dystrophic fibers together with A $\beta$  pathology in APP, APP/PS1KI<sup>he</sup>, and APP/PS1KI<sup>ho</sup> mice.** Double ABC-immunostaining showed A $\beta$  in blue using 4G8 antibodies together with visualization of fibers in reddish brown using either NF-200 or anti-pT668. The number of plaque-independent dystrophic neurites (black arrowheads) was found to increase with PS1KI gene dosage; examples of stainings from APP, APP/PS1KI<sup>he</sup>, APP/PS1KI<sup>ho</sup>, as well as PS1KI<sup>ho</sup> mice are shown using the NF-200 antibody in the pons (A-D) and anti-pT668 antibody in the spinal cord (E-H). Scale bar: 100 $\mu$ m.

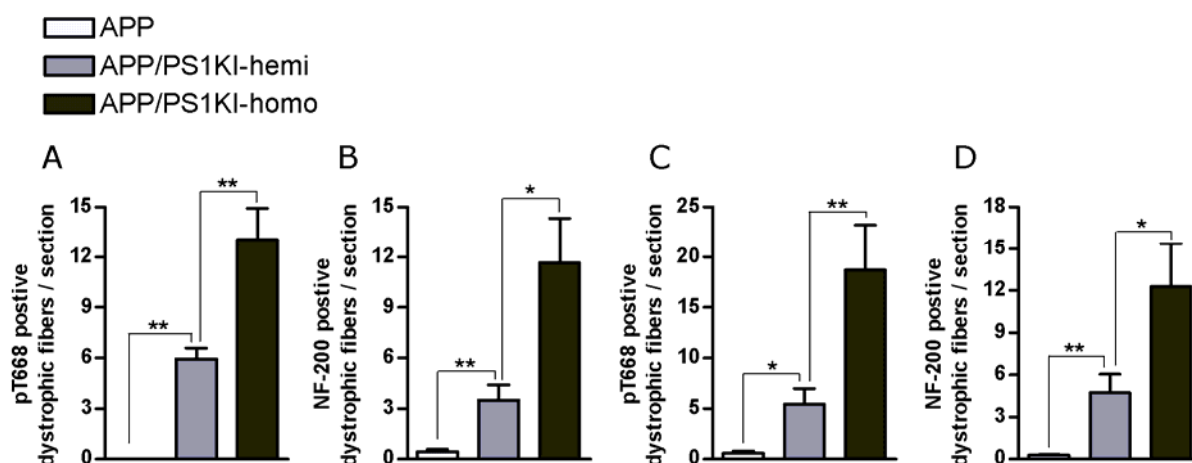


**Fig. 44 Quantification of plaque-independent dystrophic fibers in APP, APP/PS1KI<sup>he</sup>, and APP/PS1KI<sup>ho</sup> mice.** Increasing numbers of NF-200 and anti-pT668-positive plaque-independent dystrophic fibers were found with increasing PS1 gene dosage in both pons (A, B) and spinal cord (C, D) with practically no dystrophic fibers in the APP mice. Data from 6 animals of each genotype was analyzed using one-way ANOVA followed by t-tests. All error bars represent mean  $\pm$  s.e.m. **\*\*** $P < 0.01$ ; **\*** $P < 0.05$ .

### Intraneuronal accumulation of ubiquitin and A $\beta$ peptides

Immunostaining of ubiquitin in the spinal cord of 10-month-old APP, APP/PS1KI<sup>he</sup> and APP/PS1KI<sup>ho</sup> mice revealed considerable intracellular accumulation of ubiquitin in all three genotypes. However, APP/PS1KI<sup>he</sup> and APP/PS1KI<sup>ho</sup> mice in addition accumulated large amounts of ubiquitin-positive material in both plaque-independent and plaque-dependent dystrophic fibers (Fig. 45A-C). Ubiquitin western-blot analysis confirmed the finding of dramatically increased levels of ubiquitinated proteins ranging from approximately 70-180 kDa in APP/PS1KI<sup>he</sup> and APP/PS1KI<sup>ho</sup> mice as compared to wildtype (WT) and PS1KI<sup>ho</sup>

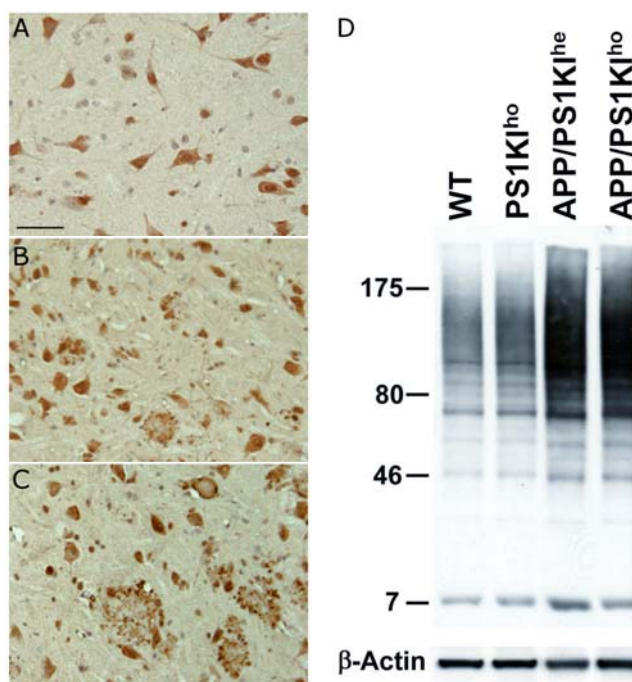


**Fig. 45 Ubiquitin in APP, APP/PS1KI<sup>he</sup>, and APP/PS1KI<sup>ho</sup> mice.** Ubiquitin staining showed many ubiquitin-positive dystrophic fibers in spinal cords of 10-month-old APP/PS1KI<sup>he</sup> (B) and APP/PS1KI<sup>ho</sup> mice (C) with only cell body staining in APP mice (A). Western-blot analysis (D) confirmed increased levels of ubiquitin in APP/PS1KI<sup>he</sup> and APP/PS1KI<sup>ho</sup> mice compared to wildtype (WT) and PS1KI<sup>ho</sup>. Protein size bar in kDa and  $\beta$ -actin blot below showing equal loading of samples. Scale bar: 50  $\mu$ m.

mice, but with no obvious difference in the amount of ubiquitin monomers (7 kDa band) (Fig. 45D).

In double ABC-immunostaining using a combination of NF-200 and 4G8 (Fig. 46A) or anti-pT668 and 4G8 (Fig. 46B), A $\beta$  could be detected in the close vicinity of plaque-independent axonal spheroids, suggesting that axonal swellings are able to release A $\beta$

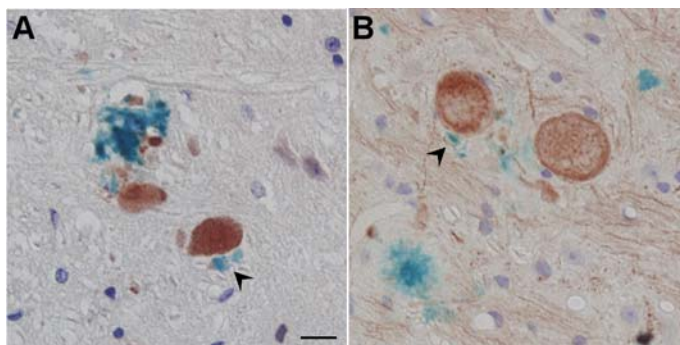


**Fig. 46 A $\beta$  deposits in the vicinity of large dystrophic neurites.** Double ABC immunostaining 4G8 antibodies (blue) together with either anti-pT668 (A) or NF-200 (B) (reddish brown) occasionally showed small A $\beta$  deposits (black arrowheads) in the vicinity of large dystrophic neurites in both APP/PS1KI<sup>hc</sup> and APP/PS1KI<sup>ho</sup> mice. Scale bar: 12.5  $\mu$ m.

peptides locally. This was confirmed by confocal imaging showing accumulation of A $\beta$  inside and in the vicinity of large plaque-independent axonal spheroids using the OC antibody recognizing fibrillar A $\beta$  oligomers and A $\beta$  fibrils (Fig. 47A-C). Generally, many plaque-

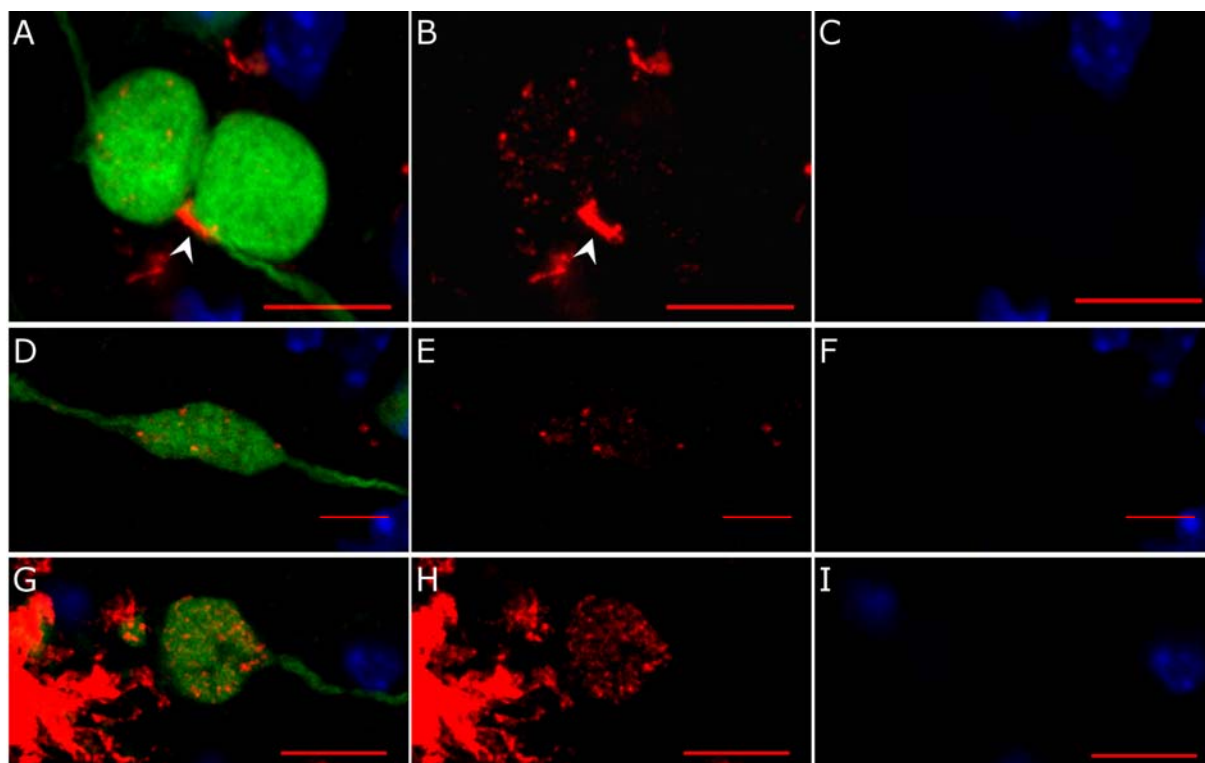


**Fig. 47 Confocal images of fibrillar A $\beta$  oligomers and A $\beta$  fibrils inside dystrophic fibers.** Using confocal imaging in 6-month-old YFP/APP/PS1KI<sup>hc</sup> mice with DAPI counterstaining confirming the lack of nuclei (blue), fibrillar A $\beta$  oligomers and A $\beta$  fibrils (OC antibody, red) were found to accumulate inside large dystrophic fibers (green). Merged images are shown (A, D, G) together with the isolated OC (B, E, H), and DAPI staining (C, F, I). Extracellular accumulation of A $\beta$  (White arrowhead) could be detected near large dystrophic fibers accumulating intracellular A $\beta$  (A-C). The intracellular accumulation of intracellular granules of OC-stained A $\beta$  peptides were observed in many large dystrophic neurites, both plaque-independent (D-F) as well as occasionally in the vicinity of plaques (G-I). A-C are generated as a sum of 20 confocal images within the dystrophic fibers, whereas D-I are images in a single confocal plane. Scale bars: 10 $\mu$ m.



independent swollen fibers were found to accumulate A $\beta$  showing a weaker scattered staining of smaller granules throughout the lumen together with the accumulation of larger A $\beta$  granules (Fig. 47D-F). The same pattern could also be found in some large dystrophic neurites in the vicinity of plaques (Fig. 47G-I). Abundant accumulation of intraneuronal A $\beta$  inside cell bodies, especially in the cortex, was confirmed using the OC antibody, where A $\beta$  granules were also observed in the axon (Fig. 48A) and large apical dendrite (Fig. 48B) projecting from the cells, indicating that A $\beta$  can be transported into axons as well as dendrites. Furthermore, occasionally, axonal swellings accumulating A $\beta$  could be found directly connected to cortical neurons accumulating abundant amounts of intraneuronal A $\beta$  at the axon hillock (Fig. 48C, D). This might indicate that the intracellular A $\beta$  accumulating in large plaque-independent dystrophic neurites originates from neurons accumulating intraneuronal A $\beta$  in their cell bodies from where it is transported into the fibers.

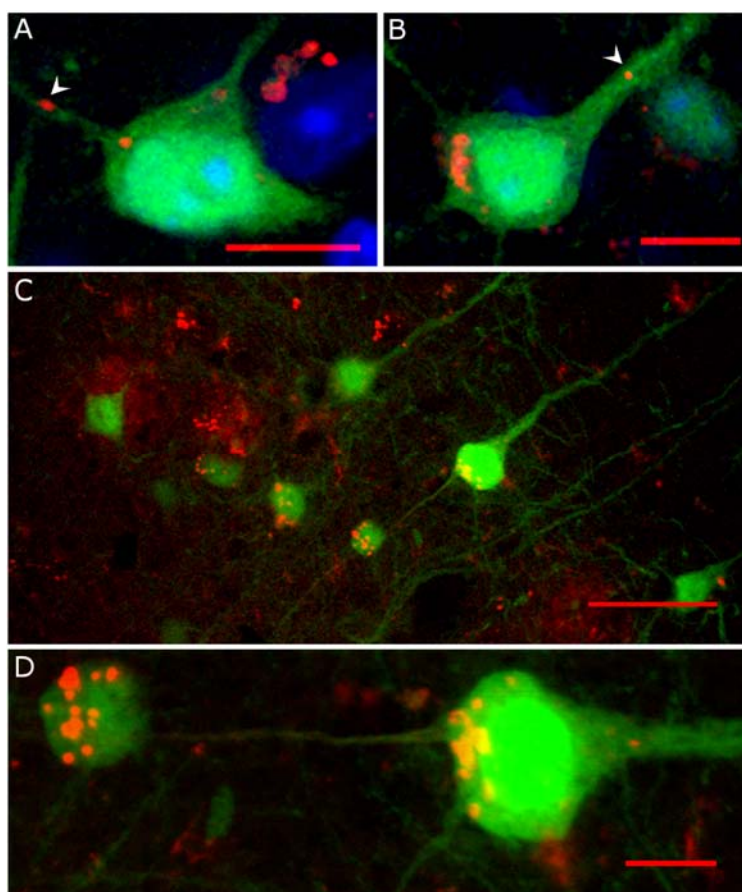


**Fig. 48 Confocal images of intraneuronal A $\beta$  accumulation in cortical neurons.** Using confocal imaging in the cortex of 6-month-old YFP/APP/PS1KI<sup>hc</sup> mice, A $\beta$  was found to accumulate inside cell bodies as well as in axons (A) and large apical dendrites (B) projecting from the cell body (OC antibody, red). Also, axonal swellings accumulating intracellular A $\beta$  were found directly connected to cortical neurons accumulating abundant amounts of intraneuronal A $\beta$  at the axon hillock (A $\beta$ [N] antibody, red) (C, D: enlargement of C). Scale bars: 10 $\mu$ m (A, B, D), 40 $\mu$ m (C).

### 3.5 Interaction between $\alpha 7$ nAChR and A $\beta$

#### Effect of an $\alpha 7$ nAChR agonist on A $\beta$ pathology

The A $\beta$  pathology of 9-month-old APP/PS1 $\Delta$ E9 mice chronically treated with saline, 10 mg/kg SSR180711, or 10 mg/kg nicotine twice daily for 10 days was assed by quantification of 4G8, LOC, and A $\beta$ [N] immunostainings (Fig. 49), where LOC is an OC-like antibody also

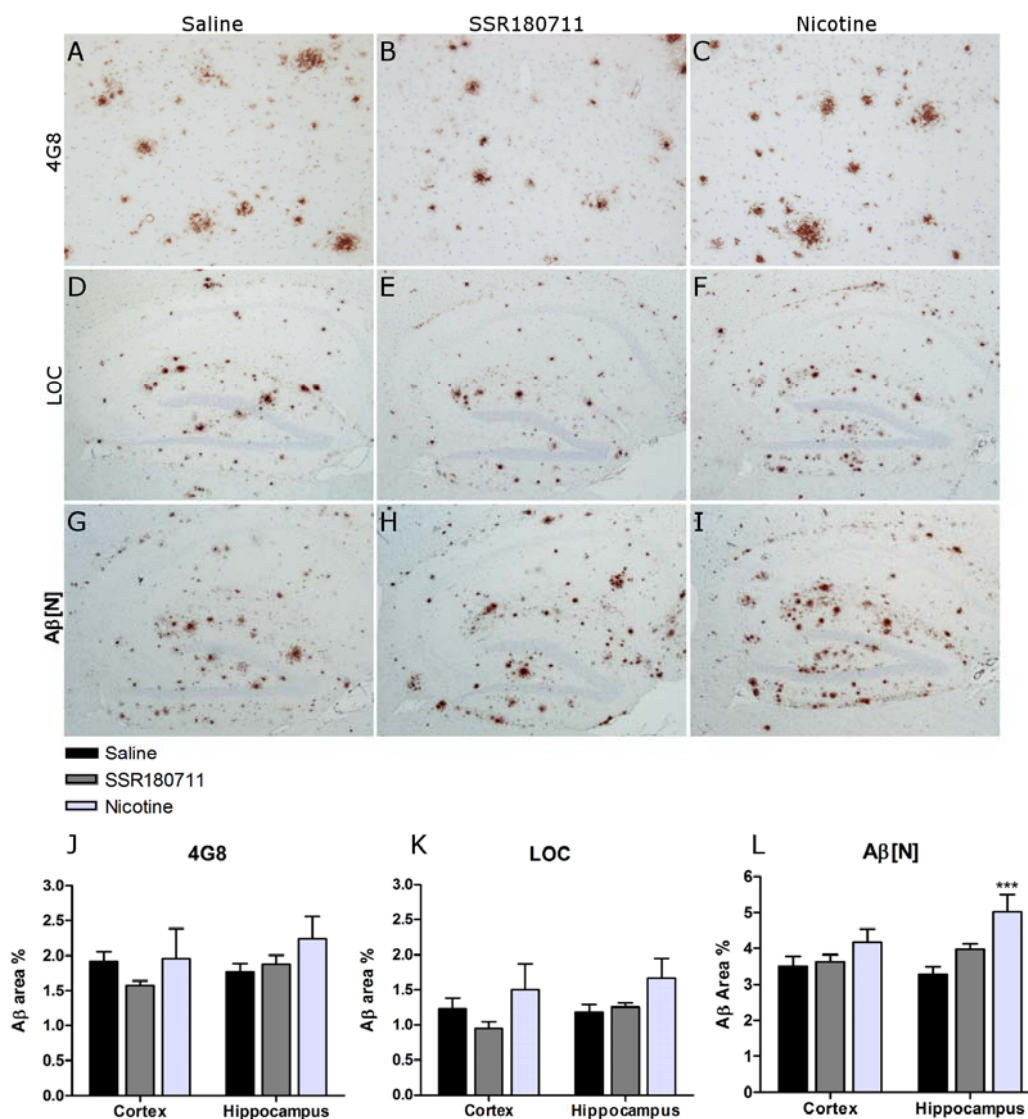


**Fig. 49 A $\beta$  staining in saline, SSR180711, and nicotine treated APP/PS1 $\Delta$ E9 mice.** Immunostaining of A $\beta$  was performed using 4G8, LOC, and A $\beta$ [N] antibodies and micrographs show 4G8 staining in the parietal cortex (A-C) and LOC (D-F) and A $\beta$ [N] (G-I) staining in the hippocampal region of 9-month-old APP/PS1 $\Delta$ E9 mice chronically treated with saline, 10 mg/kg SSR180711, or 10 mg/kg nicotine twice daily for 10 days. Quantification showed no significant differences in 4G8 (J) and LOC (K) pathology, whereas a significant increase in A $\beta$ [N] pathology (L) of the hippocampal region was observed in chronically nicotine treated animals as compared to control saline treated mice. In each group of treatment, 4-6 APP/PS1 $\Delta$ E9 mice were analyzed using one-way ANOVA followed by Dunnett's post-hoc test. Error bars represent mean  $\pm$  s.e.m. \*\*\* $P < 0.001$ .

recognizing A $\beta$  fibrils and fibrillar oligomers (Kayed et al. 2007). The percentile areas covered by A $\beta$  immunoreactivity were measured in the hippocampal formation as well as in the parietal cortex just above the hippocampal formation and showed no significant differences in either 4G8 (Fig. 49J) and LOC (Fig. 49K) pathology, however, a significant increase in A $\beta$ [N] pathology (Fig. 49L) was observed in the hippocampal region of chronically nicotine treated APP/PS1 $\Delta$ E9 mice as compared to control saline treated animals.

To assess the effect of A $\beta$  accumulation *in vivo* on the level of  $\alpha$ 7 nAChRs,  $\alpha$ -BTX autoradiographic binding studies were carried out in the 9-month-old saline treated APP/PS1 $\Delta$ E9 and wild-type mice. Measurements were performed in the medial prefrontal cortex, the parietal cortex (S1) as well as in the hippocampal region (Fig. 50A-H). No significant differences were observed in  $\alpha$ -BTX binding level between the two genotypes in any of the quantified regions (Fig. 50 I, J).

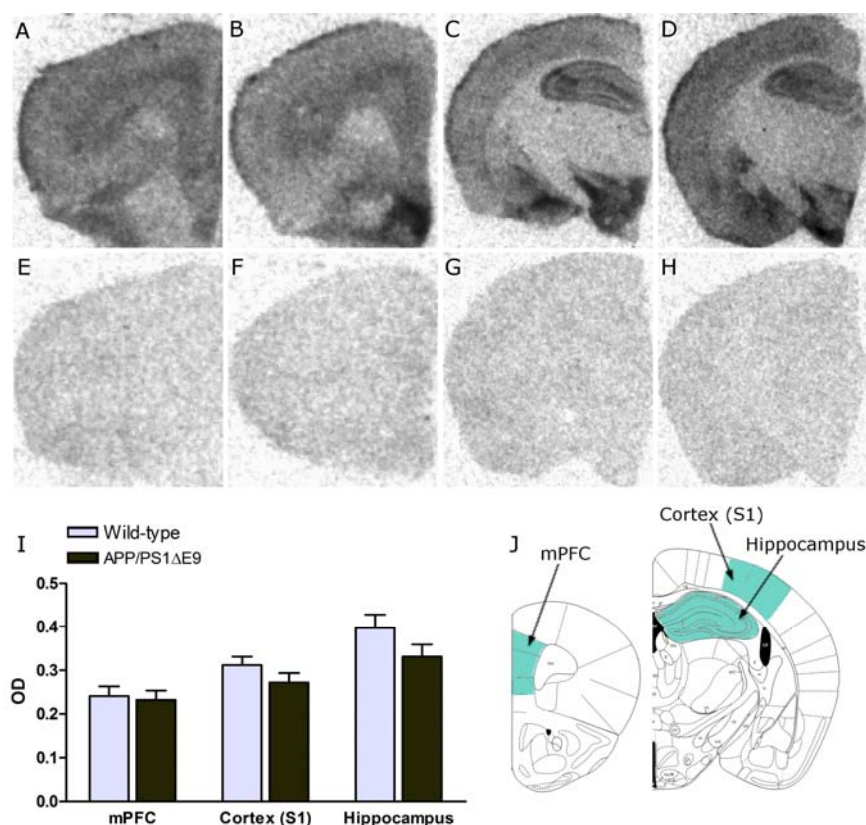


**Fig. 50  $\alpha$ -BTX radioactive ligand binding in wild-type and APP/PS1 $\Delta$ E9 mice.** Autoradiograms show total  $\alpha$ -BTX binding in coronal sections at the level of the frontal cortex and hippocampal region of 9-month-old wild-type (A, C) and APP/PS1 $\Delta$ E9 mice (B, D) together with their corresponding non-specific binding (NSB, E-H). Quantification in 5 wild-type and 6 APP/PS1 $\Delta$ E9 mice showed no significant differences in specific  $\alpha$ -BTX binding either in the medial prefrontal cortex (mPFC), the parietal cortex (S1), or the hippocampal formation (I), which were delineated as illustrated (J). Data was analyzed by unpaired Student's t-tests in each region.



### 3.6 Functional integrity of immediate early gene responses following novelty stimulation

The regulation of *Arc* and *c-fos* gene expression was measured by in situ hybridization in the mPFC, the parietal cortex (S1), CA1, CA3, and the upper DG (Fig. 51) following a single episode of novelty in APP/PS1 $\Delta$ E9 as compared to wild-type mice. Examples of the quantified autoradiograms are given for the *Arc* gene expression analysis (Fig. 52). A single episode of novelty increased *Arc* gene expression about 60% in the mPFC (Fig. 53A) and 30% in the parietal cortex (Fig. 53D) of wild-type mice, where the corresponding percentile increases in the APP/PS1 $\Delta$ E9 mice were 90% in the mPFC and 65% in the parietal cortex. The cortical inductions of *Arc* gene expression was thus higher in the transgenic mice than in the wild-type, however, basal *Arc* gene expression levels in home-cage control mice were found to be about 40% lower in APP/PS1 $\Delta$ E9 mice as compared to wild-type mice in both the mPFC (Fig. 53A) and the

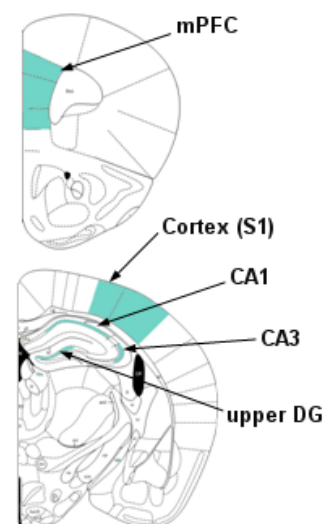


**Fig. 51 Quantified areas of the in situ hybridization analysis.** Quantification was performed in the medial prefrontal cortex (mPFC), cortex (S1), CA1, CA3, and upper DG.

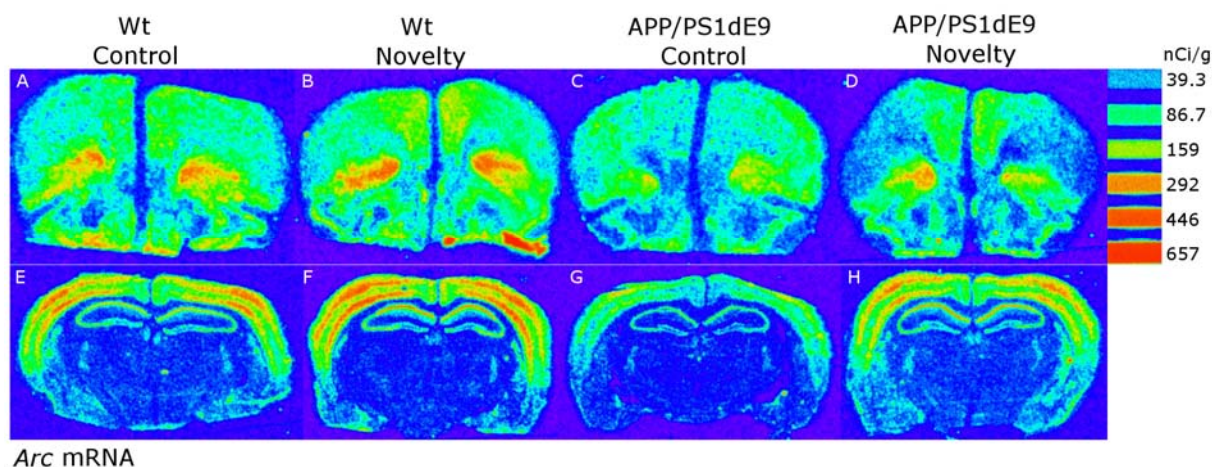


**Fig. 52 *Arc* in situ hybridization in wild-type and APP/PS1 $\Delta$ E9 novelty stimulated and control mice.** Autoradiograms show the pattern of *Arc* mRNA hybridization using pseudo colors at the level of the prefrontal cortex (A-D) and the hippocampal region (E-H) in wild-type and APP/PS1 $\Delta$ E9 mice in home-cage control (A, E and C, G, respectively) and novelty stimulated animals (B, F and D, H, respectively). To the right is found the  $^{14}$ C-calibration scale used for quantification of the autoradiograms.



---

parietal cortex (Fig. 53D). The induced levels of *Arc* gene expression after novelty thus remained significant lower in the APP/PS1 $\Delta$ E9 mice as compared to wild-type. In the hippocampal formation, percentile inductions of *Arc* gene expression following novelty were about 50%, 40%, and 35% in the CA1, CA3, and upper DG of wild-type mice as compared to 70%, 20%, and 30% in APP/PS1 $\Delta$ E9 mice (Fig. 53G, J, M), although the increase in the CA3 of APP/PS1 $\Delta$ E9 mice was only significant with a t-test ( $p=0.0043$ ) and not with the one-way ANOVA Newman-Keuls post-hoc test. Only in the CA1 was the basal level of *Arc* gene expression found to be lower in APP/PS1 $\Delta$ E9 than in wild-type mice (Fig. 53G, 26%), but induced levels of *Arc* gene expression were found to be lower in the APP/PS1 $\Delta$ E9 mice as compared to the wild-type in all three measured regions of the hippocampal formation.

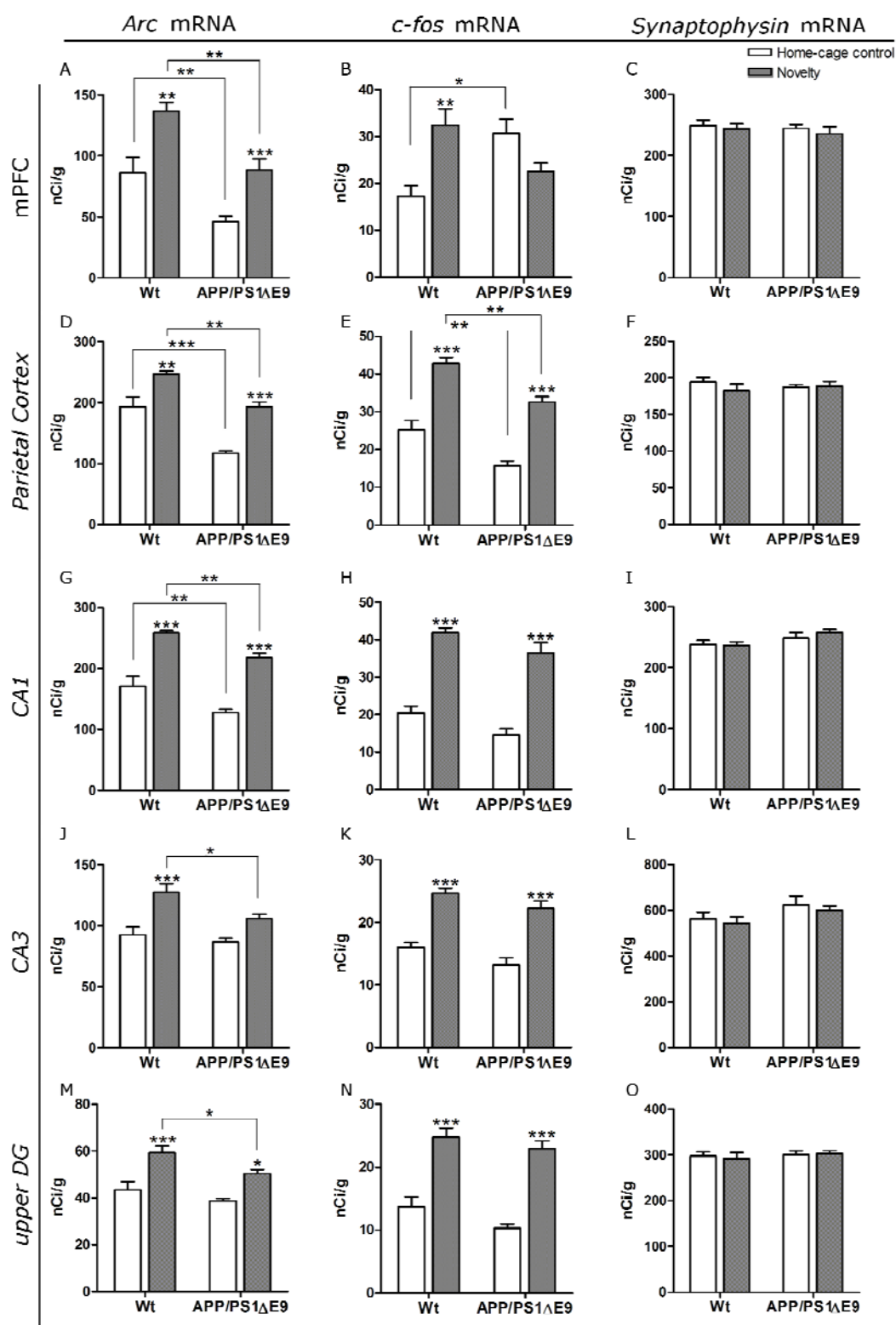


**Fig. 53 Quantification of *Arc*, *c-fos* and *synaptophysin* expression.** Mean ( $\pm$  SEM) levels of *Arc*, *c-fos* and *synaptophysin* expression is shown in the medial prefrontal cortex (mPFC, A, B, C) and parietal cortex (D, E, F) as well as in the CA1 (G, H, I), CA3 (J, K, L), and upper dentate gyrus (DG) (M, N, O) of the hippocampal formation. Data was analyzed by one-way ANOVA followed by Newman Keuls post-hoc test ( $n = 6$ ). Error bars represent mean  $\pm$  s.e.m. \* $P < 0.05$ ; \*\* $P < 0.01$ ; \*\*\* $P < 0.001$ .

In comparison, only cortical deficits in the induction of *c-fos* gene expression following a single episode of novelty were detected in the APP/PS1 $\Delta$ E9 mice compared to wild-type mice, whereas no differences in basal or induced *c-fos* expression levels were detected in either the CA1, CA3, or upper DG of the hippocampal formation (Fig. 53H, K, N). In the mPFC, APP/PS1 $\Delta$ E9 mice completely failed to up-regulate *c-fos* expression following novelty exposure and showed an 80% higher basal expression level of *c-fos* as compared to

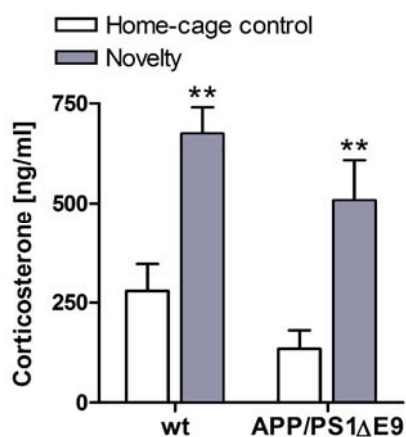


**Fig. 54 Plasma corticosterone in wild-type and APP/PS1 $\Delta$ E9 novelty stimulated and control mice.** The level of corticosterone was measured in plasma of home-cage control and novelty stimulated wild-type and APP/PS1 $\Delta$ E9 mice, and showed an increased corticosterone level after novelty exposure in both genotypes. Data was analyzed by unpaired Student's t-tests. Error bars represent mean  $\pm$  s.e.m. \*\* $P < 0.01$ .

wild-type mice (Fig. 53B). In the parietal cortex, the pattern of *c-fos* expression was similar to that of *Arc* with about 70% induction of *c-fos* expression in wild-type mice and 105% induction in APP/PS1 $\Delta$ E9 mice following novelty exposure, but with a basal difference of 40% resulting in a 25% lower induced *c-fos* expression level after novelty in APP/PS1 $\Delta$ E9 as compared to wild-type mice (Fig. 53E).

In contrast, no changes were observed in mRNA levels of the house keeping gene *synaptophysin*, in any of the quantified regions (Fig. 53C, F, I, L, O).

The five-min exposure to novelty strongly stimulated the HPA axis in mice of both genotypes as a significant increase in plasma levels of corticosterone was found in novelty exposed wild-type (2.4 fold) as well as APP/PS1 $\Delta$ E9 (3.8 fold) mice as compared to home-cage controls (Fig. 54).

## 4 Discussion

### 4.1 *Neuron loss in the cholinergic system of APP/PS1KI mice*

Numerous transgenic mouse models have been generated and investigated over the past years in order to amongst others model the cholinergic neuron loss of the basal forebrain found in AD patients. So far, most AD mouse models have shown either no change or even an increase in the number of forebrain cholinergic neurons (Boncristiano et al. 2002; Bronfman et al. 2000; German et al. 2003; Hartmann et al. 2004; Jaffar et al. 2001; Perez et al. 2007). Exceptions are the TgCRND8 mouse model of AD showing a loss of Ch4 neurons (Bellucci et al. 2006), and the Ts65Dn mouse model of Down's syndrome showing loss of Ch1/2 neurons (Salehi et al. 2006; Seo and Isacson 2005). Regarding other cholinergic regions, a neuron loss in the pons complex was described using a semi-quantitative assessment (Zhang et al. 2005), and another recent study reported a minor loss of cholinergic interneurons in the motor cortex (Perez et al. 2007). However, cholinergic cortical interneurons are bipolar GABAergic interneurons co-expressing ChAT and cannot be found in all rodent species, thus they may not be regarded as part of the cholinergic system (Bhagwandin et al. 2006). None of the studies showing loss of cholinergic neurons mentioned whether or not the degenerating neurons accumulated intraneuronal A $\beta$ , though the degenerating cholinergic forebrain neurons in the Ts65Dn mouse model of Down's syndrome were shown to accumulate APP in early endosomes, leading to a blockage of neuronal growth factor transport (Salehi et al. 2006).

The objectives of the present study were a quantitative assessment of cholinergic neuron numbers in the APP/PS1KI mouse model of AD as well as the potential impact of intraneuronal A $\beta$  deposition and accumulation on neuronal survival. Therefore, areas showing different degrees of A $\beta$  pathology were included in the quantitative analysis. The cholinergic forebrain complex consisting of Ch1-4 showed virtually no A $\beta$  pathology with neither extracellular A $\beta$  plaque deposition, nor intracellular accumulation of A $\beta$  peptides. However, fibers from this region displayed swollen ChAT-positive dystrophic neurites surrounding A $\beta$  plaques in the cortex and hippocampal formation as previously reported in other mouse models of AD (Aucoin et al. 2005; Bellucci et al. 2006; Bronfman et al. 2000; Hu et al. 2003; Luth et al. 2003; Wong et al. 1999). The Ch1/2 and Ch4 regions of the cholinergic forebrain

complex were quantified separately as they project to separate areas: the hippocampal formation and the cortex, respectively. No cholinergic neuron loss was found in either the Ch1/2 or Ch4 cholinergic nuclei. The Ch1/2 region of the forebrain complex projects to the hippocampal formation which in the present mouse model is known to develop a significant neuron loss of more than 50% in the CA1 at 10 months of age (Casas et al. 2004). This could have had additional influence on the survival of the Ch1/2 cholinergic neurons, as they have been shown to be highly dependent on external growth factor stimuli retrogradely transported from the hippocampus (Burke et al. 1994). However, growth factor stimuli could be provided by hippocampal cell types other than the degenerating CA1 neurons. In conclusion, the APP/PS1KI mouse model does not model the well-established loss of cholinergic forebrain neurons of the nucleus basalis of Meynert in AD patients (Arendt et al. 1988; Mufson et al. 1989; Whitehouse et al. 1981). However, pathological alterations in transgenic mouse models must be considered to be determined by the expression pattern of the respective transgene. Thus as the APP transgene is not expressed in the forebrain complex of the APP/PS1KI mouse model, the lack of neuron loss in this region does not subtract from the valid use of this model to study the impact of A $\beta$  in the regions of APP transgene expression. Accordingly, the motor nuclei Mo5 and 7N accumulating intracellular A $\beta$  were found to exhibit significant loss of cholinergic neurons. This loss was most prominent in the Mo5 and was found to coincide with a more robust accumulation of various A $\beta$  species including A $\beta$ <sub>1-x</sub>, fibrillar oligomers and fibrillar A $\beta$ , aggregated A $\beta$ , as well as A $\beta$ N<sub>3pE</sub> compared to the 7N. This finding is particularly interesting and corroborates our earlier reports of spinal cord axonal degeneration (Wirhth et al. 2007) and severe motor pathology in aged APP/PS1KI mice that show severe deficits in motor performance, as analyzed by a series of motor tasks including the balance beam, string suspension test, vertical grip hanging task, and rotarod (Wirhth et al. 2008b). These deficits occurred as early as at the age of 6 months and were preceded by a strong accumulation of various A $\beta$  peptides in motor neurons in the ventral horn of the spinal cord in APP/PS1KI mice (Wirhth et al. 2007). In the light of the present results this accumulation of A $\beta$  peptides could very well contribute to degeneration of the motor neurons in the spinal cord causing the detected motoric deficits.

The ChAT-positive cholinergic interneurons of the caudate putamen that did not accumulate intraneuronal A $\beta$ , but were surrounded by numerous smaller A $\beta$  plaques, also showed no loss of neurons. This adds further evidence to the assumption that extracellular plaques are not a substantial factor in mediating cell death (Wirhth et al. 2004).

In summary, A $\beta$  plaque pathology leading to plaque associated dystrophic neurites was not sufficient to cause neuron loss in the cholinergic system of APP/PS1KI mice. However, accumulation of intracellular A $\beta$  aggregates represented an early pathological alteration that strongly correlated with neuron death in brain stem motor nuclei (Fig. 55).

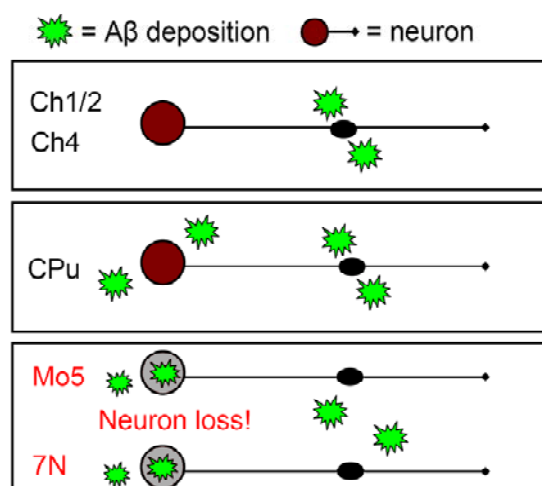


**Fig. 55 Summary of A $\beta$ -mediated cell death in the cholinergic system.** Extracellular plaque deposition leading to plaque associated dystrophic neurites was not sufficient to cause significant neuron loss in Ch1/2, Ch4, or caudate putamen (CPu). However, accumulation of intraneuronal A $\beta$  is considered an early pathological alteration that correlated with neuron loss in the Mo5 and 7N.

#### 4.2 Effect of intraneuronal A $\beta$ versus plaques on neurodegeneration

The previous study of A $\beta$  pathology and neurodegeneration in the cholinergic system of the APP/PS1KI mouse model strongly supported the hypothesis of intracellular A $\beta$  being a major trigger of neuron death in AD, and the present study was designed to more specifically investigate the toxic effect of intracellular A $\beta$  versus extracellular A $\beta$  plaques on neuronal survival. For this reason, the present study focused on two regions with distinct pathological differences regarding plaque development and intraneuronal A $\beta$  accumulation. The frontal cortex was chosen for stereological quantification representing a region with massive and early accumulation of intraneuronal A $\beta$ , with concomitant strong extracellular plaque pathology covering 12.1 % of the frontal cortex at the age of 12 months. To dissect the impact of intraneuronal A $\beta$  accumulation, the thalamus was chosen as a control region for stereological quantification representing a region with no accumulation of intraneuronal A $\beta$  but harboring a comparable amount of extracellular plaques that covered 13.1% of the region

at the age of 12 months. Despite the massive amount of plaques, the thalamus was strikingly found to suffer no neuron loss in either 6- or 12-month-old APP/PS1KI mice as compared to PS1KI control mice. This is in line with the many negative results reporting no loss of neurons in many mouse models of AD accumulating various amounts of A $\beta$  plaques (Duyckaerts et al. 2008; Games et al. 2006), and altogether suggests that plaques have no significant effect on neuronal survival. In contrast, a neuron loss of about 30 % was found in the frontal cortex already at 6 months of age, which did not significantly worsen from 6 to 12 months. Importantly, the only evident pathological difference between the two regions in question was the massive transient accumulation of intraneuronal A $\beta$  in the frontal cortex, which thus must be considered as a major trigger of the neuron loss observed in this region. Nevertheless, we can not completely rule out that thalamic neurons differ from cortical neurons in their cellular properties and may somehow be less vulnerable in general. Also, the recent finding of soluble oligomeric A $\beta$  species being highly toxic could argue that the neuron loss in the frontal cortex could be caused by the presence of extracellular soluble A $\beta$  that is, perhaps, not detected by our immunohistochemical protocol. However, in our opinion, it is unlikely that soluble extracellular A $\beta$  oligomers are causing the observed neurotoxic effects as they should be present in all plaque-rich areas including the frontal cortex as well as the thalamus. In addition, mutant PS1 may induce toxic effects due to alterations in biological functions of PS1; however, as we have used PS1KI littermates as control mice, which showed unchanged neuron numbers during aging in the thalamus as well as frontal cortex, we conclude that the applied PS1-FAD mutations have no effect on neuronal survival. Only in the combination of the PS1-FAD mutations with transgenic APP, A $\beta$ -related neurodegeneration was observed.

The transient nature of the intraneuronal accumulation of A $\beta$  observed in the frontal cortex adds further support to the hypothesis of its toxicity. Thus significant neuron loss became evident at the age of 6 months; exactly the time point when a decreased intraneuronal A $\beta$  accumulation was evident. This corresponds to the possibility that the neurons accumulating intracellular A $\beta$  at earlier time points are those lost at a time between the age of 2 and 6 months and correlates with an earlier report claiming that neurons which accumulate A $\beta$  peptides undergo lysis to give rise to extracellular deposits (D'Andrea et al. 2001). However, the strong accumulation of plaques in the thalamus of the present mouse model which contains no neurons expressing the APP transgene suggests that plaques can be formed by A $\beta$

deposition from fibers. Thus other hypotheses exist for plaque formation, and compact plaques with high A $\beta$ 40 load are suggested to have a different etiology than diffuse plaques with predominant A $\beta$ 42 deposition, as in the current model. The transient nature of intraneuronal A $\beta$  accumulation preceding massive extracellular plaque pathology has been previously reported in a different APP/PS1 transgenic mouse model (Langui et al. 2004; Wirths et al. 2002). The relevance of this finding of an early transient accumulation of A $\beta$  is supported from studies in Down's syndrome (DS) patients who develop A $\beta$  plaques and NFTs as found in AD patients. Intraneuronal A $\beta$ 42 was found to accumulate only in younger DS patients declining with the development and maturation of plaques (Gyure et al. 2001; Mori et al. 2002). In addition, another study claims that intraneuronal A $\beta$ 42 in human AD is only detectable in patients with low Braak stages and short disease duration and that the intraneuronal A $\beta$  immunoreactivity is lost in patients with more progressive AD (Gouras et al. 2000). This would correlate with the fact that neurons are not yet lost in pre-clinical AD (West et al. 2004) where intraneuronal accumulation of A $\beta$ 42 would still be detectable; however, with the transition to AD, the intraneuronal immunoreactivity will be strongly decreased or undetectable, due to the loss of the respective neurons. The possibility of a transient intraneuronal A $\beta$  accumulation is of great importance for the difficulties of providing proof of the intracellular A $\beta$  hypothesis in human AD tissue. As this most often represents end stage pathology where adverse neuron loss has already occurred, intraneuronal A $\beta$  may no longer be present.

Altogether, the present study strongly suggests that plaques have no effect on neuronal survival, but that a transient intraneuronal accumulation of A $\beta$  coincides with neuron loss. These findings are in line with the modified  $\beta$ -amyloid cascade hypothesis, in which early intraneuronal A $\beta$  accumulation represents the central pathological alteration upstream of extracellular plaque deposition and neuronal dysfunction (Wirths et al. 2004).



### **4.3 Intra-neuronal A $\beta$ staining in AD patients and transgenic AD mouse models**

#### **Optimization for staining of intra-neuronal A $\beta$ in mouse models of AD**

FA is widely used to enhance immunostaining of plaques and has been shown to covalently modify A $\beta$  by formate esterification of serine residues, leading to solubilization of the peptide (Alafuzoff et al. 2008; Klunk et al. 1994). The effect of FA on the immunohistochemical staining of intra-neuronal A $\beta$  is currently debated with reports of low or similar effects to heat, as well as FA having a counteracting effect on the heat-induced enhanced intra-neuronal A $\beta$  staining in human AD tissue (D'Andrea et al. 2003; Ohyagi et al. 2007). In addition, the exposure time for FA pretreatment varies greatly between studies; however, one study showed no significant difference in the intensity of the amyloid plaque detection between 10 min and 12 hours of FA pretreatment in AD tissue (D'Andrea et al. 2003). Corroborating this result, we did not find any significant difference between 3 and 10 min FA treatment in the percentile area of intra-neuronal A $\beta$  or plaque staining in the CA1 and thalamus of APP/PS1KI mice, respectively. The effect of a short FA exposure is also in line with other studies in mice where intra-neuronal A $\beta$  could be detected in paraffin embedded sections using only 5 min FA incubation (Knobloch et al. 2007; Van Broeck et al. 2008).

Regarding the effects of heat versus FA on intra-neuronal A $\beta$  detection, FA pretreatment was found to be essential for the staining of A $\beta_{1-x}$  peptides in the CA1 of APP/PS1KI mice, whereas no or heat antigen retrieval alone disclosed no or very little detection of intra-neuronal A $\beta_{1-x}$ . Yet, the combination of FA and heat seemed to even further intensify the staining of intra-neuronal A $\beta_{1-x}$ , although no significant increase in the stained area was observed compared to FA pretreatment alone. Regarding the detection of plaques, heat and FA were found to have an equal enhancing effect on the extracellular staining of A $\beta$  plaques in the thalamus of APP/PS1KI mice. This finding of FA to enhance staining of plaques is in general agreement with the literature (Alafuzoff et al. 2008; Kitamoto et al. 1987), however, the equally enhancing effect of heat pretreatment does not seem to have been systematically investigated in AD tissue. The enhancing effect of FA on intra-neuronal A $\beta$  staining in mouse tissue is in contrast to the observations in human AD tissue reporting FA to have no effect or

even to counteract the heat-inducing effect on staining of intracellular A $\beta$  (D'Andrea et al. 2003; Ohyagi et al. 2007).

To further compare the effect of heat and FA pretreatment on the detection of intraneuronal A $\beta$ , the three protocols using heat, 3 min FA exposure, or their combination were compared to no pretreatment in three additional mouse models. Corroborating the observations in APP/PS1KI mice, 3 min FA was confirmed to have a markedly increasing effect on the staining of intraneuronal A $\beta_{1-x}$  peptides revealing an intense staining of large granules at the axon hillock of cortical neurons in APP, APP/PS1, and 5xFAD mice, whereas heat pretreatment was found to have a minor increasing effect on intracellular A $\beta$  staining. Yet, the combination of heat and FA pretreatment showed the highest staining intensity. The same protocols were applied for immunostaining with the 4G8 antibody, recognizing the central epitope A $\beta_{17-24}$ . The 4G8 is a highly sensitive antibody used in routine staining of A $\beta$  in AD tissue (Alafuzoff et al. 2008), and was found not to cross-react with full length APP at high dilutions (1:10.000) using a combined heat and FA protocol in the APP/PS1KI mouse model (Christensen et al. 2008). With the application of FA, the 4G8 antibody revealed the same intense granular staining pattern as the A $\beta$ [N] antibody, however, surprisingly, heat pretreatment alone disclosed an obvious homogenous staining pattern of smaller granules dispersed throughout the cytoplasm in all four mouse models investigated that decreased upon the combination with FA. When the two protocols of heat and heat + FA were compared in a fluorescent double labeling of APP and 4G8, the fainter heat-induced intraneuronal A $\beta$  staining turned out to largely co-localize with APP, in contrast to the FA-induced staining of larger granules, suggesting that heat pretreatment alone increases the cross-reaction of the 4G8 antibody to APP. Alternatively, heat and FA could induce the staining of A $\beta$  peptides of different aggregation states corresponding to a suggestion that two unique forms of A $\beta$  exist as a function of their sensitivity to FA (D'Andrea et al. 2003). These heat-induced 4G8 stained A $\beta$  peptides would then be co-localized with APP in intracellular compartments and their decreased reactivity by FA corroborates a previous result of a counteracting effect of FA on heat enhanced A $\beta$  staining in human AD tissue (Ohyagi et al. 2007).

To investigate the aggregation state of the intraneuronal A $\beta$  revealed by FA pretreatment, the immunohistochemical stainings were compared to a Thioflavin S staining labeling aggregated A $\beta$  peptides (LeVine 1993). In all four mouse models, the Thioflavin S pattern was found to correspond to the intense granular intraneuronal A $\beta$  staining disclosed by FA or FA together

with heat using 4G8 as well as A $\beta$ [N] antibodies, suggesting that the intraneuronal A $\beta$  peptides induced by FA are highly aggregated in mouse models of AD. That FA reveals aggregated A $\beta$  is further supported by the observation that the FA worked best in the three mouse models with PS1 mutations, and to a lesser extent in the APP single transgenic mice not harboring the PS1 mutations that are known to increase the production of the more aggregation prone A $\beta$ 42 peptides (Guo et al. 1999; Jankowsky et al. 2004).

Our optimization of the staining protocol with regard to FA and heat shows that the two antigen retrieval methods may disclose separate species of A $\beta$  peptides with FA, especially detecting aggregated A $\beta$ , leading to the assumption that in mouse models of AD, FA is an essential pretreatment for immunohistochemical detection of intraneuronal aggregated A $\beta$  peptides.

### **Staining of intraneuronal A $\beta$ in brain tissue of AD patients**

The four protocols qualitatively investigated in the mouse models were applied to human AD tissue using A $\beta$ [N] antibodies specific to A $\beta$ <sub>1-x</sub>. The optimization was performed in paraffin embedded hippocampal sections from sporadic as well as Swedish and Arctic FAD brain tissue since the familial cases were considered more likely to show similarities to the mouse models and thus accumulate intraneuronal A $\beta$ . Also, the Arctic mutation has been shown to favor intracellular A $\beta$  production in cultured cells and mouse models (Sahlin et al. 2007). Some intraneuronal A $\beta$ <sub>1-x</sub> staining was evident even without any pretreatment, but heat dramatically increased the intraneuronal staining of smaller granules throughout the cytoplasm concentrating around the nucleus in all three types of AD hippocampal tissues, especially in the CA4 region. In contrast, FA pretreatment did not increase the staining of intraneuronal A $\beta$ <sub>1-x</sub> as compared to no antigen retrieval and even counteracted the enhancing effect of heat as the combination of heat and FA only slightly increased the staining of A $\beta$ <sub>1-x</sub> as compared to no pretreatment with much less inducing effect than heat alone. The counteracting effect of FA on the heat-induced staining of intraneuronal A $\beta$ <sub>1-x</sub> peptides corroborates one other study using an A $\beta$ 42(43) specific antibody (BC-05) and an autoclave heating protocol reporting a counteracting effect of FA on heat-induced A $\beta$ 42 staining (Ohyagi et al. 2007). These findings are in contrast to the observations in the mouse models where FA clearly enhanced the staining of intraneuronal A $\beta$  peptides and heat had no or only a minor increasing effect. The difference in the effect of heat and FA between mouse and

human tissue could be explained by differences in A $\beta$  species accumulating within the cells. In the AD mouse models, much of the intraneuronal A $\beta$  induced by FA pretreatment seemed to be aggregated peptides. Possibly, the intraneuronal A $\beta_{1-x}$  in AD tissue could be mostly soluble oligomeric species that may be enhanced by heat but counteracted by FA. In agreement, low-n oligomeric A $\beta$  have been detected inside primary human neurons (Walsh et al. 2000). The presence of soluble oligomeric A $\beta$  inside neurons would add further importance to the impact of intraneuronal A $\beta$  since two studies have so far indicated that soluble A $\beta$  may be the best correlate of cognitive decline in AD (McLean et al. 1999; Naslund et al. 2000).

The presence of intraneuronal A $\beta$  in sporadic AD tissue was confirmed by staining with the polyclonal OC antibody recognizing fibrillar A $\beta$  oligomers and A $\beta$  fibrils (Kayed et al. 2007). The OC antibody disclosed an intense intraneuronal A $\beta$  staining with heat as well as with additional FA pretreatment that had an intensifying effect on the intraneuronal OC staining. This is in contrast to the counteracting effect of FA on the detection of A $\beta_{1-x}$ , but is in line with the suggestion that FA enhances the staining of aggregated A $\beta$  fibrils that are recognized by the OC antibody. The staining disclosed by heat could be owing to detection of oligomeric A $\beta$  fibrils that are also recognized by the OC antibody and would thus agree with two previous studies stating that A $\beta$  oligomerization starts within neurons (Takahashi et al. 2004; Walsh et al. 2000).

It was attempted to further confirm the presence of intraneuronal A $\beta$  using the 4G8 antibody recognizing the central epitope A $\beta_{17-24}$ , as this is a commercially available widely used A $\beta$  antibody. However, the 4G8 antibody produced an intracellular staining pattern with a large granular cap-like staining adjacent to the nucleus that was completely different from the staining patterns of the A $\beta$ [N] and OC antibodies. This 4G8 staining proved to be caused by a cross-reaction with lipofuscin as Sudan Black B pretreatment abolished all intraneuronal fluorescence detected with the 4G8 antibody as well as autofluorescence from the UV and red channel. This observation corroborates another study suggesting cross-reaction between lipofuscin and several monoclonal antibodies toward the A $\beta_{17-24}$  sequence, including the 4G8 antibody (Baner et al. 1989). Despite this report of cross-reactivity to lipofuscin, the 4G8 antibody has been repeatedly applied to show intraneuronal A $\beta$  in AD disclosing this large granular cap-like staining adjacent to the nucleus characteristic of lipofuscin (LaFerla et al. 1997; Ohyagi et al. 2007; Wegiel et al. 2007). In contrast, the A $\beta$ [N] antibody disclosed a

highly specific staining pattern of small granules throughout the cytoplasm that remained following Sudan Black B pretreatment, which thereby is in good agreement with a previous study showing that lipofuscin and A $\beta$  peptides do not co-localize inside neurons (D'Andrea et al. 2002a).

The mechanism whereby intraneuronal A $\beta$  could mediate toxicity is yet unclear. Most evidence points to the accumulation of A $\beta$  in the endocytic pathway where it has been reported to accumulate in multi-vesicular bodies (MVB) (Takahashi et al. 2002) and impair their sorting (Almeida et al. 2006). In agreement, we observed a staining pattern of smaller granules dispersed throughout the cytoplasm, but often concentrated around the nucleus with both the A $\beta$ [N] and OC antibodies. This corresponds to earlier observations using an A $\beta$ 42 specific antibody (D'Andrea et al. 2002a) and cell biology studies locating the intracellular generation of A $\beta$  from the endoplasmic reticulum to the trans-Golgi network and the endosomal-lysosomal system (Cook et al. 1997; Perez et al. 1999; Rajendran et al. 2007; Selkoe 1998; Xu et al. 1997). Accordingly, abnormalities in the endocytic pathway have been reported to precede A $\beta$  plaque deposition in sporadic AD as well as Down's syndrome patients (Cataldo et al. 2000), indicating that intraneuronal A $\beta$  may be a mediator of early pathological changes.

Whether intraneuronal A $\beta$  originates exclusively from intraneuronal sources or if it can in addition be internalized from external sources is not yet clarified. Yet, much evidence supports the possibility of reuptake of A $\beta$  peptides into cells by endocytosis. Thus members of the lipoprotein receptor (LDLR) family (Bu et al. 2006),  $\alpha$ 7 nicotinic receptors (Nagele et al. 2002), as well as scavenger receptors for advanced glycation end products (RAGE) (Deane et al. 2003; Sasaki et al. 2001; Yan et al. 1996) have all been reported to interact with A $\beta$  and lead to internalization of extracellular A $\beta$  peptides. In particular, RAGE-A $\beta$  complexes have been shown to be internalized and co-localize with the lysosomal pathway in astrocytes in AD brains (Sasaki et al. 2001), which is supported by our observation of astrocytes accumulating high amounts of intraneuronal A $\beta$  granules. The LDLR-related protein (LRP) is a member of the LDLR family and functions as an ApoE receptor. LRP has been shown to facilitate rapid endocytosis of APP thereby promoting APP processing and thus A $\beta$  generation. In addition to the effect on APP trafficking, LRP-induced rapid endocytosis also facilitates cellular uptake of A $\beta$  peptides from the extracellular space, either directly through binding to A $\beta$  or indirectly through interaction with ligands such as ApoE (Bu et al. 2006). Accordingly, knock out of

*APOE* in PDAPP transgenic mice reduced the accumulation of intracellular A $\beta$  (Zerbinatti et al. 2006). With these implications for a role of ApoE in the accumulation of intraneuronal A $\beta$ , we correlated the intensity of the intraneuronal A $\beta_{1-x}$  staining in the hippocampal regions of 20 AD patients and 10 controls to ApoE genotype and found a highly significant correlation between the intensity of intraneuronal A $\beta_{1-x}$  staining and the presence of at least one ApoE4 allele ( $P=0.002$ ). This correlation nicely concurs with the observation of ApoE4 being a major risk factor of sporadic AD (Ashford 2004; Raber et al. 2004) and further supports an important role of intraneuronal A $\beta$  in the pathogenesis of AD.

A possible criticism of the importance of intraneuronal A $\beta$  is its presence in AD patients as well as in non-demented controls, which could be observed in the present study and is also reported by others (D'Andrea et al. 2002a; D'Andrea et al. 2002b; D'Andrea et al. 2001; Gouras et al. 2000; Wegiel et al. 2007). However, this is to be expected since plaques are likewise found in non-demented controls (Aizenstein et al. 2008) and the pools of intracellular and extracellular A $\beta$  most likely have a common origin. What needs to be investigated is whether there are differences in the A $\beta$  species accumulating within neurons of AD patients versus non-demented controls. Furthermore, an obstacle in immunopathological studies is that we are most often dealing with end-stage pathology where many neurons are already lost and early pathological mechanisms are not easily identified. Thus a transient nature of intraneuronal A $\beta$  accumulation preceding massive extracellular plaque pathology has previously been reported in transgenic mouse models (Christensen et al. 2008; Langui et al. 2004; Wirths et al. 2002), as well as in Down's syndrome (DS) patients (Gyure et al. 2001; Mori et al. 2002), and intraneuronal A $\beta_{42}$  in human AD has been claimed to be most detectable in patients with low Braak stages and short disease duration (Gouras et al. 2000). It is therefore very likely that the accumulation of intraneuronal A $\beta$  may be much more prominent in MCI patients in which AD symptoms only begin to emerge and neurons have not yet been lost (West et al. 2004).

The present study is a thorough report of intraneuronal N-terminal A $\beta$  species in human AD which have so far believed not to accumulate inside neurons (Chui et al. 2001; Mori et al. 2002) and confirmed the presence of intraneuronal A $\beta$  in human AD by staining with the OC antibody recognizing fibrillar oligomers and fibrillar A $\beta$ . Our optimization of the staining protocol regarding FA and heat shows that heat is essential for the detection of intraneuronal A $\beta_{1-x}$  peptides in human AD tissue and is counteracted by FA. However, the effects of heat

and FA seem to depend on the specificity of the antibody applied since intraneuronal staining with the OC antibody was increased and not counteracted by FA, probably owing to the observation from AD mouse models that FA enhances the staining of aggregated A $\beta$  peptides. In addition, a highly significant correlation was identified between the accumulation of intraneuronal A $\beta_{1-x}$  peptides and ApoE4 genotype, supporting the view that the ApoE4 isoform is a major risk factor of AD.

#### **4.4 Effect of A $\beta$ on axonopathy in transgenic AD mouse models**

Axonal deficits and impairment of motor performance are common pathological alterations in mouse models expressing different isoforms of human mutant tau protein (reviewed in (Wirhth and Bayer 2008)). However, in recent years, similar phenotypes have been reported for AD mouse models based on APP overexpression (Stokin et al. 2005; Wirhth et al. 2007; Wirhth et al. 2006), and disturbances of axonal transport rates have been reported in APP-based transgenic mouse models of Down syndrome (Salehi et al. 2003) and AD (Smith et al. 2007). Accordingly, APP has been demonstrated to undergo fast axonal transport (Koo et al. 1990), presumably by a kinesin-I-mediated mechanism (Kamal et al. 2000). In addition, the  $\beta$ -site cleaving enzyme (BACE) and PS1 have been shown to be associated with APP-resident membranous cargos, implying that A $\beta$  can be produced directly in the axons (Kamal et al. 2001), although this finding has recently been questioned (Lazarov et al. 2005). Accordingly, APP, BACE and PS1 were found to co-accumulate in swollen axons following traumatic brain injury (Chen et al. 2004).

A recent report claiming that axonopathies in APP-transgenic mouse models entirely depend on APP overexpression and that co-expression of FAD-linked PS1 mutants and related increased A $\beta$  levels suppress axonal defects (Stokin et al. 2008), prompted us to analyze axonal degeneration in our APP/PS1KI<sup>ho</sup> mouse model, as well as in APP single transgenic and APP/PS1KI<sup>he</sup> mice, all harboring equal APP transgene expression. Previous work in the APP/PS1KI<sup>ho</sup> mouse model has demonstrated a severe age-dependent axonal degeneration phenotype, which is characterized by the accumulation of large axonal swellings. These swellings were most abundant in fiber-rich regions of the central nervous system such as corpus callosum, pons, medulla, and spinal cord. We demonstrated a significant increase in these swellings between 6 and 10 months of age, which only marginally worsened at the age

of 14 months (Wirhth et al. 2007). The mice used in the present study are based on Thy1-driven overexpression of APP751 with the Swedish and London mutations and carry either no (APP), one (APP/PS1KI<sup>he</sup>) or two (APP/PS1KI<sup>ho</sup>) mutant murine PS1 alleles under the control of the endogenous PS1 promoter. Using this strategy, we ensured that the APP expression level did not differ between the different mouse lines, which was confirmed by immunostaining using APP antibodies and western-blotting. However, the amount of A $\beta$  peptides differs significantly between the analyzed mouse lines, leading to dramatic increases in the A $\beta$  load comprising plaques as well as intraneuronal A $\beta$  depending on the mutant PS1KI gene dosage. It has been previously shown that expression of mutant PS1 allele together with an APP transgene does not only lead to a higher overall A $\beta$  load, but in addition causes a significant rise in the A $\beta$ 42/A $\beta$ 40-total ratio and an earlier plaque onset (6m in APP versus 2 m in APP/PS1KI<sup>ho</sup> mice) (Casas et al. 2004).

To quantify axonal defects we applied antibodies toward phosphorylated APP as well as NF-200 as markers of axonal degeneration. Upon quantification of pAPP as well as NF-200-positive plaque-independent axonal swellings in the pons and spinal cord, significant increases in the numbers of dystrophic spheroids were detected in APP/PS1KI<sup>he</sup> mice compared to APP single transgenic mice, which were almost devoid of any axonal swellings in the analyzed regions. When comparing APP/PS1KI<sup>he</sup> with APP/PS1KI<sup>ho</sup>, a further 2 – 4 times increase of spheroids was detected in both pons and spinal cord. This result is in apparent contradiction to the recently published finding that axonal defects were unchanged or even suppressed in mice expressing FAD mutant PS1 in combination with FAD mutant APP (Stokin et al. 2008). One major difference between the APP/PS1 double-transgenic mice used in this report and our mouse model is the fact that the endogenous murine PS1 gene was still present in the APP/PS1 transgenic mice, whereas it has been sequentially replaced by the FAD mutant form in our APP/PS1KI model. It has been hypothesized that kinesin-based axonal transport is compromised by mutations in PS1 via interaction with glycogen synthase kinase 3 $\beta$  (GSK3 $\beta$ ) and it has been recently reported that the relative levels of GSK3 $\beta$  activity were increased in the presence of mutant PS1, as well as in the absence of wildtype PS1. This results in increased phosphorylation of kinesin-light chain and reduced anterograde transport (Pigino et al. 2003). In addition, anterograde fast axonal transport of APP and Trk receptors is impaired in the sciatic nerve of mice expressing FAD-linked PS1 mutations, resulting in an increased phosphorylation of tau and neurofilaments in the spinal cord (Lazarov et al. 2007).



No fiber pathology was detected in PS1KI mice, however, it is possible that disturbances in axonal transport may become evident upon additional mutant APP overexpression thereby contributing to the observed fiber disturbances in the APP/PS1KI mice.

Ubiquitinated proteins were found to accumulate in the fibers of APP/PS1KI<sup>he</sup> and APP/PS1KI<sup>ho</sup> mice in higher levels than in APP single transgenic mice, indicating an overload of the protein degrading system in the transgenic mice carrying the PS1KI allele. This could be explained by the dramatically increased accumulation of A $\beta$  peptides in these two models resulting in general accumulation of ubiquitinated proteins in the fibers that could contribute to the observed dystrophic axons. Furthermore, A $\beta$  peptides were found to accumulate in the axonal swellings being plaque-independent as well as in the vicinity of plaques, raising the possibility that these swellings precede and contribute to the formation of extracellular plaques. Whether A $\beta$  peptides are generated and released at the site of axonal swellings is currently unclear, however, A $\beta$ -positive granules were also detected in the axons and apical dendrites of cortical neurons, indicating that A $\beta$  can be transported within fibers. It has been hypothesized that if A $\beta$  generation occurs at the sites of axonal blockage, amyloid deposition might be due to focally increased A $\beta$  secretion or lysis of axonal spheroids that were enriched in A $\beta$  peptides (Stokin et al. 2005). Our finding of A $\beta$  transport and accumulation in fibers together with diffuse extracellular A $\beta$  deposits in the close vicinity of axonal spheroids adds further evidence to the hypothesis that A $\beta$  can be released from fiber swellings.

#### **4.5 Interaction between $\alpha 7$ nAChR and A $\beta$**

Much evidence supports a role of the  $\alpha 7$  nAChR in the pathological mechanism of AD. Thus a direct interaction between the  $\alpha 7$  nAChR and A $\beta 42$  has been reported stating that A $\beta 42$  displaces  $\alpha$ -BTX binding specific for  $\alpha 7$ nAChRs (Wang et al. 2000), although this has recently been questioned by a study reporting that A $\beta$  does not bind to  $\alpha 7$ nAChRs, but to lipids within the plasma membrane (Small et al. 2007). However, A $\beta 42$  has been shown to specifically block the response evoked by ACh or nicotine of  $\alpha 7$  nAChRs in cell culture and hippocampal neurons (Liu et al. 2001; Pettit et al. 2001; Spencer et al. 2006), and  $\alpha 7$  nAChR activation protected against A $\beta$ -induced neurotoxicity (Kihara et al. 1997). In AD post-mortem studies, reduction of the  $\alpha 7$  subunit have been reported in the cortex and hippocampal formation (Guan et al. 2000; Teaktong et al. 2004), and  $\alpha 7$  nAChRs have shown co-localise as

well as co-immunoprecipitate with A $\beta$ 42 in AD hippocampal neurons (Wang et al. 2000). *In vivo*, smoking was found to have a lowering effect on A $\beta$  in the human brain (Hellstrom-Lindahl et al. 2004b), which was supported by a study in APP<sup>sw $e$</sup>  mice where 10 days of treatment with nicotine reduced insoluble A $\beta$ 40 and A $\beta$ 42 levels by 80% in the mouse brain tissue (Hellstrom-Lindahl et al. 2004a). This prompted us to study whether this lowering effect of nicotine on A $\beta$  levels could be mediated through the  $\alpha$ 7 nAChR and we thus chronically treated 9-month-old APP/PS1 $\Delta$ E9 mice with nicotine as a positive control, saline as a negative control, and the  $\alpha$ 7 nAChR agonist SSR180711 twice daily for 10 days. Surprisingly, no changes in 4G8 and LOC immunohistochemical pathology were found in the hippocampal formation or parietal cortex of the nicotine treated animals that even showed an increase in A $\beta$ [N] pathology of the hippocampal formation. The mice treated with  $\alpha$ 7 nAChR agonist showed no difference in A $\beta$  pathology with any of the three applied antibodies, and we were thus not able to replicate the findings of nicotine to lower A $\beta$  levels using the same dosing scheme as in the study of APP<sup>sw $e$</sup>  mice (Hellstrom-Lindahl et al. 2004a). Two main differences could potentially explain the lack of effect from the administration of nicotine in our studies versus its beneficial effect in the previous study in APP<sup>sw $e$</sup>  mice. First, our mouse model contains a familial PS1 mutation in addition to the Swedish mutations in APP and thus if any effect of nicotine should be mediated through interaction with PS1 they could be prevented by PS1 mutations as is observed for some  $\gamma$ -secretase inhibitors that only show effects on wild-type PS1 activity (Czirr et al. 2007). However, to the best of our knowledge, no studies have suggested such an interaction. In AD, it has been mainly suggested that the effects of nicotine are mediated through a direct interaction of the  $\alpha$ 7 nAChR with A $\beta$ . Secondly, we evaluated the drug effects by quantification of immunostainings applying A $\beta$  specific antibodies, whereas the study in the APP<sup>sw $e$</sup>  mice measured A $\beta$  levels in brain homogenates by ELISAs. Although our method may only be semi-quantitative, the study in the APP<sup>sw $e$</sup>  mice reported an 80% lowering effect of nicotine on insoluble A $\beta$ 40 as well as A $\beta$ 42 levels, and such a dramatic effect should also have been evident by our method of quantification, especially with the application of the LOC antibody recognizing fibrillar A $\beta$  oligomers and A $\beta$  fibrils that should be part of the insoluble A $\beta$  species (Kayed et al. 2007).

If A $\beta$  interacts with the  $\alpha$ 7 nAChR it could mediate part of its toxic effect by inducing desensitization of the  $\alpha$ 7 nAChR, and we therefore measured the binding level of  $\alpha$ 7 nAChRs in APP/PS1 $\Delta$ E9 mice as compared to wild-type C57Bl6 mice. No significant differences

could be detected in the mPFC, the parietal cortex, or the hippocampal formation; although a weak tendency towards lower  $\alpha 7$  nAChR levels seemed to be present, especially in the hippocampal formation, which might become significant with the inclusion of more animals.

In summary, our studies of a potential interaction between the  $\alpha 7$  nAChR and A $\beta$  in APP/PS1 $\Delta$ E9 mice were not sufficient to support a role of the  $\alpha 7$  nAChR in AD. However, a recent study showed that deletion of the  $\alpha 7$  nAChR gene in an AD mouse model actually improved cognitive deficits and synaptic pathology without any evident effect on 4G8-reactive A $\beta$  immunoreactivity (Dziewczapolski et al. 2009). Interestingly, this is consistent with the intraneuronal A $\beta$  hypothesis of AD since the  $\alpha 7$  nAChR has been reported to mediate endocytosis of A $\beta$ 42 facilitating intraneuronal accumulation of A $\beta$  and deletion of the  $\alpha 7$  nAChR may thus decrease the level of intraneuronal A $\beta$  peptides (Nagele et al. 2002). It is therefore possible that  $\alpha 7$  nAChR antagonists rather than agonists may be beneficial in AD patients.

#### **4.6 Functional integrity of immediate early gene responses following novelty stimulation**

It is well known that the expression levels of *Arc* together with other IEGs are significantly up-regulated in response to various stimuli. Seizure activity upregulates *Arc* mRNA levels in the hippocampal region and parietal cortex (Guzowski et al. 1999). Arousal stimuli such as acute restraint stress up-regulate *Arc* mRNA levels in the mPFC but not in the hippocampal formation or parietal cortex (Guzowski et al. 1999; Mikkelsen and Larsen 2006). Novel environment, a further emotional stressor, induces *Arc* and *c-fos* gene expression in the parietal cortex and the hippocampus as well as in forebrain regions including the mPFC and orbitofrontal cortex, and one study even saw an up-regulation in the caudate nucleus (Klebaur et al. 2002; Ons et al. 2004; Pinaud et al. 2001). However, there seem to be some anatomical specificity to the regulation of IEG mRNA where seizure activity upregulates *Arc* expression in neurons of the hippocampal formation or parietal cortex, whereas the pure stress stimuli up-regulate *Arc* mRNA in the forebrain region, but not in the hippocampal region. This regional specificity could be explained by the effect of corticosterone on cognitive function. Thus two systems within memory generation have received a lot of attention: The hippocampal system and the caudate nucleus system each depending on the surrounding cortices (Packard and

Knowlton 2002). The hippocampal memory system is thought to be predominately cognitively driven depending on spatial cues, whereas the caudate nucleus memory system is thought to be driven more by instinct depending on single cues and is termed “stimulus-response” or “habit” memory. Corticosterone is known to influence memory through corticosteroid receptors located in the hippocampal region as well as in the amygdala, and it has been shown in humans as well as mice that increased stress levels leading to increased blood corticosterone levels do not decrease the learning ability in total. However, they facilitate stimuli-response learning strategies at the expense of hippocampal-dependent cognitive learning strategies (Kim et al. 2001; Schwabe et al. 2007). Thus an increased corticosterone level seems to work as a switch between the hippocampal and the caudate nucleus based memory systems, which may explain why *Arc* mRNA is up-regulated only in mPFC and not in hippocampus or surrounding cortices after pure stress stimuli. The induction of *Arc* gene expression in the mPFC by acute stressors emphasizes that the mPFC is a central component of stress perception and the region is accordingly considered a key component of the neuronal circuitry mediating responses to stressful situations and contributes to the interplay between emotions and memory (Roozendaal 2002). The novelty paradigm is only a light stressor and has in addition the element of exploration; however, we found considerable increased plasma corticosterone levels in both genotypes and accordingly found the highest induction of *Arc* and *c-fos* gene expression following novelty in the mPFC providing input to the caudate nucleus. Relating to the genotypes, we found a difference in basal levels of *Arc* gene expression being most pronounced in the cortices (40%). The APP/PS1ΔE9 mice were generally capable of increasing the *Arc* gene expression in response to a novel environment, in some regions even with higher percentages; however, the absolute *Arc* mRNA level never reached the same level as in the wild-type mice. This could mean that a lesser number of neurons is activated in the APP/PS1ΔE9 mice or that their neurons are not activated as much as in the wild-type mice. Basal differences and deficits in *c-fos* expression and induction following novelty were only identified in the cortical regions with the parietal cortex showing the same pattern as for *Arc* mRNA, but with dramatically increased basal *c-fos* mRNA levels in the mPFC of APP/PS1ΔE9 mice and an inability to up-regulate *c-fos* expression in this region upon a novel environment. As no effect of novelty or genotype was observed in the house keeping gene *synaptophysin*, the effects on *Arc* and *c-fos* gene expression are not

artifacts of the plaque deposition and no neuron loss has been observed in any of the investigated regions of this AD mouse model (Oh et al. 2008).

Three other studies have previously investigated the effect of novelty on the expression of immediate early genes in AD mouse models. One was conducted in another APP + PS1 transgenic model and reported reduced basal expression levels of *Arc*, *Nur 77*, and *Zif 268* in 6-month-old APP + PS1 transgenic mice by qRT-PCR in hippocampus, posterior cortex, and caudate nucleus. Following 5 min environmental novelty in 18-month-old mice, they observed a decreased percentile induction of *Arc* and *Nur77* expression in the hippocampal region by qRT-PCR in transgenic mice compared to littermate controls (Dickey et al. 2004). The finding of decreased basal cortical EIG expression levels is in agreement with our observations; however, we only found a minor decrease in basal expression of *Arc* in the CA1 of the hippocampal formation in contrast to no difference in the CA3 or upper DG. No basal hippocampal differences were found in *c-fos* expression of the hippocampal formation. Likewise, the blunted induction of *Arc* gene expression following novelty observed by qRT-PCR agrees partly with our findings as we observe a reduced percentile reduction of *Arc* gene expression in the CA3, however, in the CA1 and upper DG, the percentile inductions are equal or even higher in the transgenic animals, but reach a lower absolute level of *Arc* gene expression due to reduced basal expressions. However, in relation to *c-fos*, we did not observe any deficits in the functional response to novel environment in the hippocampal formation. Another study investigated EIG gene expression following novelty in hAPP<sub>FAD</sub> mice carrying the Swedish and Indiana FAD mutations using in situ hybridization and immunohistochemistry in the neocortex, CA1, and granular layer of the DG. They found decreased basal *Arc* and *c-fos* expression as well as protein accumulation only in the DG, which was also the only investigated region to show a complete abolishment of induced *Arc* and *c-fos* gene expression after novelty in the transgenic mice (Palop et al. 2005). We did not observe the same reduced basal expression levels of *Arc* and *c-fos* in the DG, and only found a minor decrease in the induction of *Arc* expression following novelty in this region, whereas no deficits were found in *c-fos* induction. Generally, we observe much greater deficits in the functional response of *Arc* and *c-fos* expression following novelty in cortical regions as compared to the hippocampal formation, which seems to have been the greater focus of earlier studies. A very recent study investigated the impact of different amyloid pathologies in three AD mouse models including an APP/PS1 model overexpressing APP carrying the Swedish

mutations together with hPS1 carrying the L166P mutation, the APP23 model harboring the Swedish double mutation, and APPDutch mice (Wegenast-Braun et al. 2009). By in situ hybridization as well as stereological quantification of *Arc* mRNA positive cells, this study reports decreased percentile inductions of *Arc* mRNA in the neocortex and granular cell layer of the DG following novelty in all three mouse models at old age compared to age-matched non-transgenic mice, which is in general agreement with our results. Interestingly, this study also found decreased induction of *Arc* mRNA before plaque deposition in young APP23 and APPDutch mice, but not in young APP/PS1 mice, correlating with only APP23 and APPDutch mice accumulating intraneuronal A $\beta$  at young age. However, as the accumulation of intraneuronal A $\beta$  was transient and APP/PS1 mice also develop deficits in *Arc* mRNA induction with advanced age, intraneuronal A $\beta$ , plaques, as well as vascular CAA pathology were suggested to cause separate deficits in the induction of *Arc* mRNA expression (Wegenast-Braun et al. 2009). Not much intraneuronal A $\beta$  could be detected in our 9-month-old APP/PS1 $\Delta$ E9 mice; however, they accumulated a vast amount of A $\beta$  plaques as well as vascular CAA depositions, which, according to the previous results, are then both likely to contribute to the observed deficits.

The present data reveal a suppressing effect of A $\beta$  on basal and novelty induced neuronal activity in APP/PS1 $\Delta$ E9 mice being most pronounced in cortical regions, where the mPFC seems to be especially affected showing an increased basal level of *c-fos* expression that did not increase upon novelty stimulation. This finding is in line with data from AD patients where increased protein levels of *c-fos*, *c-jun*, and *Arc* have been reported (Engidawork et al. 2001; Marcus et al. 1998). It is thus possible that a decreased functional response in IEG systems could in part mediate cognitive deficits relating to environmental encoding as well as the interplay between emotions and memory in AD patients.

## 5 Summary and Conclusions

The present thesis investigated the role of intraneuronal A $\beta$  in pathological alterations in AD on a neuroanatomical level by the application of methods such as immunohistochemistry, image analysis, stereological quantification, as well as in situ hybridization and radioactive ligand binding. In two independent studies, the accumulation of intraneuronal A $\beta$  was found to correlate with neuron loss in the APP/PS1KI mouse model of AD. Thus in the brain cholinergic system of APP/PS1KI mice, accumulation of intracellular A $\beta$  aggregates represented an early pathological alteration that strongly correlated with neuron death in brain stem motor nuclei. In contrast, A $\beta$  plaque pathology leading to plaque associated dystrophic neurites was not sufficient to cause neuron loss. A second study comparing neuron numbers in two regions accumulating either intraneuronal A $\beta$  together with plaque pathology or plaques only, found that neurons were lost only in the region with accumulation of intraneuronal A $\beta$ , whereas no neuron loss was observed in the region accumulating only extracellular plaques. Furthermore, the presence of intraneuronal A $\beta$  was found to be transient and was virtually absent at the age where neuron loss was first detected, indicating that the neurons accumulating intraneuronal A $\beta$  were the ones to be lost.

The current ongoing debate concerning the presence of intraneuronal A $\beta$  in human AD brains prompted an optimization of the immunohistochemical staining method for the detection of intraneuronal A $\beta$  peptides. The optimization provided a strong and robust staining of intraneuronal N-terminal A $\beta$  peptides as well as fibrillar oligomers and A $\beta$  fibrils in the hippocampal formation of AD tissue, adding a valuable contribution to the evidence of intraneuronal A $\beta$  in human AD brains. In the same experiment, a highly significant correlation between the accumulation of intraneuronal N-terminal A $\beta$  peptides and the ApoE4 genotype was identified, further emphasizing the impact of intraneuronal A $\beta$  in AD pathology as the ApoE4 isoform is recognized to be the major risk factor for sporadic AD.

Axonopathy recognized by dystrophic swellings of fibers is a well-known pathological alteration found in the human AD brain as well as in mouse models of AD; however, the origin of the dystrophic fibers is presently unclear. Using YFP transgenic mice crossed with APP/PS1KI<sup>he</sup> mice and confocal imaging, A $\beta$ -positive granules were detected in the axons and apical dendrites of cortical neurons, indicating that A $\beta$  can be transported within fibers.

Accumulation of intracellular A $\beta$  was also identified within large dystrophic fibers independent of plaques as well as in the vicinity of plaques and with diffuse A $\beta$  deposits nearby the axonal swelling, suggesting that A $\beta$  accumulation inside fibers may contribute to the generation of axonal spheroids and adding further evidence to the hypothesis that A $\beta$  can be released from fiber swellings.

Concerning functional deficits, the studies of an interaction between A $\beta$  and the  $\alpha$ 7 nAChR in APP/PS1 $\Delta$ E9 mice were not sufficient to support a role of the  $\alpha$ 7 nAChR in AD. Furthermore, the reported lowering effect of nicotine on A $\beta$  pathology could not be confirmed; on the contrary, an increase in full-length A $\beta$  plaques was observed in the hippocampal formation of nicotine treated APP/PS1 $\Delta$ E9 mice. However, in the studies of the functional integrity of the IEG response systems, a suppressing effect of A $\beta$  on basal and novelty induced expression of *Arc* and *c-fos* was identified in the APP/PS1 $\Delta$ E9 mice being most pronounced in cortical regions, where the mPFC seemed to be especially affected showing an increased basal level of *c-fos* expression that did not increase upon novelty stimulation. Such a decreased functional response in IEG systems could in part mediate cognitive deficits relating to environmental encoding as well as the interplay between emotions and memory in AD patients.

In conclusion, the present thesis corroborates the modified intraneuronal A $\beta$  cascade hypothesis. It provides additional evidence for the presence of intraneuronal A $\beta$  in human AD tissue and supports the view of intraneuronal A $\beta$  as an early pathological initiator contributing strongly to pathological alterations in AD including large plaque-independent dystrophic fiber pathology and neuronal loss. In contrast, plaques are found likely to cause functional disturbances such as deficits in the induction of IEG systems upon neuronal activity, but seem not to be involved in the loss of neurons.



## 6 References

- Aizenstein HJ, Nebes RD, Saxton JA, Price JC, Mathis CA, Tsopelas ND, Ziolkowski SK, James JA, Snitz BE, Houck PR, Bi W, Cohen AD, Lopresti BJ, DeKosky ST, Halligan EM, Klunk WE. 2008. Frequent amyloid deposition without significant cognitive impairment among the elderly. *Arch Neurol* 65(11):1509-1517.
- Alafuzoff I, Pikkarainen M, Arzberger T, Thal DR, Al-Sarraj S, Bell J, Bodi I, Budka H, Capetillo-Zarate E, Ferrer I, Gelpi E, Gentleman S, Giaccone G, Kavantzias N, King A, Korkolopoulou P, Kovacs GG, Meyronet D, Monoranu C, Parchi P, Patsouris E, Roggendorf W, Stadelmann C, Streichenberger N, Tagliavini F, Kretzschmar H. 2008. Inter-laboratory comparison of neuropathological assessments of beta-amyloid protein: a study of the BrainNet Europe consortium. *Acta Neuropathol* 115(5):533-546.
- Alkondon M, Albuquerque EX. 2004. The nicotinic acetylcholine receptor subtypes and their function in the hippocampus and cerebral cortex. *Prog Brain Res* 145:109-120.
- Allinson TM, Parkin ET, Turner AJ, Hooper NM. 2003. ADAMs family members as amyloid precursor protein alpha-secretases. *J Neurosci Res* 74(3):342-352.
- Almeida CG, Takahashi RH, Gouras GK. 2006. Beta-amyloid accumulation impairs multivesicular body sorting by inhibiting the ubiquitin-proteasome system. *J Neurosci* 26(16):4277-4288.
- Almeida CG, Tampellini D, Takahashi RH, Greengard P, Lin MT, Snyder EM, Gouras GK. 2005. Beta-amyloid accumulation in APP mutant neurons reduces PSD-95 and GluR1 in synapses. *Neurobiol Dis* 20(2):187-198.
- Alzheimer's Association Brochure. 2005. Basics of Alzheimer's Disease. Alzheimer's Association.
- Alzheimer's Association Report. 2009. Alzheimer's Disease Facts and Figures. Alzheimer's and Dementia 5(3).
- Ancolio K, Dumanchin C, Barelli H, Warter JM, Brice A, Campion D, Frebourg T, Checler F. 1999. Unusual phenotypic alteration of beta amyloid precursor protein (betaAPP) maturation by a new Val-715 --> Met betaAPP-770 mutation responsible for probable early-onset Alzheimer's disease. *Proc Natl Acad Sci U S A* 96(7):4119-4124.
- Aoki M, Volkman I, Tjernberg LO, Winblad B, Bogdanovic N. 2008. Amyloid beta-peptide levels in laser capture microdissected cornu ammonis 1 pyramidal neurons of Alzheimer's brain. *Neuroreport* 19(11):1085-1089.
- Arendt T, Stieler J, Strijkstra AM, Hut RA, Rudiger J, Van der Zee EA, Harkany T, Holzer M, Hartig W. 2003. Reversible paired helical filament-like phosphorylation of tau is an adaptive process associated with neuronal plasticity in hibernating animals. *J Neurosci* 23(18):6972-6981.
- Arendt T, Taubert G, Bigl V, Arendt A. 1988. Amyloid deposition in the nucleus basalis of Meynert complex: a topographic marker for degenerating cell clusters in Alzheimer's disease. *Acta Neuropathol* 75(3):226-232.

- Ashford JW. 2004. APOE genotype effects on Alzheimer's disease onset and epidemiology. *J Mol Neurosci* 23(3):157-165.
- Aucoin JS, Jiang P, Aznavour N, Tong XK, Buttini M, Descarries L, Hamel E. 2005. Selective cholinergic denervation, independent from oxidative stress, in a mouse model of Alzheimer's disease. *Neuroscience* 132(1):73-86.
- Bancher C, Grundke-Iqbal I, Iqbal K, Kim KS, Wisniewski HM. 1989. Immunoreactivity of neuronal lipofuscin with monoclonal antibodies to the amyloid beta-protein. *Neurobiol Aging* 10(2):125-132.
- Baron R, Harpaz I, Nemirovsky A, Cohen H, Monsonogo A. 2007. Immunity and neuronal repair in the progression of Alzheimer's disease: a brief overview. *Exp Gerontol* 42(1-2):64-69.
- Beer J, Masters CL, Beyreuther K. 1995. Cells from peripheral tissues that exhibit high APP expression are characterized by their high membrane fusion activity. *Neurodegeneration* 4(1):51-59.
- Bellucci A, Luccarini I, Scali C, Prosperi C, Giovannini MG, Pepeu G, Casamenti F. 2006. Cholinergic dysfunction, neuronal damage and axonal loss in TgCRND8 mice. *Neurobiol Dis* 23(2):260-272.
- Bentahir M, Nyabi O, Verhamme J, Tolia A, Horre K, Wiltfang J, Esselmann H, De Strooper B. 2006. Presenilin clinical mutations can affect gamma-secretase activity by different mechanisms. *J Neurochem* 96(3):732-742.
- Bhagwandin A, Fuxe K, Manger PR. 2006. Choline acetyltransferase immunoreactive cortical interneurons do not occur in all rodents: a study of the phylogenetic occurrence of this neural characteristic. *J Chem Neuroanat* 32(2-4):208-216.
- Birks J. 2006. Cholinesterase inhibitors for Alzheimer's disease. *Cochrane Database Syst Rev* 25(1):CD005593.
- Blanchard V, Moussaoui S, Czech C, Touchet N, Bonici B, Planche M, Canton T, Jedidi I, Gohin M, Wirths O, Bayer TA, Langui D, Duyckaerts C, Tremp G, Pradier L. 2003. Time sequence of maturation of dystrophic neurites associated with Abeta deposits in APP/PS1 transgenic mice. *Experimental neurology* 184(1):247-263.
- Boncrisiano S, Calhoun ME, Kelly PH, Pfeifer M, Bondolfi L, Stalder M, Phinney AL, Abramowski D, Sturchler-Pierrat C, Enz A, Sommer B, Staufenbiel M, Jucker M. 2002. Cholinergic changes in the APP23 transgenic mouse model of cerebral amyloidosis. *J Neurosci* 22(8):3234-3243.
- Borchelt DR, Thinakaran G, Eckman CB, Lee MK, Davenport F, Ratovitsky T, Prada CM, Kim G, Seekins S, Yager D, Slunt HH, Wang R, Seeger M, Levey AI, Gandy SE, Copeland NG, Jenkins NA, Price DL, Younkin SG, Sisodia SS. 1996. Familial Alzheimer's disease-linked presenilin 1 variants elevate Abeta1-42/1-40 ratio in vitro and in vivo. *Neuron* 17(5):1005-1013.
- Breyhan H, Wirths O, Duan K, Marcello A, Rettig J, Bayer TA. 2009. APP/PS1KI bigenic mice develop early synaptic deficits and hippocampus atrophy. *Acta Neuropathol* 117(6):677-685.

- Briski KP. 1996. Stimulatory vs. inhibitory effects of acute stress on plasma LH: differential effects of pretreatment with dexamethasone or the steroid receptor antagonist, RU 486. *Pharmacol Biochem Behav* 55(1):19-26.
- Bronfman FC, Moechars D, Van Leuven F. 2000. Acetylcholinesterase-positive fiber deafferentation and cell shrinkage in the septohippocampal pathway of aged amyloid precursor protein london mutant transgenic mice. *Neurobiol Dis* 7(3):152-168.
- Braak H, Alafuzoff I, Arzberger T, Kretschmar H, Del Tredici K. 2006. Staging of Alzheimer disease-associated neurofibrillary pathology using paraffin sections and immunocytochemistry. *Acta Neuropathol* 112(4):389-404.
- Braak H, Braak E. 1991. Neuropathological staging of Alzheimer-related changes. *Acta Neuropathol* 82(4):239-259.
- Bu G. 2009. Apolipoprotein E and its receptors in Alzheimer's disease: pathways, pathogenesis and therapy. *Nature reviews* 10(5):333-344.
- Bu G, Cam J, Zerbinatti C. 2006. LRP in amyloid-beta production and metabolism. *Ann N Y Acad Sci* 1086:35-53.
- Burgos I, Cuello AC, Liberini P, Pioro E, Masliah E. 1995. NGF-mediated synaptic sprouting in the cerebral cortex of lesioned primate brain. *Brain Res* 692(1-2):154-160.
- Burke MA, Mobley WC, Cho J, Wiegand SJ, Lindsay RM, Mufson EJ, Kordower JH. 1994. Loss of developing cholinergic basal forebrain neurons following excitotoxic lesions of the hippocampus: rescue by neurotrophins. *Experimental neurology* 130(2):178-195.
- Capsoni S, Ugolini G, Comparini A, Ruberti F, Berardi N, Cattaneo A. 2000. Alzheimer-like neurodegeneration in aged antinerve growth factor transgenic mice. *Proc Natl Acad Sci U S A* 97(12):6826-6831.
- Carson R, Craig D, McGuinness B, Johnston JA, O'Neill FA, Passmore AP, Ritchie CW. 2008. Alpha7 nicotinic acetylcholine receptor gene and reduced risk of Alzheimer's disease. *J Med Genet* 45(4):244-248.
- Casas C, Sergeant N, Itier JM, Blanchard V, Wirths O, van der Kolk N, Vingtdeux V, van de Steeg E, Ret G, Canton T, Drobecq H, Clark A, Bonici B, Delacourte A, Benavides J, Schmitz C, Tremp G, Bayer TA, Benoit P, Pradier L. 2004. Massive CA1/2 neuronal loss with intraneuronal and N-terminal truncated Abeta42 accumulation in a novel Alzheimer transgenic model. *Am J Pathol* 165(4):1289-1300.
- Cataldo AM, Peterhoff CM, Troncoso JC, Gomez-Isla T, Hyman BT, Nixon RA. 2000. Endocytic pathway abnormalities precede amyloid beta deposition in sporadic Alzheimer's disease and Down syndrome: differential effects of APOE genotype and presenilin mutations. *Am J Pathol* 157(1):277-286.
- Chandramohan Y, Droste SK, Reul JM. 2007. Novelty stress induces phospho-acetylation of histone H3 in rat dentate gyrus granule neurons through coincident signalling via the N-methyl-D-aspartate receptor and the glucocorticoid receptor: relevance for c-fos induction. *J Neurochem* 101(3):815-828.

- Charles V, Mufson EJ, Friden PM, Bartus RT, Kordower JH. 1996. Atrophy of cholinergic basal forebrain neurons following excitotoxic cortical lesions is reversed by intravenous administration of an NGF conjugate. *Brain Res* 728(2):193-203.
- Chawla MK, Guzowski JF, Ramirez-Amaya V, Lipa P, Hoffman KL, Marriott LK, Worley PF, McNaughton BL, Barnes CA. 2005. Sparse, environmentally selective expression of Arc RNA in the upper blade of the rodent fascia dentata by brief spatial experience. *Hippocampus* 15(5):579-586.
- Chen XH, Siman R, Iwata A, Meaney DF, Trojanowski JQ, Smith DH. 2004. Long-term accumulation of amyloid-beta, beta-secretase, presenilin-1, and caspase-3 in damaged axons following brain trauma. *Am J Pathol* 165(2):357-371.
- Christensen DZ, Kraus SL, Flohr A, Cotel MC, Wirths O, Bayer TA. 2008. Transient intraneuronal A $\beta$  rather than extracellular plaque pathology correlates with neuron loss in the frontal cortex of APP/PS1KI mice. *Acta Neuropathol* 116(6):647-655.
- Chui DH, Dobo E, Makifuchi T, Akiyama H, Kawakatsu S, Petit A, Checler F, Araki W, Takahashi K, Tabira T. 2001. Apoptotic neurons in Alzheimer's disease frequently show intracellular A $\beta$ 42 labeling. *J Alzheimers Dis* 3(2):231-239.
- Chui DH, Tanahashi H, Ozawa K, Ikeda S, Checler F, Ueda O, Suzuki H, Araki W, Inoue H, Shirotani K, Takahashi K, Gallyas F, Tabira T. 1999. Transgenic mice with Alzheimer presenilin 1 mutations show accelerated neurodegeneration without amyloid plaque formation. *Nat Med* 5(5):560-564.
- Cook DG, Forman MS, Sung JC, Leight S, Kolson DL, Iwatsubo T, Lee VM, Doms RW. 1997. Alzheimer's A $\beta$ (1-42) is generated in the endoplasmic reticulum/intermediate compartment of NT2N cells. *Nat Med* 3(9):1021-1023.
- Corder EH, Saunders AM, Strittmatter WJ, Schmechel DE, Gaskell PC, Small GW, Roses AD, Haines JL, Pericak-Vance MA. 1993. Gene dose of apolipoprotein E type 4 allele and the risk of Alzheimer's disease in late onset families. *Science* 261(5123):921-923.
- Coulson EJ, Paliga K, Beyreuther K, Masters CL. 2000. What the evolution of the amyloid protein precursor supergene family tells us about its function. *Neurochem Int* 36(3):175-184.
- Counts SE, He B, Che S, Ikonomic MD, DeKosky ST, Ginsberg SD, Mufson EJ. 2007. Alpha7 nicotinic receptor up-regulation in cholinergic basal forebrain neurons in Alzheimer disease. *Arch Neurol* 64(12):1771-1776.
- Counts SE, Mufson EJ. 2005. The role of nerve growth factor receptors in cholinergic basal forebrain degeneration in prodromal Alzheimer disease. *J Neuropathol Exp Neurol* 64(4):263-272.
- Coyle JT, Price DL, DeLong MR. 1983. Alzheimer's disease: a disorder of cortical cholinergic innervation. *Science* 219(4589):1184-1190.
- Cras P, Kawai M, Lowery D, Gonzalez-DeWhitt P, Greenberg B, Perry G. 1991. Senile plaque neurites in Alzheimer disease accumulate amyloid precursor protein. *Proc Natl Acad Sci U S A* 88(17):7552-7556.
- Cross DJ, Flexman JA, Anzai Y, Maravilla KR, Minoshima S. 2008. Age-related decrease in axonal transport measured by MR imaging in vivo. *Neuroimage* 39(3):915-926.

- Cutler RG, Kelly J, Storie K, Pedersen WA, Tammara A, Hatanpaa K, Troncoso JC, Mattson MP. 2004. Involvement of oxidative stress-induced abnormalities in ceramide and cholesterol metabolism in brain aging and Alzheimer's disease. *Proc Natl Acad Sci U S A* 101(7):2070-2075.
- Czirr E, Leuchtenberger S, Dorner-Ciossek C, Schneider A, Jucker M, Koo EH, Pietrzik CU, Baumann K, Weggen S. 2007. Insensitivity to Abeta42-lowering nonsteroidal anti-inflammatory drugs and gamma-secretase inhibitors is common among aggressive presenilin-1 mutations. *J Biol Chem* 282(34):24504-24513.
- D'Andrea MR, Nagele RG. 2006. Targeting the alpha 7 nicotinic acetylcholine receptor to reduce amyloid accumulation in Alzheimer's disease pyramidal neurons. *Curr Pharm Des* 12(6):677-684.
- D'Andrea MR, Nagele RG, Gumula NA, Reiser PA, Polkovitch DA, Hertzog BM, Andrade-Gordon P. 2002a. Lipofuscin and Abeta42 exhibit distinct distribution patterns in normal and Alzheimer's disease brains. *Neurosci Lett* 323(1):45-49.
- D'Andrea MR, Nagele RG, Wang HY, Lee DH. 2002b. Consistent immunohistochemical detection of intracellular beta-amyloid42 in pyramidal neurons of Alzheimer's disease entorhinal cortex. *Neurosci Lett* 333(3):163-166.
- D'Andrea MR, Nagele RG, Wang HY, Peterson PA, Lee DH. 2001. Evidence that neurones accumulating amyloid can undergo lysis to form amyloid plaques in Alzheimer's disease. *Histopathology* 38(2):120-134.
- D'Andrea MR, Reiser PA, Polkovitch DA, Gumula NA, Branchide B, Hertzog BM, Schmidheiser D, Belkowski S, Gastard MC, Andrade-Gordon P. 2003. The use of formic acid to embellish amyloid plaque detection in Alzheimer's disease tissues misguides key observations. *Neurosci Lett* 342(1-2):114-118.
- Dani JA, Bertrand D. 2007. Nicotinic acetylcholine receptors and nicotinic cholinergic mechanisms of the central nervous system. *Annu Rev Pharmacol Toxicol* 47:699-729.
- Davies P. 1979. Neurotransmitter-related enzymes in senile dementia of the Alzheimer type. *Brain Res* 171(2):319-327.
- Davies P, Maloney AJ. 1976. Selective loss of central cholinergic neurons in Alzheimer's disease. *Lancet* 2(8000):1403.
- Deane R, Du Yan S, Submamaryan RK, LaRue B, Jovanovic S, Hogg E, Welch D, Manness L, Lin C, Yu J, Zhu H, Ghiso J, Frangione B, Stern A, Schmidt AM, Armstrong DL, Arnold B, Liliensiek B, Nawroth P, Hofman F, Kindy M, Stern D, Zlokovic B. 2003. RAGE mediates amyloid-beta peptide transport across the blood-brain barrier and accumulation in brain. *Nat Med* 9(7):907-913.
- DeKosky ST, Scheff SW. 1990. Synapse loss in frontal cortex biopsies in Alzheimer's disease: correlation with cognitive severity. *Ann Neurol* 27(5):457-464.
- Delatour B, Blanchard V, Pradier L, Duyckaerts C. 2004. Alzheimer pathology disorganizes cortico-cortical circuitry: direct evidence from a transgenic animal model. *Neurobiol Dis* 16(1):41-47.

- Dickey CA, Gordon MN, Mason JE, Wilson NJ, Diamond DM, Guzowski JF, Morgan D. 2004. Amyloid suppresses induction of genes critical for memory consolidation in APP + PS1 transgenic mice. *J Neurochem* 88(2):434-442.
- Dickson DW. 1997. The pathogenesis of senile plaques. *J Neuropathol Exp Neurol* 56(4):321-339.
- Dickson DW, Crystal HA, Bevona C, Honer W, Vincent I, Davies P. 1995. Correlations of synaptic and pathological markers with cognition of the elderly. *Neurobiol Aging* 16(3):285-298; discussion 298-304.
- Duyckaerts C, Potier MC, Delatour B. 2008. Alzheimer disease models and human neuropathology: similarities and differences. *Acta Neuropathol* 115(1):5-38.
- Dziewczapolski G, Glogowski CM, Masliah E, Heinemann SF. 2009. Deletion of the alpha7 nicotinic acetylcholine receptor gene improves cognitive deficits and synaptic pathology in a mouse model of Alzheimer's disease. *J Neurosci* 29(27):8805-8815.
- Eikelenboom P, Veerhuis R, Scheper W, Rozemuller AJ, van Gool WA, Hoozemans JJ. 2006. The significance of neuroinflammation in understanding Alzheimer's disease. *J Neural Transm* 113(11):1685-1695.
- Engidawork E, Gulesserian T, Yoo BC, Cairns N, Lubec G. 2001. Alteration of caspases and apoptosis-related proteins in brains of patients with Alzheimer's disease. *Biochem Biophys Res Commun* 281(1):84-93.
- Erkinjuntti T, Lee DH, Gao F, Steenhuis R, Eliasziw M, Fry R, Merskey H, Hachinski VC. 1993. Temporal lobe atrophy on magnetic resonance imaging in the diagnosis of early Alzheimer's disease. *Arch Neurol* 50(3):305-310.
- Feng G, Mellor RH, Bernstein M, Keller-Peck C, Nguyen QT, Wallace M, Nerbonne JM, Lichtman JW, Sanes JR. 2000. Imaging neuronal subsets in transgenic mice expressing multiple spectral variants of GFP. *Neuron* 28(1):41-51.
- Fernandez-Vizarra P, Fernandez AP, Castro-Blanco S, Serrano J, Bentura ML, Martinez-Murillo R, Martinez A, Rodrigo J, Encinas JM, Munoz P, Alonso D, Gomez MB, Sanchez J, Rios-Tejada F, Salas E, Lisazoain I, Leza JC, Lopez JC, Manuel Encinas J, Lorenzo P, Pedrosa JA, Peinado MA, Richart A, Santacana M, Cuttitta F, Uttenthal LO, Bosca L, Rodriguez I, Ruiz-Cabello J. 2004. Intra- and extracellular Abeta and PHF in clinically evaluated cases of Alzheimer's disease. *Histol Histopathol* 19(3):823-844.
- Folstein MF, Folstein SE, McHugh PR. 1975. "Mini-mental state". A practical method for grading the cognitive state of patients for the clinician. *J Psychiatr Res* 12(3):189-198.
- Games D, Buttini M, Kobayashi D, Schenk D, Seubert P. 2006. Mice as models: Transgenic approaches and Alzheimer's disease. *J Alzheimers Dis* 9(3 Suppl):133-149.
- Gandy S. 2005. The role of cerebral amyloid beta accumulation in common forms of Alzheimer disease. *J Clin Invest* 115(5):1121-1129.
- Geerts H, Grossberg GT. 2006. Pharmacology of acetylcholinesterase inhibitors and N-methyl-D-aspartate receptors for combination therapy in the treatment of Alzheimer's disease. *J Clin Pharmacol* 46(7 Suppl 1):8S-16S.

- German DC, Yazdani U, Speciale SG, Pasbakhsh P, Games D, Liang CL. 2003. Cholinergic neuropathology in a mouse model of Alzheimer's disease. *J Comp Neurol* 462(4):371-381.
- Glenner GG, Wong CW. 1984. Alzheimer's disease: initial report of the purification and characterization of a novel cerebrovascular amyloid protein. *Biochem Biophys Res Commun* 120(3):885-890.
- Gomez-Isla T, Hollister R, West H, Mui S, Growdon JH, Petersen RC, Parisi JE, Hyman BT. 1997. Neuronal loss correlates with but exceeds neurofibrillary tangles in Alzheimer's disease. *Ann Neurol* 41(1):17-24.
- Gomez-Isla T, Price JL, McKeel DW, Jr., Morris JC, Growdon JH, Hyman BT. 1996. Profound loss of layer II entorhinal cortex neurons occurs in very mild Alzheimer's disease. *J Neurosci* 16(14):4491-4500.
- Gouras GK, Almeida CG, Takahashi RH. 2005. Intraneuronal Abeta accumulation and origin of plaques in Alzheimer's disease. *Neurobiol Aging* 26(9):1235-1244.
- Gouras GK, Tsai J, Naslund J, Vincent B, Edgar M, Checler F, Greenfield JP, Haroutunian V, Buxbaum JD, Xu H, Greengard P, Relkin NR. 2000. Intraneuronal Abeta42 accumulation in human brain. *Am J Pathol* 156(1):15-20.
- Grimm MO, Grimm HS, Patzold AJ, Zinser EG, Halonen R, Duering M, Tschape JA, De Strooper B, Muller U, Shen J, Hartmann T. 2005. Regulation of cholesterol and sphingomyelin metabolism by amyloid-beta and presenilin. *Nat Cell Biol* 7(11):1118-1123.
- Grossberg GT, Edwards KR, Zhao Q. 2006. Rationale for combination therapy with galantamine and memantine in Alzheimer's disease. *J Clin Pharmacol* 46(7 Suppl 1):17S-26S.
- Grundke-Iqbal I, Iqbal K, George L, Tung YC, Kim KS, Wisniewski HM. 1989. Amyloid protein and neurofibrillary tangles coexist in the same neuron in Alzheimer disease. *Proc Natl Acad Sci U S A* 86(8):2853-2857.
- Gsell W, Jungkunz G, Riederer P. 2004. Functional neurochemistry of Alzheimer's disease. *Curr Pharm Des* 10(3):265-293.
- Guan ZZ, Zhang X, Ravid R, Nordberg A. 2000. Decreased protein levels of nicotinic receptor subunits in the hippocampus and temporal cortex of patients with Alzheimer's disease. *J Neurochem* 74(1):237-243.
- Guo Q, Fu W, Sopher BL, Miller MW, Ware CB, Martin GM, Mattson MP. 1999. Increased vulnerability of hippocampal neurons to excitotoxic necrosis in presenilin-1 mutant knock-in mice. *Nat Med* 5(1):101-106.
- Guzowski JF. 2002. Insights into immediate-early gene function in hippocampal memory consolidation using antisense oligonucleotide and fluorescent imaging approaches. *Hippocampus* 12(1):86-104.
- Guzowski JF, Lyford GL, Stevenson GD, Houston FP, McGaugh JL, Worley PF, Barnes CA. 2000. Inhibition of activity-dependent arc protein expression in the rat hippocampus impairs the maintenance of long-term potentiation and the consolidation of long-term memory. *J Neurosci* 20(11):3993-4001.



- Guzowski JF, McNaughton BL, Barnes CA, Worley PF. 1999. Environment-specific expression of the immediate-early gene Arc in hippocampal neuronal ensembles. *Nat Neurosci* 2(12):1120-1124.
- Gyure KA, Durham R, Stewart WF, Smialek JE, Troncoso JC. 2001. Intraneuronal abeta-amyloid precedes development of amyloid plaques in Down syndrome. *Arch Pathol Lab Med* 125(4):489-492.
- Hanger DP, Anderton BH, Noble W. 2009. Tau phosphorylation: the therapeutic challenge for neurodegenerative disease. *Trends Mol Med* 15(3):112-119.
- Hardy J. 2006. A hundred years of Alzheimer's disease research. *Neuron* 52(1):3-13.
- Hardy J, Allsop D. 1991. Amyloid deposition as the central event in the aetiology of Alzheimer's disease. *Trends Pharmacol Sci* 12(10):383-388.
- Hartmann J, Erb C, Ebert U, Baumann KH, Popp A, Konig G, Klein J. 2004. Central cholinergic functions in human amyloid precursor protein knock-in/presenilin-1 transgenic mice. *Neuroscience* 125(4):1009-1017.
- Hasselmo ME. 2006. The role of acetylcholine in learning and memory. *Curr Opin Neurobiol* 16(6):710-715.
- He W, Barrow CJ. 1999. The A beta 3-pyroglutamyl and 11-pyroglutamyl peptides found in senile plaque have greater beta-sheet forming and aggregation propensities in vitro than full-length A beta. *Biochemistry* 38(33):10871-10877.
- Hefti F. 1986. Nerve growth factor promotes survival of septal cholinergic neurons after fimbrial transections. *J Neurosci* 6(8):2155-2162.
- Hellstrom-Lindahl E, Court J, Keverne J, Svedberg M, Lee M, Marutle A, Thomas A, Perry E, Bednar I, Nordberg A. 2004a. Nicotine reduces A beta in the brain and cerebral vessels of APPsw mice. *Eur J Neurosci* 19(10):2703-2710.
- Hellstrom-Lindahl E, Mousavi M, Ravid R, Nordberg A. 2004b. Reduced levels of Abeta 40 and Abeta 42 in brains of smoking controls and Alzheimer's patients. *Neurobiol Dis* 15(2):351-360.
- Holton JL, Ghiso J, Lashley T, Rostagno A, Guerin CJ, Gibb G, Houlden H, Ayling H, Martinian L, Anderton BH, Wood NW, Vidal R, Plant G, Frangione B, Revesz T. 2001. Regional distribution of amyloid-Bri deposition and its association with neurofibrillary degeneration in familial British dementia. *Am J Pathol* 158(2):515-526.
- Hu L, Wong TP, Cote SL, Bell KF, Cuellar AC. 2003. The impact of Abeta-plaques on cortical cholinergic and non-cholinergic presynaptic boutons in alzheimer's disease-like transgenic mice. *Neuroscience* 121(2):421-432.
- Huesgen CT, Burger PC, Crain BJ, Johnson GA. 1993. In vitro MR microscopy of the hippocampus in Alzheimer's disease. *Neurology* 43(1):145-152.
- Hussain I, Powell D, Howlett DR, Tew DG, Meek TD, Chapman C, Gloger IS, Murphy KE, Southan CD, Ryan DM, Smith TS, Simmons DL, Walsh FS, Dingwall C, Christie G. 1999. Identification of a novel aspartic protease (Asp 2) as beta-secretase. *Mol Cell Neurosci* 14(6):419-427.

- Ittner LM, Gotz J. 2007. Pronuclear injection for the production of transgenic mice. *Nat Protoc* 2(5):1206-1215.
- Iwatsubo T. 1998. Abeta42, presenilins, and Alzheimer's disease. *Neurobiol Aging* 19(1 Suppl):S11-13.
- Jaffar S, Counts SE, Ma SY, Dadko E, Gordon MN, Morgan D, Mufson EJ. 2001. Neuropathology of mice carrying mutant APP(swe) and/or PS1(M146L) transgenes: alterations in the p75(NTR) cholinergic basal forebrain septohippocampal pathway. *Experimental neurology* 170(2):227-243.
- Jankowsky JL, Fadale DJ, Anderson J, Xu GM, Gonzales V, Jenkins NA, Copeland NG, Lee MK, Younkin LH, Wagner SL, Younkin SG, Borchelt DR. 2004. Mutant presenilins specifically elevate the levels of the 42 residue beta-amyloid peptide in vivo: evidence for augmentation of a 42-specific gamma secretase. *Hum Mol Genet* 13(2):159-170.
- Janssen JC, Beck JA, Campbell TA, Dickinson A, Fox NC, Harvey RJ, Houlden H, Rossor MN, Collinge J. 2003. Early onset familial Alzheimer's disease: Mutation frequency in 31 families. *Neurology* 60(2):235-239.
- Kamal A, Almenar-Queralt A, LeBlanc JF, Roberts EA, Goldstein LS. 2001. Kinesin-mediated axonal transport of a membrane compartment containing beta-secretase and presenilin-1 requires APP. *Nature* 414(6864):643-648.
- Kamal A, Stokin GB, Yang Z, Xia CH, Goldstein LS. 2000. Axonal transport of amyloid precursor protein is mediated by direct binding to the kinesin light chain subunit of kinesin-I. *Neuron* 28(2):449-459.
- Kamenetz F, Tomita T, Hsieh H, Seabrook G, Borchelt D, Iwatsubo T, Sisodia S, Malinow R. 2003. APP processing and synaptic function. *Neuron* 37(6):925-937.
- Kang J, Lemaire HG, Unterbeck A, Salbaum JM, Masters CL, Grzeschik KH, Multhaup G, Beyreuther K, Muller-Hill B. 1987. The precursor of Alzheimer's disease amyloid A4 protein resembles a cell-surface receptor. *Nature* 325(6106):733-736.
- Kawas C, Gray S, Brookmeyer R, Fozard J, Zonderman A. 2000. Age-specific incidence rates of Alzheimer's disease: the Baltimore Longitudinal Study of Aging. *Neurology* 54(11):2072-2077.
- Kayed R, Head E, Sarsoza F, Saing T, Cotman CW, Necula M, Margol L, Wu J, Breydo L, Thompson JL, Rasool S, Gurlo T, Butler P, Glabe CG. 2007. Fibril specific, conformation dependent antibodies recognize a generic epitope common to amyloid fibrils and fibrillar oligomers that is absent in prefibrillar oligomers. *Mol Neurodegener* 2:18.
- Kesslak JP, Nalcioglu O, Cotman CW. 1991. Quantification of magnetic resonance scans for hippocampal and parahippocampal atrophy in Alzheimer's disease. *Neurology* 41(1):51-54.
- Kihara T, Sawada H, Nakamizo T, Kanki R, Yamashita H, Maelicke A, Shimohama S. 2004. Galantamine modulates nicotinic receptor and blocks Abeta-enhanced glutamate toxicity. *Biochem Biophys Res Commun* 325(3):976-982.

- Kihara T, Shimohama S, Sawada H, Kimura J, Kume T, Kochiyama H, Maeda T, Akaike A. 1997. Nicotinic receptor stimulation protects neurons against beta-amyloid toxicity. *Ann Neurol* 42(2):159-163.
- Kim JJ, Lee HJ, Han JS, Packard MG. 2001. Amygdala is critical for stress-induced modulation of hippocampal long-term potentiation and learning. *J Neurosci* 21(14):5222-5228.
- Kinoshita A, Fukumoto H, Shah T, Whelan CM, Irizarry MC, Hyman BT. 2003. Demonstration by FRET of BACE interaction with the amyloid precursor protein at the cell surface and in early endosomes. *J Cell Sci* 116(Pt 16):3339-3346.
- Kitamoto T, Ogomori K, Tateishi J, Prusiner SB. 1987. Formic acid pretreatment enhances immunostaining of cerebral and systemic amyloids. *Lab Invest* 57(2):230-236.
- Klebaur JE, Ostrander MM, Norton CS, Watson SJ, Akil H, Robinson TE. 2002. The ability of amphetamine to evoke arc (Arg 3.1) mRNA expression in the caudate, nucleus accumbens and neocortex is modulated by environmental context. *Brain Res* 930(1-2):30-36.
- Klunk WE, Xu CJ, Pettegrew JW. 1994. NMR identification of the formic acid-modified residue in Alzheimer's amyloid protein. *J Neurochem* 62(1):349-354.
- Knobloch M, Konietzko U, Krebs DC, Nitsch RM. 2007. Intracellular Abeta and cognitive deficits precede beta-amyloid deposition in transgenic arcAbeta mice. *Neurobiol Aging* 28(9):1297-1306.
- Koo EH, Sisodia SS, Archer DR, Martin LJ, Weidemann A, Beyreuther K, Fischer P, Masters CL, Price DL. 1990. Precursor of amyloid protein in Alzheimer disease undergoes fast anterograde axonal transport. *Proc Natl Acad Sci U S A* 87(4):1561-1565.
- Kuhar JM, Unnerstall JR, Yamamura HI, Enna SJ, Kuhar MJ. 1990. Receptor Autoradiography. *Methods in Neurotransmitter Receptor Analysis*. New York: Raven Press. p 177-218.
- Kumar-Singh S, Theuns J, Van Broeck B, Pirici D, Vennekens K, Corsmit E, Cruts M, Dermaut B, Wang R, Van Broeckhoven C. 2006. Mean age-of-onset of familial Alzheimer disease caused by presenilin mutations correlates with both increased Abeta42 and decreased Abeta40. *Hum Mutat* 27(7):686-695.
- Kumar-Singh S, Van Broeckhoven C. 2007. Frontotemporal lobar degeneration: current concepts in the light of recent advances. *Brain Pathol* 17(1):104-114.
- Kuo YM, Webster S, Emmerling MR, De Lima N, Roher AE. 1998. Irreversible dimerization/tetramerization and post-translational modifications inhibit proteolytic degradation of A beta peptides of Alzheimer's disease. *Biochim Biophys Acta* 1406(3):291-298.
- Lad SP, Neet KE, Mufson EJ. 2003. Nerve growth factor: structure, function and therapeutic implications for Alzheimer's disease. *Curr Drug Targets CNS Neurol Disord* 2(5):315-334.
- Laferla FM, Green KN, Oddo S. 2007. Intracellular amyloid-beta in Alzheimer's disease. *Nature reviews* 8(7):499-509.

- LaFerla FM, Troncoso JC, Strickland DK, Kawas CH, Jay G. 1997. Neuronal cell death in Alzheimer's disease correlates with apoE uptake and intracellular Abeta stabilization. *J Clin Invest* 100(2):310-320.
- Langui D, Girardot N, El Hachimi KH, Allinquant B, Blanchard V, Pradier L, Duyckaerts C. 2004. Subcellular topography of neuronal Abeta peptide in APPxPS1 transgenic mice. *Am J Pathol* 165(5):1465-1477.
- Lazarov O, Morfini GA, Lee EB, Farah MH, Szodorai A, DeBoer SR, Koliatsos VE, Kins S, Lee VM, Wong PC, Price DL, Brady ST, Sisodia SS. 2005. Axonal transport, amyloid precursor protein, kinesin-1, and the processing apparatus: revisited. *J Neurosci* 25(9):2386-2395.
- Lazarov O, Morfini GA, Pigino G, Gadadhar A, Chen X, Robinson J, Ho H, Brady ST, Sisodia SS. 2007. Impairments in fast axonal transport and motor neuron deficits in transgenic mice expressing familial Alzheimer's disease-linked mutant presenilin 1. *J Neurosci* 27(26):7011-7020.
- Lesne S, Koh MT, Kotilinek L, Kaye R, Glabe CG, Yang A, Gallagher M, Ashe KH. 2006. A specific amyloid-beta protein assembly in the brain impairs memory. *Nature* 440(7082):352-357.
- Levey A, Lah J, Goldstein F, Steenland K, Bliwise D. 2006. Mild cognitive impairment: an opportunity to identify patients at high risk for progression to Alzheimer's disease. *Clin Ther* 28(7):991-1001.
- LeVine H, 3rd. 1993. Thioflavine T interaction with synthetic Alzheimer's disease beta-amyloid peptides: detection of amyloid aggregation in solution. *Protein Sci* 2(3):404-410.
- Liu Q, Kawai H, Berg DK. 2001. beta -Amyloid peptide blocks the response of alpha 7-containing nicotinic receptors on hippocampal neurons. *Proc Natl Acad Sci U S A* 98(8):4734-4739.
- Livak KJ, Schmittgen TD. 2001. Analysis of relative gene expression data using real-time quantitative PCR and the 2(-Delta Delta C(T)) Method. *Methods* 25(4):402-408.
- Loo DT, Copani A, Pike CJ, Whittemore ER, Walencewicz AJ, Cotman CW. 1993. Apoptosis is induced by beta-amyloid in cultured central nervous system neurons. *Proc Natl Acad Sci U S A* 90(17):7951-7955.
- Lord A, Kalimo H, Eckman C, Zhang XQ, Lannfelt L, Nilsson LN. 2006. The Arctic Alzheimer mutation facilitates early intraneuronal Abeta aggregation and senile plaque formation in transgenic mice. *Neurobiol Aging* 27(1):67-77.
- Lucas-Meunier E, Fossier P, Baux G, Amar M. 2003. Cholinergic modulation of the cortical neuronal network. *Pflugers Arch* 446(1):17-29.
- Luna-Munoz J, Garcia-Sierra F, Falcon V, Menendez I, Chavez-Macias L, Mena R. 2005. Regional conformational change involving phosphorylation of tau protein at the Thr231, precedes the structural change detected by Alz-50 antibody in Alzheimer's disease. *J Alzheimers Dis* 8(1):29-41.
- Luth HJ, Apelt J, Ihunwo AO, Arendt T, Schliebs R. 2003. Degeneration of beta-amyloid-associated cholinergic structures in transgenic APP SW mice. *Brain Res* 977(1):16-22.

- Mann DM, Sumpter PQ, Davies CA, Yates PO. 1987. Glycogen accumulations in the cerebral cortex in Alzheimer's disease. *Acta Neuropathol* 73(2):181-184.
- Marcus DL, Strafaci JA, Miller DC, Masia S, Thomas CG, Rosman J, Hussain S, Freedman ML. 1998. Quantitative neuronal c-fos and c-jun expression in Alzheimer's disease. *Neurobiol Aging* 19(5):393-400.
- Martin L, Fluhrer R, Reiss K, Kremmer E, Saftig P, Haass C. 2008. Regulated intramembrane proteolysis of Bri2 (Itm2b) by ADAM10 and SPPL2a/SPPL2b. *J Biol Chem* 283(3):1644-1652.
- Masters CL, Simms G, Weinman NA, Multhaup G, McDonald BL, Beyreuther K. 1985. Amyloid plaque core protein in Alzheimer disease and Down syndrome. *Proc Natl Acad Sci U S A* 82(12):4245-4249.
- McGehee DS, Heath MJ, Gelber S, Devay P, Role LW. 1995. Nicotine enhancement of fast excitatory synaptic transmission in CNS by presynaptic receptors. *Science* 269(5231):1692-1696.
- McLean CA, Cherny RA, Fraser FW, Fuller SJ, Smith MJ, Beyreuther K, Bush AI, Masters CL. 1999. Soluble pool of Abeta amyloid as a determinant of severity of neurodegeneration in Alzheimer's disease. *Ann Neurol* 46(6):860-866.
- Mesulam MM, Mufson EJ, Wainer BH, Levey AI. 1983. Central cholinergic pathways in the rat: an overview based on an alternative nomenclature (Ch1-Ch6). *Neuroscience* 10(4):1185-1201.
- Mikkelsen JD, Larsen MH. 2006. Effects of stress and adrenalectomy on activity-regulated cytoskeleton protein (Arc) gene expression. *Neurosci Lett* 403(3):239-243.
- Minoshima S, Cross D. 2008. In vivo imaging of axonal transport using MRI: aging and Alzheimer's disease. *Eur J Nucl Med Mol Imaging* 35 Suppl 1:S89-92.
- Mochizuki A, Tamaoka A, Shimohata A, Komatsuzaki Y, Shoji S. 2000. Abeta42-positive non-pyramidal neurons around amyloid plaques in Alzheimer's disease. *Lancet* 355(9197):42-43.
- Moir RD, Soscia SJ, Tucker S, Burton MA, Goldstein LE, Kirby JE, Tanzi RE. 2009. The Abeta protein of Alzheimer's disease is an antimicrobial peptide of the innate immune system. *Neurodegenerative Diseases* 6, Suppl. 1:2047.
- Montero CN, Hefti F. 1988. Rescue of lesioned septal cholinergic neurons by nerve growth factor: specificity and requirement for chronic treatment. *J Neurosci* 8(8):2986-2999.
- Mori C, Spooner ET, Wisniewsk KE, Wisniewski TM, Yamaguch H, Saido TC, Tolan DR, Selkoe DJ, Lemere CA. 2002. Intraneuronal Abeta42 accumulation in Down syndrome brain. *Amyloid* 9(2):88-102.
- Moya KL, Benowitz LI, Schneider GE, Allinquant B. 1994. The amyloid precursor protein is developmentally regulated and correlated with synaptogenesis. *Dev Biol* 161(2):597-603.
- Mufson EJ, Bothwell M, Kordower JH. 1989. Loss of nerve growth factor receptor-containing neurons in Alzheimer's disease: a quantitative analysis across subregions of the basal forebrain. *Experimental neurology* 105(3):221-232.

- Mufson EJ, Conner JM, Kordower JH. 1995. Nerve growth factor in Alzheimer's disease: defective retrograde transport to nucleus basalis. *Neuroreport* 6(7):1063-1066.
- Muller U, Cristina N, Li ZW, Wolfer DP, Lipp HP, Rulicke T, Brandner S, Aguzzi A, Weissmann C. 1994. Behavioral and anatomical deficits in mice homozygous for a modified beta-amyloid precursor protein gene. *Cell* 79(5):755-765.
- Nagele RG, D'Andrea MR, Anderson WJ, Wang HY. 2002. Intracellular accumulation of beta-amyloid(1-42) in neurons is facilitated by the alpha 7 nicotinic acetylcholine receptor in Alzheimer's disease. *Neuroscience* 110(2):199-211.
- Naslund J, Haroutunian V, Mohs R, Davis KL, Davies P, Greengard P, Buxbaum JD. 2000. Correlation between elevated levels of amyloid beta-peptide in the brain and cognitive decline. *JAMA* 283(12):1571-1577.
- Nitsch RM, Slack BE, Wurtman RJ, Growdon JH. 1992. Release of Alzheimer amyloid precursor derivatives stimulated by activation of muscarinic acetylcholine receptors. *Science* 258(5080):304-307.
- Nordberg A, Alafuzoff I, Winblad B. 1992. Nicotinic and muscarinic subtypes in the human brain: changes with aging and dementia. *J Neurosci Res* 31(1):103-111.
- Oakley H, Cole SL, Logan S, Maus E, Shao P, Craft J, Guillozet-Bongaarts A, Ohno M, Disterhoft J, Van Eldik L, Berry R, Vassar R. 2006. Intraneuronal beta-amyloid aggregates, neurodegeneration, and neuron loss in transgenic mice with five familial Alzheimer's disease mutations: potential factors in amyloid plaque formation. *J Neurosci* 26(40):10129-10140.
- Oddo S, Caccamo A, Shepherd JD, Murphy MP, Golde TE, Kaye R, Metherate R, Mattson MP, Akbari Y, LaFerla FM. 2003. Triple-transgenic model of Alzheimer's disease with plaques and tangles: intracellular Abeta and synaptic dysfunction. *Neuron* 39(3):409-421.
- Oh ES, Savonenko AV, King JF, Fangmark Tucker SM, Rudow GL, Xu G, Borchelt DR, Troncoso JC. 2008. Amyloid precursor protein increases cortical neuron size in transgenic mice. *Neurobiol Aging*.
- Ohyagi Y, Tsuruta Y, Motomura K, Miyoshi K, Kikuchi H, Iwaki T, Taniwaki T, Kira J. 2007. Intraneuronal amyloid beta42 enhanced by heating but counteracted by formic acid. *J Neurosci Methods* 159(1):134-138.
- Ons S, Marti O, Armario A. 2004. Stress-induced activation of the immediate early gene Arc (activity-regulated cytoskeleton-associated protein) is restricted to telencephalic areas in the rat brain: relationship to c-fos mRNA. *J Neurochem* 89(5):1111-1118.
- Packard MG, Knowlton BJ. 2002. Learning and memory functions of the Basal Ganglia. *Annu Rev Neurosci* 25:563-593.
- Palop JJ, Chin J, Bien-Ly N, Massaro C, Yeung BZ, Yu GQ, Mucke L. 2005. Vulnerability of dentate granule cells to disruption of arc expression in human amyloid precursor protein transgenic mice. *J Neurosci* 25(42):9686-9693.
- Paxinos G, Franklin KBJ. 2001. *The mouse brain in stereotaxic coordinates*: Academic Press.
- Perez RG, Soriano S, Hayes JD, Ostaszewski B, Xia W, Selkoe DJ, Chen X, Stokin GB, Koo EH. 1999. Mutagenesis identifies new signals for beta-amyloid precursor protein

- endocytosis, turnover, and the generation of secreted fragments, including Abeta42. *J Biol Chem* 274(27):18851-18856.
- Perez SE, Dar S, Ikonovic MD, DeKosky ST, Mufson EJ. 2007. Cholinergic forebrain degeneration in the APP<sup>swe</sup>/PS1<sup>DeltaE9</sup> transgenic mouse. *Neurobiol Dis* 28(1):3-15.
- Petersen RC, Doody R, Kurz A, Mohs RC, Morris JC, Rabins PV, Ritchie K, Rossor M, Thal L, Winblad B. 2001. Current concepts in mild cognitive impairment. *Arch Neurol* 58(12):1985-1992.
- Petersen RC, Smith GE, Waring SC, Ivnik RJ, Tangalos EG, Kokmen E. 1999. Mild cognitive impairment: clinical characterization and outcome. *Arch Neurol* 56(3):303-308.
- Pettit DL, Shao Z, Yakel JL. 2001. beta-Amyloid(1-42) peptide directly modulates nicotinic receptors in the rat hippocampal slice. *J Neurosci* 21(1):RC120.
- Pierce JE, Trojanowski JQ, Graham DI, Smith DH, McIntosh TK. 1996. Immunohistochemical characterization of alterations in the distribution of amyloid precursor proteins and beta-amyloid peptide after experimental brain injury in the rat. *J Neurosci* 16(3):1083-1090.
- Pigino G, Morfini G, Atagi Y, Deshpande A, Yu C, Jungbauer L, LaDu M, Busciglio J, Brady S. 2009. Disruption of fast axonal transport is a pathogenic mechanism for intraneuronal amyloid beta. *Proc Natl Acad Sci U S A* 106(14):5907-5912.
- Pigino G, Morfini G, Pelsman A, Mattson MP, Brady ST, Busciglio J. 2003. Alzheimer's presenilin 1 mutations impair kinesin-based axonal transport. *J Neurosci* 23(11):4499-4508.
- Pike CJ, Overman MJ, Cotman CW. 1995. Amino-terminal deletions enhance aggregation of beta-amyloid peptides in vitro. *J Biol Chem* 270(41):23895-23898.
- Pinaud R, Penner MR, Robertson HA, Currie RW. 2001. Upregulation of the immediate early gene arc in the brains of rats exposed to environmental enrichment: implications for molecular plasticity. *Brain Res Mol Brain Res* 91(1-2):50-56.
- Pluck A, Klasen C. 2009. Generation of chimeras by microinjection. *Methods Mol Biol* 561:199-217.
- Praprotnik D, Smith MA, Richey PL, Vinters HV, Perry G. 1996. Filament heterogeneity within the dystrophic neurites of senile plaques suggests blockage of fast axonal transport in Alzheimer's disease. *Acta Neuropathol (Berl)* 91(3):226-235.
- Price JL, Ko AI, Wade MJ, Tsou SK, McKeel DW, Morris JC. 2001. Neuron number in the entorhinal cortex and CA1 in preclinical Alzheimer disease. *Arch Neurol* 58(9):1395-1402.
- Raber J, Huang Y, Ashford JW. 2004. ApoE genotype accounts for the vast majority of AD risk and AD pathology. *Neurobiol Aging* 25(5):641-650.
- Rajendran L, Knobloch M, Geiger KD, Dienel S, Nitsch R, Simons K, Konietzko U. 2007. Increased Abeta production leads to intracellular accumulation of Abeta in flotillin-1-positive endosomes. *Neurodegener Dis* 4(2-3):164-170.

- Reisberg B. 2006. Diagnostic criteria in dementia: a comparison of current criteria, research challenges, and implications for DSM-V. *J Geriatr Psychiatry Neurol* 19(3):137-146.
- Riddell DR, Christie G, Hussain I, Dingwall C. 2001. Compartmentalization of beta-secretase (Asp2) into low-buoyant density, noncaveolar lipid rafts. *Curr Biol* 11(16):1288-1293.
- Roozendaal B. 2002. Stress and memory: opposing effects of glucocorticoids on memory consolidation and memory retrieval. *Neurobiol Learn Mem* 78(3):578-595.
- Roy S, Zhang B, Lee VM, Trojanowski JQ. 2005. Axonal transport defects: a common theme in neurodegenerative diseases. *Acta Neuropathol (Berl)* 109(1):5-13.
- Roychoudhuri R, Yang M, Hoshi MM, Teplow DB. 2008. Amyloid beta -protein assembly and Alzheimer's disease. *J Biol Chem*.
- Ruberti F, Capsoni S, Comparini A, Di Daniel E, Franzot J, Gonfloni S, Rossi G, Berardi N, Cattaneo A. 2000. Phenotypic knockout of nerve growth factor in adult transgenic mice reveals severe deficits in basal forebrain cholinergic neurons, cell death in the spleen, and skeletal muscle dystrophy. *J Neurosci* 20(7):2589-2601.
- Russo C, Violani E, Salis S, Venezia V, Dolcini V, Damonte G, Benatti U, D'Arrigo C, Patrone E, Carlo P, Schettini G. 2002. Pyroglutamate-modified amyloid beta-peptides--AbetaN3(pE)--strongly affect cultured neuron and astrocyte survival. *J Neurochem* 82(6):1480-1489.
- Sahlin C, Lord A, Magnusson K, Englund H, Almeida CG, Greengard P, Nyberg F, Gouras GK, Lannfelt L, Nilsson LN. 2007. The Arctic Alzheimer mutation favors intracellular amyloid-beta production by making amyloid precursor protein less available to alpha-secretase. *J Neurochem* 101(3):854-862.
- Saido TC, Iwatsubo T, Mann DM, Shimada H, Ihara Y, Kawashima S. 1995. Dominant and differential deposition of distinct beta-amyloid peptide species, A beta N3(pE), in senile plaques. *Neuron* 14(2):457-466.
- Salehi A, Delcroix JD, Belichenko PV, Zhan K, Wu C, Valletta JS, Takimoto-Kimura R, Kleschevnikov AM, Sambamurti K, Chung PP, Xia W, Villar A, Campbell WA, Kulnane LS, Nixon RA, Lamb BT, Epstein CJ, Stokin GB, Goldstein LS, Mobley WC. 2006. Increased App expression in a mouse model of Down's syndrome disrupts NGF transport and causes cholinergic neuron degeneration. *Neuron* 51(1):29-42.
- Salehi A, Delcroix JD, Mobley WC. 2003. Traffic at the intersection of neurotrophic factor signaling and neurodegeneration. *Trends in neurosciences* 26(2):73-80.
- Sandberg G, Stewart W, Smialek J, Troncoso JC. 2001. The prevalence of the neuropathological lesions of Alzheimer's disease is independent of race and gender. *Neurobiol Aging* 22(2):169-175.
- Sang TK, Jackson GR. 2005. Drosophila models of neurodegenerative disease. *NeuroRx* 2(3):438-446.
- Sarter M, Hasselmo ME, Bruno JP, Givens B. 2005. Unraveling the attentional functions of cortical cholinergic inputs: interactions between signal-driven and cognitive modulation of signal detection. *Brain Res Brain Res Rev* 48(1):98-111.



- Sasaki N, Toki S, Chowei H, Saito T, Nakano N, Hayashi Y, Takeuchi M, Makita Z. 2001. Immunohistochemical distribution of the receptor for advanced glycation end products in neurons and astrocytes in Alzheimer's disease. *Brain Res* 888(2):256-262.
- Scheff SW, DeKosky ST, Price DA. 1990. Quantitative assessment of cortical synaptic density in Alzheimer's disease. *Neurobiol Aging* 11(1):29-37.
- Scheuner D, Eckman C, Jensen M, Song X, Citron M, Suzuki N, Bird TD, Hardy J, Hutton M, Kukull W, Larson E, Levy-Lahad E, Viitanen M, Peskind E, Poorkaj P, Schellenberg G, Tanzi R, Wasco W, Lannfelt L, Selkoe D, Younkin S. 1996. Secreted amyloid beta-protein similar to that in the senile plaques of Alzheimer's disease is increased in vivo by the presenilin 1 and 2 and APP mutations linked to familial Alzheimer's disease. *Nat Med* 2(8):864-870.
- Schilling S, Lauber T, Schaupp M, Manhart S, Scheel E, Bohm G, Demuth HU. 2006. On the seeding and oligomerization of pGlu-amyloid peptides (in vitro). *Biochemistry* 45(41):12393-12399.
- Schilling S, Zeitschel U, Hoffmann T, Heiser U, Francke M, Kehlen A, Holzer M, Hutter-Paier B, Prokesch M, Windisch M, Jagla W, Schlenzig D, Lindner C, Rudolph T, Reuter G, Cynis H, Montag D, Demuth HU, Rossner S. 2008. Glutaminy cyclase inhibition attenuates pyroglutamate Abeta and Alzheimer's disease-like pathology. *Nat Med* 14(10):1106-1111.
- Schmechel DE, Goldgaber D, Burkhart DS, Gilbert JR, Gajdusek DC, Roses AD. 1988. Cellular localization of messenger RNA encoding amyloid-beta-protein in normal tissue and in Alzheimer disease. *Alzheimer Dis Assoc Disord* 2(2):96-111.
- Schmechel DE, Saunders AM, Strittmatter WJ, Crain BJ, Hulette CM, Joo SH, Pericak-Vance MA, Goldgaber D, Roses AD. 1993. Increased amyloid beta-peptide deposition in cerebral cortex as a consequence of apolipoprotein E genotype in late-onset Alzheimer disease. *Proc Natl Acad Sci U S A* 90(20):9649-9653.
- Schmitz C, Hof PR. 2005. Design-based stereology in neuroscience. *Neuroscience* 130(4):813-831.
- Schmitz C, Rutten BP, Pielen A, Schafer S, Wirths O, Tremp G, Czech C, Blanchard V, Multhaup G, Rezaie P, Korr H, Steinbusch HW, Pradier L, Bayer TA. 2004. Hippocampal neuron loss exceeds amyloid plaque load in a transgenic mouse model of Alzheimer's disease. *Am J Pathol* 164(4):1495-1502.
- Schnell SA, Staines WA, Wessendorf MW. 1999. Reduction of lipofuscin-like autofluorescence in fluorescently labeled tissue. *J Histochem Cytochem* 47(6):719-730.
- Schwabe L, Oitzl MS, Philippson C, Richter S, Bohringer A, Wippich W, Schachinger H. 2007. Stress modulates the use of spatial versus stimulus-response learning strategies in humans. *Learn Mem* 14(1):109-116.
- Scott SA, Mufson EJ, Weingartner JA, Skau KA, Crutcher KA. 1995. Nerve growth factor in Alzheimer's disease: increased levels throughout the brain coupled with declines in nucleus basalis. *J Neurosci* 15(9):6213-6221.
- Seaman MN. 2004. Cargo-selective endosomal sorting for retrieval to the Golgi requires retromer. *J Cell Biol* 165(1):111-122.

- Selkoe DJ. 1989. Biochemistry of altered brain proteins in Alzheimer's disease. *Annu Rev Neurosci* 12:463-490.
- Selkoe DJ. 1998. The cell biology of beta-amyloid precursor protein and presenilin in Alzheimer's disease. *Trends Cell Biol* 8(11):447-453.
- Selkoe DJ. 2001. Alzheimer's disease: genes, proteins, and therapy. *Physiol Rev* 81(2):741-766.
- Senechal Y, Larmet Y, Dev KK. 2006. Unraveling in vivo functions of amyloid precursor protein: insights from knockout and knockdown studies. *Neurodegener Dis* 3(3):134-147.
- Seo H, Isacson O. 2005. Abnormal APP, cholinergic and cognitive function in Ts65Dn Down's model mice. *Experimental neurology* 193(2):469-480.
- Simic G, Kostovic I, Winblad B, Bogdanovic N. 1997. Volume and number of neurons of the human hippocampal formation in normal aging and Alzheimer's disease. *J Comp Neurol* 379(4):482-494.
- Simons M, Schwarzler F, Lutjohann D, von Bergmann K, Beyreuther K, Dichgans J, Wormstall H, Hartmann T, Schulz JB. 2002. Treatment with simvastatin in normocholesterolemic patients with Alzheimer's disease: A 26-week randomized, placebo-controlled, double-blind trial. *Ann Neurol* 52(3):346-350.
- Sinha S, Anderson JP, Barbour R, Basi GS, Caccavello R, Davis D, Doan M, Dovey HF, Frigon N, Hong J, Jacobson-Croak K, Jewett N, Keim P, Knops J, Lieberburg I, Power M, Tan H, Tatsuno G, Tung J, Schenk D, Seubert P, Suomensaaari SM, Wang S, Walker D, Zhao J, McConlogue L, John V. 1999. Purification and cloning of amyloid precursor protein beta-secretase from human brain. *Nature* 402(6761):537-540.
- Small DH, Maksel D, Kerr ML, Ng J, Hou X, Chu C, Mehrani H, Unabia S, Azari MF, Loiacono R, Aguilar MI, Chebib M. 2007. The beta-amyloid protein of Alzheimer's disease binds to membrane lipids but does not bind to the alpha7 nicotinic acetylcholine receptor. *J Neurochem* 101(6):1527-1538.
- Small DH, McLean CA. 1999. Alzheimer's disease and the amyloid beta protein: What is the role of amyloid? *J Neurochem* 73(2):443-449.
- Small SA, Gandy S. 2006. Sorting through the cell biology of Alzheimer's disease: intracellular pathways to pathogenesis. *Neuron* 52(1):15-31.
- Smith KD, Kallhoff V, Zheng H, Pautler RG. 2007. In vivo axonal transport rates decrease in a mouse model of Alzheimer's disease. *Neuroimage* 35(4):1401-1408.
- Sola C, Mengod G, Probst A, Palacios JM. 1993. Differential regional and cellular distribution of beta-amyloid precursor protein messenger RNAs containing and lacking the Kunitz protease inhibitor domain in the brain of human, rat and mouse. *Neuroscience* 53(1):267-295.
- Sparks DL, Sabbagh MN, Connor DJ, Lopez J, Launer LJ, Browne P, Wasser D, Johnson-Traver S, Lochhead J, Ziolkowski C. 2005. Atorvastatin for the treatment of mild to moderate Alzheimer disease: preliminary results. *Arch Neurol* 62(5):753-757.

- Spencer JP, Weil A, Hill K, Hussain I, Richardson JC, Cusdin FS, Chen YH, Randall AD. 2006. Transgenic mice over-expressing human beta-amyloid have functional nicotinic alpha 7 receptors. *Neuroscience* 137(3):795-805.
- Steward O, Worley P. 2002. Local synthesis of proteins at synaptic sites on dendrites: role in synaptic plasticity and memory consolidation? *Neurobiol Learn Mem* 78(3):508-527.
- Steward O, Worley PF. 2001. Selective targeting of newly synthesized Arc mRNA to active synapses requires NMDA receptor activation. *Neuron* 30(1):227-240.
- Stokin GB, Almenar-Queralt A, Gunawardena S, Rodrigues EM, Falzone T, Kim J, Lillo C, Mount SL, Roberts EA, McGowan E, Williams DS, Goldstein LS. 2008. AMYLOID PRECURSOR PROTEIN-INDUCED AXONOPATHIES ARE INDEPENDENT OF AMYLOID- $\beta$  PEPTIDES. *Hum Mol Genet*.
- Stokin GB, Goldstein LS. 2006. Axonal transport and Alzheimer's disease. *Annu Rev Biochem* 75:607-627.
- Stokin GB, Lillo C, Falzone TL, Brusch RG, Rockenstein E, Mount SL, Raman R, Davies P, Masliah E, Williams DS, Goldstein LS. 2005. Axonopathy and transport deficits early in the pathogenesis of Alzheimer's disease. *Science* 307(5713):1282-1288.
- Strachan T, Read AP. 1999. *Human Molecular Genetics*. Kingston F, editor. Bath, UK: The Bath Press Ltd.
- Strittmatter WJ, Weisgraber KH, Huang DY, Dong LM, Salvesen GS, Pericak-Vance M, Schmechel D, Saunders AM, Goldgaber D, Roses AD. 1993. Binding of human apolipoprotein E to synthetic amyloid beta peptide: isoform-specific effects and implications for late-onset Alzheimer disease. *Proc Natl Acad Sci U S A* 90(17):8098-8102.
- Takahashi RH, Almeida CG, Kearney PF, Yu F, Lin MT, Milner TA, Gouras GK. 2004. Oligomerization of Alzheimer's beta-amyloid within processes and synapses of cultured neurons and brain. *J Neurosci* 24(14):3592-3599.
- Takahashi RH, Milner TA, Li F, Nam EE, Edgar MA, Yamaguchi H, Beal MF, Xu H, Greengard P, Gouras GK. 2002. Intraneuronal Alzheimer abeta42 accumulates in multivesicular bodies and is associated with synaptic pathology. *Am J Pathol* 161(5):1869-1879.
- Tanaka S, Shiojiri S, Takahashi Y, Kitaguchi N, Ito H, Kameyama M, Kimura J, Nakamura S, Ueda K. 1989. Tissue-specific expression of three types of beta-protein precursor mRNA: enhancement of protease inhibitor-harboring types in Alzheimer's disease brain. *Biochem Biophys Res Commun* 165(3):1406-1414.
- Tanzi RE, Gusella JF, Watkins PC, Bruns GA, St George-Hyslop P, Van Keuren ML, Patterson D, Pagan S, Kurnit DM, Neve RL. 1987. Amyloid beta protein gene: cDNA, mRNA distribution, and genetic linkage near the Alzheimer locus. *Science* 235(4791):880-884.
- Teaktong T, Graham AJ, Court JA, Perry RH, Jaros E, Johnson M, Hall R, Perry EK. 2004. Nicotinic acetylcholine receptor immunohistochemistry in Alzheimer's disease and dementia with Lewy bodies: differential neuronal and astroglial pathology. *J Neurol Sci* 225(1-2):39-49.

- Teipel SJ, Stahl R, Dietrich O, Schoenberg SO, Perneczky R, Bokde AL, Reiser MF, Moller HJ, Hampel H. 2007. Multivariate network analysis of fiber tract integrity in Alzheimer's disease. *Neuroimage* 34(3):985-995.
- Terry RD, Masliah E, Salmon DP, Butters N, DeTeresa R, Hill R, Hansen LA, Katzman R. 1991. Physical basis of cognitive alterations in Alzheimer's disease: synapse loss is the major correlate of cognitive impairment. *Ann Neurol* 30(4):572-580.
- Thomann PA, Dos Santos V, Seidl U, Toro P, Essig M, Schroder J. 2009. MRI-Derived Atrophy of the Olfactory Bulb and Tract in Mild Cognitive Impairment and Alzheimer's Disease. *J Alzheimers Dis* 17(1):213-221.
- Tiraboschi P, Hansen LA, Alford M, Masliah E, Thal LJ, Corey-Bloom J. 2000. The decline in synapses and cholinergic activity is asynchronous in Alzheimer's disease. *Neurology* 55(9):1278-1283.
- Tsai J, Grutzendler J, Duff K, Gan WB. 2004. Fibrillar amyloid deposition leads to local synaptic abnormalities and breakage of neuronal branches. *Nat Neurosci* 7(11):1181-1183.
- Tuszynski MH, Gage FH. 1995. Bridging grafts and transient nerve growth factor infusions promote long-term central nervous system neuronal rescue and partial functional recovery. *Proc Natl Acad Sci U S A* 92(10):4621-4625.
- Tuszynski MH, Thal L, Pay M, Salmon DP, U HS, Bakay R, Patel P, Blesch A, Vahlsing HL, Ho G, Tong G, Potkin SG, Fallon J, Hansen L, Mufson EJ, Kordower JH, Gall C, Conner J. 2005. A phase 1 clinical trial of nerve growth factor gene therapy for Alzheimer disease. *Nat Med* 11(5):551-555.
- Van Broeck B, Vanhoutte G, Pirici D, Van Dam D, Wils H, Cuijt I, Vennekens K, Zabielski M, Michalik A, Theuns J, De Deyn PP, Van der Linden A, Van Broeckhoven C, Kumar-Singh S. 2008. Intraneuronal amyloid beta and reduced brain volume in a novel APP T714I mouse model for Alzheimer's disease. *Neurobiol Aging* 29(2):241-252.
- Vas CJ, Rajkumar S, Tanyakitpisal P, Chandra V. 2002. Regional Health Forum report. World Health Organization (WHO), South-East Asia Region 6(1).
- Vassar R, Bennett BD, Babu-Khan S, Kahn S, Mendiaz EA, Denis P, Teplow DB, Ross S, Amarante P, Loeloff R, Luo Y, Fisher S, Fuller J, Edenson S, Lile J, Jarosinski MA, Biere AL, Curran E, Burgess T, Louis JC, Collins F, Treanor J, Rogers G, Citron M. 1999. Beta-secretase cleavage of Alzheimer's amyloid precursor protein by the transmembrane aspartic protease BACE. *Science* 286(5440):735-741.
- Vazdarjanova A, Guzowski JF. 2004. Differences in hippocampal neuronal population responses to modifications of an environmental context: evidence for distinct, yet complementary, functions of CA3 and CA1 ensembles. *J Neurosci* 24(29):6489-6496.
- Vazdarjanova A, McNaughton BL, Barnes CA, Worley PF, Guzowski JF. 2002. Experience-dependent coincident expression of the effector immediate-early genes arc and Homer 1a in hippocampal and neocortical neuronal networks. *J Neurosci* 22(23):10067-10071.

- Vetrivel KS, Cheng H, Lin W, Sakurai T, Li T, Nukina N, Wong PC, Xu H, Thinakaran G. 2004. Association of gamma-secretase with lipid rafts in post-Golgi and endosome membranes. *J Biol Chem* 279(43):44945-44954.
- Vidal R, Frangione B, Rostagno A, Mead S, Revesz T, Plant G, Ghiso J. 1999. A stop-codon mutation in the BRI gene associated with familial British dementia. *Nature* 399(6738):776-781.
- Vidal R, Revesz T, Rostagno A, Kim E, Holton JL, Bek T, Bojsen-Moller M, Braendgaard H, Plant G, Ghiso J, Frangione B. 2000. A decamer duplication in the 3' region of the BRI gene originates an amyloid peptide that is associated with dementia in a Danish kindred. *Proc Natl Acad Sci U S A* 97(9):4920-4925.
- Wahle T, Prager K, Raffler N, Haass C, Famulok M, Walter J. 2005. GGA proteins regulate retrograde transport of BACE1 from endosomes to the trans-Golgi network. *Mol Cell Neurosci* 29(3):453-461.
- Wallace CS, Lyford GL, Worley PF, Steward O. 1998. Differential intracellular sorting of immediate early gene mRNAs depends on signals in the mRNA sequence. *J Neurosci* 18(1):26-35.
- Walsh DM, Lomakin A, Benedek GB, Condron MM, Teplow DB. 1997. Amyloid beta-protein fibrillogenesis. Detection of a protofibrillar intermediate. *J Biol Chem* 272(35):22364-22372.
- Walsh DM, Selkoe DJ. 2007. A beta oligomers - a decade of discovery. *J Neurochem* 101(5):1172-1184.
- Walsh DM, Tseng BP, Rydel RE, Podlisny MB, Selkoe DJ. 2000. The oligomerization of amyloid beta-protein begins intracellularly in cells derived from human brain. *Biochemistry* 39(35):10831-10839.
- Wang HY, D'Andrea MR, Nagele RG. 2002. Cerebellar diffuse amyloid plaques are derived from dendritic Abeta42 accumulations in Purkinje cells. *Neurobiol Aging* 23(2):213-223.
- Wang HY, Lee DH, D'Andrea MR, Peterson PA, Shank RP, Reitz AB. 2000. beta-Amyloid(1-42) binds to alpha7 nicotinic acetylcholine receptor with high affinity. Implications for Alzheimer's disease pathology. *J Biol Chem* 275(8):5626-5632.
- Wegenast-Braun BM, Fulgencio Maisch A, Eicke D, Radde R, Herzog MC, Staufenbiel M, Jucker M, Calhoun ME. 2009. Independent effects of intra- and extracellular Abeta on learning-related gene expression. *Am J Pathol* 175(1):271-282.
- Wegiel J, Kuchna I, Nowicki K, Frackowiak J, Mazur-Kolecka B, Imaki H, Mehta PD, Silverman WP, Reisberg B, DeLeon M, Wisniewski T, Pirttilla T, Frey H, Lehtimäki T, Kivimäki T, Visser FE, Kamphorst W, Potempska A, Bolton D, Currie JR, Miller DL. 2007. Intraneuronal Abeta immunoreactivity is not a predictor of brain amyloidosis-beta or neurofibrillary degeneration. *Acta Neuropathol* 113(4):389-402.
- West MJ. 1993. New stereological methods for counting neurons. *Neurobiol Aging* 14(4):275-285.
- West MJ. 2002. Design-based stereological methods for counting neurons. *Prog Brain Res* 135:43-51.

- West MJ, Coleman PD, Flood DG, Troncoso JC. 1994. Differences in the pattern of hippocampal neuronal loss in normal ageing and Alzheimer's disease. *Lancet* 344(8925):769-772.
- West MJ, Kawas CH, Stewart WF, Rudow GL, Troncoso JC. 2004. Hippocampal neurons in pre-clinical Alzheimer's disease. *Neurobiol Aging* 25(9):1205-1212.
- West MJ, Slomianka L, Gundersen HJ. 1991. Unbiased stereological estimation of the total number of neurons in the subdivisions of the rat hippocampus using the optical fractionator. *AnatRec* 231(4):482-497.
- Whitehouse PJ, Price DL, Clark AW, Coyle JT, DeLong MR. 1981. Alzheimer disease: evidence for selective loss of cholinergic neurons in the nucleus basalis. *Ann Neurol* 10(2):122-126.
- Whitehouse PJ, Price DL, Struble RG, Clark AW, Coyle JT, DeLong MR. 1982. Alzheimer's disease and senile dementia: loss of neurons in the basal forebrain. *Science* 215(4537):1237-1239.
- Williams LR, Varon S, Peterson GM, Victorin K, Fischer W, Bjorklund A, Gage FH. 1986. Continuous infusion of nerve growth factor prevents basal forebrain neuronal death after fimbria fornix transection. *Proc Natl Acad Sci U S A* 83(23):9231-9235.
- Wirhns O, Bayer TA. 2008. Motor impairment in Alzheimer's disease and transgenic Alzheimer's disease mouse models. *Genes Brain Behav* 7 Suppl 1:1-5.
- Wirhns O, Breyhan H, Cynis H, Schilling S, Demuth HU, Bayer TA. 2009. Intraneuronal pyroglutamate-Abeta 3-42 triggers neurodegeneration and lethal neurological deficits in a transgenic mouse model. *Acta Neuropathol*.
- Wirhns O, Breyhan H, Marcello A, Cotel MC, Bruck W, Bayer TA. 2008a. Inflammatory changes are tightly associated with neurodegeneration in the brain and spinal cord of the APP/PS1KI mouse model of Alzheimer's disease. *Neurobiol Aging*.
- Wirhns O, Breyhan H, Schafer S, Roth C, Bayer TA. 2008b. Deficits in working memory and motor performance in the APP/PS1ki mouse model for Alzheimer's disease. *Neurobiol Aging* 29(6):891-901.
- Wirhns O, Multhaup G, Bayer TA. 2004. A modified beta-amyloid hypothesis: intraneuronal accumulation of the beta-amyloid peptide--the first step of a fatal cascade. *J Neurochem* 91(3):513-520.
- Wirhns O, Multhaup G, Czech C, Blanchard V, Moussaoui S, Tremp G, Pradier L, Beyreuther K, Bayer TA. 2001. Intraneuronal Abeta accumulation precedes plaque formation in beta-amyloid precursor protein and presenilin-1 double-transgenic mice. *Neurosci Lett* 306(1-2):116-120.
- Wirhns O, Multhaup G, Czech C, Feldmann N, Blanchard V, Tremp G, Beyreuther K, Pradier L, Bayer TA. 2002. Intraneuronal APP/A beta trafficking and plaque formation in beta-amyloid precursor protein and presenilin-1 transgenic mice. *Brain Pathol* 12(3):275-286.
- Wirhns O, Weickert S, Majtenyi K, Havas L, Kahle PJ, Okochi M, Haass C, Multhaup G, Beyreuther K, Bayer TA. 2000. Lewy body variant of Alzheimer's disease: alpha-synuclein in dystrophic neurites of Abeta plaques. *Neuroreport* 11(17):3737-3741.

- Wirhth O, Weis J, Kaye R, Saido TC, Bayer TA. 2007. Age-dependent axonal degeneration in an Alzheimer mouse model. *Neurobiol Aging* 28(11):1689-1699.
- Wirhth O, Weis J, Szczygielski J, Multhaup G, Bayer TA. 2006. Axonopathy in an APP/PS1 transgenic mouse model of Alzheimer's disease. *Acta Neuropathol (Berl)* 111(4):312-319.
- Wisniewski K, Howe J, Williams DG, Wisniewski HM. 1978. Precocious aging and dementia in patients with Down's syndrome. *Biol Psychiatry* 13(5):619-627.
- Wong TP, Debeir T, Duff K, Cuello AC. 1999. Reorganization of cholinergic terminals in the cerebral cortex and hippocampus in transgenic mice carrying mutated presenilin-1 and amyloid precursor protein transgenes. *J Neurosci* 19(7):2706-2716.
- Xu H, Sweeney D, Wang R, Thinakaran G, Lo AC, Sisodia SS, Greengard P, Gandy S. 1997. Generation of Alzheimer beta-amyloid protein in the trans-Golgi network in the apparent absence of vesicle formation. *Proc Natl Acad Sci U S A* 94(8):3748-3752.
- Yagishita S. 1978. Morphological investigations on axonal swellings and spheroids in various human diseases. *Virchows Arch A Pathol Anat Histol* 378(3):181-197.
- Yan SD, Chen X, Fu J, Chen M, Zhu H, Roher A, Slattery T, Zhao L, Nagashima M, Morser J, Migheli A, Nawroth P, Stern D, Schmidt AM. 1996. RAGE and amyloid-beta peptide neurotoxicity in Alzheimer's disease. *Nature* 382(6593):685-691.
- Yankner BA. 1996. New clues to Alzheimer's disease: unraveling the roles of amyloid and tau. *Nat Med* 2(8):850-852.
- Yankner BA, Duffy LK, Kirschner DA. 1990. Neurotrophic and neurotoxic effects of amyloid beta protein: reversal by tachykinin neuropeptides. *Science* 250(4978):279-282.
- Zerbinatti CV, Wahrle SE, Kim H, Cam JA, Bales K, Paul SM, Holtzman DM, Bu G. 2006. Apolipoprotein E and low density lipoprotein receptor-related protein facilitate intraneuronal A $\beta$ 42 accumulation in amyloid model mice. *J Biol Chem* 281(47):36180-36186.
- Zhang B, Veasey SC, Wood MA, Leng LZ, Kaminski C, Leight S, Abel T, Lee VM, Trojanowski JQ. 2005. Impaired rapid eye movement sleep in the Tg2576 APP murine model of Alzheimer's disease with injury to pedunculopontine cholinergic neurons. *Am J Pathol* 167(5):1361-1369.
- Zheng H, Jiang M, Trumbauer ME, Sirinathsinghji DJ, Hopkins R, Smith DW, Heavens RP, Dawson GR, Boyce S, Conner MW, Stevens KA, Slunt HH, Sisodia SS, Chen HY, Van der Ploeg LH. 1995. beta-Amyloid precursor protein-deficient mice show reactive gliosis and decreased locomotor activity. *Cell* 81(4):525-531.
- Zhu X, Moreira PI, Smith MA, Perry G. 2005. Alzheimer's disease: an intracellular movement disorder? *Trends Mol Med* 11(9):391-393.

## 7 Curriculum Vitae

### Personal Data

- Full name: Ditte Zerlang Christensen
- Date of birth: August 16<sup>th</sup>, 1980
- Nationality: Danish

### Education

---

10/2006 – 10/2009 3 years	<i>University of Goettingen</i> <b>PhD-student</b> The PhD is part of NEURAD which is an EU funded Marie-Curie PhD school focusing on Alzheimer's disease ( <a href="http://www.neurad-alzheimer.de">www.neurad-alzheimer.de</a> ). Thesis title: "Intraneuronal beta amyloid in Alzheimer's disease".	<i>Germany</i>
08/2003 – 03/2006 2 years, 8 months	<i>University of Copenhagen</i> <b>M.Sc. (Human Biology)</b> The master project was conducted in 1 year at the laboratory of Neuropsychiatry, department of pharmacology, University of Copenhagen. Thesis title: "Neuropeptide Y in electroconvulsive seizures and depression" (Mark: 11).	<i>Denmark</i>
01/2003 – 06/2003 6 months	<i>University of Manchester</i> <b>Studentship abroad</b> I studied at the Institute of Biosciences and the exchange was conducted through the international Erasmus program.	<i>England</i>
08/1999 – 01/2003 3 years, 6 months	<i>Technical University of Denmark (DTU)</i> <b>Bachelor of Chemistry/biotechnology engineering</b> Bachelor project: "Immunogenesitet af hypoallergene modermælkserstatninger" (Mark 11).	<i>Denmark</i>

### Professional experience

---

04/2008 – 06/2008 & 12/2008 – 03/2009 5 months	<i>Neurosearch A/S</i> <b>Consultant</b> I worked in the department of translational medicine with Jens D.	<i>Ballerup, Denmark</i>
--	--	--------------------------



- Mikkelsen setting up autoradiographic binding assays and working with the nicotinic alpha 7 receptor in Alzheimer's disease.
- 04/2006 – 10/2006  
6 months  
*University of Copenhagen* *Copenhagen, Denmark*  
**Research Assistant**  
In the laboratory of Neuropsychiatry I extended the work of my master project on Neuropeptide Y in neurogenesis.
- 06/2005 – 11/2005  
4 months  
*CMC Biopharmaceuticals* *Søborg, Denmark*  
**Student Assistant** (part-time during study in human biology)  
Main assignment was to check that the equipment was running with the correct settings according to GMP.
- 08/2000 – 08/2003  
3 years  
*Tolleruphøj* *Frederikssund, Denmark*  
**Assistant** (part-time during study at DTU)  
Residential home for elderly people.

### Awards and Scholarships

---

- 09/2008  
**1. Prize** for best oral presentation of PhD project at the NEURAD annual meeting in Leuven, Belgium.
- 09/2007  
**1. Prize** for best oral presentation of PhD project at the NEURAD annual meeting in Göttingen, Germany.
- 09/2005  
**Biocampus scholarship** during master project, University of Copenhagen, DK.

### Publications

---

**Christensen DZ**, Olesen MV, Kristiansen H, Mikkelsen JD, Woldbye DPD. Unaltered neuropeptide Y (NPY) stimulated z-GTP $\gamma$ S binding suggests a net increase in NPY signalling after electroconvulsive seizures in mice. *Journal of Neuroscience Research*, 84:1282–1291 (2006).

**Christensen DZ**, Kraus SL, Flohr A, Cotel MC, Wirths O, Bayer TA. Transient intraneuronal A $\beta$  rather than extracellular plaque pathology correlates with neuron loss in the frontal cortex of APP/PS1KI mice. *Acta Neuropathol* 2008;116(6):647-55.

**Christensen DZ**, Bayer TA, Wirths O. Intracellular A $\beta$  triggers neuron loss in the cholinergic system of the APP/PS1KI mouse model of Alzheimer's disease. *Neurobiology of Aging*, in press (EPUB Sep 3<sup>rd</sup> 2008, DOI: 10.1016/j.neurobiolaging.2008.07.022).

Thomsen MS, **Christensen DZ**, Hansen HH, Redrobe J, Mikkelsen JD. Alpha 7 nicotinic acetylcholine receptor activation prevents behavioural and molecular changes induced by repeated phencyclidine treatment. *Neuropharmacology* 56(6-7):1001-9 (2009).

Olling JD, Ulrichsen J, **Christensen DZ**, Woldbye DPD. Complex Plastic Changes in the Neuropeptide Y (NPY) System During Ethanol Intoxication and Withdrawal in the Rat Brain. *Journal of Neuroscience Research*, in press (2009).